Drug Discoveries & Therapeutics

ISSN 1881-7831 Online ISSN 1881-784X
Volume 2, Number 2, April 2008
www.ddtjournal.com

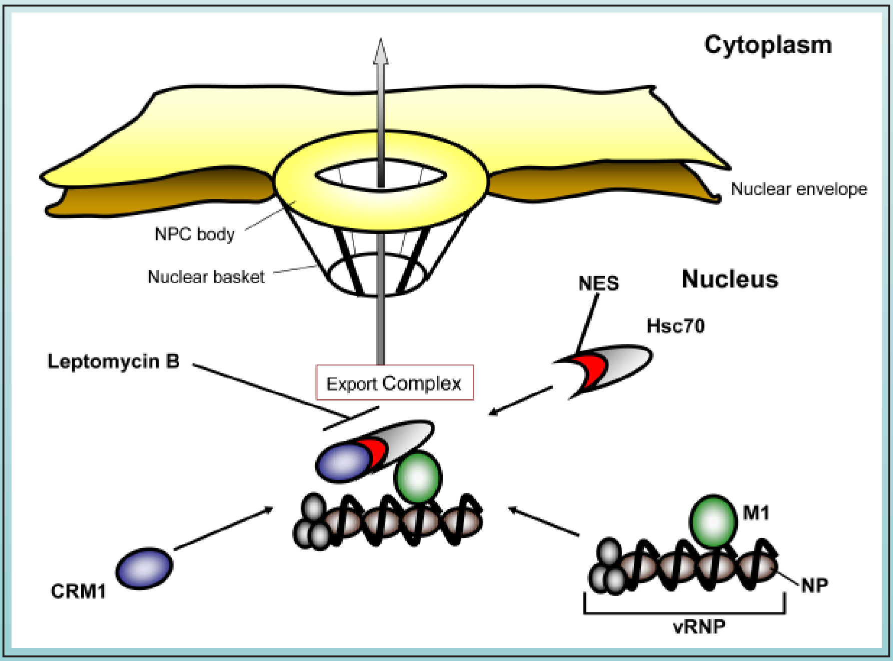
Cytoplasm
Nuclear envelope
NPC body
Nuclear basket
NES
Nucleus
Hsc70
Leptomycin B
Export Complex
M1
CRM1
NP
vRNP

Shandong University China-Japan Cooperation Center for Drug Discovery & Screen
International Advancement Center for Medicine & Health Research

Drug Discoveries & Therapeutics

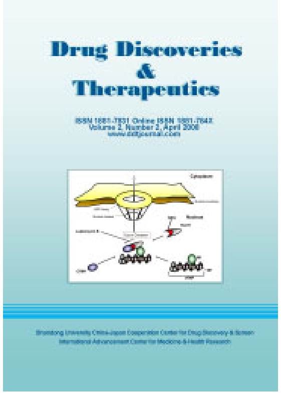

Editor-in-Chief:

Kazuhisa SEKIMIZU
(*The University of Tokyo, Tokyo, Japan*)

Associate Editor:

Norihiro KOKUDO
(*The University of Tokyo, Tokyo, Japan*)

Drug Discoveries & Therapeutics is a peer-reviewed international journal published bimonthly by *Shandong University China-Japan Cooperation Center for Drug Discovery & Screen* (SDU-DDSC) and *International Advancement Center for Medicine & Health Research Co., Ltd.* (IACMHR Co., Ltd.).

Drug Discoveries & Therapeutics mainly publishes articles related to basic and clinical pharmaceutical research such as pharmaceutical and therapeutical chemistry, pharmacology, pharmacy, pharmacokinetics, industrial pharmacy, pharmaceutical manufacturing, pharmaceutical technology, drug delivery, toxicology, and traditional herb medicine. Studies on drug-related fields such as biology, biochemistry, physiology, microbiology, and immunology are also within the scope of this journal.

Subject Coverage: Basic and clinical pharmaceutical research including Pharmaceutical and therapeutical chemistry, Pharmacology, Pharmacy, Pharmacokinetics, Industrial pharmacy, Pharmaceutical manufacturing, Pharmaceutical technology, Drug delivery, Toxicology, and Traditional herb medicine.

Language: English
Issues/Year: 6
Published by: IACMHR and SDU-DDSC
ISSN: 1881-7831 (**Online ISSN** 1881-784X)

Editorial and Head Office

Wei TANG, MD PhD
Secretary-in-General

TSUIN-IKIZAKA 410
2-17-5 Hongo, Bunkyo-ku
Tokyo 113-0033, Japan
Tel: 03-5840-9697
Fax: 03-5840-9698
E-mail: office@ddtjournal.com
URL: www.ddtjournal.com

IACMHR CO., LTD.

Drug Discoveries & Therapeutics

Editorial Board

Editor-in-Chief:
Kazuhisa SEKIMIZU (*The University of Tokyo, Tokyo, Japan*)

Associate Editor:
Norihiro KOKUDO (*The University of Tokyo, Tokyo, Japan*)

Secretary-in-General:
Wei TANG (*The University of Tokyo, Tokyo, Japan*)

Office Manager:
Munehiro NAKATA *(Tokai University, Kanagawa, Japan*)

Web Editor:
Yu CHEN (*The University of Tokyo, Tokyo, Japan*)

English Editor:
Curtis BENTLEY (*Roswell, GA, USA*)

China Office:
Wenfang XU (*Shandong University, Shandong, China*)

Editors:

Yoshihiro ARAKAWA (*Tokyo, Japan*)
Santad CHANPRAPAPH (*Bangkok, Thailand*)
Fen Er CHEN (*Shanghai, China*)
Guanhua DU (*Beijing, China*)
Chandradhar DWIVEDI (*Brookings, SD, USA*)
Mohamed F. EL-MILIGI (*Cairo, Egypt*)
Harald HAMACHER (*Tuebingen, Germany*)
Hiroshi HAMAMOTO (*Tokyo, Japan*)
Xiao-Jiang HAO (*Kunming, China*)
Langchong HE (*Xi'an, China*)
David A. HORNE (*Duarte, CA, USA*)
Yongzhou HU (*Hangzhou, China*)
Wei HUANG (*Shanghai, China*)
Hans E. JUNGINGER (*Phitsanulok, Thailand*)
Toshiaki KATADA (*Tokyo, Japan*)
Ibrahim S. KHATTAB (*Safat, Kuwait*)
Hiromichi KIMURA (*Tokyo, Japan*)
Shiroh KISHIOKA (*Wakayama, Japan*)
Kam Ming KO (*Hong Kong, China*)
Nobuyuki KOBAYASHI (*Nagasaki, Japan*)
Toshiro KONISHI (*Tokyo, Japan*)
Masahiro KUROYANAGI (*Hiroshima, Japan*)
Chun Guang LI (*Victoria, Australia*)
Hongmin LIU (*Zhengzhou, China*)
Ji-Kai LIU (*Kunming, China*)
Hongxiang LOU (*Jinan, China*)
Ken-ichi MAFUNE (*Tokyo, Japan*)
Norio MATSUKI (*Tokyo, Japan*)
Tohru MIZUSHIMA (*Kumamoto, Japan*)
Abdulla M. MOLOKHIA (*Alexandria, Egypt*)
Masahiro MURAKAMI (*Osaka, Japan*)
Yoshinobu NAKANISHI (*Ishikawa, Japan*)
Yutaka ORIHARA (*Tokyo, Japan*)
Xiao-Ming OU (*Jackson, MS, USA*)
Wei-San PAN (*Shenyang, China*)
Shafiqur RAHMAN (*Brookings, SD, USA*)
Adel SAKR (*Cincinnati, OH, USA*)
Abdel Aziz M. SALEH (*Cairo, Egypt*)
Tomofumi SANTA (*Tokyo, Japan*)
Yasufumi SAWADA (*Tokyo, Japan*)
Brahma N. SINGH (*Commack, NY, USA*)
Hongbin SUN (*Nanjing, China*)
Benny K. H. TAN (*Singapore, Singapore*)
Ren-Xiang TAN (*Nanjing, China*)
Murat TURKOGLU (*Istanbul, Turkey*)
Stephen G. WARD (*Bath, UK*)
Takako YOKOZAWA (*Toyama, Japan*)
Liangren ZHANG (*Beijing, China*)
Jian-Ping ZUO (*Shanghai, China*)

CONTENTS

Volume 2, Number 2, 2008

Reviews

58-63 **Roles of the Duffy antigen and glycophorin A in malaria infection and erythrocyte.**

Hiroshi Hamamoto, Nobuyoshi Akimitsu, Nagisa Arimitsu, Kazuhisa Sekimizu

64-73 **Dermal drug delivery: Revisited.**

Sateesh Khandavilli, Ramesh Panchagnula

Brief Report

74-76 **On the temperature dependence of the unbound drug fraction in plasma: Ultrafiltration method may considerably underestimate the true value for highly bound drugs.**

Leonid M. Berezhkovskiy

Original Articles

77-84 **Hsc70 regulates the nuclear export but not the import of influenza viral RNP: A possible target for the development of anti-influenza virus drugs.**

Ken Watanabe, Naoki Takizawa, Saiko Noda, Fujiko Tsukahara, Yoshiro Maru, Nobuyuki Kobayashi

85-93 **UVB-dependent generation of reactive oxygen species by catalase and IgG under UVB light: Inhibition by antioxidants and anti-inflammatory drugs.**

Masahiro Murakami, Masakazu Taniguchi, Masashi Takama, Jinghao Cui, Yoshihiko Oyanagui

94-107 **Formulation and hypoglycemic activity of pioglitazone-cyclodextrin inclusion complexes.**

Ahmed Abd Elbary, Mahfouz A. Kassem, Mona M. Abou Samra, Rawia M. Khalil

CONTENTS (*Continued*)

108-114 **Reconstituted powder for suspension of antitubercular drugs formulated as microspheres for pediatric use.**

Abdus Samad, Yasmin Sultana, Roop K. Khar, Mohd Aqil, Krishna Chuttani, Anil K. Mishra

115-121 **Synthesis and biological evaluation of substituted phenylpyrazole[4,5-*b*]oleanane derivatives as inhibitors of glycogen phosphorylase.**

Jun Chen, Yanchun Gong, Jun Liu, Luyong Zhang, Weiyi Hua, Hongbin Sun

122-127 **Using factorial design to improve the solubility and *in-vitro* dissolution of nimesulide hydrophilic polymer binary systems.**

Ibrahim S. Khattab, Saleh M. Al-Saidan, Aly H. Nada, Abdel-Azim A. Zaghloul

128-135 **Iontophoretic delivery of 5-fluorouracil through excised human stratum corneum.**

Brahma N. Singh, Shyam B. Jayaswal

Guide for Authors

Copyright

Drug Discov Ther 2008; 2(2):58-63.

Review

Roles of the Duffy antigen and glycophorin A in malaria infection and erythrocyte

Hiroshi Hamamoto[1], Nobuyoshi Akimitsu[2], Nagisa Arimitsu[3], Kazuhisa Sekimizu[1,]*

[1] *Laboratory of Microbiology, Graduate School of Pharmaceutical Sciences, The University of Tokyo, Bunkyo-ku, Tokyo, Japan;*
[2] *Radioisotope Center, The University of Tokyo, Bunkyo-ku, Tokyo, Japan*
[3] *School of Life Science, Tokyo University of Pharmacy and Life Science, Hachioji, Tokyo, Japan.*

ABSTRACT: We constructed gene knockout mice lacking either the Duffy antigen (*Dfy*) or glycophorin A (*GPA*), major glycoproteins that are expressed on erythrocyte membranes, to examine the role of these proteins in malaria infection and erythrocyte. All of the rodent malarias examined proliferated in the erythrocytes of these knockout mice, indicating that neither the Duffy antigen nor GPA has an essential role as a receptor for malaria parasites. Duffy antigen knockout mice infected by *Plasmodium yoelii* 17XL exhibited autotherapy. At the early stage of the infection, the parasite proliferated exponentially, whereas at the late stage, parasitemia decreased to a level at which the mice were considered cured. The results of depletion experiments with anti-CD4 antibodies suggested that CD4-positive cells in the Duffy antigen knockout mice were responsible for the autotherapy effect. The Duffy antigen is a chemokine receptor. Compared to wild-type mice, chemokines which have affinities for the Duffy antigen injected intravenously more rapidly disappeared from the Duffy antigen knockout mice. Stimulation of the immune response by the increase of leukocytes might lead to the suppression of parasitemia in the Duffy antigen knockout mice. The absence of GPA decreased the amount of *O*-linked oligosaccharides on the erythrocyte membranes. The erythrocyte membranes of the GPA knockout mice decreased several *O*-linked glycoproteins and TER-119 protein. GPA has an essential role in the expression of *O*-linked antigens on erythrocyte membranes, but these proteins are not important for malaria parasite invasion of erythrocytes.

Keywords: Duffy antigen, Glycophorin A, Malaria, Knockout mouse

**Correspondence to:* Dr. Kazuhisa Sekimizu, Laboratory of Microbiology, Graduate School of Pharmaceutical Sciences, The University of Tokyo, Bunkyo-ku, Tokyo 113-0033, Japan;
e-mail: sekimizu@mol.f.u-tokyo.ac.jp

Introduction

The initial step in the life cycle of malaria parasites in blood, is their invasion of the erythrocyte membranes (*1-3*). There have been several efforts to identify the malaria parasite receptors on the erythrocyte membranes (*4,5*). In humans, the Duffy antigen (*6-9*) and glycophorin A (GPA) (*10,11*) are thought to have roles as malaria receptors (*12*). In mice, however, little is known about the malaria receptors. To understand the roles of the Duffy antigen and GPA in malaria infection, we constructed mice with gene knockout mice lacking these proteins (*13,14*). In this review, we describe some characteristic features of the knockout mice to elucidate the physiologic functions of the Duffy antigen and glycophorin A proteins on erythrocyte and their roles on malarial infection.

Construction of gene knockout mice lacking either the Duffy antigen or glycophorin A

The gene encoding the Duffy antigen contains two exons (*15*). We deleted the chromosomal region of embryonic stem cells encoding the protein by homologous recombination followed by germ line transmission to construct the gene knockout mice (*13*). Inter-crossing of heterozygote mice resulted in the appearance of a homozygous deletion of the *Dfy* gene, according to Mendelian laws of inheritance (Table 1). The knockout mice appeared normal, and had no reproductive problems. These results demonstrated that the Duffy antigen is not essential for mouse development.

GPA contains a transmembrane domain (*16,17*). The *N*-terminal region of the protein is modified by *O*-linked oligosaccharides (*18,19*). To construct of gene knockout mice, we attempted to delete exons 4, 5, 6, and 7, which encode the transmembrane region of GPA (*14*). Inter-crossing of mice with a heterozygous deletion of the GPA gene resulted in he appearance of a homozygous deletion according to Mendelian law, indicating that

GPA is also not essential for mouse development (Table 1).

Growth of rodent malaria parasites in erythrocyte at the early stage of infection

Both the Duffy antigen knockout mice and the GPA knockout mice were susceptible to all types of rodent malaria examined; *Plasmodium berghei* NK65, *Plasmodium chabaudi*, *Plasmodium vinckei*, and *Plasmodium yoelii* 17XL. These results suggest that neither the Duffy antigen nor GPA do not function as receptors for these malarias (*20*). However, the Duffy antigen knockout mice infected with *Plasmodium yoelii* 17XL exhibited autotherapy (Figure 1). In wild-type mice, parasitemia increased to more than 80% within 5 days after infection, and the mice began to die. In the Duffy antigen knockout mice, parasitemia did not increase to more than 50%, and was maintained at a similar level for 2 weeks, then decreased to zero 3 weeks after infection.

Effect of the Duffy antigen on immunity

Because *Plasmodium yoelii* 17XL proliferated in the erythrocytes of Duffy antigen-knockout mice in the early stage of infection, we assumed that the autotherapy was due to an immunologic event in the host. The number of leukocytes in the blood of the Duffy antigen knockout mice increased twice as much as that in wild-type mice 5 days after infection (Figure 2A). The numbers of neutrophils, monocytes, and lymphocytes increased were much higher in Duffy antigen knockout mice than in wild-type mice, whereas the number of eosinophilic leukocytes was not different (Figure 2B).

Table 1. Genotype of glycophorin A and the Duffy antigen knockout mouse heterozygote intercrossed pups

Glycophorin A	genotype		
	+/+	+/–	–/–
Number of pups	18	37	22

Duffy antigen	genotype		
	+/+	+/–	–/–
Number of pups	106	201	77

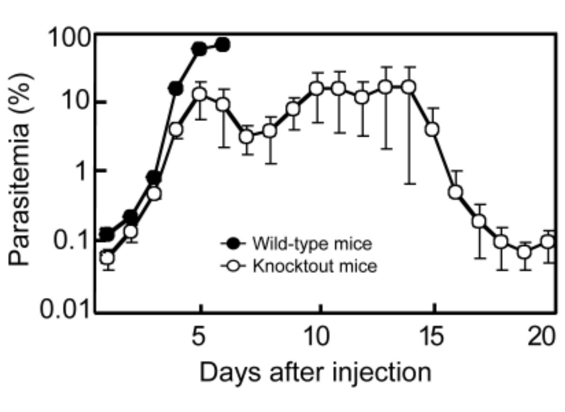

Figure 1. Resistance and invasion of *P. yoelii* 17XL infection in the Duffy antigen knockout mice. Mice were intravenously injected with erythrocyte suspension containing 105 erythrocytes parasitized with *P. yoelii* 17XL.

We then examined the types of leukocytes responsible for the autotherapy depletion experiments by using carrageenan and CD4 and CD8 antibodies. The decrease in parasitemia in the Duffy antigen knockout mice was not affected by carrageenan treatment, which depletes phagocytosis-active lymphocytes (Figure 3). When CD4-positive cells were depleted with antibodies against CD4, the decrease in parasitemia was blocked (Figure 4). When the mice were treated with anti-CD8 antibody to deplete CD8-positive cells, the decrease in parasitemia resumed. These results suggest that CD4-positive cells, but not CD8-positive cells or macrophages, were responsible for the autotherapy in the Duffy antigen knockout mice infected with *Plasmodium yoelii* 17XL.

A role for the Duffy antigen in maintaining the plasma concentration of chemokines

The Duffy antigen has affinities for various types of chemokines (*15,21,22*). The Duffy antigen selectively

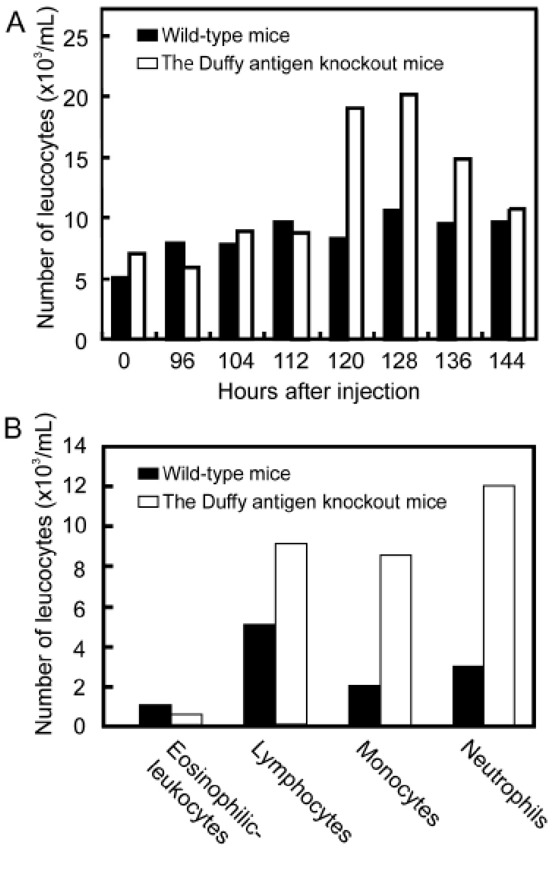

Figure 2. Increase of leukocytes in the Duffy antigen knockout mice 5 days after infection of *P. yoelii* 17XL. A: Blood was collected from mice at the indicated periods and stained with Turk's stain solution, and the number of leukocytes was counted with a hemocytometer. B: Tail blood smears were prepared 5 d after infection followed by staining with the Write-Giemsa method. Each type of leukocyte was determined based on the staining pattern and the number of leukocytes in the blood was calculated.

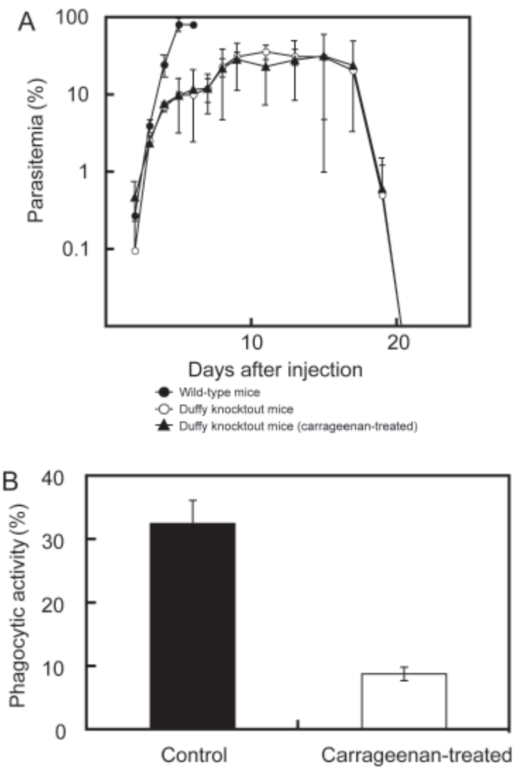

Figure 3. Effect of carrageenan on infection by *P. yoelii* 17XL in erythrocytes in the Duffy antigen knockout mice. A: Mice were intravenously injected with an erythrocyte suspension containing 105 erythrocytes parasitized with *P. yoelii* 17XL. Parasitemia was assessed by microscopic examination of Giemsa-stained smears of tail blood. B: Inhibition of phagocytotic activity of adherent spleen cells by carrageenan. Adherent spleen cells from carrageenan-treated or control mice were incubated with fluorescein isothiocyanate-conjugated beads at 37˚C for 30 min. Phagocytic activity was assayed by FACScan analysis with gating on a Mac-1 high population. Data are mean ± SD.

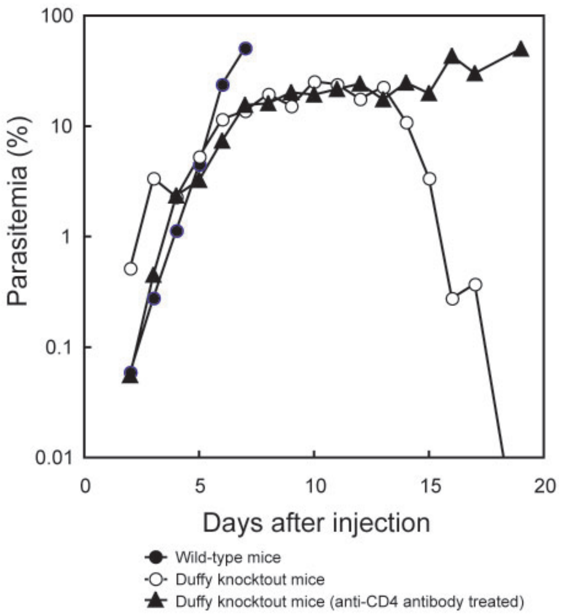

Figure 4. Effect of injection with anti-CD4 antibody or anti-CD8 antibody to the Duffy antigen knockout mice infected with *P. yoelii* 17XL. Mice were intravenously injected with an erythrocyte suspension containing 105 erythrocytes parasitized with *P. yoelii* 17XL. Parasitemia was assessed by microscopic examination of Giemsa-stained tail blood smears.

Table 2. Plasma concentrations of chemokines in wild-type and the Duffy antigen knockout mice

Chemokine	Genotype of the *Dfy* gene	
	+/+	–/–
Eotaxin (pg/mL)	4,200 ± 1,800	930 ± 30
MCP-1 (pg/mL)	110 ± 40	< 40

binds distinct members of the pro-inflammatory chemokines such as CXCL1, CXCL5, CCL2, CCL5, and CCL7, but not lymphoid chemokines such as CCL21, CCL19, CXCL12, and CXCL13 (*23*). The Duffy antigen is suggested to act as a chemokine "sink", thereby excluding plasma chemokines from being reutilized (*22,24*). We examined the plasma concentrations of eotaxin and MCP-1, which have affinities for the Duffy antigen. The plasma concentrations of these chemokines were much lower in Duffy antigen-knockout mice than in wild-type mice (Table 2). We also the examined clearance rate of these chemokines in both the Duffy antigen knockout mice and wild-type mice. In this experiment, we injected intravenously recombinant chemokines such as eotaxin, hMGSA, and MCP-1, which bind to the Duffy antigen, and hIP-10 and interferon-γ, which do not bind the Duffy antigen (*25-28*), then determined the plasma concentrations by enzyme-linked immunosorbent assay. The results indicated that concentration of eotaxin, hMGSA, and MCP-1 in blood were less stable in the plasma of the Duffy antigen knockout mice than in that of the wild-type mice (Figure 5) (*13,29*). A recent study also demonstrated rapidly vanishing of chemokines in the Duffy antigen knockout mice (*30*). We propose that the Duffy antigen acts as a "reservoir" to regulate plasma chemokine concentrations (*13*).

Therefore, a lack of the Duffy antigen should negatively affect the plasma concentrations of a set of chemokines. Interleukin-27 acts as a negative regulator of inflammatory T-cell responses against parasitic infections (*31*). Based on these findings, we propose a model to explain autotherapy in the Duffy antigen knockout mice infected with *P. yoelii* 17XL (Figure 6). At the initial infection, *P. yoelii* 17XL induces certain cytokines, which function to repress CD4-positive cell activity and whose plasma concentrations are maintained by the Duffy antigen. The plasma concentrations of these cytokines were lower in the Duffy antigen knockout mice than in wild-type mice; thus CD4-positive cell activity was enhanced and the autotherapeutic phenotype was observed.

Characterization of GPA knockout mice

GPA is a major glycoprotein on erythrocyte membranes. This protein contains *O*-linked oligosaccharides on the *N*-terminal regions locating in the external space of the erythrocytes. We extracted the oligosaccharides from erythrocyte membranes of the GPA knockout

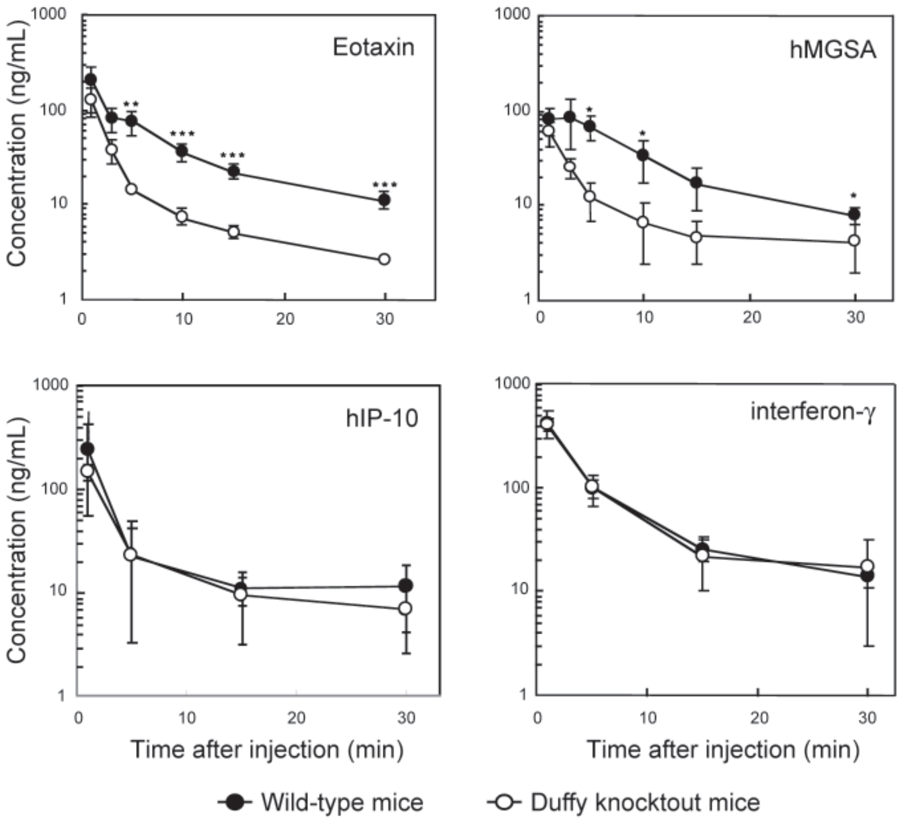

Figure 5. Clearance of eotaxin, hMGSA, hIP-10, and interferon-g from plasma. After intravenous injection of these chemokines and IFN-γ, blood samples were collected from tails using heparinized capillary tubes. Chemokines in the plasma concentration were determined by enzyme-linked immunosorbent assay. *** $P < 0.005$, ** $P < 0.02$, * $P < 0.05$, n = 3-5, mean ± SD.

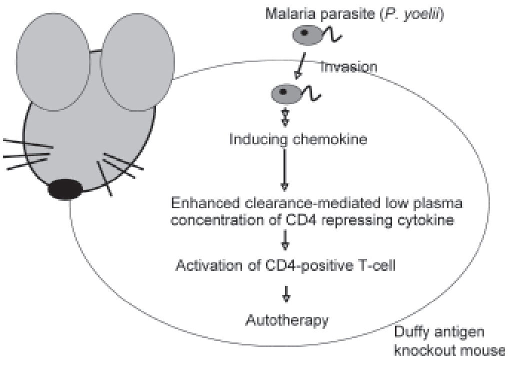
Malaria parasite (P. yoelii)
Invasion
Inducing chemokine
Enhanced clearance-mediated low plasma concentration of CD4 repressing cytokine
Activation of CD4-positive T-cell
Autotherapy
Duffy antigen knockout mouse

Figure 6. Scheme of autotherapy in the Duffy antigen knockout mice infected with *P. yoelii* 17XL.

Table 3. Comparison of monosaccharides amount on the erythrocyte membrane of wild-type and GPA knockout mouse

Monosaccharides	Amount of monosaccharides (nmol/mg protein)	
	WT	KO
Fucose	17 ± 4	17 ± 6
GalNAc	23 ± 3*	14 ± 3*
GlcNAc	97 ± 29	112 ± 34
Galactose	82 ± 22	75 ± 22
Mannose	68 ± 6	94 ± 38
NeuAc	182 ± 33	135 ± 22

(* $P < 0.01$)

mice, followed by acid-hydrolysis of the materials, and analysis by high performance liquid chromatography with an anion-exchange column. The amounts of all of three different species of oligosaccharide chains were decreased in the erythrocyte membranes of the GPA mice compared to the wild-type mice (Figure 7).

We then analyzed the monosaccharide composition of the oligosaccharides. Isolated oligosaccharides were further hydrolyzed, followed by analysis on high performance liquid chromatography. The amount of *N*-acetylgalactosamine (GalNAc) was decreased in the fraction from the GPA knockout mice (Table 3). Because GalNAc is a characteristic of *O*-linked sugars (*32*), the results suggest that the amount of *O*-linked sugars in the erythrocyte membrane was decreased in the GPA knockout mice.

TER-119 antigens are localized on the erythrocyte membrane in close relation to GPA (*33*). Therefore, we tested for the presence of TER-119 antigens on the erythrocyte membranes of the GPA knockout mice. Immunofluorescence staining using an antibody against TER-119 antigens demonstrated the presence of TER-119 antigens on the erythrocyte membranes of wild-type mice. TER-119 antigens were not present, however, in the erythrocyte membranes of GPA knockout mice (Figure 8A). Fluorescence-activated cell-sorting analysis using the antibody also revealed

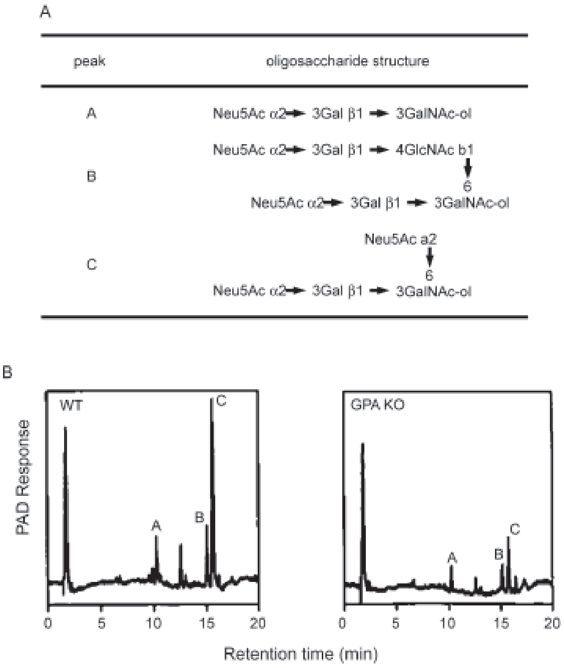

Figure 7. Decrease of *O*-glycans on the erythrocytes of GPA knockout mice. A: Schematics of *O*-glycans on the murine erythrocyte. B: Analysis of *O*-glycans by high-performance anion-exchange chromatography with pulsed amperometric detection.

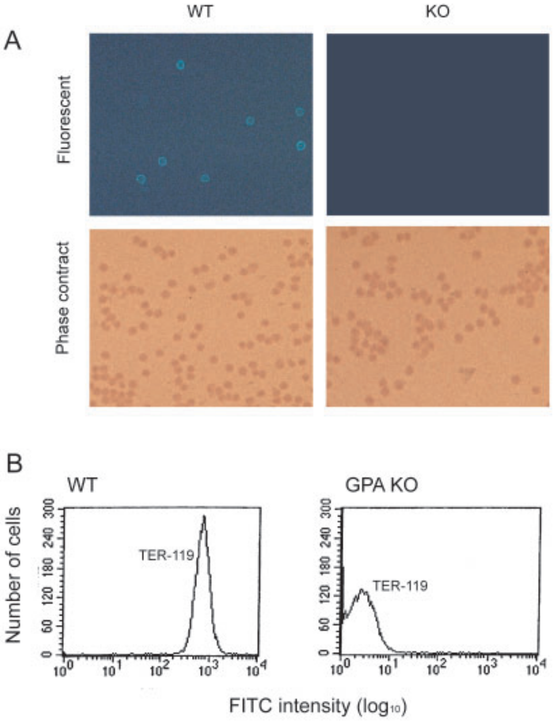

Figure 8. Disappearance of TER-119 antigens on the erythrocytes of GPA knockout mice. Blood cells isolated from wild-type and GPA knockout mice were stained with TER-119 antibody, followed by staining with fluorescein isothiocyanate-conjugated secondary antibody (A). Samples were analyzed by FACScan (B).

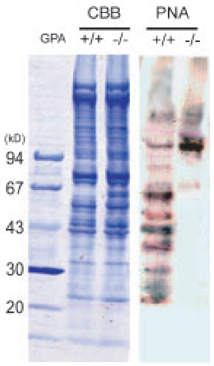

Figure 9. Lectin stain of GPA knockout mouse. Erythrocyte membranes prepared from wild-type and GPA knockout mice were fractionated by sodium dodecyl sulfate-polyacrylamide gel electrophoresis, After transferring, glycoproteins were detected using PNA.

the absence of TER-119-positive erythrocytes in the knockout mice (Figure 8B) (*14*). The absence of the TER-119 antigen on the erythrocyte membranes was further confirmed by Western blot analysis using the anti-TER-119 antibody. Two bands stained with the anti-TER-119 antigen in the sample from wild-type mice were not present in the sample from the GPA knockout mice (*14*). Because the TER-119 antigens are distinct from GPA, the results indicate that the amounts of proteins other than GPA were also decreased in the erythrocyte membranes of GPA knockout mice.

Peanut agglutinin is a lectin that has affinities for *O*-linked sugars (*34*). Western blot analysis probing with Peanut agglutinin demonstrated the lack of some glycoproteins with *O*-linked sugars in the erythrocyte membranes of GPA knockout mice (Figure 9). GPA seems to have an essential role in the expression of those glycoproteins with *O*-linked sugars onto the red blood cell surface. The results considering with the sugar analysis suggest that not only GPA, but also some of other glycoproteins with *O*-linked sugars are lost in the erythrocyte membrane of GPA knockout mice. Because the rodent malaria parasites initially proliferated in the GPA knockout mice, the present results suggest neither GPA nor glycoproteins with *O*-linked sugars have a role as receptors for rodent malarias.

In this review, we discussed about our research findings regarding the functions of two erythrocyte membrane proteins, GPA and the Duffy antigen, in malaria infection and in the physiology. We hope to further clarify the function of the erythrocyte membranes, which comprise 40% to 50% of the blood.

References

1 Oh SS, Chishti AH. Host receptors in malaria merozoite invasion. Curr Top Microbiol Immunol 2005; 295:203-232.

2 Cowman AF, Crabb BS. Invasion of red blood cells by malaria parasites. Cell 2006; 124:755-766.

3 O'Donnell RA, Blackman MJ. The role of malaria merozoite proteases in red blood cell invasion. Curr Opin Microbiol 2005; 8:422-427.

4 Gaur D, Mayer DC, Miller LH. Parasite ligand-host receptor interactions during invasion of erythrocytes by Plasmodium merozoites. Int J Parasitol 2004; 34:1413-1429.

5 Chitnis CE. Molecular insights into receptors used by

malaria parasites for erythrocyte invasion. Curr Opin Hematol 2001; 8:85-91.

6 Horuk R, Chitnis CE, Darbonne WC, Colby TJ, Rybicki A, Hadley TJ, Miller LH. A receptor for the malarial parasite Plasmodium vivax: the erythrocyte chemokine receptor. Science 1993; 261:1182-1184.

7 Haynes JD, Dalton JP, Klotz FW, McGinniss MH, Hadley TJ, Hudson DE, Miller LH. Receptor-like specificity of a *Plasmodium knowlesi* malarial protein that binds to Duffy antigen ligands on erythrocytes. J Exp Med 1988; 167:1873-1881.

8 Miller LH, Mason SJ, Dvorak JA, McGinniss MH, Rothman IK. Erythrocyte receptors for (*Plasmodium knowlesi*) malaria: Duffy blood group determinants. Science 1975; 189:561-563.

9 Swardson-Olver CJ, Dawson TC, Burnett RC, Peiper SC, Maeda N, Avery AC. *Plasmodium yoelii* uses the murine Duffy antigen receptor for chemokines as a receptor for normocyte invasion and an alternative receptor for reticulocyte invasion. Blood 2002; 99:2677-2684.

10 Pasvol G, Jungery M, Weatherall DJ, Parsons SF, Anstee DJ, Tanner MJ. Glycophorin as a possible receptor for *Plasmodium falciparum*. Lancet 1982; 2:947-950.

11 Sim BK, Chitnis CE, Wasniowska K, Hadley TJ, Miller LH. Receptor and ligand domains for invasion of erythrocytes by *Plasmodium falciparum*. Science 1994; 264:1941-1944.

12 Miller LH, Mason SJ, Clyde DF, McGinniss MH. The resistance factor to Plasmodium vivax in blacks. The Duffy-blood-group genotype, FyFy. N Engl J Med 1976; 295:302-304.

13 Fukuma N, Akimitsu N, Hamamoto H, Kusuhara H, Sugiyama Y, Sekimizu K. A role of the Duffy antigen for the maintenance of plasma chemokine concentrations. Biochem Biophys Res Commun 2003; 303:137-139.

14 Arimitsu N, Akimitsu N, Kotani N, Takasaki S, Kina T, Hamamoto H, Kamura K, Sekimizu K. Glycophorin A requirement for expression of *O*-linked antigens on the erythrocyte membrane. Genes Cells 2003; 8:769-777.

15 Luo H, Chaudhuri A, Johnson KR, Neote K, Zbrzezna V, He Y, Pogo AO. Cloning, characterization, and mapping of a murine promiscuous chemokine receptor gene: homolog of the human Duffy gene. Genome Res 1997; 7:932-941.

16 Matsui Y, Natori S, Obinata M. Isolation of the cDNA clone for mouse glycophorin, erythroid-specific membrane protein. Gene 1989; 77:325-332.

17 Challou N, Goormaghtigh E, Cabiaux V, Conrath K, Ruysschaert JM. Sequence and structure of the membrane-associated peptide of glycophorin A. Biochemistry 1994; 33:6902-6910.

18 Furthmayr H. Structural analysis of a membrane glycoprotein: glycophorin A. J Supramol Struct 1977; 7:121-134.

19 Marchesi VT, Tillack TW, Jackson RL, Segrest JP, Scott RE. Chemical characterization and surface orientation of the major glycoprotein of the human erythrocyte membrane. Proc Natl Acad Sci USA 1972; 69:1445-1449.

20 Akimitsu N, Kim HS, Hamamoto H, Kamura K, Fukuma N, Arimitsu N, Ono K, Wataya Y, Torii M, Sekimizu K. Duffy antigen is important for the lethal effect of the lethal strain of *Plasmodium yoelii* 17XL. Parasitol Res 2004; 93:499-503.

21 Chaudhuri A, Zbrzezna V, Polyakova J, Pogo AO, Hesselgesser J, Horuk R. Expression of the Duffy antigen in K562 cells. Evidence that it is the human erythrocyte chemokine receptor. J Biol Chem 1994; 269:7835-7838.

22 Dawson TC, Lentsch AB, Wang Z, Cowhig JE, Rot A, Maeda N, Peiper SC. Exaggerated response to endotoxin in mice lacking the Duffy antigen/receptor for chemokines (DARC). Blood 2000; 96:1681-1684.

23 Kashiwazaki M, Tanaka T, Kanda H, Ebisuno Y, Izawa D, Fukuma N, Akimitsu N, Sekimizu K, Monden M, Miyasaka M. A high endothelial venule-expressing promiscuous chemokine receptor DARC can bind inflammatory, but not lymphoid, chemokines and is dispensable for lymphocyte homing under physiological conditions. Int Immunol 2003; 15:1219-1227.

24 Darbonne WC, Rice GC, Mohler MA, Apple T, Hebert CA, Valente AJ, Baker JB. Red blood cells are a sink for interleukin 8, a leukocyte chemotaxin. J Clin Invest 1991; 88:1362-1369.

25 Neote K, Darbonne W, Ogez J, Horuk R, Schall TJ. Identification of a promiscuous inflammatory peptide receptor on the surface of red blood cells. J Biol Chem 1993; 268:12247-12249.

26 Hadley TJ, Peiper SC. From malaria to chemokine receptor: the emerging physiologic role of the Duffy blood group antigen. Blood 1997; 89:3077-3091.

27 Horuk R, Wang ZX, Peiper SC, Hesselgesser J. Identification and characterization of a promiscuous chemokine-binding protein in a human erythroleukemic cell line. J Biol Chem 1994; 269:17730-17733.

28 Bryan SA, Jose PJ, Topping JR, Wilhelm R, Soderberg C, Kertesz D, Barnes PJ, Williams TJ, Hansel TT, Sabroe I. Responses of leukocytes to chemokines in whole blood and their antagonism by novel CC-chemokine receptor 3 antagonists. Am J Respir Crit Care Med 2002; 165:1602-1609.

29 Jilma B, Akimitsu N, Fukuma N, Sekimizu K, Jilma-Stohlawetz P. Man, mouse and Duffy genotype-phenotype-specific pharmacokinetics of monocyte chemotactic protein-1. Transfus Med 2004; 14:251-252.

30 Rot A. Contribution of Duffy antigen to chemokine function. Cytokine Growth Factor Rev 2005; 16:687-694.

31 Hunter CA, Villarino A, Artis D, Scott P. The role of IL-27 in the development of T-cell responses during parasitic infections. Immunol Rev 2004; 202:106-114.

32 Hanisch FG. *O*-glycosylation of the mucin type. Biol Chem 2001; 382:143-149.

33 Kina T, Ikuta K, Takayama E, Wada K, Majumdar AS, Weissman IL, Katsura Y. The monoclonal antibody TER-119 recognizes a molecule associated with glycophorin A and specifically marks the late stages of murine erythroid lineage. Br J Haematol 2000; 109:280-287.

34 Bruneau N, Nganga A, Fisher EA, Lombardo D. *O*-Glycosylation of *C*-terminal tandem-repeated sequences regulates the secretion of rat pancreatic bile salt-dependent lipase. J Biol Chem 1997; 272:27353-27361.

(*Received April 26, 2008; Accepted April 29, 2008*)

Review

Dermal drug delivery: Revisited

Sateesh Khandavilli, Ramesh Panchagnula*

Department of Pharmaceutics, National Institute of Pharmaceutical Education and Research (NIPER), Sector 67, Mohali, Punjab 160062, India.

ABSTRACT: The unique histological and molecular organization of skin poses a formidable barrier to drug delivery into and across skin. Due to the severe restrictions on molecular transport, only potent and lipophilic drug candidates have been able to successfully enter the market. New drug discovery programs based on high-throughput screening and combinatorial chemistry have lead to synthesis of potent but highly lipophilic molecules, and yet these molecules are difficult to deliver by conventional routes of administration. (trans)dermal delivery offers an attractive route of administration for these lipophilic molecules. Further, the diverse opportunities offered by genomics and proteomics cannot be effectively utilized without an equally diverse delivery approach. Skin offers a convenient and effective route for those genes and proteins due to the presence of the stem cell compartment in the epidermis.

Keywords: Dermal, Localized delivery, Penetration, Body burden

The recent advances in formulation and drug discovery programs have brought an increased number of molecules within the purview of (trans)dermal delivery. This review critically analyzes the challenges and opportunities offered by (trans)dermal drug delivery for the delivery of lipophilic molecules and genes as well as polypeptides. It also addresses the issue of skin localization of drugs with respect to systemic delivery, where systemic escape of a drug is not desirable. Finally, a survey of clinical trials on psoriasis and melanoma therapy by localized administration of drugs is presented as an example of the recent enhanced interest in (trans)dermal delivery.

1. Skin: an efficient barrier

In order to physically protect an organism from the rigors of its environment and to maintain its water homeostasis, nature has molded skin into an excellent barrier with a unique histological and molecular organization (*1*). It is equally adept in limiting molecular transport both from and into the body. Overcoming this barrier, for the purpose of (trans)dermal drug delivery, has been a challenge for the pharmaceutical scientist (*2*). Various approaches such as chemical penetration enhancers (*3,4*), iontophoresis (*5,6*), electroporation (*7,8*), and sonophoresis (*9*) have been tried in order to overcome the skin barrier. Apart from these widely reported approaches, various novel formulation methodologies such as microspheres (*10,11*), nanoparticles (*12,13*), hydrogels (*14,15*), liposomes (*16-18*), and nanoemulsions (*19-21*) were also employed to enhance the transdermal or dermal delivery of drugs.

1.1. *Dermal delivery vis-à-vis oral delivery*

From the drug delivery point of view, skin differs from the gastro-intestinal tract (GIT) both structurally and functionally. It imposes a formidable challenge in the form of a very impermeable, lipophilic, and highly tortuous barrier, unlike GIT, which is much more permeable. Research has now established that the main barrier to cutaneous penetration lies in the outer most layer of skin, the stratum corneum (SC). The SC, consists of flat, hexagonal corneocytes which are tightly packed by intercellular cement consisting of primarily ceramides, and is approximately 0.3 μm thick (*22*). Immediately below the SC lies the viable dermis, followed by the dermis. The confluence of the lipidic epidermis and predominantly aqueous dermis makes the drug delivery of molecules at both extremes in terms of their lipophilicity index difficult. While the lipidic SC determines the rate of permeation of hydrophilic solutes, the dermis limits the transdermal transport of lipophilic molecules. Furthermore, immunogenicity of the organ, by virtue of its status as the first line of immunological defense, will limit the deliverability of proteins and peptides. On the other hand, skin also provides drug delivery scientists with distinctive opportunities. It is the only organ, apart from oral route, which has been found to provide zero-order delivery for up to a week (*2*). In addition, the skin has been widely explored

---

**Correspondence to:* Dr. Ramesh Panchagnula, Pharmaceutical R&D, VMPS, Pfizer Pharmaceutical India Pvt. Ltd., Thane Belapur Road, Turbhe, K.U. Bazar Post, Navi Mumbai 400705, India;
e-mail: Panchagnula@yahoo.com

for the delivery of potent molecules with high hepatic extraction due to its relatively subtle enzymatic activity. Moreover, formulation of delivery systems should be easier given the vast repertoire of excipients approved for topical or transdermal use. Quite uniquely, the existence of the stem cell compartment in the epidermis (*23,24*) has provided an exclusive opportunity for delivery of genes and anti-sense nucleotides. Further, lipophilic molecules that are otherwise potent but are orally non-deliverable due to poor aqueous solubility (anti-fungals, anti-psoriatics, anti-neoplastics, *etc*.) can be delivered to their site of action inside skin layers and thereby considerably reduce the systemic drug burden. Moreover, up to 95% of pathogens cross epithelial barriers, so attempts to manipulate specific immune responses at inductive sites (*25*) such as skin could lead to development of new vaccines against established and emerging diseases.

1.2. *Dermal delivery is as difficult as transdermal delivery*

Primary objective of transdermal delivery is to deliver a drug into systemic circulation while minimizing the local drug concentration in the skin. However, the objective of dermal delivery is to maximize the drug concentration in the desired skin layer with a minimal net drug transport across the skin into the blood, or in other words, to minimize 'systemic escape' of the drug. More often than not, in many pathological situations involving skin the target skin layer is not known and, furthermore, the target within the skin layer is seldom known (*26*). Therefore, contrary to general belief, the development of dermal products is more complex than that for transdermal products. Apart from the uncertainty in target location, the required local concentrations in the biophase at the tissue level is seldom known, mainly because required local drug concentrations can vary with the state of a disease. In the case of transdermal delivery, drug pharmacokinetics is modeled based on systemic drug concentrations by compartment or non-compartment-based modeling. In localized delivery, though, systemic drug pharmacokinetics are limited only to assessment of drug leakage from the target site. However, some recent attempts were made to model regional pharmacokinetics of drug absorption into various skin layers using multi-compartment models (*27-29*). Unlike the enhanced permeation and retention effect observed in tumors as facilitates local targeting, such phenomena do not prevail in the case of non-malignant diseases such as psoriasis. Bucks *et al.* have proposed that specific interaction with skin components may be required for long-term skin reservoir formation (*30*). Hence, the delivery technologies must mature far beyond their current level in order to enhance the local targeting of drugs to skin layers with greater reproducibility and reliability. Delivery is further complicated by the lack of knowledge on how a drug redistributes amongst different layers of skin and then into blood.

Contrary to accepted beliefs, blood supply to the dermis is not capable of resorbing certain drugs proportionate to their penetration through the epidermis. High lipophilicity, and molecular weight (MW), together with a slow rate of dissolution, or a rapid intake by dermatological tissues such as keratinocytes could be responsible for this preferential distribution of drug into these high-perfusion tissues. Due to this restricted systemic distribution of drugs applied dermally *via* systemic circulation (*27-29,31*), new avenues have opened up in the area of localized drug delivery *via* the skin. Therapeutically, localized dermal delivery can achieve two goals: delivery to superficial skin layers, *i.e.*, the SC and epidermis, and delivery to deeper layers such as the dermis, subcutaneous tissue, and finally into muscles directly beneath the area of application.

1.3. *Factors affecting molecular transport across skin*

Although the histological and molecular organization of skin is highly complex and heterogeneous, the transport of molecules across this barrier is surprisingly Fickian (*32*). The passive flux (J) of a drug across the skin is a function of diffusivity (D), its partition coefficient (K), and the concentration gradient (C/h) prevailing across the barrier with a diffusion path length (h) and is governed by equation 1.

$$J = DKC/h \text{ ----------- Equation 1}$$

Thus, the permeability of drugs can be enhanced by altering K, D and C of a drug with an appropriate choice of a solvent system, penetration enhancers, or by means of super saturation of a vehicle with the drug. According to lipid-protein-partitioning (LPP) theory (*33*), the penetration enhancers act by alteration of intercellular lipids or intracellular protein domains or by enhancing partitioning of a drug into the skin. Thus, permeation of drugs within the lipid bilayer can be enhanced by targeting the hydrophilic head groups or lipophilic fatty acyl chains of the lipid bilayer or by enhancing the partitioning of the drug into the aqueous space between the polar heads by the appropriate choice of a vehicle. At the current point in time, bilayer disruption by azone (*34,35*), terpenes (*36-39*), and fatty acids (*40-42*) has been reported to increase the flux of hydrophilic and lipophilic drugs of different MW varying from 200 to 500 Da. However, few studies reported using permeants with MWs above 500 Da and instead used chemical penetration enhancement such as insulin (*5,43,44*) and FITC-dextrans (*45,46*). As the MW exceeds 500 Da, the penetration characteristics of normal skin decrease significantly (*47*). According to free volume theory for molecular transport across a membrane (*48*), there exists an inverse relationship between the diffusion coefficient (D) and MW, and D of a molecule decreases exponentially with MW (Equation 2)

$$D = DO.\ EXP^{(-\beta.MW)} \text{ ----------- Equation 2}$$

where, DO → Diffusivity of molecule at zero molecular volume; β → Constant

Similar to other biological lipid membranes, in the SC diffusivity also decreases exponentially with increasing MW (*49*). Further, the skin permeation of molecules is also dependent on lipophilicity along with MW; based on these physicochemical properties, a model was proposed to predict the skin permeability of molecules (*50*).

1.4. *Penetration-permeation balance*

Many predictive approaches were tried to describe molecular transport across the skin (*27-29,50,51*) based on the various physicochemical properties of solutes, such as octanol-water partition coefficient (log P), MW, melting point, and concentration of unbound drug in the skin. Despite the variety of approaches employed, they shared an emphasis on the importance of lipophilicity and MW as the primary determinants of solute transport across skin.

A generally accepted precept is the larger the MW, the lesser drug permeation due to the slower diffusion coefficient. However, based on permeation data obtained from a series of alkanols, Behl *et al.* proposed that lipophilicity may play a larger role than MW (*26*). In the current authors' opinion, this trend may be valid for molecules less than 500 Da, upon which the analysis by Behl *et al.* was based. At higher MWs, which factor plays a predominant role is unclear since an increase in carbon chain length leads to both MW and lipophilicity enhancement. Thus, interaction between these two factors and their individual as well as cumulative influence on skin penetration and permeation has to be explored. This will help to better understand the influence of physico-chemical properties of molecules on dermal-transdermal delivery. Apart from this, the manner in which vehicles influence transdermal delivery differs from the way they affect local delivery to the skin. The vehicle can move into skin layers and alter skin integrity as well as the microenvironment, thus affecting drug uptake dramatically without significantly influencing transdermal permeation. Under these circumstances, studying the efficacy of vehicles and penetration enhancers on drug penetration and localization into skin using conventional transdermal permeation experiments is problematic since drug permeation into the receptor phase does not guarantee drug localization and *vice versa*.

Although several studies have dealt with the influence of penetration enhancers on transdermal delivery, few have actually focused on dermatological drug localization in skin. In the case of dermal penetration enhancers, a desirable trait would be to promote penetration, and thus drug localization, while decreasing drug permeation. Chemical substances that break the SC barrier may enhance both events simultaneously while those enhancers that act purely by enhancing the partitioning of the drug into the SC subsequent to the alteration of the microenvironment may help in maximizing penetration and form a depot of the drug.

In transdermal delivery literature, the terms "penetration" and "permeation" are often used interchangeably. However, these are two distinct events, essentially separated at the level of the main barrier to molecular transport, the SC. "Penetration" specifically describes the entry of molecules into the SC, and "permeation" describes the mass transfer from the SC across different layers of skin into the systemic circulation. However, since these events overlap during permeation studies, they may not be quantified separately, but dermal and transdermal delivery can be delineated by the penetration/permeation balance, which in turn is a complex function of the MW and the lipophilicity of a drug and is further influenced by the extent of enhancement provided by a formulation strategy (Figure 1). If a drug is hydrophilic (log P < 1) and its MW < 500 Da, it can be made to penetrate into skin using a penetration enhancer, as in the case of zidovudine (*52*), but its localization *in vivo* is difficult due to the hydrophilic environment existing after the dermo-epidermal junction. In contrast, a lipophilic molecule with a lower MW, such as naloxone, can easily be made to penetrate as well as permeate, thus enabling transdermal delivery (*53,54*). However, a permeation retardant or depot former such as propylene glycol is needed for retention in the skin (*55*). In contrast, a hydrophilic molecule with a high MW, such as insulin, can be made to penetrate with a high degree of penetration enhancement (*5,43,44*) but is very difficult to localize inside the skin. Similarly, a lipophilic molecule with a high MW, such as paclitaxel (PCL), can be made to penetrate using formulation strategies (*3*); due to its high lipophilicity, it would not require any permeation retardant for its localization, and therapeutically effective concentrations could be built up in the biophase (*56*).

Rapid advances in drug discovery with the advent of combinatorial chemistry and receptor-based drug design, enabled by high-throughput screening methodologies and further accelerated by genomics and proteomics, have lead to discovery of millions of molecules that have been pharmacodynamically optimized. However, drug optimization is not complete

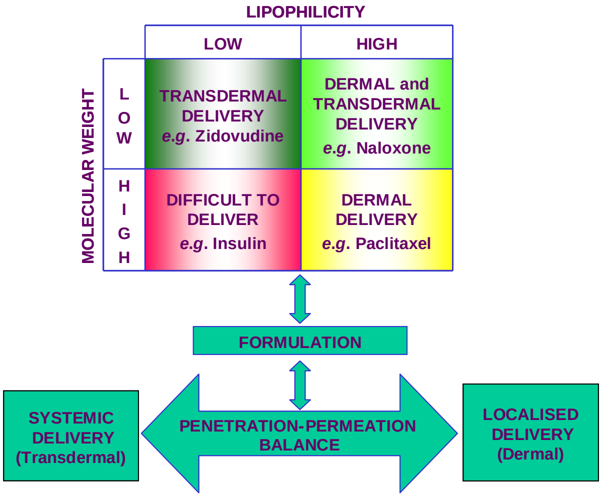
LIPOPHILICITY
LOW
HIGH
MOLECULAR WEIGHT
LOW
HIGH
TRANSDERMAL DELIVERY e.g. Zidovudine
DERMAL and TRANSDERMAL DELIVERY e.g. Naloxone
DIFFICULT TO DELIVER e.g. Insulin
DERMAL DELIVERY e.g. Paclitaxel
FORMULATION
SYSTEMIC DELIVERY (Transdermal)
PENETRATION-PERMEATION BALANCE
LOCALISED DELIVERY (Dermal)

Figure 1. Schematic representation of penetration-permeation balance and its correlation with physicochemical properties. Dermal and transdermal delivery can be delineated by the penetration/permeation balance, which in turn is a complex function of lipophilicity and MW. A small hydrophilic molecule like zidovudine can be made to penetrate the skin easily using penetration enhancers, and from there it quickly permeates to produce systemic levels due to its small MW and the aqueous environment in deeper skin layers. A small lipophilic molecule like naloxone can be made to localize in skin using a skin depot former like propylene glycol or systemic therapeutic concentrations can be effected using oleic acid as a permeation enhancer. However, delivery of a hydrophilic macromolecule such as insulin would be difficult since it has trouble penetrating the lipophilic SC despite enhancement by iontophoresis and/or penetration enhancers. Further, a lipophilic drug with a high molecular weight such as paclitaxel can penetrate into deeper skin layers and form a depot through use of a proper formulation strategy.

without drug development essentially consisting of biopharmaceutic and pharmacokinetic optimization. Although this later aspect was initially neglected, biopharmaceutic and pharmacokinetic optimization has assumed renewed importance with the review of the causes of the failure of preclinical candidates indicating their poor biopharmaceutic properties (*57*). Further, choice of delivery system is as important as the drug itself, since even the best biopharmaceutically optimized drug cannot deliver itself (*58*); hence, it has to be developed with its delivery characteristics incorporating excipients in mind, ultimately yielding a dosage form that is administrable. This has ultimately led to the evolution of BCS for peroral drug candidates. Such a unified classification is warranted for other routes of delivery but is rather difficult if not impossible, primarily due to the difference in the role of physicochemical properties influencing each route. Another problem with modern drug discovery technologies is their inherent bias towards more lipophilic, and thus orally difficult-to-deliver, molecules, necessitating the search for non-peroral drug delivery strategies. The cutaneous route is correctly positioned to provide unique opportunities for delivery of class II and IV drugs and genes and localized delivery of dermatopharmaceuticals.

2. Dermal delivery of genes and antisense nucleotides (ANs)

Although genomics have opened up many avenues for therapeutic intervention, the full potential of these therapies cannot be realized until an understanding of the choice of vector and delivery strategies has matured (*59*). There is currently no practical method, either viral or non-viral, available to allow safe and efficient delivery in most clinical situations. Broad applicability of gene therapy will invariably require diversity in formulation and routes of administration. Although the oral route of delivery has been explored (*60,61*), significant success has yet to be achieved. Skin, by virtue of its ready accessibility and non-invasiveness, is an obvious target for both systemic and local delivery. Advances in delivery methods are increasing the feasibility of this delivery route (*62*). Dermal formulations can modulate gene expression within the skin, an application that would be useful for the inhibition of viral genes in skin lesions or inhibition of genes associated with ongoing pathology in the skin. Further, transdermal delivery for systemic administration can provide reliable sustained release, reduced enzymatic and first-pass metabolism, and improved patient compliance. Moreover, skin is the anatomical site where most exogenous antigens are encountered first, so *in vivo* transfection of epidermal or dermal cells by DNA would be expected to provide an efficient route to gene immunization that mimics a physiological response to an infection (*63*).

ANs mainly permeate through intra-appendageal route through hair follicles. Approximately 0.5% of the applied dose of a 22-25-base oligomer was observed to be delivered to the hair bulbs and deeper strata (*64*). Keratinocytes are particularly sensitive to ANs and provide an excellent target for dermal administration. These cells can internalize ANs very rapidly in 30-60 min after exposure (*65*), and uptake of these molecules proceeds without cell surface accumulation or endosomal sequestration (*66*). Internalization of ANs is dependent upon molecular size and sequence (*67*). Furthermore, uptake is also influenced by concentration, exposure time, and temperature (*68*). Once a drug passes through viable epidermis, it reaches the vascular and lymphatic systems for potential systemic availability. However, this systemic escape is preceded by keratinocyte internalization, and an inverse relation between transdermal permeation of phosphorothioate ANs and internalization by keratinocytes has been observed. This presents the possibility that ANs may be designed to treat skin diseases with little systemic availability, and conversely that ANs may also be designed for systemic treatment with little local interaction in the skin. Vlassov *et al.* were the first to report the transdermal permeation of ANs (*69*), in which they described systemic availability of a ^{32}P-labelled oligonucleotide following application of a lotion of AN to mouse ear helices. Further, they reported the iontophoretic delivery of oligonucleotides and noted accumulation of intact AN in mouse tumors (*70*). Other physical enhancement strategies like electroporation (*71*), gold micro projectiles (*72*), gene guns (*73*), and microprojection patches (*74*) have also been explored to deliver genes into the skin.

Gillardon *et al*. reported a complete blockade of *c-fos* gene expression in a UV-irradiated rat upon topical application of an AN to *c-fos* to tape-stripped skin and further suggested its applicability to intact skin (*75*). The ability of an AN to TGF-β1 to control the healing of incisional wounds in mice was tested by applying an AN to the site, and the AN was observed to decrease scarring (*76*). A chimeric AN (TYR-A) designed to correct a point mutation in the tyrosinase gene was able to restore melanin synthesis by topical and intradermal administrations for at least 3 months after application (*77*). Topical delivery of a cream consisting of AN to intercellular adhesion molecule-1 (ICAM-1) effectively inhibited 66% mRNA synthesis in the skin of human skin-transplanted immunodeficient mice. Upon topical administration, local concentrations were 3 times as high in the epidermis and 2 times as high in the dermis than with intravenous (*i.v.*) administration. AN metabolism was also considerably lower upon topical administration (*78*). However, few studies have been performed to study the *in vivo* efficacy of chemical enhancement as a means to achieve transdermal delivery. Brand *et al*. have reported a modified backbone AN transdermal delivery in rats using propylene glycol and linoleic acid as enhancers (*79*). Zhang *et al*. reported the application of pressure-mediated electroporation to deliver a *LacZ* reporter gene *in vivo* into hairless mouse skin, and gene expression was observed up to a depth of 370 μm (*80*).

3. Dermal delivery of class II and IV drugs

Dermal delivery is an attractive option for the molecules of classes II and IV of the Biopharmaceutic Classification System (BCS) as they are otherwise very difficult to deliver orally (Figure 1). By virtue of their high lipophilicity, they will readily partition into and permeate through skin, rendering themselves deliverable by this route. Delivery across and into skin would be the more natural route for drugs that are intended to act in the skin, such as anti-psoriatics, anti-fungals, anti-neoplastics, anti-leishmanials, and antibiotics. This would give the delivery strategy an element of passive targeting together with a reduction in non-target organ toxicity (Figure 2).

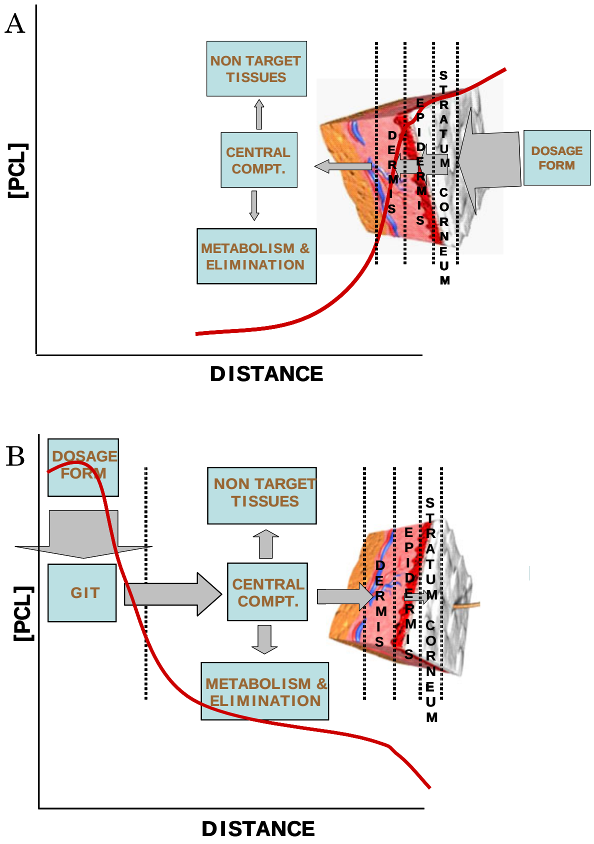

Figure 2. An illustration of the regional pharmacokinetic advantage offered by (A) Localized (Dermal) delivery over (B) Systemic (Oral) delivery for a lipophilic drug. The thickness of arrows schematically represents the local concentrations of drug. When a drug with a therapeutic target lying in skin layers is given by the systemic route (situation B), the local concentrations decrease exponentially (assuming passive diffusion with first-order kinetics) as the drug crosses each barrier. Under these circumstances, final concentrations achievable at the target will be a small fraction of the dose administered. Such severe pharmacokinetic limitations lead to the failure of drugs that are proven to be effective against the disease in pharmacological screening. Alternatively, if the same drug is administered locally (situation A), much higher concentrations are achievable at the biophase, while considerably reducing the non-target organ concentration. The regional pharmacokinetic advantage of dermal delivery of dermatopharmaceuticals is shown here as an illustration and is not drawn to scale.

Methotrexate, which is normally given systemically by *i.v.* or orally, has been developed for topical application for the treatment of psoriasis. Alvarez-Figueroa *et al*. reported on the topical delivery of methotrexate by both iontophoresis and passive delivery using microemulsions (*21,81*). Enhanced transdermal delivery of methotrexate was also reported using penetration enhancers (*82*). PCL, an effective antineoplastic agent given by *i.v.*, is being explored for use in psoriasis therapy *via* dermal application (*3,56,83*). 5-fluorouracil *via* dermal application has been used to treat epidermal dysplasia (*84*) and pre-malignant actinic keratoses (*85*). Topical therapy using paromomycin ointment was reported to be effective against cutaneous leishmaniasis without any local or systemic side effects (*86*). Amphotericin B, an antibiotic with several systemic side effects, was delivered effectively to the skin in order to treat cutaneous leishmaniasis. Vardy *et al*. reported the effectiveness of a lipidic formulation of amphotericin B for cutaneous leishmaniasis in a prospective placebo-controlled clinical study (*87*). Topical and transdermal delivery of cyclosporin is being explored as a therapy for various inflammatory skin diseases such as psoriasis, atopic dermatitis, and diseases of hair follicles like alopecia areata (*88,89*). Tacrolimus, a cyclosporine-like inhibitor of T-cell activation, is currently available for the treatment of atopic dermatitis (*90*). Steroids and non-steroidal anti-inflammatory drugs (NSAIDs) by far comprise the largest group of topical medications. The dermal delivery of triamcinolone acetonide was found to improve upon administration as transfersomes in comparison to its gel formulations (*91*). NSAIDS such as diclofenac (*92,93*), piroxicam (*94*), ketoprofen (*95*), and flurbiprofen (*96*) are actively being studied for use in *in vivo* dermal delivery.

4. Dermal delivery systems in clinical trials

The past few years have witnessed a dramatic increase in therapies aimed at the treatment of many dermatological disorders, with special emphasis on psoriasis and melanoma. Unlike previous approaches that were mainly symptomatic, recent therapies have essentially focused on the cause of the disease.

4.1. *Psoriasis*

Psoriasis is a chronic, hyperproliferative, inflammatory disease of the skin that affects 1-3% of the world's population. The annual cost of psoriasis outpatient care in the US is estimated to be between US$1.6 billion and US$3.2 billion (*www.angiotech.com* accessed on 23.08.2005). A comprehensive survey of various treatments for psoriasis and psoriatic arthritis in the development stage or late development stage (updated until May 2005) can be found at *http://www.psoriasis.org/research/pipeline/*.

Since the disease's pathogenesis involves a complex series of molecular events, various molecular targets are being targeted to treat psoriasis. The delivery approaches are mainly concentrating on localized dermal delivery in comparison to oral and other systemic routes.

Vitamin D analogs were found to be efficacious in the treatment of psoriasis, but their therapy is limited by the development of hypocalcaemia. Becocalcidiol, a vitamin D analog without this adverse effect, has recently completed phase IIB clinical trials for the topical treatment of mild to moderate psoriasis (*www.quatrx.com*). Ligands of nuclear hormone receptors such as glucocorticoids, retinoids, and vitamin D are useful antipsoriatic drugs. Peroxisome proliferator-activated receptors (PPARs), which also belong to the nuclear hormone receptor super family, were also reported to be effective *in vitro* against psoriasis. However, a pilot *in vivo* study found their efficacy to be inadequate (*97*). The marketed PPAR-γ agonist rosiglitazone was found not to be efficacious against psoriasis in phase III clinical trials (*http://science.gsk.com/pipeline/index.htm*). A novel class of drugs called Retinoic Acid Metabolism Blocking Agents (RAMBA) uses the body's own endogenous retinoic acid to provide a therapeutic effect against ichthyosis, psoriasis, and acne. RAMBAs have been shown to be safer than retinoids. Rambazole, a second generation RAMBA, has completed early Phase II testing in topical clinical studies (*http://khandekar.com* accessed on 22.08.2005). Stimulation of epidermal keratinocytes by insulin-like growth factor I (IGF-I) is essential for cell division, and increased sensitivity to IGF-I occurs in psoriasis. A second-generation antisense drug (ATL1101) was designed by Antisense Therapeutics to silence or suppress the gene for the insulin-like growth factor-I receptor (IGF-Ir). IGF-Ir's pivotal role in the regulation of cell over-growth in psoriasis was previously established (*98-100*). ATL1101 is being developed by Antisense Therapeutics as a cream for treatment of mild-to-moderate cases of psoriasis. In a novel extension to its established activity as antineoplastic, paclitaxel is being developed as an anti-psoriatic by Angiotech Pharmaceuticals (*www.angiotech.com*). The topical gel has completed phase I clinical trials for mild to moderate psoriasis. Micellar paclitaxel for treatment of rheumatoid arthritis and severe psoriasis is in phase II clinical trials. Selectins are the cell surface proteins involved in the recruitment of leucocytes during inflammation. A new topical formulation of the small molecule pan-selectin antagonist bimosiamose was recently found to be effective in the treatment of psoriasis during a phase IIa clinical trial (*101*). Tacrolimus and pimecrolimus, immunosuppressant calcineurin inhibitors, are approved in the US for the treatment of atopic dermatitis by topical application and are in a phase IIIb clinical trial for the treatment of inverse psoriasis (*www.novartisclinicaltrials.com*).

4.2. *Melanoma*

Melanoma is a skin cancer involving melanocytes. According to the Melanoma Research Foundation (*www.melanoma.org*), this is the fastest growing cancer in the US and worldwide, with its incidence increasing at the rate of 3% every year. Various innovative approaches are being explored for the treatment of melanoma including gene therapy, immunological intervention using vaccines, and molecular targeting-based therapies.

Appreciative of the skin's function as a barrier, many clinical trials involving macromolecules such as vaccines oligonucleotides, genes, and large proteins have been performed using either an intradermal or subcutaneous route. Vaccine-based preparations were mainly prepared as emulsions in montanide ISA-51 (mannide oleate), which itself can act as an immuno adjuvant. However, delivery approaches must still mature in order to harness the full therapeutic potential of these novel molecules.

Recently, the National Cancer Institute (NCI) started a phase II clinical trial on vaccine therapy using melanoma peptides for cytotoxic T cells and helper T cells by a dermal/subcutaneous route. In another phase I/II clinical trial, the multiple synthetic melanoma peptide sargramostim is being evaluated for stage III/IV melanoma involving the eye. The biological response modifier imiquimod is also being tried in a phase I clinical trial as an adjuvant to enhance the response of transdermal vaccines consisting of multi-epitope melanoma peptides. Subcutaneous Interferon-β is in a phase II clinical trial for the treatment of metastatic cutaneous melanoma or ocular melanoma.

5. Conclusion

Despite the toughness and complexity of the skin barrier, (trans)dermal delivery remains an innovative and successful route of drug administration. Recent developments in drug discovery technologies coupled with high-throughput screening have lead to discovery of highly lipophilic and poorly permeating drugs. Further, biopharmaceuticals arising from genomics and proteomics research may not be amenable to oral delivery due to the abundance of enzymes in GIT. Due to the poor peroral bioavailability of such poorly soluble and permeating molecules and given the unique advantages offered by skin with respect to localized delivery, this route has received renewed attention. With the likelihood of an imminent increase in biopharmaceuticals and vaccines, (trans)dermal delivery has come into its own.

References

1. Blank IH. Cutaneous barriers. J Invest Dermatol 1965; 45:249-256.
2. Naik A, Kalia YN, Guy RH. Transdermal drug delivery: overcoming the skin's barrier function. PSTT 2000; 3:318-326.
3. Panchagnula R, Desu H, Jain A, Khandavilli S. Effect of lipid bilayer alteration on transdermal delivery of high molecular weight and lipophilic drug: studies with paclitaxel. J Pharm Sci 2004; 93:2177-2183.
4. Narishetty STK, Panchagnula R. Transdermal delivery of zidovudine: effect of terpenes and their mechanism of action. J Control Release 2004; 95:367-379.
5. Pillai O, Panchagnula R. Transdermal delivery of insulin from poloxamer gel: *ex vivo* and *in vivo* skin permeation studies in rat using iontophoresis and chemical enhancers. J Control Release 2003; 89:127-140.
6. Nair VB, Panchagnula R. Effect of iontophoresis and fatty acids on permeation of arginine vasopressin through rat skin. Pharmacol Res 2003; 47:563-569.
7. Prausnitz MR. The effects of electric current applied to skin: A review for transdermal drug delivery. Adv Drug Del Rev 1996; 18:395-425.
8. Prausnitz MR, Lee CS, Liu CH, Pang JC, Tej Preet S, Langer R, Weaver JC. Transdermal transport efficiency during skin electroporation and iontophoresis. J Control Release 1996; 38:205-217.
9. Mitragotri S, Farrell J, Tang H, Terahara T, Kost J, Langer R. Determination of threshold energy dose for ultrasound-induced transdermal drug transport. J Control Release 2000; 63:41-52.
10. Perugini P, Genta I, Pavanetto F, Conti B, Scalia S, Baruffini A. Study on glycolic acid delivery by liposomes and microspheres. Int J Pharm 2000; 196:51-61.
11. Giandalia G, De Caro V, Cordone L, Giannola LI. Trehalose-hydroxyethylcellulose microspheres containing vancomycin for topical drug delivery. Eur J Pharm Biopharm 2001; 52:83-89.
12. Lippacher A, Muller RH, Mader K. Preparation of semisolid drug carriers for topical application based on solid lipid nanoparticles. Int J Pharm 2001; 214:9-12.
13. Langer K, Mutschler E, Lambrecht G, Mayer D, Troschau G, Stieneker F, Kreuter J. Methylmethacrylate sulfopropylmethacrylate copolymer nanoparticles for drug delivery: Part III: Evaluation as drug delivery system for ophthalmic applications. Int J Pharm 1997; 158:219-231.
14. Walters KA, Brain KR, Green DM, James VJ, Watkinson AC, Sands RH. Comparison of the transdermal delivery of estradiol from two gel formulations. Maturitas 1998; 29:189-195.
15. Sateesh K Sharma P, Panchagnula R. Stability, biophysical, and *in vivo* toxicity evaluation of a novel naloxone transdermal gel formulation. Fifth International Symposium on Advances in Technology and Business Potential of New Drug Delivery Systems. Mumbai, India, 2004.
16. Touitou E, Levi Schaffer F, Dayan N, Alhaique F, Riccieri F. Modulation of caffeine skin delivery by carrier design: liposomes versus permeation enhancers. Int J Pharm 1994; 103:131-136.
17. Hwang BY, Jung BH, Chung SJ, Lee MH, Shim CK. *In vitro* skin permeation of nicotine from proliposomes. J Control Release 1997; 49:177-184.
18. Dayan N, Touitou E. Carriers for skin delivery of trihexyphenidyl HCl: Ethosomes *vs*. liposomes. Biomaterials 2000; 21:1879-1885.
19. Wu H, Ramachandran C, Weiner ND, Roessler BJ. Topical transport of hydrophilic compounds using water-in-oil nanoemulsions. Int J Pharm 2001; 220:63-75.
20. Rhee YS, Choi JG, Park ES, Chi SC. Transdermal delivery of ketoprofen using microemulsions. Int J Pharm 2001; 228:161-170.
21. Alvarez-Figueroa MJ, Delgado-Charro MB, Blanco-Méndez J. Transdermal delivery of methotrexate: iontophoretic delivery from hydrogels and passive delivery from microemulsions. Int J Pharm 2001; 215:57-65.
22. Asbill CS, Michniak BB. Percutaneous penetration enhancers: local versus transdermal activity. PSTT 2000; 3:36-41.
23. Lako M, Armstrong L, Cairns PM, Harris S, Hole N, Jahoda CAB. Hair follicle dermal cells repopulate the mouse haematopoietic system. J Cell Sci 2002; 115:3967-3974.
24. Frye M, Gardner C, Li ER, Arnold I, Watt FM. Evidence that Myc activation depletes the epidermal stem cell compartment by modulating adhesive interactions with the local microenvironment. Development 2003; 130:2793-2808.
25. Brayden DJ, Jepson MA, Baird AW. Intestinal peyers patch M cells and oral vaccine targeting. Drug Discov Today 2005; 10:1145-1157.
26. Behl C, Char H, Patel S, Mehta D, Piemontere D, Malick

A. *In vivo* and *in vitro* skin uptake and permeation studies: critical considerations and factors which affect them. In: Topical Drug Bioavailability, Bioequivalence, and Penetration (Shah VP, Maibach HI, eds.) Plenum Press, New York, 1993; pp. 225-259.

27. Higaki K, Asai M, Suyama T, Nakayama K, Ogiwara K, Kimura T. Estimation of intradermal disposition kinetics of drugs: II. Factors determining penetration of drugs from viable skin to muscular layer. Int J Pharm 2002; 239:129-141.
28. Nakayama K, Matsuura H, Asai M, Ogawara K, Higaki K, Kimura T. Estimation of intradermal disposition kinetics of drugs: I. Analysis by compartmental model with contralateral tissues. Pharm Res 2002; 16:302-308.
29. Singh P, Roberts M. Local deep tissue penetration of compounds after dermal application: Structure-tissue penetration relationships. J Pharmacol Exp Ther 1996; 279:908-917.
30. Bucks D, McMaster J, Maibach HI, Guy RH. Prolonged residence of topically applied chemicals in the stratum corneum. J Pharm Sci 1987; 76:S125.
31. Guy RH, Maibach HI. Drug delivery to local subcutaneous structures following topical administration. J Pharm Sci 1983; 72:1375-1380.
32. Kalia Y, Guy RH. Modeling transdermal drug release. Adv Drug Del Rev 2001; 48:159-172.
33. Barry BW. Lipid-protein-partition theory of skin penetration enhancement. J Control Release 1991; 15:237-248.
34. Ito Y, Ogiso T, Iwaki M. Thermodynamic study on enhancement of percutaneous penetration of drugs by Azone. J Pharmacobiodyn 1988; 11:749-757.
35. Afouna M, Fincher T, Zaghloul A, Reddy I. Effect of Azone upon the *in vivo* antiviral efficacy of cidofovir or acyclovir topical formulations in treatment/prevention of cutaneous HSV-1 infections and its correlation with skin target site free drug concentration in hairless mice. Int J Pharm 2003; 253:159-168.
36. Yamane MA, Williams AC, Barry BW. Terpene penetration enhancers in propylene glycol/water co-solvent systems: effectiveness and mechanism of action. J Pharm Pharmacol 1995; 47:978-989.
37. Moghimi HR, Williams AC, Barry BW. A lamellar matrix model for stratum corneum intercellular lipids. V. Effects of terpene penetration enhancers on the structure and thermal behaviour of the matrix. Int J Pharm 1997; 146:41-54.
38. Cornwell PA, Barry BW. The routes of penetration of ions and 5-fluorouracil across human skin and the mechanism of action of terpene skin penetration enhancers. Int J Pharm 1993; 94:189-194.
39. Jain AK, Thomas NS, Panchagnula R. Transdermal drug delivery of imipramine hydrochloride: I. Effect of terpenes. J Control Release 2002; 79:93-101.
40. Tanojo H, Boelsma E, Junginger HE, Ponec M, Bodde HE. *In vivo* human skin barrier modulation by topical application of fatty acids. Skin Pharmacol Appl Skin Physiol 1998; 11:87-97.
41. Santoyo S, Ygartua P. Effect of skin pretreatment with fatty acids on percutaneous absorption and skin retention of piroxicam after its topical application. Eur J Pharm Biopharm 2000; 50:245-250.
42. Aungst BJ, Rogers NJ, Shefter E. Enhancement of naloxone penetration through human skin *in vitro* using fatty acids, fatty alcohols, surfactants, sulfoxides and amides. Int J Pharm 1986; 33:225-234.
43. Pillai O, Borkute SD, Sivaprasad N, Panchagnula R. Transdermal iontophoresis of insulin: II. Physicochemical considerations. Int J Pharm 2003; 254:271-280.
44. Pillai O, Panchagnula R. Transdermal iontophoresis of insulin: V. Effect of terpenes. J Control Release 2003; 88:287-296.
45. Ogiso T, Paku T, Iwaki M, Tanino T. Mechanism of the enhancement effect of *n*-octyl-beta-*D*-thioglucoside on the transdermal penetration of fluorescein isothiocyanate-labeled dextrans and the molecular weight dependence of water-soluble penetrants through stripped skin. J Pharm Sci 1994; 83:1676-1681.
46. Ogiso T, Paku T, Iwaki M, Tanino T. Percutaneous penetration of fluorescein isothiocyanate-dextrans and the mechanism for enhancement effect of enhancers on the intercellular penetration. Biol Pharm Bull 1995; 18:1566-1571.
47. Bos JD, Meinardi MMHM. The 500 Dalton rule for the skin penetration of chemical compounds and drugs. Exp Dermatol 2000; 9:165-169.
48. Cohen MH, Turnbull D. Molecular transport in liquids and gases. J Chem Phys 1959; 31:1164-1169.
49. Kasting GB, Smith RL, Cooper ER. Effect of lipid solubility and molecular size on percutaneous absorption. In: Skin Pharmacokinetics (Shroot B, Schaefer H, eds.) Karger, Basel, 1987; pp. 138-153.
50. Potts RO, Guy RH. Predicting skin permeability. Pharm Res 1992; 9:663-669.
51. Magnusson B, Anissimov Y, Cross S, Roberts M. Molecular size as the main determinant of solute maximum flux across the skin. J Invest Dermatol 2004; 122:993-999.
52. Thomas NS, Panchagnula R. Transdermal delivery of zidovudine: effect of vehicles on permeation across rat skin and their mechanism of action. Eur J Pharm Sci 2003; 18:71-79.
53. Panchagnula R, Khandavilli S. *In vitro* and *in vivo* evaluation of gel formulation for the transdermal delivery of naloxone. Pharm Ind 2004; 66:228-233.
54. Panchagnula R, Bokalial R, Sharma P, Khandavilli S. Transdermal delivery of naloxone: skin permeation, pharmacokinetic, irritancy and stability studies. Int J Pharm 2005; 293:213-223.
55. Jaiswal J, Poduri R, Panchagnula R. Transdermal delivery of naloxone: *ex vivo* permeation studies. Int J Pharm 1999; 179:129-134.
56. Kandavilli S, Panchagnula R. Trans(Dermal) delivery of high molecular weight and lipophilic drug Paclitaxel: Influence of lipidic vehicles and penetration enhancers. American Association for Pharmaceutical Scientists (AAPS) Conference. Baltimore, USA, 2004.
57. Prentis R, Lis Y, Walker S. Pharmaceutical innovation by the seven UK-owned pharmaceutical companies (1964-1985). Br J Clin Pharmacol 1988; 25:387-396.
58. Davis S, Illum L. Drug delivery systems for challenging molecules. Int J Pharm 1998; 176:1-8.
59. Anderson W. Human gene therapy. Nature 1998; 392:25-30.
60. Agrawal S, Zhang X, Lu Z, Zhao H, Tamburin JM, Yan J, Cai H, Diasia RB. Absorption,tissue distribution and *in vivo* stability in rats of a hybrid antisense oligonucleotide following oral administration. Biochem Pharmacol 2005; 50:571-576.
61. Beck GR, Irwin WJ, Nicklin PL, Akhtar S. Interactions

of phosphodiester and phosphothiolate oligonucleotides with intestinal epithelial Caco-2 cells. Pharm Res 2005; 13:1028-1037.
62. Luo D, Saltzman WM. Synthetic DNA delivery systems. Nat Biotechnol 2000; 18:33-37.
63. Raz E, Carson DA, Parker SE, Parr TB, Abai AM. Intradermal gene immunization: The possible role of DNA uptake in the induction of cellular immunity to viruses. Proc Natl Acad Sci USA 1994; 91:9519-9523.
64. Lieb LM, Liimatta AP, Bryan RN, Brown BD, Krueger GG. Description of the intrafollicular delivery of large molecular weight molecules to follicles of human scalp skin *in vitro*. J Pharm Sci 1997; 86:1022-1029.
65. Nestle F O, Mitra RS, Bennett CF, Chan H, Nickoloff BJ. Cationic lipid is not required for uptake and selective inhibitory activity of ICAM-1 phosphorothiolate antisense oligonucleotides in keratinocytes. J Invest Dermatol 1994; 103:569-575.
66. Noonberg SB, Garovoy MR, Hunt CA. Characteristics of oligonucleotide uptake in human keratinocyte cultures. J Invest Dermatol 1993; 101:727-731.
67. Brand RM, Haase K, Hannah TL, Iversen PL. An experimental model for interpreting percutaneous penetration of oligonucleotides that incorporates the role of keratinocytes. J Invest Dermatol 1998; 111:1166-1171.
68. Wigens M, vanHooijdonk CA, deJongh DJ, Schalkwijk J, vanErp PE. Flowcytometric and microscopic characterization of the uptake and distribution of phosphorothiolate oligonucleotides in human keratinocytes. Arch Dematol Res 1998; 290:119-125.
69. Vlassov VV, Karamyshev VN, Yakubov LA. Penetration of oligonucleotides into mouse organism through mucosa and skin. FEBS Lett 1993; 327:271-274.
70. Vlassov VV, Nechaeva MV, Karamyshev VN, Yakubov LA. Iontophoetic delivery of oligonucleotide derivatives into mouse tumour. Antisense Res Dev 1994; 4:291-293.
71. Zevert TE, Pliquett UF, Langer R, Weaver JC. Transdermal transport of DNA antisense oligonucleotides by electroporation. Biochem Biophys Res Commun 1995; 212:286-292.
72. Tang DC, DeVit M, Johnston SA. Genetic immunization is a simple method for eliciting an immune response. Nature 1992; 356:152-154.
73. Fynan EF, Webster RG, Fuller DH, Haynes JR, Santoro JC, Robinson HL. DNA vaccines: protective immunizations by parenteral, mucosal, and gene-gun inoculations. Proc Natl Acad Sci USA 1993; 90:11478-11482.
74. Lin W, Cormier M, Samiee A, Griffin A, Johnson B, Teng CL, Hardee GE, Daddona PE. Transdermal delivery of antisense oligonucleotides with microprojection patch (Macroflux) technology. Pharm Res 2001; 18:1789-1793.
75. Gillardon F, Mill I, Uhlmann E. Inhibition of *c-fos* expression in the UV-irradiated epidermis by topical application of antisense oligodeoxynucleotides suppresses activation of proliferating cell nuclear antigen. Carcinogenesis 1995; 16:1853-1856.
76. Choi BM, Kwak HJ, Jun CD, Park SD, Kim KY. Control of scarring in adult wounds using antisense transforming growth factor-B1 oligodeoxynucleotides. Immunol Cell Biol 1996; 174:144-150.
77. Alexeev VIO, Domashenko A, Cotsarelis G, Yoon K. Localized *in vivo* genotypic and phenotypic correction of the albino mutation in skin by RNA-DNA oligonucleotide. Nat Biotechnol 2000; 18:43-47.
78. Mehta RC, Stecker KK, Cooper SR, Templin MV, Tsai YJ. Intercellular adhesion molecule-1 suppression in skin by topical delivery of antisense oligonucleotides. J Invest Dermatol 2000; 115:805-812.
79. Brand RM, Hannah TL, Norris J, Iversen PL. Transdermal delivery of antisense oligonucleotides can induce changes in gene expression *in vivo*. Antisense Nucleic Acid Drug Dev 2001; 11:1-6.
80. Zhang L, Li L. An Z, Hoffman RM, Hofmann GA. *In vivo* transdermal delivery of large molecules by pressure-mediated electroincorporation and electroporation: a novel method for drug and gene delivery. Bioelectrochem Bioenerg 1997; 42:283-292.
81. Alvarez-Figueroa MJ, Delgado-Charro MB, Blanco-Méndez J. Passive and iontophoretic transdermal penetration of methotrexate. Int J Pharm 2001; 212:101-107.
82. Matsuyama K, Nakashima M, Nakaboh Y, Ichikawa M, Yano T, Satoh S. Application of *in vivo* microdialysis to transdermal absorption of methotrexate in rats. Pharm Res 1994; 11:684-686.
83. Panchagnula R, Desu H, Jain A, Khandavilli S. Feasibility studies of dermal delivery of paclitaxelwith binary combinations of ethanol and isopropyl myristate: role of solubility, partitioning and lipid bilayer perturbation. IL Farmaco 2005; 59:839-842.
84. Simeonova M, Velichkova R, Ivanova G, Enchev V, Abrahams I. Poly(butylcyanoacrylate) nanoparticles for topical delivery of 5-fluorouracil. Int J Pharm 2003; 263:133-140.
85. Pearlman DL. Weekly pulse dosing: effective and comfortable 5-fluorouracil treatment of multiple facial actinic keratoses. J Am Acad Dermatol 1991; 25:665-667.
86. Stanimirovic A, Stipic T, Skerlev M, Basta Juzbas A. Treatment of cutaneous leishmaniasis with 20% paromomycin ointment. J Eur Acad Dermatol Venereol 1999; 13:214-217.
87. Vardy D, Barenholz Y, Naftoliev N, Klaus S, Gilead L, Frankenburq S. Efficacious topical treatment for human cutaneous leishmaniasis with ethanolic lipid amphotericin B. Trans Royal Soc Trop Med Hygiene 2001; 95:184-186.
88. Wang S, Kara M, Krishnan TR. Transdermal delivery of cyclosporin-A using electroporation. J Control Release 1998; 50:61-70.
89. Verma DD, Fahr A. Synergistic penetration enhancement effect of ethanol and phospholipids on the topical delivery of cyclosporin A. J Control Release 2004; 97:55-66.
90. Russel JJ. Topical tacrolimus: A new therapy for atopic dermatitis. Am Fam Physician 2002; 66:1899-1902.
91. Cevc G, Blume G. Biological activity and characteristics of triamcinolone-acetonide formulated with the self-regulating drug carriers, Transfersomes. Biochim Biophys Acta 2003; 1614:156-164.
92. Cevc G, Blume G. New, highly efficient formulation of diclofenac for the topical, transdermal administration in ultradeformable drug carriers, Transfersomes. Biochim Biophys Acta - Biomembranes 2001; 1514:191-205.
93. Escribano E, Calpena AC, Queralt J, Obach R, Doménech J. Assessment of diclofenac permeation with different formulations: anti-inflammatory study of a selected formula. Eur J Pharm Sci 2003; 19:203-210.
94. Curdy C, Kalia YN, Naik A, Guy RH. Piroxicam

delivery into human stratum corneum *in vivo*: iontophoresis versus passive diffusion. J Control Release 2001; 76:73-79.

95. Paolino D, Ventura CA, Nisticò S, Puglisi G, Fresta M. Lecithin microemulsions for the topical administration of ketoprofen: percutaneous adsorption through human skin and *in vivo* human skin tolerability. Int J Pharm 2002; 244:21-31.
96. Sugibayashi K, Yanagimoto G, Hayashi T, Seki T, Juni K, Morimoto Y. Analysis of skin disposition of flurbiprofen after topical application in hairless rats. J Control Release 1999; 62:193-200.
97. Stéphane Kuenzli, Jean Hilaire Saurat. Effect of topical PPARb/d and PPARg agonists on plaque psoriasis: A pilot study. Dermatology 2003; 206:252-256.
98. Wraight CJ, White PJ, McKean SC, Fogarty RD, Venables DJ, Liepe IJ, Edmondson SR, Werther GA. Reversal of epidermal hyperproliferation in psoriasis by insulin-like growth factor I receptor antisense oligonucleotides. Nat Biotechnol 2000; 18:521-526.
99. Hodak E, Gottlieb AB, Anzilotti M, Krueger JG. The insulin-like growth factor 1 receptor is expressed by epithelial cells with proliferative potential in human epidermis and skin appendages: correlation of increased expression with epidermal hyperplasia. J Invest Dermatol 1996; 106:564-570.
100. White PJ, Fogarty RD, Werther GA, Wraight CJ. Antisense inhibition of IGF receptor expression in HaCaT keratinocytes: a model for antisense strategies in keratinocytes. Antisense Nucleic Acid Drug Dev 2000; 10:195-203.
101. M Friedrich, K Vollhardt, R Zahlten, W Sterry, G Wolff. Demonstration of antipsoriatic efficacy of a new topical formulation of the small molecule selectin antagonist bimosiamose. European Congress on Psoriasis 2004. Paris, France, 2004.

(*Received March 8, 2008; Revised March 27, 2008; Accepted April 7, 2008*)

Brief Report

On the temperature dependence of the unbound drug fraction in plasma: Ultrafiltration method may considerably underestimate the true value for highly bound drugs

Leonid M. Berezhkovskiy

Genetech Inc., 1 DNA Way, South San Francisco, CA 94080, USA.

ABSTRACT: The value of the unbound drug fraction in plasma is a common characteristic required for drug discovery and development. The communication considers an important possibility that the unbound drug fraction at physiological temperature (37˚C) could be substantially greater (more than 5 times) than the value measured by traditionally set ultrafiltration method with the incubation of drug plasma solution at 37˚C followed by the centrifugation at room temperature. The consideration is based on the general thermodynamic theory of chemical equilibrium, which is applied to the particular problem of determination of protein binding by ultrafiltration method.

Keywords**:** Protein binding, Unbound drug fraction, Equilibrium dissociation constant, Ultrafiltration, Pharmacokinetics, Thermodynamics

---

Introduction

Binding of drugs to plasma proteins is an important feature affecting their pharmacodynamic and pharmacokinetic properties. Generally the free drug fraction is available for diffusion and transport across cell membranes to reach the activity site. The ultrafiltration and equilibrium dialysis are the methods traditionally used for determination of protein binding, which are based on the separation of free drug from bound one at equilibrium (*1*). The nonspecific adsorption of drugs (especially lipophylic ones) to the separation membrane and a relatively long and uncertain time of reaching equilibrium for the equilibrium dialysis are the major inconveniences in using these methods. In equilibrium dialysis method the initial total drug concentration in plasma decreases during the dialysis, so that there is no control on what would be the drug concentration at which protein binding is measured. This creates a complexity when binding is nonlinear and requires additional computational adjustments (*2*).

A quite short equilibration time and also the ability to measure protein binding at a given drug concentration are the advantages of the commonly used ultrafiltration method. Ultrafiltration method does not have control over temperature and provides the value of protein binding at room temperature because of a very quick temperature adjustment of equilibrium. For a typical value of the on-rate binding constant (*3*) $k_{on} \gtrsim 3.5\times10^4\ M^{-1}\ s^{-1}$ and albumin concentration P_o = 670 μM, the time scale of reaching equilibrium is about $\tau \sim (k_{on}P_o + k_{off})^{-1} \lesssim 4.2\times10^{-2}$ s (the off-rate constant k_{off} was taken as zero in this estimation). A more accurate calculation of τ requires knowing the k_{off}, which strongly depends on the binding energy and can be estimated (*4*). For the binding energy of 10 kcal/mole $k_{off} \sim 4\times10^4\ s^{-1}$, which makes the time scale of reaching equilibrium extremely short $\tau \lesssim 10^{-4}$ s. If incubation is done at 37˚C, and after that plasma is transferred to ultrafiltration device at room temperature for centrifugation, then the temperature of plasma would drop to room temperature with consequent instant adjustment of drug-protein binding equilibrium. Thus after centrifugation we would be measuring the free drug concentration, which corresponds to the equilibrium at room temperature. Only if all procedures were performed at 37˚C until plasma ultrafiltrate containing the free drug fraction is separated, then we would be able to measure the protein binding at controlled temperature. Thus to obtain the value of protein binding at physiological conditions actually requires doing not only the incubation, but also plasma transfer to ultrafiltration device and subsequent centrifugation in a 37˚C room.

Though the influence of the temperature on protein binding is known, the analysis of the dependence of

---

**Correspondence to:* Dr. Leonid M. Berezhkovskiy, Genetech Inc., 1 DNA Way, South San Francisco, CA 94080, USA;
e-mail: berezhkovskiy.leo@gene.com

possible error in determination of the unbound drug fraction on temperature variation and the strength of protein binding was not reported in literature. The goal of this communication is to show that temperature dependence of protein binding (decrease of fraction bound at 37˚C compared the value measured at room temperature) might be quite significant and should be taken into account, especially for the highly bound drugs. This is considered in detail in the next section.

Determination of the temperature dependence of the unbound drug fraction

Generally there are several binding sites on each type of plasma protein (commonly albumin and α_1 - acid glycoprotein) involved in drug binding. The equilibrium binding to each binding site i of a single type of protein

$$R + P_i \rightleftharpoons Ci$$

is characterized by the affinity K_i (equilibrium dissociation constant), so that according to the mass action law

$$K_i = R{*}P_i/C_i \tag{1}$$

where R is the equilibrium concentrations of the unbound drug, P_i and C_i are respectively the concentrations of free and occupied i-th binding site. The mass balance equation for a drug and each binding sites can be written as $R_o = R + \Sigma C_i$, $P_o = P_i + C_i$, where R_o is the total drug concentration in plasma, and P_o is the plasma concentration of the protein. The unbound drug fraction is defined as $f_u = R/R_o$. Using Eq. 1 and the mass balance relation, we get

$$f_u = R/(R + \Sigma C_i) = 1/(1 + \Sigma P_i/K_i) \tag{2}$$

The concentration of free i-th binding site $P_i = P_o – C_i > P_o – R_o$ because $C_i < R_o$. The protein binding experiment is commonly performed at drug concentration much less than that of a protein, $R_o << P_o$. The unbound protein concentration P_i can then be assumed equal to P_o, so that Eq. 2 yields the minimum value of the unbound drug fraction, f_u^o, which corresponds to $R_o \rightarrow 0$

$$f_u^o = 1/(1 + k) \tag{3}$$

where $k = P_o \Sigma 1/K_i$. For a drug, which binds to several types of proteins in plasma, similarly as done above (*5*), we would obtain $f_u^o = 1/(1 + k_p)$, where k_p is equal to the sum of the parameters k, which characterize drug affinities of individual proteins.

Let us estimate the influence of temperature on the value of the unbound drug fraction. The traditional ultrafiltration method, when the separation of the unbound drug fraction is commonly performed at room temperature, yields the value of drug protein binding at t = 20˚C. The unbound drug fraction at body temperature (t = 37˚C) is actually pertinent to drug development. To estimate f_u^o (37˚C) from the known value of f_u^o (20˚C) let us assume that all n binding sites of the protein have the same affinity, *i.e.* $K_i = K_d$ in Eq. 1, so that the unbound drug fraction calculated by Eq. 3 is then equal to

$$f_u^o = 1/(1 + nP_o/K_d). \tag{4}$$

The temperature dependence of the equilibrium constant (at constant ambient pressure) is given by the Vant Hoff equation (*6*)

$$d(\ln K_d)/dT = \Delta H^o/(RT^2) \tag{5}$$

where ΔH^o is the enthalpy change of the reaction for each binding site ($\Delta H^o > 0$ for dissociation), R = 1.98 cal/(mole∗°K) is the gas constant and T = t + 273.15 is the absolute temperature. Integrating Eq. 5, using a common assumption that ΔH^o is constant in the narrow temperature interval between 20˚C and 37˚C, yields

$$K_d(37˚C) = K_d(20˚C){*}\exp[\Delta H^o(T_2 – T_1)/(RT_1T_2)] \tag{6}$$

where T_1 = 20 + 273.15 = 293.15 °K and T_2 = 37 + 273.15 = 310.15 °K. The unbound drug fraction at 37˚C is calculated as

$$f_u^o(37˚C) = 1/[1 + nP_o/K_d(37˚C)] \tag{7}$$

Substituting K_d(37˚C) from Eq. 6 in Eq. 7 and taking into account Eq. 4 written for f_u^o(20˚C), we obtain the equation for the calculation of the unbound drug fraction at 37˚C from the known value at 20˚C

$$f_u^o(37˚C) = 1/\{1 + (1/f_u(20˚C) – 1){*}\exp[\Delta H^o (T_1 – T_2)/(RT_1T_2)]\} \tag{8}$$

or the bound fraction $f_b^o = 1 – f_u^o$

$$f_b^o(37˚C) = 1/\{1 + (1/f_b(20˚C) –1){*}\exp[\Delta H^o (T_2 – T_1)/(RT_1T_2)]\} \tag{9}$$

Eq. 8 readily allows to estimate the temperature change of f_u^o using the values of f_u^o (20˚C) and ΔH^o. The decrease of f_u^o with temperature change from 20˚C to 37˚C strongly depends on the enthalpy change of the reaction. This is shown in Figure 1. Typically the value of ΔH^o ranges from 4 to 18 kcal/mole (*7*), though it could be as large as 30 kcal/mole (*8*). The largest relative increase of f_u^o (37˚C)/f_u^o (20˚C) occurs for highly bound drugs, $f_b^o \rightarrow 1$. For instance for a drug with f_u^o (20˚C) = 0.01 (99% protein binding) and ΔH^o = 12 kcal/mole (which corresponds to the two strong hydrogen bonds) the unbound drug fraction at 37˚C would be f_u^o (37˚C)

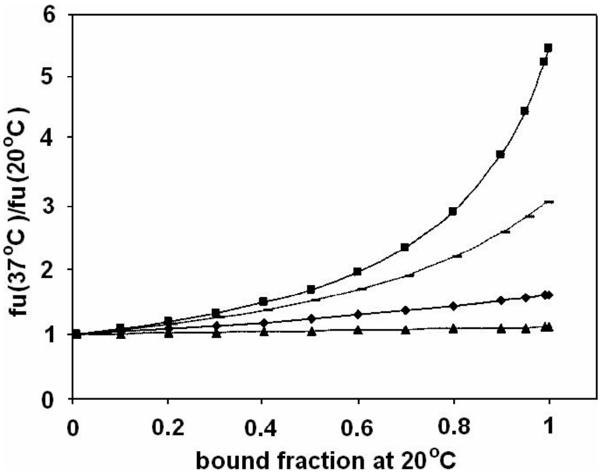

Figure 1. Temperature dependence of the unbound drug fraction. The relative increase of the unbound drug fraction, f_u^o(37˚C)/f_u^o (20˚C), with temperature change from 20˚C to 37˚C as a function of the enthalpy change of drug - protein complex dissociation reaction (Eq. 8): ▲, ΔH^o = 1 kcal/mole; ◆, ΔH^o = 5 kcal/mole; ▬, ΔH^o = 12 kcal/mole; ■, ΔH^o = 18 kcal/mole.

= 0.03. This is a 3-fold increase of the unbound drug fraction. If the enthalpy change for the drug binding reaction were ΔH^o = 18 kcal/mole, we would get more than a 5-fold increase of the unbound drug fraction at 37˚C (94.8 % protein binding). On the other hand for a drug with f_u^o = 0.03 (97% protein binding) at room temperature and ΔH^o = 1 kcal/mole there is relatively small change in protein binding at 37˚C, f_u^o (37˚C) = 0.033. It is most likely to have the greater value of ΔH^o for the highly bound drug compared to that with low protein binding. Thus for highly bound drugs it is more likely to expect a considerable temperature decrease of f_u^o at 37˚C compared to the value measured at 20˚C.

Conclusion

The rejection of drug candidates for a particular project when a relatively high value of the unbound drug fraction is desirable, based exclusively on the high level of protein binding obtained by regularly set ultra filtration method (*i.e.* plasma incubation at 37˚C and subsequent centrifugation at room temperature), might result in missing of potentially active compounds. The actual protein binding at physiological conditions could be substantially lower than that obtained by regularly set ultrafiltration method (which eventually yields the value of protein binding at room temperature). Ultrafiltration method requires control over temperature to obtain protein binding at physiological conditions – thus the method should be performed at 37˚C until plasma ultrafiltrate, which contains the free drug fraction, is separated.

References

1. Kwon I. Handbook of Essential Pharmacokinetics, Pharmacodynamics and Drug Metabolism for Industrial Scientists. Kluwer Academic/Plenum Publishers: New-York, 2001, and references therein.
2. Boudinot FD, Jusko WJ. Fluid shifts and other factors affecting plasma protein binding of prednisolone by equilibrium dialysis. J Pharm Sci 1984; 73:774-780.
3. Freedman FB, Johnson A. Equilibrium and kinetic properties of the Evan blue-albumin system. Am J Physiol 1969; 216:675-681.
4. Berezhkovskiy LM. Determination of volume of distribution at steady state with complete consideration of the kinetics of protein and tissue binding in linear pharmacokinetics. J Pharm Sci 2004; 93:364-374.
5. Berezhkovskiy LM. On the concentration dependence of drug binding to plasma proteins with multiple binding sites of different affinities: determination of the possible variation of the unbound drug fraction and the number of binding sites of the protein. J Pharm Sci 2004; 93:364-374.
6. Levine I. Physical Chemistry. McGrow-Hill: New-York, 1978.
7. Aki H, Yamamoto M. Thermodynamic characterization of drug binding to human serum albumin by isothermal titration microcalorimetry. J Pharm Sci 1994; 83:1712-1716.
8. Chen W, Chang CE, Gilson MK. Calculation of cyclodextrin binding affinities: energy, entropy, and implications for drug design. Biophys J 2004; 87:3035-3049.

(*Received March 22, 2008; Revised April 10, 2008; Accepted April 16, 2008*)

Original Article

Hsc70 regulates the nuclear export but not the import of influenza viral RNP: A possible target for the development of anti-influenza virus drugs

Ken Watanabe[1], Naoki Takizawa[1], Saiko Noda[1], Fujiko Tsukahara[2], Yoshiro Maru[2], Nobuyuki Kobayashi[1, 3,]*

[1] *Laboratory of Molecular Biology of Infectious Agents, Graduate School of Biomedical Sciences, Nagasaki University, Nagasaki, Japan;*
[2] *Department of Pharmacology, Tokyo Women's Medical University, School of Medicine, Tokyo, Japan;*
[3] *Central Research Center, AVSS Corporation, Nagasaki, Japan.*

ABSTRACT: In our previous report, we demonstrated that the matrix 1 (M1) protein of influenza virus directly binds to heat shock cognate protein 70 (Hsc70). The down-regulation of Hsc70 resulted in the reduction of influenza virus production, thus suggesting that Hsc70 plays a crucial role for viral replication. However, the detailed role of Hsc70 in viral replication remains to be elucidated. Hsc70 has been suggested to play a significant role in both the nuclear import and export processes. In this report, using leptomycin B (LMB), a CRM1-mediated nuclear export inhibitor, we demonstrated that Hsc70 forms a complex with vRNP through M1 in infected cells and in the virion, thus playing a significant role in the export of vRNP from the nucleus but not in the import of vRNP into the nucleus. The regulation of Hsc70 may therefore lead to the development of new anti-influenza virus drugs without raising mutant viruses.

Keywords: Influenza virus, Heat shock protein, Hsc70, Nuclear export signal, Leptomycin B

Introduction

The type A influenza virus genome has eight segmented single-stranded RNAs in negative polarity. Its genome in the virion exists as a vRNP complex with RNA-dependent RNA polymerase (RdRp) and nucleocapsid protein (NP). The vRNP is surrounded by matrix protein 1 (M1), which is also associated with the lipid bilayer. After the adsorption of the virion to the host cell, the incoming vRNPs are imported into the nucleus where early transcription of the influenza virus occurs. The early gene products, three subunits of RdRp (PB1, PB2, and PA), and NP are synthesized immediately after infection and then are subsequently transported to the nucleus where they form new vRNPs. These newly formed vRNPs are used as a template for late transcription. The gene products, such as hemagglutinin (HA), neuraminidase (NA), M1, M2, and NS2, are synthesized at the late stage of infection. These proteins are essential for the formation of mature virus particles in the cytoplasm and plasma membrane (for a review, see *Ref. 1*).

M1 has been suggested to play an important role in the nuclear export of vRNPs (*2,3*). Using leptomycinB (LMB), an inhibitor of CRM1-dependent nuclear export, we previously found the export of vRNP to be efficiently inhibited (*4*), although M1, NP and RdRp do not have a nuclear export signal (NES). Recently, we identified heat shock cognate protein 70 (Hsc70) as a host factor which bind to M1 protein in infected cells and our results suggest that Hsc70 directly interacts with M1 (*5*). However, its detailed role still remains unclear.

Heat shock proteins (Hsps) are induced by various types of stimulation, such as heat treatments, chemicals, UV, and viral infection, as a cellular defense mechanism. For example, prostaglandins induce the expression of Hsps (Hsp70, Hsc70) and inhibit the replication of a variety of RNA viruses, including paramyxoviruses, rhabdoviruses, rotaviruses, retroviruses and influenza virus (for a review, see *Ref. 6*). On the other hand, some viruses utilize specific Hsps for their propagation. Hsp70, an inducible form of the Hsp70 family protein, is reported to be involved in the polymerase activity of Canine distemper virus and in the growth of measles virus by associating

---

**Correspondence to:* Dr. Nobuyuki Kobayashi, Laboratory of Molecular Biology of Infectious Agents, Graduate School of Biomedical Sciences, Nagasaki University, 1-14 Bunkyo-machi, Nagasaki 852-8521, Japan;
e-mail: nobnob@nagasaki-u.ac.jp

with N protein (*7*). Hsc70, a constitutive form of the Hsp70 family protein, is involved in the cell entry of rotavirus (*8*).

Hsc70 is a molecular chaperone which consists of the ATPase domain (residues 1-384 in human), the protein binding domain (residues 385-543), and the variable domain (residues 544-646). Hsc70 mediates not only protein folding but also protein translocation across nuclear membrane. We found that Hsc70 has leucine-rich NES (^{394}LDVTPLSL^{401}) (*9*) and it is also involved in the nuclear export of the import receptors, importin and transportin (*10*). Hsc70 has been reported to have NLS(^{246}KRKHKKDISENKRAVRR^{262}) (*11*). Antibodies against Hsc70 inhibit the nuclear import of karyophilic proteins, suggesting the essential role of Hsc70 in nuclear import (*12*). In the case of viral lifecycle, Hsc70 is required for the nuclear import of Adenovirus DNA (*13*), and papillomavirus capsid (*14*), however, the involvement of Hsc70 in the influenza viral nuclear traffic process is unknown.

This study examined the mechanism of Hsc70 in the nuclear localization of influenza viral RNP. We showed that Hsc70-M1-vRNP complex is detected in both infected cells and in virions. NP accumulates in the nucleus in transfected cells without nuclear accumulation of Hsc70. The nuclear export of Hsc70 is inhibited by LMB treatment in infected cells. These results suggest that Hsc70 is thus required for the nuclear export of influenza viral RNP components, but not for the nuclear import thereof.

Materials and Methods

Virus, cells, antibodies, chemicals and plasmids

Influenza virus A/WSN/33 (H1N1) was propagated in 10-day-old embryonic eggs and the allantoic fluid (~1 × 10^7 PFU/mL) was used for the infection procedures. Purified virions were obtained as described previously (*5*). For the preparation of vRNP, purified virions (8 mg total protein) were treated with 1 mL of disruption buffer consisting of 100 mM Tirs-HCl (pH 8.0), 100 mM NaCl, 5 mM $MgCl_2$, 1% lysolecitin (Sigma Aldrich), 1% Triton X-100, 1 mM DTT and 5% glycerol for 30 min at 30°C. The solution was directly subjected to centrifugation on a 30-60% linear gradient of glycerol on an 80% glycerol cushion in 50 mM Tris-HCl (pH 7.9), 100 mM NaCl, and 1 mM DTT in a Beckman SW40Ti rotor at 36,000 rpm for 4 h at 4°C. Madin-Darby canine kidney (MDCK) cells and HeLa cells were maintained in MEM supplemented with 10% FBS. The preparation of anti-M1 and anti-NP rabbit polyclonal Ab were previously described (*15*). Anti-NP mouse mAb was kindly supplied by Dr. Fumitaka Momose (Kitazato University) (*16*). Anti-Hsc70 (SPA-815) rat mAb was purchased from Stressgen (Victoria BC, Canada). Anti-B23 rabbit antiserum was kindly supplied by Dr. Mitsuru Okuwaki (Tsukuba University). LMB was purchased from LC Laboratories, Inc (Woburn, MA).

Immunoprecipitation

HeLa cells grown in 90-mm dish (~1 × 10^7 cells) were infected with influenza virus at a MOI of 1 for 12 h. The cells were washed twice with 3 mL of PBS and then were lysed with 400 µL of the ice-cold lysis buffer (50 mM Tris (pH7.5), 150 mM NaCl, 0.5% Triton X-100, 2 mM EDTA, 1 mM DTT, and 1 mM PMSF) for 30 min, followed by centrifugation at 15,000 g for 10 min. In a total volume of 200 µL, the reaction mixture containing 20 µL of the cell lysate, 10 µL of Ab-bound proteinA sepharose beads, and the lysis buffer containing 0.1% BSA was incubated at 4°C for overnight. After successive washings with a wash buffer (the lysis buffer containing 300 mM NaCl), Ab-bound proteins were eluted by Laemili SDS sample buffer and loaded onto SDS-PAGE and then they were analyzed by Western blotting.

Permeabilization of MDCK cells and in vitro export assays

In vitro export assays were performed as previously described (*4*) with some modifications. Briefly, MDCK cells were washed with an ice-cold transport buffer (20 mM Hepes-KOH (pH 7.4), 100 mM potassium acetate, 5 mM sodium acetate, and 1 mM EGTA). The cells were treated with the ice-cold transport buffer containing 100 µg/mL digitonin (Wako) for 20 min at 0°C. After successive washings at 0°C, the export assays were performed in the transport buffer by incubating the cells at 30°C for indicated time in each figure legends. The supernatant was recovered as an "exported fraction", and then it was analyzed by Western blotting. Digitonin-permeabilized cells before performing export assays were also lysed with Laemili SDS sample buffer and loaded onto SDS-PAGE to estimate the total protein remaining in nucleus ("Permeabilized cells" in each figure).

Indirect immunofluorescence

HeLa cells were grown on glass coverslips and incubated for 24 h to a density of ~50% confluence. The cells were then transfected with pCAGGS-M1 or pCAGGS-NP (Figure 3A) using lipofectamine 2000 (Invitrogen) or were infected with influenza virus and then were further incubated at 37°C for 9 h. The following procedure was performed at room temperature: The cells were fixed with 4% paraformaldehyde in PBS for 10 min and treated with a wash buffer (0.1% NP-40 in PBS) for 20 min. The cells were immersed for 1 h in a blocking solution (1% skim milk in PBS) and then were incubated for 1 h with anti-Hsc70 rat mAb, anti-NP mouse mAb, or anti-M1 rabbit antiserum in the blocking solution. After washing with the wash buffer, the cells were incubated for 1 h with the secondary antibodies, Alexa488-conjugated anti-rat Ig, Alexa546-conjugated anti-mouse Ig or Alexa546-conjugated anti-rabbit Ig. The cells were washed with the wash buffer, and then were observed by microscopy (Axiophot, Carl Zeiss).

Results

Detection of Hsc70-M1-vRNP complex

Recently, we identified Hsc70 (Figure 1A) to be a M1 binding protein using MALDI-TOF MS (*5*). An X-ray structure analysis showed helix 6 (amino acid residues 91-105) of M1 to be involved in the binding with viral RNP (*17*). The interaction between Hsc70, M1 and vRNP was confirmed using co-immunoprecipitation assay (Figure 2A). The infected cells were lysed with the lysis buffer and subjected to immunoprecipitation using anti-Hsc70, NP, or M1 antibody. These results showed that Hsc70 co-precipitates with M1 and NP. Next, the purified virion was lysed by the addition of Triton X-100 and lysolecitin, and then it was separated by glycerol density gradient centrifugation (Figure 2B). The vRNP fractions were pooled, and then were subjected to a Western blotting analysis (Figure 2C). Hsc70 was detected both in the virion and in the vRNP fraction. A far-western blotting analysis confirmed that Hsc70 directly interacts with M1 *in vitro* (Figure 2D). These results suggest that Hsc70-M1-vRNP complex exist in infected cells and in the virion.

LMB inhibits the nuclear export of vRNPs and Hsc70 and suppresses virus production

We hypothesized that Hsc70 shuttles between nucleus and cytoplasm, thus utilizing its NES, NLS, and NLRS (see Figure 1A), and the export of Hsc70 is also mediated by CRM1-dependent pathway in both uninfected cells and influenza virus infected cells. To monitor the nuclear export processes directly, we established a novel *in vitro* nuclear export assay using digitonin-permeabilized cells (*4*) (Figure 3). LMB-treated uninfected cells (Figure 3A) or infected cells (Figure 3B) were permeabilized with digitonin at 0°C and washed successively with the ice-cold transport buffer to remove soluble cytosol components such as viral proteins and nuclear import factors, then subjected to the nuclear export assay. We confirmed that digitonin-permeabilization (100 μg/mL) specifically permeabilize the plasma membrane, whereas the nuclear envelope was kept intact by monitoring GFP-Hsc70 fluorescence (data not shown). The export of Hsc70 from the nucleus occured in a temperature-dependent manner, and it was inhibited by LMB treatment (Figure 3B, lanes 5-7 and 9-11), whereas

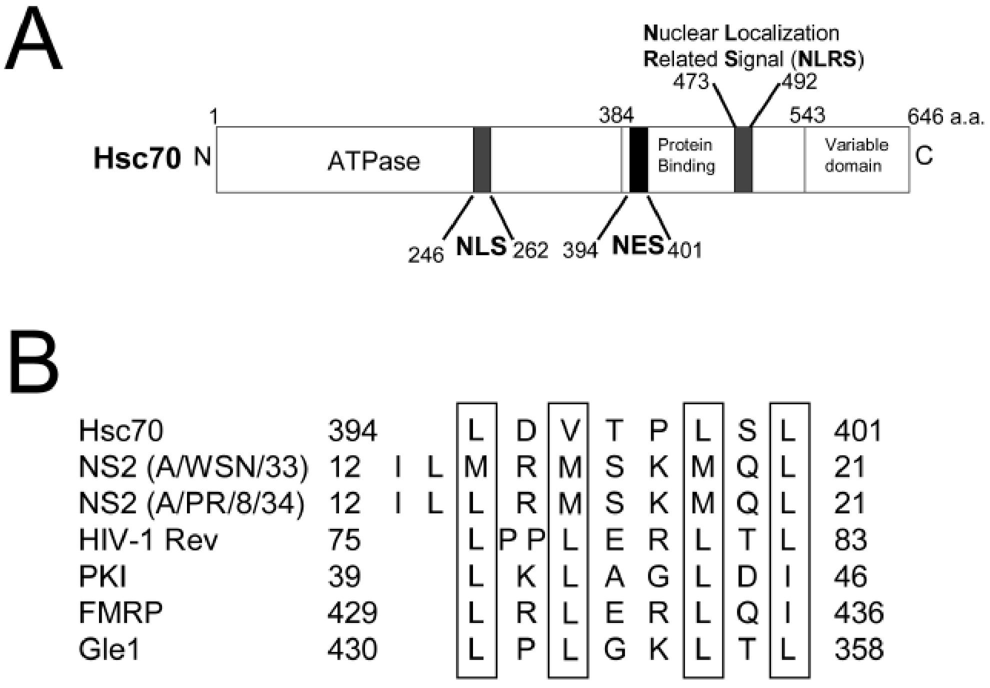

Hsc70	394			L	D	V	T	P	L	S	L	401
NS2 (A/WSN/33)	12	I	L	M	R	M	S	K	M	Q	L	21
NS2 (A/PR/8/34)	12	I	L	L	R	M	S	K	M	Q	L	21
HIV-1 Rev	75			L	P P	L	E	R	L	T	L	83
PKI	39			L	K	L	A	G	L	D	I	46
FMRP	429			L	R	L	E	R	L	Q	I	436
Gle1	430			L	P	L	G	K	L	T	L	358

Figure 1. (A) Diagram of functional domain of human Hsc70. Hsc70 contains NLS, NES and Nuclear localization related signal (NLRS) (*9*). (B) Comparison of the NES of Hsc70, influenza NS2, HIV-1 Rev and representative host proteins. The consensus sequence for leucine- rich NESs is shown. The consensus sequence contains hydrophobic residues, including leucine, isoleucine methionine and valine. PKI; protein kinase inhibitor, FMRP; fragile X metal retardation protein.

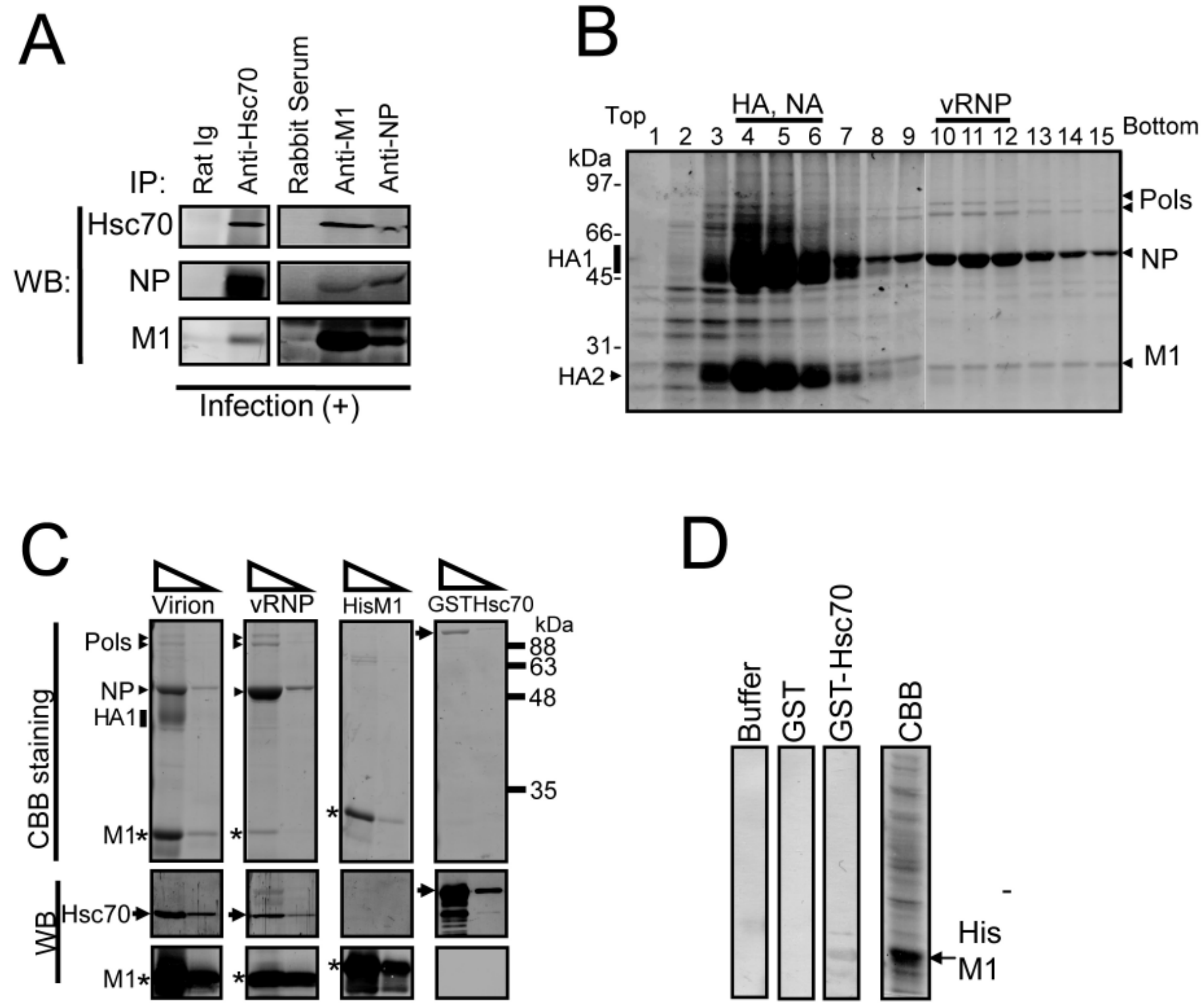

Figure 2. Detection of Hsc70-M1-vRNP interaction. (A) Immunoprecipitation. HeLa cells were infected with the influenza virus A/WSN/33 (MOI = 1) for 12 h. The total cell lysates were immunoprecipitated with anti-M1 antiserum, anti-NP antiserum, or anti-Hsc70 mAb and then were visualized with anti-M1 antiserum, anti-NP mAb, or anti-Hsc70 mAb after 10% SDS-PAGE as indicated. (B) Separation of vRNP-associated factors by glycerol density gradient centrifugation. Virions were purified on a sucrose step gradient (indicated as virion in Figure 2C) and were disrupted by the addition of Triton X-100 and lysolecitin as described in materials and methods. Fractions (1-15) were collected, then separated by a 10% SDS-PAGE, followed by visualization by CBB staining. The vRNP fractions (Fraction numbers 10-12) were pooled, mixed, and subjected to Western blotting using anti-Hsc70 antibody (see Figure 2C). Separately, marker proteins were also subjected to the same glycerol density gradient. Trypsin inhibitor (21 kD), BSA (66 kD) and myosin (200 kD) sediments in fraction number 2, 3 and 4-5, respectively. (C) Detection of virion- and vRNP-associated Hsc70. Purified virion (5 µg and 500 ng), purified vRNP, purified recombinant His-M1 (1 µg and 100 ng), or GST-Hsc70 (300 ng and 30 ng) were loaded onto 10% SDS-PAGE. The gels were either stained with CBB (upper panel) or subjected to Western blotting using anti-Hsc70 (middle panel) or anti-M1 antibody (lower panel). The asterisks and arrows indicate M1 protein and Hsc70, respectively. The arrowheads indicate NP and Polymerases (Pols; PA, PB1 and PB2). (D) Far-Western Blotting. *E. coli*-expressed crude lysate of His-M1 was separated by 10% SDS-PAGE, transferred onto the PVDF membrane, then followed by denaturation with 6 M guanidine HCl in TBST for 10 min. After stepwise renaturing, the membrane was incubated with 1 µg/mL of each purified GST-Hsc70 or GST in TBST at 4°C for 4 h. Specific signals were detected by a Western blotting procedure using anti-Hsc70 mAb.

Nucleophosmin/B23, which is known to localize in the nucleolus, did not come out of the nucleus. Next, the infected MDCK cells (7 hpi) were also subjected to the *in vitro* export assays and the exported fraction was detected by Western blotting (Figure 3B). Viral RNP, M1, and Hsc70 were exported from nucleus at 30°C and the export processes were inhibited when the cells were pretreated with LMB (lanes 5-7 and 9-11). These results suggest that Hsc70, M1, and vRNP are exported from the nucleus to the cytoplasm *via* the CRM1-dependent pathway. To determine whether LMB affects the influenza virus production, MDCK cells were infected with the influenza virus A/WSN/33 at a MOI of 0.1 in the presence (1 or 10 ng/mL) or absence of LMB (Figure 3C). At 12 or 24 h post infection, the supernatants of the infected cells were recovered and subjected to the plaque assay. The virus titer in the supernatant was markedly reduced when cells were treated with LMB in dose dependent manner. In uninfected cells, 10 ng/mL of LMB treatment did not affect cell viability significantly (data not shown). In infected cells, at 12 h post infection, the cell viability was > 90% in the presence or absence of LMB. At 24 h post infection, the cell viability was 32.6% in the absence of LMB whereas that of LMB treated cells (1 ng/mL or 10 ng/mL) was 40.8% or 61.8%, thus suggesting that cell death by the

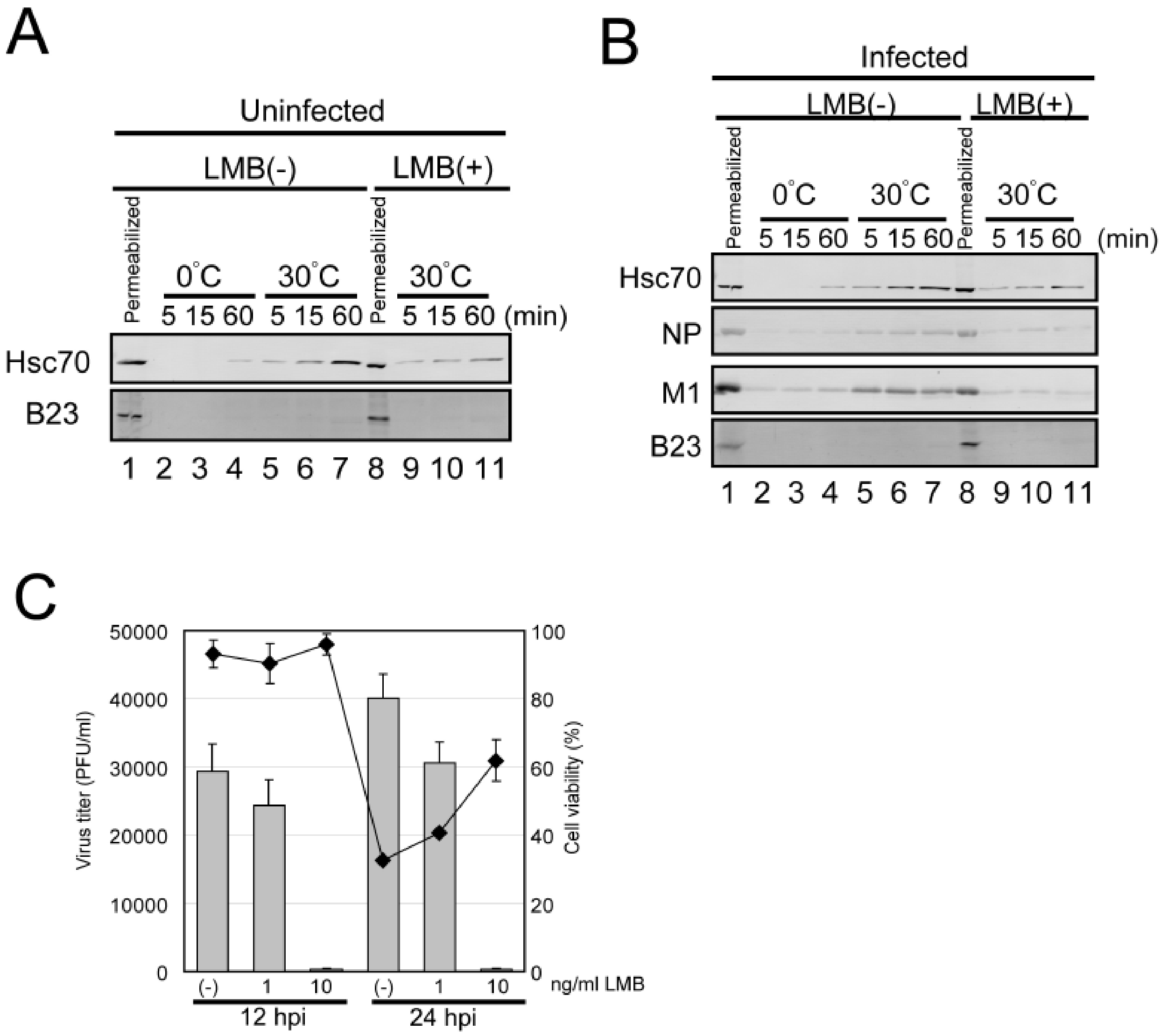

Figure 3. (A) (B) *In vitro* export assays. MDCK cells were uninfected or infected in the absence or presence of 10 ng/mL LMB for 7 h as indicated. The cells were treated with ice-cold 100 μg/mL Digitonin, the permeabilized cells were incubated at 0°C or 30°C. (A) The export of the endogenous Hsc70 was detected by the *in vitro* export assays using uninfected MDCK cells. The permeabilized cells lysed by Laemili SDS sample buffer (indicated as "Permeabilized", lanes 1 and 8) or the exported supernatant fraction was recovered at 5, 15 and 60 min were loaded onto 10% SDS-PAGE, then detected by the Western blotting using anti-Hsc70 (upper panel) and anti-B23 antibodies (lower panel). (B) Export of the endogenous Hsc70 and viral proteins. MDCK cells were infected with A/WSN/33 at a MOI of 1 for 7 h. The cells were treated with digitonin and subjected to the *in vitro* export assays. The permeabilized cells lysed by Laemili SDS sample buffer (indicated as "Permeabilized", lanes 1 and 8) or the exported supernatant fractions from digitonin-permeabilized cells were separated by 10% SDS-PAGE and then visualized by Western blotting using anti-Hsc70 mAb, anti-M1 antiserum and anti-NP antiserum as indicated. (C) The effect of LMB on the propagation of the influenza virus. MDCK cells were infected with A/WSN/33 at a MOI of 0.1 for 60 min. After successive washing, the cells were further incubated without or with 1 ng or 10 ng/mL of LMB. The culture supernatant was recovered at 12 and 24 h after infection, then subjected to plaque assays. The viability of the cells was determined by trypanblue staining. The virus titer (PFU/mL) is shown as solid bar, and the viability (%) was shown as a line. The experiments were performed in triplicate and the mean + SD was shown.

infection was suppressed by LMB treatment.

Hsc70 does not regulate the nuclear import of vRNP components but regulate the export of vRNP

It has been reported that the dissociation of M1 from vRNP is required for the nuclear import of incoming vRNP in the early stages of infection (*2*) and the nuclear import of newly synthesized vRNP components such as NP is mediated by importin family proteins (for a review, see *Ref. 18*). To rule out the possibility that Hsc70 regulate nuclear import of vRNP components *via* M1, we monitored the localization of Hsc70, NP, or M1 in transiently transfected HeLa cells. Hsc70 and M1 localized in both nucleus and cytoplasm (Figure 4A, panels a and b) where NP accumulated in nucleus (c), suggesting that Hsc70 does not regulate nuclear import processes of viral proteins. Next, we monitored the localization of Hsc70 and NP at the late stages of infection (9 h) when nuclear export of vRNP mainly occurs (Figure 4B). NP and Hsc70 localized dominantly in the nucleus (panels b and e). Clearly, in the presence of LMB, NP was localized exclusively in the nucleus (c). The localization of Hsc70 was more extensively

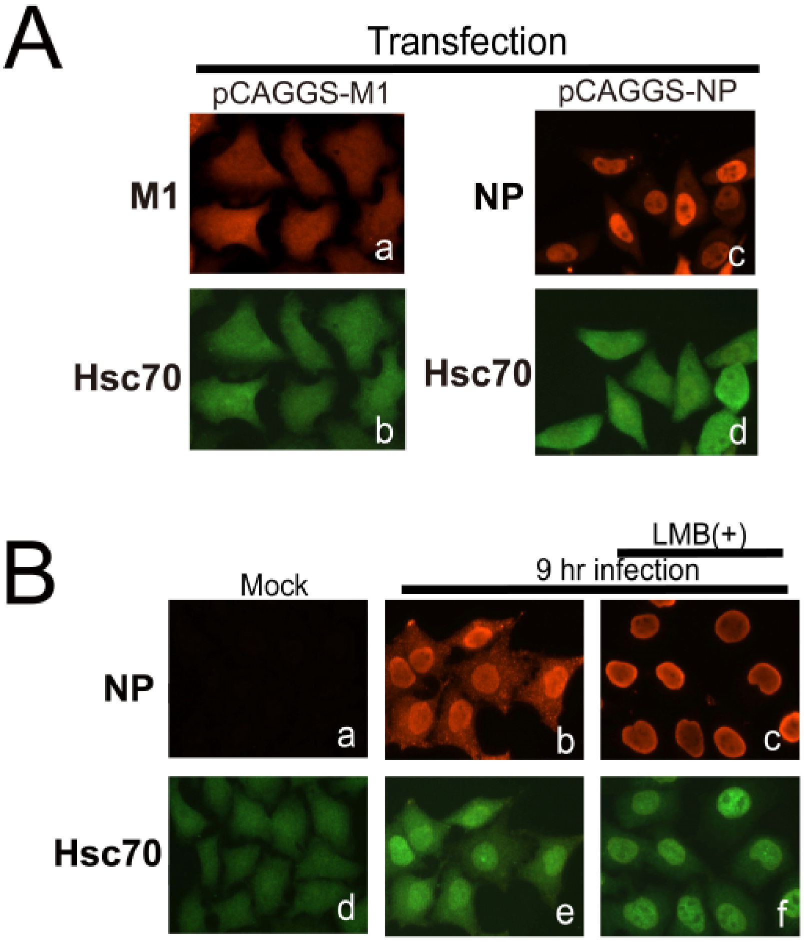
A
Transfection
pCAGGS-M1
pCAGGS-NP
M1
NP
a
c
Hsc70
Hsc70
b
d
B
LMB(+)
9 hr infection
Mock
NP
a
b
c
Hsc70
d
e
f

Figure 4. Hsc70 regulates the nuclear export of vRNP. HeLa cells were transiently transfected with NP- or M1-expressing plasmids (A) or were infected with A/WSN/33 (MOI = 5) in the absence or presence of 10 ng/mL LMB (B). The cells were fixed and stained with anti-Hsc70 mAb, anti-NP mAb, and anti-M1 antiserum as indicated. NP (Alexa 546: Red), M1 (Alexa 546: Red) and Hsc70 (Alexa488: Green) were observed under microscopy.

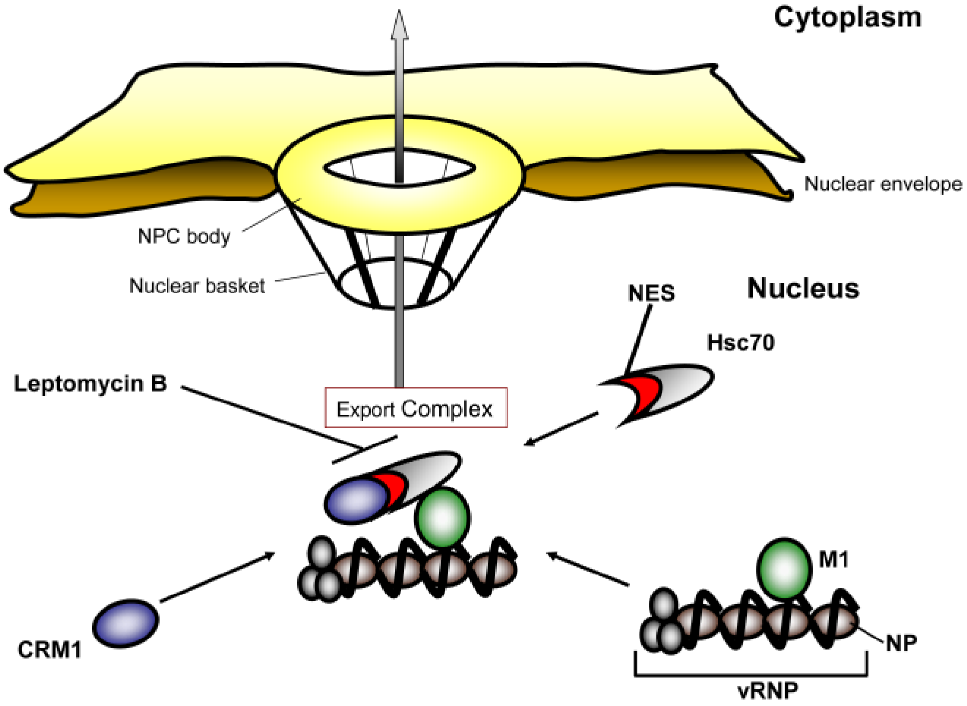
Cytoplasm
Nuclear envelope
NPC body
Nuclear basket
NES
Nucleus
Hsc70
Leptomycin B
Export Complex
M1
CRM1
NP
vRNP

Figure 5. A model for Hsc70-related nuclear export of the influenza virus RNP complexes. Hsc70 interacts with CRM1 *via* its NES, and M1 interacts with Hsc70. CRM1-Hsc70-M1-vRNP complex is formed and exported from the nucleus and concomitantly CRM1 is released from Hsc70. A part of Hsc70 may incorporate into the virions.

accumulated in the nucleus in the presence of LMB in infected cells (f). These results suggest that Hsc70 regulates vRNP export from the nucleus in the late stages of infection, while having no such effect in the early stages of infection.

Discussion

This study demonstrated that Hsc70 regulates the nuclear export of vRNP. The nuclear export of Hsc70 and vRNP was LMB sensitive. In infected cells, M1 and NP co-precipitated with Hsc70, and the Hsc70-M1-vRNP complex exported from the nucleus *via* the CRM1-dependent pathway.

Because the transcription and replication of influenza virus occurs in nucleus, nuclear import and export of vRNP is one of the most important steps for the virus life cycle. It has been reported that nuclear export of vRNP is mediated by M1 and viral NS2 protein (*2,19*), and is inhibited by LMB (*20,21*). Although M1 does not have NES, it plays a key role as a mediator to bind both vRNP and NS2. NS2 have leucine rich NES which binds to a nuclear export factor, CRM1 (Figure 1B). Thus, vRNP is thought to be exported by the vRNP-M1-NS2-CRM1complex (for a review, see *Ref. 18*). However, we previously found that the effect of LMB on the nuclear export of the NS2 was a partial effect (*4*), suggesting the existence of other host factors which is essential for the nuclear export of vRNP. We explored M1 binding protein using MALDI-TOF MS and identified Hsc70 (*5*). Hsc70 was complexed with M1 and NP in infected cells and in the virion (Figure 2). Hsc70 has both NES and NLS, and is known to shuttle between the nucleus and cytoplasm. To monitor the export processes, an *in vitro* export assay system was developed (Figure 3A and 3B) and showed that export of Hsc70 and vRNP was CRM1 dependent. The inhibition of the export of vRNP by LMB (Figure 3B) resulted in the reduction of virus production (Figure 3C) in MDCK cells. MDCK cell is usually used for viral infection experiments, because it support multiple cycle of the virus infection and efficient virus production. However, the cytopathic effect (CPE) occurs very fast in the MDCK cells. Therefore, for the detection of viral protein, HeLa cell was used for immunoprecipitation (Figure 2A) and indirect immunofluorescence (Figure 4). The nuclear import of NP was not related with Hsc70 (Figure 4A), whereas the nuclear export of NP and Hsc70 was inhibited by LMB. Taking these observations into account, we therefore hypothesize that vRNP is exported as Hsc70-M1-vRNP *via* the CRM1-dependent pathway (Figure 5). Further studies are essential to elucidate the involvement of NS2 in the export complex.

The anti-influenza drugs available today are directed against essential viral protein functions. Amantadine blocks the ion-channel activity of the viral M2 protein, which is required for virus entry steps. Zanamivir and oseltamivir, block the receptor-destorying activity of viral NA protein, prevent viral budding form the cell surface. These drugs are approved and commercially available in many countries. However, the influenza virus easily change its genome sequence and many drug-resistant mutated viruses has been reported (for a review, see *Ref. 22*). Specific cellular proteins essential for virus propagation such as Hsc70 may therefore be a good target for the development of drugs which can suppress viral diseases (*23*).

Acknowledgements

We thank Dr. Y. Kawaoka (the University of Tokyo) for providing M1 and NP expression vectors. This work was partly supported by a Grant-in-Aid for Ministry of Education, Culture, Sports, Science and Technology and by a Grant-in-Aid for Scientific Research from Nagasaki University, Japan (K.W.).

References

1. Nayak DP, Hui EK, Barman S. Assembly and budding of influenza virus. Virus Res 2004; 106:147-165.
2. Martin K, Helenius A. Nuclear transport of influenza virus ribonucleoproteins: the viral matrix protein (M1) promotes export and inhibits import. Cell 1991; 67:117-130.
3. Bui M, Wills EG, Helenius A, Whittaker GR. Role of the influenza virus M1 protein in nuclear export of viral ribonucleoproteins. J Virol 2000; 74:1781-1786.
4. Watanabe K, Takizawa N, Katoh M, Hoshida K, Kobayashi N, Nagata K. Inhibition of nuclear export of ribonucleoprotein complexes of influenza virus by leptomycin B. Virus Res 2001; 77:31-42.
5. Watanabe K, Fuse T, Asano I, Tsukahara F, Maru Y, Nagata K, Kitazato K, Kobayashi N. Identification of Hsc70 as an influenza virus matrix protein (M1) binding factor involved in the virus life cycle. FEBS Lett 2006; 580:5785-5790.
6. Santoro MG. Antiviral activity of cyclopentenone prostanoids. Trends Microbiol 1997; 5:276-281.
7. Zhang X, Bourhis JM, Longhi S, Carsillo T, Buccellato M, Morin B, Canard B, Oglesbee M. Hsp72 recognizes a P binding motif in the measles virus N protein C-terminus. Virology 2005; 337:162-174.
8. Perez-Vargas J, Romero P, Lopez S, Arias CF. The peptide-binding and ATPase domains of recombinant hsc70 are required to interact with rotavirus and reduce its infectivity. J Virol 2006; 80:3322-3331.
9. Tsukahara F, Maru Y. Identification of novel nuclear export and nuclear localization-related signals in human heat shock cognate protein 70. J Biol Chem 2004; 279:8867-8872.
10. Kose S, Furuta M, Koike M, Yoneda Y, Imamoto N. The 70-kD heat shock cognate protein (hsc70) facilitates the nuclear export of the import receptors. J Cell Biol 2005; 171:19-25.
11. Lamian V, Small GM, Feldherr CM. Evidence for the

existence of a novel mechanism for the nuclear import of Hsc70. Exp Cell Res 1996; 228:84-91.

12. Imamoto N, Matsuoka Y, Kurihara T, Kohno K, Miyagi M, Sakiyama F, Okada Y, Tsunasawa S, Yoneda Y. Antibodies against 70-kD heat shock cognate protein inhibit mediated nuclear import of karyophilic proteins. J Cell Biol 1992; 119:1047-1061.
13. Saphire AC, Guan T, Schirmer EC, Nemerow GR, Gerace L. Nuclear import of adenovirus DNA *in vitro* involves the nuclear protein import pathway and hsc70. J Biol Chem 2000; 275:4298-4304.
14. Florin L, Becker KA, Sapp C, Lambert C, Sirma H, Muller M, Streeck RE, Sapp M. Nuclear translocation of papillomavirus minor capsid protein L2 requires Hsc70. J Virol 2004; 78:5546-5553.
15. Takizawa N, Watanabe K, Nouno K, Kobayashi N, Nagata K. Association of functional influenza viral proteins and RNAs with nuclear chromatin and sub-chromatin structure. Microbes Infect 2006; 8:823-833.
16. Momose F, Kikuchi Y, Komase K, Morikawa Y. Visualization of microtubule-mediated transport of influenza viral progeny ribonucleoprotein. Microbes Infect 2007; 9:1422-1433.
17. Sha B, Luo M. Structure of a bifunctional membrane-RNA binding protein, influenza virus matrix protein M1. Nat Struct Biol 1997; 4:239-244.
18. Boulo S, Akarsu H, Ruigrok RW, Baudin F. Nuclear traffic of influenza virus proteins and ribonucleoprotein complexes. Virus Res 2007; 124:12-21.
19. O'Neill RE, Talon J, Palese P. The influenza virus NEP (NS2 protein) mediates the nuclear export of viral ribonucleoproteins. Embo J 1998; 17:288-296.
20. Elton D, Simpson-Holley M, Archer K, Medcalf L, Hallam R, McCauley J, Digard P. Interaction of the influenza virus nucleoprotein with the cellular CRM1-mediated nuclear export pathway. J Virol 2001; 75:408-419.
21. Ma K, Roy AM, Whittaker GR. Nuclear export of influenza virus ribonucleoproteins: identification of an export intermediate at the nuclear periphery. Virology 2001; 282:215-220.
22. De Clercq E. Antiviral agents active against influenza A viruses. Nat Rev Drug Discov 2006; 5:1015-1025.
23. Watanabe K, Saiko N, Kobayashi N. Establishment of a new cell line for performing sensitive screening of nuclear export inhibitors. Drug Discov Ther 2008; 2:7-9.

(*Received February 12, 2008; Revised February 19, 2008; Accepted February 26, 2008*)

Original Article

UVB-dependent generation of reactive oxygen species by catalase and IgG under UVB light: Inhibition by antioxidants and anti-inflammatory drugs

Masahiro Murakami[1,]*, Masakazu Taniguchi[2], Masashi Takama[1], Jinghao Cui[2,], Yoshihiko Oyanagui[3]**

[1] *Laboratory of Pharmaceutics, Faculty of Pharmacy, Osaka Ohtani University, 3-11-1 Nishikiori-kita, Tondabayashi, Osaka, Japan;*
[2] *Discovery Research Laboratory, Amato Pharmaceutical Co., 995 Sasao, Fukuchiyama, Kyoto, Japan;*
[3] *Redox Research Laboratory, 97-1 Gokasho-ishizuka, Higashi-ohmi-shi, Shiga, Japan.*

ABSTRACT: Catalase, which can decompose H_2O_2, has recently been found to generate unspecified reactive oxygen species (ROS) as a result of ultraviolet B (UVB) irradiation. Many proteins, hemes, and iron compounds were first tested to determine that this ROS generation was unique to catalase and immunoglobulin G (IgG). An increase in absorbance at 502 nm due to 2',7'-dichlorofluorescein, the oxidized product of 2',7'-dichlorodihydrofluorecein diacetate as a result of UVB (310 nm) irradiation, was measured in order to estimate this ROS generation. Catalase and IgG generated a pronounced amount of ROS when irradiated with UVB. Another heme protein, cytochrome c, and heat-inactivated catalase had no such effect. ROS generation by catalase was at least 5 times more potent than that reported for IgG with UVB and without antigens. This catalase-mediated ROS generation was largely temperature-dependent in the range of 25 to 42°C. As IgG is considered an evolutionally important bactericidal component, the same was considered true for this enzyme. Next, inhibitory effects of various drugs, including antioxidants and anti-inflammatory drugs, on catalase-mediated and UVB-induced ROS generation were examined. Many of the drugs, including catalase inhibitors, had inhibitory effects with different potencies. Melanin was found to be the most effective inhibitor of this ROS generation (IC_{30}, 0.2 µg/mL), followed by Indigo Carmine and rutin. Also inhibiting this ROS generation were ascorbic acid, α-tocopherol, indomethacin, coenzyme Q10, β-carotene, uric acid, piroxicam, diclofenac, and glutathione, in that order of potency. Various ROS were apparently generated by catalase under UVB, creating a cycle or chain which was thought due to the biphasic effects of some drugs such as 3-aminotriazole or sodium azide. Excess ROS generation induces inflammation. Catalase might serve dual roles, removing H_2O_2 and generating various ROS depending on the H_2O_2 concentration and other factors.

Keywords: Catalase, IgG, UVB, Reactive oxygen species (ROS), Antioxidant, Anti-inflammatory drug, Melanin

Introduction

This study primarily sought to verify and expand upon two recent reports (*1*,*2*) that found unexpected generation of reactive oxygen species (ROS) as a result of ultraviolet (UV) light irradiation of catalase and immunoglobulins. Heck *et al.* (*1*) found a material in keratinocyte lysates capable of generating ROS responding to UVB (290-320 nm) irradiation. They purified this material into a protein of 240 kDa and verified that it was catalase using antibodies; this finding was surprising as this enzyme is the only one to degrade H_2O_2, a typical ROS that can be scavenged by catalase and glutathione peroxidase (GSH•Px). The current study attempted to identify the type of ROS generated by UVB and catalase and indicate which drugs can inhibit the generation of this ROS. The study measured the fluorescence (495 nm excitation and 520 nm emission) due to 2',7'-dichlorofluorescein (DCF), the oxidized product of 2',7'--dichlorodihydrofluorecein

---

**Correspondence to:* Dr. Masahiro Murakami, Laboratory of Pharmaceutics, Faculty of Pharmacy, Osaka Ohtani University, 3-11-1 Nishikiori-kita, Tondabayashi, Osaka 584-8540, Japan;
e-mail: murakam@osaka-ohtani.ac.jp

**Present address: Department of Pharmaceutics, College of Pharmacy, Soochow University, No.1 Heng 1 Road, SIP, Suzhou City, Jiangsu 215123, China.

diacetate (DCFH•DA) (*1*). Valkonen *et al*. (*3*) noted that DCFH can also be assayed by spectrophotometry as an increase in optical density (O.D.) at 504 nm; therefore, this method of spectrophotometry was used in the current study to facilitate testing the effects of numerous drugs. Another fascinating finding is that of Wentworth, Jr. *et al*. (*2*), who reported that UVB (312 nm) irradiation of immunoglobulins (IgG, IgM, IgA) and T-cell receptor resulted in ROS generation from water. The inter-Greek key domain interface (IGKD), formed by heavy and light chains of the IgG molecule, is considered to be the site of H_2O_2 generation from singlet oxygen ($^1O_2$) or hydrogen trioxide (HOOOH) generated by UV light (*4*). As $^1O_2$ has a short life span (4 μs), it must be converted into H_2O_2 to maintain continuous microbicidal action for the immune system. $^1O_2$ can also be formed from hypochlorite (HOCl) plus H_2O_2 and superoxide radical (O_2^-) plus nitric oxide (*5*). This means that the generation of $^1O_2$ is not limited to UV irradiation. In addition to $^1O_2$, ozone (O_3) was reported to be involved in leukocyte antibacterial action (*6*). Contrary to the generally accepted concept that $^1O_2$ is an end-product ROS, antibodies have an intrinsic ability to generate $^1O_2$ in the first step of ROS generation. The strongest oxidant is the hydroxyl radical (•OH), which can be produced by ferrous ion from H_2O_2; thus, the participation of •OH could not be ignored in the current experiments. *In vivo*, the main sources of $^1O_2$ and H_2O_2 generation are NAD(P)H oxidase in leucocytes and xanthine oxidase in organs such as the liver and intestines. However, the participation of these enzymes should be excluded in this *in vitro* report. The current authors previously reported that UV irradiation (260-340 nm) for 60 min generated H_2O_2 from 100 μg/mL IgG that was inhibited by dexamethasone and piroxicam (*7*). This suggested that anti-inflammatory drugs could block the ROS (H_2O_2 or its derived oxidants). The current study found that catalase's ROS-generating capacity under UV light was more evident than that of IgG. None of the other proteins examined was capable of generating more ROS than catalase or IgG. The nature of ROS generated by catalase under UVB light was further investigated using various medications including catalase inhibitors, antioxidants, and anti-inflammatory drugs.

Materials and Methods

Materials

2',7'-dichloro-5-fluorecein diacetate (DCFH•DA) and Arabia gum were obtained from Wako Pure Chemical Industries, Ltd. (Osaka, Japan). Catalase (from bovine liver, approx. activity = 50,000 units/mg/protein, 2 × crystallized), Cu, Zn-superoxide dismutase (Cu, Zn-SOD, from bovine erythrocytes, lyophilized powder, approx. activity = 3,000 unit/mg/protein), and glutathione peroxidase (GSH•Px, from bovine erythrocytes, lyophilized powder containing approx. 20% protein) were from Sigma Co. (St. Louis, USA). Polyclonal anti-human immunoglobulin G (IgG from fraction powder from rabbit, H&L, 9.7 mg/mL) was obtained from Inter-Cell Technologies, Inc. (New Jersey, USA). Dexamethasone acetate (Decadron-A 8 mg/mL) was from Banyu Pharmaceutical Co. (Tokyo, Japan). Desferoxamine mesylate (Desferal) was purchased from Ciba-Geigy Co. (Takarazuka, Japan). All other reagents were from Nakalai Tesque Co. (Kyoto, Japan), Wako Pure Chemical Industries, Ltd. (Osaka, Japan) or Sigma Co. (St. Louis, USA).

UVB irradiation

Mixed with 1.5 mL of water were 0.3 mL phosphate buffer (1 M, pH 7.4) and 0.3 mL catalase (250 μM), followed by the addition of 0.3 mL Arabia gum suspension (100 mg/mL) with or without a drug. A fresh DCFH•DA solution (15 mM, 0.6 mL) was added to a total volume of 3.0 mL. An aliquot (0.3 mL) was transferred to a quartz cell containing 2.7 mL water maintained at 37°C. Absorption at 502 nm was measured (value A_0) by a spectrophotometer (Shimadzu UV-1200, Japan). The resulting mixture (2.7 mL) was irradiated with UVB (310 nm) for 15 min. An aliquot (0.3 mL) of this UVB-irradiated mixture was added to another quartz cell containing 2.7 mL water kept at 37°C. The absorbance was next measured at 502 nm to yield an A_{15} value. The irradiation measurement slit was 5 mm × 10 mm (50 mm^2), and the cell surface area 300 mm^2; therefore, the sample received one-sixth of the irradiation. The beam power was 0.012 $\mu W/mm^2$ at 310 nm (as measured by the manufacturer) so that 0.002 $\mu W/mm^2$ (= 2 $\mu W/cm^2$) was irradiated for 15 min (in general), resulting in 30 mJ/cm^2. Measurement was performed at various irradiation (210-650 nm) and absorption (480-520 nm) wavelengths. Irradiation time-dependency for an increase in 502 nm absorption was confirmed over 60 min.

Measurement of DCFH•DA oxidation

In this report, the increase in O.D. at 502 nm due to DCF (an oxidative product of DCFH•DA) was generally measured following UV (310 nm) irradiation for 15 min at 37°C. Various compounds including catalase, IgG, and cytochrome c were assayed for their ability to increase O.D. at 502 nm as a result of irradiation. The scavengers of $^1O_2$, O_3, *etc*. and various kinds of drugs were tested to ascertain the nature of catalase-generated ROS under UVB irradiation. Drug inhibition was calculated by the following formula:

$$\textbf{Inhibition \%} = \left[1 - \frac{\textbf{Drug } (A_{15}\text{-}A_0)}{\textbf{Control } (A_{15}\text{-}A_0)}\right] \times 100$$

where A_0 and A_{15} are the absorbances at 502 nm before and after, respectively, irradiation at 310 nm.

Arabic gum was used to dissolve drugs in a final concentration of 10 mg/mL. The concentration needed to obtain 30% inhibition (IC_{30}) was estimated from drug concentration-% inhibition curves as an index of the drug's inhibitory potency.

Results

ROS generated by catalase with light of different wavelengths

As expected, the maximum wavelength at which ROS were generated by catalase (25 µM) was 310 nm (UVB) (Figure 1). However, 210 and 280 nm (UVC) for 15 min also increased ROS, as did 350 nm (UVA). Visible blue light (450 nm) resulted in a 77% increase over the generation at 310 nm. Even red light (650 nm) generated about half the ROS generated at 310 nm. Spectra from DCF were observed between 480 and 520 nm (data not shown). Optimal O.D. was between 503 and 510 nm. A sharp decrease occurred near 504 nm, which has been adopted for assay by other investigators (*1*), so 502 nm was chosen for measurement of ROS generation in the current study. Nadirs of spectra were also seen at 486, 493-497, and 510-528 nm.

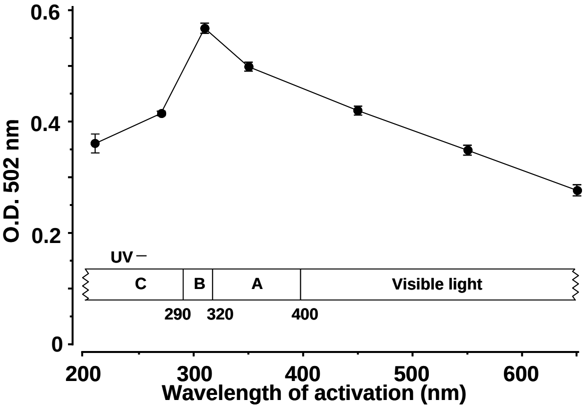

Figure 1. Effect of irradiation on catalase-mediated ROS generation. DCFH•DA solution (3 mM, pH 7.4) was irradiated for 30 min at 37°C in the presence of 25 µM catalase. The increase in absorbance at 502 nm (O.D. at 502 nm) was measured. Bars indicate S.E. of the mean (*n* = 3).

ROS generation by various proteins, iron compounds, and dyes

To determine whether only catalase generated ROS, other compounds were investigated. Concentrations of the compounds were set at 10 mg/mL; the corresponding calculated molar concentrations are noted in Table 1. Catalase generated the largest quantity of ROS, followed by IgG. However, heat-inactivated catalase lacked the capacity to generate ROS. Cu, Zn-SOD, bovine serum albumin (BSA), myoglobin, and $FeSO_4$ also enhanced ROS generation in high concentrations. Mn-SOD, monoamine oxidase, RNase A, lysozyme and ubiquitin failed to generate ROS. No noticeable ROS generation was observed with L-histidine. Some amino acids are reported to scavenge rather than generate $^1O_2$ and O_2^- like, for example, L-histidine and L-tryptophan, respectively (*10,11*). Rose Bengal (*12*) and methylene blue (*13*), photosensitizers that generate $^1O_2$, did not increase O.D. at 502 nm under the experimental conditions, suggesting that catalase generated ROS in a different way than these dyes did. Since catalase is an enzyme that contains heme, some hemes and inorganic irons were also then examined. Hemes (hematin and hemin) and heme-containing proteins (cytochrome c and myoglobin) did not generate ROS in the current system. Hematoporphyrin, which does not possess

Table 1. ROS generated by UVB irradiation in the presence of various proteins, iron compounds, and dyes

Agent (10 mg/mL)	Conc. (M)	ΔO.D. at 502 nm (× 10^{-3})[a]
Catalase	4.2×10^{-5}	489 ± 28
Inactivated Catalase	4.2×10^{-5}	26 ± 3
Immunoglobulin G (IgG)	1.5×10^{-5}	253 ± 24
Cytochrome C	8.0×10^{-4}	33 ± 11
Cu, Zn-SOD	3.2×10^{-4}	124 ± 29
Mn-SOD	2.5×10^{-4}	89 ± 31
Bovine serum albumin (BSA)	1.5×10^{-4}	127 ± 9
Monoamineoxidase (MAO)	3.8×10^{-5}	91 ± 17
Myoglobin	5.9×10^{-4}	156 ± 16
Hematin	1.6×10^{-2}	9 ± 6
Hemin·Cl	1.5×10^{-2}	12 ± 8
$FeSO_4 \cdot 7H_2O$	3.6×10^{-2}	136 ± 43
$FeCl_3 \cdot 6H_2O$	4.0×10^{-2}	4 ± 3
Hematoporphyrin·2HCl	1.4×10^{-2}	13 ± 2
Rose Bengal	9.8×10^{-3}	23 ± 8
Methylene blue	2.7×10^{-2}	17 ± 6
RNase	7.1×10^{-4}	46 ± 38
Lysozyme	6.9×10^{-4}	4 ± 3
Ubiquitin	1.2×10^{-3}	13 ± 8
L-Histidine·H_2O	4.8×10^{-2}	11 ± 6

[a] Absorbance increase at 502 nm was measured after 15 min of UVB (310 nm) irradiation with DCFH•DA (3 mM) at 37°C, pH 7.4. Molar concentration was calculated from each reported molecular weight.

iron, also failed to generate ROS. Inorganic ferrous iron ($FeSO_4$) generated a small amount of ROS, albeit only in high concentrations, but ferric iron ($FeCl_3$) generated none whatsoever. Thus, the possibility that trace iron contaminating the tested proteins was a ROS-generating component can be negated. Some conformational structure(s) in catalase and IgG may be responsible for generating the unspecified but obvious ROS observed in this experiment.

The concentration-dependency of three representative compounds is shown in Figure 2. Almost linear concentration-dependent increases of O.D. at 502 nm (ROS generation) were observed with catalase. Catalase is clearly shown to be the best mediator to generate ROS, followed by IgG. Cytochrome c was ineffective. Other compounds that were tested in various concentrations showed much less ROS generation than did IgG (data not shown).

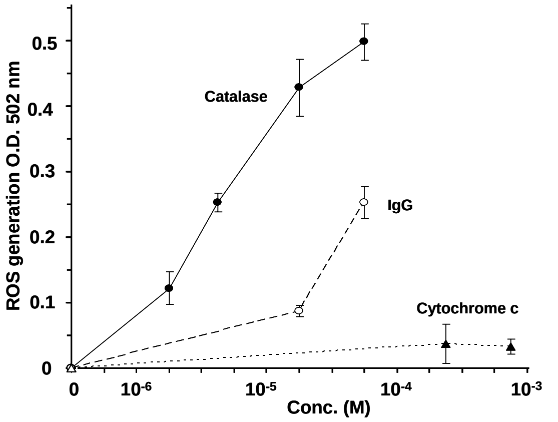

Figure 2. ROS generation mediated by catalase (●), IgG (○) or cytochrome (▲) when irradiated with UVB (310 nm) for 15 min at 37°C. Bars indicate S.E. of the mean (*n* = 3).

Catalase- and DCFH•DA-concentration dependency of ROS generation

DCFH•DA concentration dependency was confirmed up to 4 mM, with 10, 25 and 50 µM of catalase (Figure 3). Therefore, inhibition of ROS generation by drugs was examined using 3 mM DCFH•DA and 25 µM catalase. The time course of this ROS generation was linear up to 30 min of irradiation (data not shown), so a UV irradiation time of 15 min was chosen to evaluate a drug's inhibitory effect.

Temperature-, pH- and phosphate buffer concentration-dependency of ROS generation by catalase as a result of UVB irradiation

ROS generation was temperature-dependent (Figure 4). Drug inhibition was tested at 37°C with 25 µM catalase, which had a sufficient increase in O.D. at 502 nm. Five different pHs of 100 µM potassium phosphate buffer were selected. ROS generation (O.D. at 502 nm) of 0.512, 0.502, and 0.510 (*n* = 3) was almost equal at pH 6.8, 7.4, and 8.0, respectively. ROS generation of 0.419 and 0.346 was lower at pH 5.6 and at pH 8.6, respectively. When phosphate buffer was replaced with water, ROS generation was 0.422 (*n* = 3). At potassium phosphate concentrations of 50, 100, and 200 mM (pH 7.4) ROS generation was 0.532, 0.502 and 0.411, respectively (*n* = 3). Hence, phosphate was not essential for ROS generation.

Effect of moderately soluble or suspended drugs

ROS generation (O.D. at 502 nm, 0.469, *n* = 3) significantly increased in the presence of dimethyl formamide (DMF) (0.5-2.0%, Figure 5A). The DMF concentration required to solubilize water-insoluble drugs in a final concentration of 100 µg/mL was above

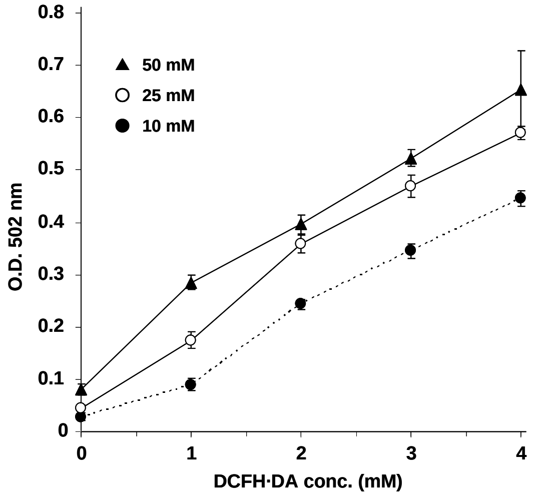

Figure 3. The concentration dependency of catalase-mediated and UVB-induced ROS generation. DCFH•DA (0-4 mM) and catalase (10-50 µM) solutions (pH 7.4) were irradiated with UVB for 15 min at 37°C.

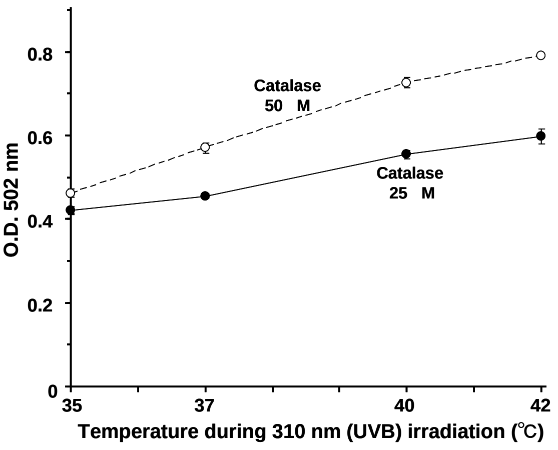

Figure 4. The temperature dependency of catalase-mediated and UVB-induced ROS generation. A 50 µM (○) or 25 µM (●) catalase-DCFH•DA (3 mM) solution (pH 7.4) was irradiated with UVB for 15 min at 37°C. Bars indicate S.E. of the mean (*n* = 3).

1.0%. This concentration of DMF alone markedly increased O.D. at 502 nm by approximately 45% (Figure 5A). Dimethyl sulfoxide (DMSO) alone resulted in a similar enhancement of O.D. at 502 nm (data not shown). On the other hand, Arabia gum (5-20 mg/mL) slightly decreased ROS generation (Figure 5B) and did not precipitate the drugs. In addition, 5, 10, and 20 mg/mL of Arabic gum did not affect the inhibitory potencies on ROS generation of Indigo Carmine, ascorbic acid, rutin, and indomethacin (data not shown). Therefore, 10 mg/mL Arabia gum, which only inhibited ROS generation by 11%, was selected because of its suitability in homogeneously suspending different kinds of drugs.

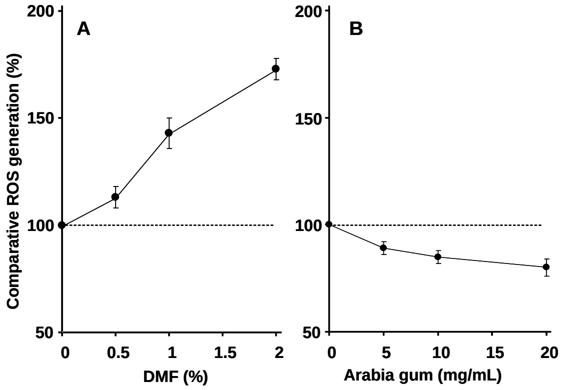

Figure 5. Effects of dimethyl formamide (DMF) (A) and Arabic gum (B) on catalase-mediated and UVB-induced ROS generation. Bars indicate S.E. of the mean ($n = 3$).

Drug inhibition of ROS generation

In the current assay system, drugs could have reacted directly with DCFH•DA, without catalase or UVB participation, resulting in an artificial increase in absorption at 502 nm. Therefore, a continuous curve at 502 nm was registered for up to 15 min without catalase or UVB light in a separate experiment. There was neither a remarkable increase nor decrease in absorption with any drug without catalase. When catalase was absent, some drugs increased absorption before the start (A_0) and maintained the same O.D. until the end of irradiation (data not shown). Figure 6 shows the inhibitory effects up to 100 μg/mL of 12

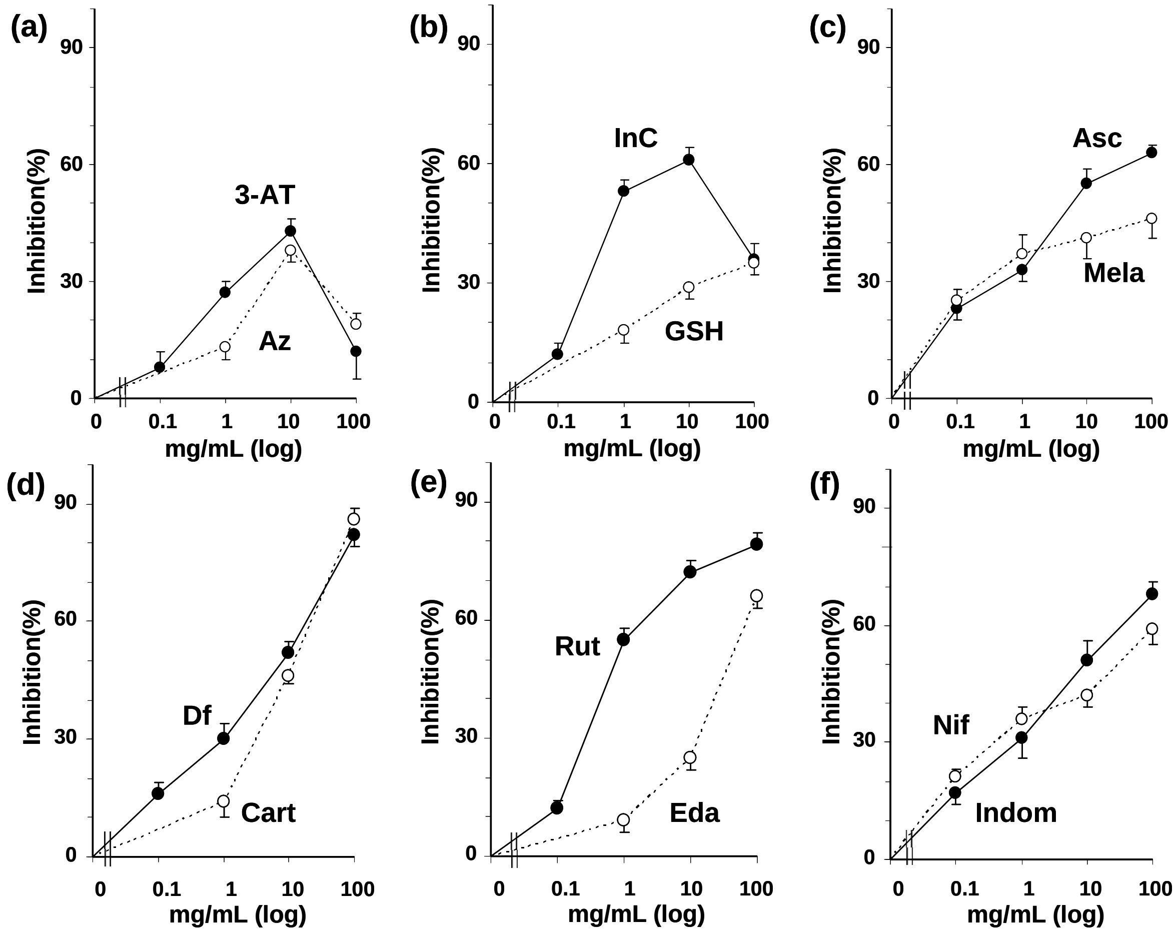

Figure 6. Inhibitory effects of various drugs on ROS generation induced by catalase under UVB irradiation. Drugs were suspended in 100 mM phosphate buffered solution (pH 7.4) containing 10 mg/mL Arabic gum, 25 μM catalase, and 3 mM DCFH•DA. Irradiation with UVB was carried out for 15 min at 37°C. 3-AT, 3-aminotriazole; Az, azide; InC, Indigocarmin; GSH, reduced glutathione; Asc, ascorbic acid; Mela, melanin; Df, diphenylisobenzofuran; Cart, β-carotene; Rut, rutin; Eda, edaravone; Nif, nifedipine; Indom, indomethacin. Bars indicate S.E. of the mean ($n = 3$).

Table 2. Summary of inhibitory effects of various drugs on catalase-mediated and UVB-induced ROS generation[a]

IC_{30} < 1 µg/mL	1 < IC_{30} < 10 µg/mL	10 < IC_{30} < 100 µg/mL
Melanin (0.2)	Diphenylisobenzofuran (2)*	GSH (12)
Indigo carmine (0.3)*	Coenzyme Q10 (2)	Edaravone (12)
Rutin (0.3)	β-Carotene (3)	Nimesulide (15)
Ascorbic acid (0.6)	Uric acid (3)	Cis-Pt (30)
α-Tocopherol (0.8)	Piroxicam (3)	NADH (100)
Indomethacin (0.8)	Diclofenac (3)	
	Oxyphenbutazone (3)	
	Ibuprofen (7)	
	Aspirin (8)*	
	Azide (8)*	
1000 µg/mL < IC_{30} (Weak or No-inhibitory drug)		
Cu, Zn-SOD, GSH•Px*, Mannitol, DMTU, Desferal, BHT, Propyl gallate, Fenofibrate, Dexamethasone, Verapamil, DetaNONOate		

[a] IC_{30} (30% inhibitory concentration) was obtained from the inhibition curve of the drug. IC_{30} is indicated as µg/mL in parentheses. Drugs that showed biphasic inhibition where inhibitions were lower at high concentrations are marked with an asterisk (*).

drugs that appeared to have physiological significance. To compare potencies, drug concentrations here are expressed in µg/mL. A catalase inhibitor, 3-amino-1,2,4 triazole (3-AT), had biphasic inhibition reaching a peak of 43% at 10 µg/mL. Heck *et al.* (*1*) reported 45% and 25% stimulation at 1 mM (84 µg/mL) and 0.1 mM (8.4 µg/mL), respectively. However, they apparently neglected the inhibitory effect below 0.1 mM, and the current data showed no stimulatory effect over 100 µg/mL (1.2 mM). The same inhibitor, 3-AT, was also tested at 1,000 µg/mL and was found to stimulate 35% of the ROS generation occurring with catalase and UVB (data not shown).

A similar biphasic inhibition resulted with another catalase inhibitor, sodium azide (Figure 6a). Indigo Carmine, which is believed to quench O_3, inhibited ROS generation, resulting in 53% and 63% generation at 1 and 10 µg/mL (= 0.021 mM), respectively. Its dose-inhibition curve was also bell-shaped (Figure 6b). Its ROS generation was 36% at 100 µg/mL. The ROS observed here might include ozone, even if its existence is just transient. Reduced glutathione (GSH) inhibited ROS generation, resulting in 35% generation at 100 µg/mL (= 0.33 mM) (Figure 6b). A general antioxidant, ascorbic acid, inhibited ROS in the current system in a dose-dependent manner, and melanin (a skin product induced by sunlight and a polymer of tyrosine) inhibited ROS more potently (Figure 6c). The $^1O_2$ scavenger diphenylisobenzofuran (*14*) was a strong inhibitor of ROS generation (Figure 6d); thus, $^1O_2$ may also participate in the generation of ROS in the current system. Beta-carotene is a strong $^1O_2$ scavenger (*11*), and its inhibition was also strong (Figure 6d). Rutin scavenges various ROS and was found to inhibit ROS effectively in the current system (Figure 6e). Edaravone (3-methyl-1-phenyl-2-pyrazolin-5-one), a radical scavenger that is generally believed to quench •OH radicals but may also react with other ROS, was effective especially in higher concentrations (Figure 6e). Both indomethacin, a non-steroidal anti-inflammatory (NSAID), and nifedipine (Nif, a Ca-entry blocker and anti-inflammatory drug) showed strong inhibitory effects, with similar dose-dependent inhibition curves (Figure 6f).

The IC_{30} values of the drugs determined are listed in Table 2. The strong inhibitory effects on ROS generation in the current system were detected as an IC_{30} of less than 1 µg/mL for five drugs, *i.e.* melanin, rutin, ascorbic acid, α-tocopherol, and indomethacine. Ten medications, including several other antioxidants and NSAIDs, had moderate suppressive effects with an IC_{30} of less than 10 µg/mL, followed by GSH and four other drugs with an IC_{30} of less than 100 µg/mL. In contrast, deta NONOate, a NO donor, and dexamethasone had no effect, showing that NO and steroidals may not inhibit ROS generated by catalase under UVB irradiation. Two antioxidants (BHT, propyl gallate) also had no capacity for suppressing ROS generation. An anti-lipidemic drug, fenofibrate, was not effective, along with verapamil, a non-dihydropyridine Ca-entry blocker. Some important drugs, marked with an asterisk in the table, had biphasic inhibition, the mechanism and significance of which have yet to be clarified.

Discussion

Catalase catalyzes H_2O_2 and ROOH to ($H_2O + O_2$) and (H_2O + ROH), respectively, in a reaction that consists of two steps mediated by the compound I (catalase-[O]). An assay of catalase solutions that are pure enough to yield negligible absorption at 230 to 250 nm can be performed spectrophotometrically (*15*). Catalase works as a tetramer of the same or almost the same subunit, and enzymatic activity can be maintained only when all subunits are active (*16*). The reason for this is unclear. Catalase can remove high concentrations of H_2O_2, in contrast to glutathione peroxidase (GSH•Px), which is believed to play a main role in eliminating low concentrations of H_2O_2 *in vivo*. Nevertheless, catalase contains one hard-bound NADPH per subunit that offers a reductive power to GSH•Px; therefore, this function of catalase cannot be ignored because of its importance at removing H_2O_2 *in vivo*. In fact, catalase has been reported to act as more of a primary defense against oxidative stress from H_2O_2 and UVB light than GSH•Px in human fibroblasts (*17*). UV light evidently generates ROS, but the species are unclear. Singlet oxygen is the most noted ROS generated by UV light (*18*); yet, at the same time $^1O_2$ also inactivates catalase (*19*). The discovery by Heck *et al.* (*1*) that catalase generates ROS despite its widely believed ability to reduce ROS (H_2O_2) was the first indication that catalase both removes and generates ROS. These contrasting reactions may occur depending on the concentrations of H_2O_2 and other ROS such as $^1O_2$. Recently, ROS generation by UV light and immunoglobulins has been highlighted (*2*). Immunoglobulins are reported to be antibacterial without binding to antigens. This concept could be enlarged to encompass catalase because this enzyme showed more ROS generation than IgG and both proteins specifically generated ROS under UVB (310 nm) irradiation (Figure 2). In terms of evolution, catalase is older than immunoglobulins if one is to speculate on the significance of a general host defense. However, catalase and IgG, and only high concentrations of Cu, Zn-SOD, BSA, myoglobin and FeSO4, generated ROS among the 20 compounds tested here (Table 1); catalase is worthy of consideration as an important specific source of ROS generation under UV light.

Because heat-inactivated catalase was inactive, a special peptide conformation of catalase appears to be important for ROS generation. Iron-containing cytochrome c, hematin, and hemin did not generate ROS. Ferrous iron, but not ferric iron itself, might increase this ROS generation slightly (Table 1). ROS generation was rather dependent on temperature, with generation occurring from 35-42°C (Figure 4). Catalase decreases in tumors (*20*), which might result in less in situ ROS generation by this enzyme, thus permitting tumor growth. Hyperthermia cancer therapy, which is generally carried out at 42°C, may possibly involve the effect of this increased ROS generation.

To ascertain whether UV light is specifically required for catalase to generate ROS, a separate experiment was performed in which UV irradiation was replaced with a typical radical initiator, 2,2'-azobis-2-1-amidinopropane (APPH) (*2*). This reagent works on unsaturated fatty acids, forming hydroperoxide (LOOH), malondialdehyde, or alkoxyl radical (LO•), but failed to generate ROS by reacting with catalase. AAPH (0, 50, 100 mM) with 25 μM catalase resulted in nearly the same absorption increase (0.56-0.60) (data not shown). Increased catalase (50 μM) also showed no difference, suggesting that AAPH had no effect on catalase-mediated ROS generation. Therefore, UV or visible light is essential for this ROS generation by catalase. However, what ROS are generated by UV light and catalase is unknown. A DCFH•DA oxidation method was used here to compare data with that from Heck *et al.* (*1*); this reagent is the best ROS detector but is not specific to a particular ROS. DCFH•DA does not detect H_2O_2 and lipid peroxides well because these reactions are very slow (*21*). DCFH•DA can be transformed to DCFH, which is oxidized by ROS to DCF. Here, DCF formed from DCFH•DA *in vitro* as a result of its reacting with mainly the •OH, peroxynitrite ($ONOO^-$), and the peroxyl radical (ROO•) must have been measured. Hypochlorite (OCl^-), $^1O_2$, O_2^-, and NO are weak at oxidizing DCFH to DCF. Less participation of $^1O_2$ in the oxidization of DCFH is reported (*22*). Bovine erythrocytes, Cu, Zn-SOD, and bacterial Mn-SOD did not generate much ROS under UV light (Table 1), even though Cu, Zn-SOD (SOD-1) have been reported to form •OH through co-existing H_2O_2 (*23*). Only catalase generated ROS under UVB irradiation; Cu, Zn-SOD, Mn-SOD and GSH•Px did not. DCFH•DA must indeed react with all ROS, but with different levels of reactivity. A catalase-UVB system might generate various ROS in numerous steps, creating chains or cycles among the ROS. If electron spin resonance (ESR) with a proper radical trap is used instead of DCFH•DA, O_2^- or •OH can be more specifically detected. However, their half-lives are limited and their roles in biological materials are not ROS-specific. In fact, there is little meaning in detecting these ROS to ascertain the role of catalase-generated ROS, and ESR methods cannot detect $^1O_2$, O_3, and H_2O_2. For now, the DCFH•DA method seems to be the best detector as it reacts with all kinds of ROS. Two •OH scavengers failed to inhibit catalase-generated ROS; therefore, •OH might not be one of the first ROS generated by catalase-UVB. ROS such as $^1O_2$ or O_3 could be among the first ROS generated and then be transformed to O_2^-, •OH, or the like. The increase of O.D. at 502 nm would be the sum of DCF formed by all of the ROS.

Effects of various ROS scavengers or antioxidants were examined in the system with 25 μM catalase under UVB (310 nm) irradiation. Catalase inhibitors 3-AT and sodium azide showed optimal inhibition of about 40% at 10 μg/mL (Figure 6a), but at higher concentrations stimulated ROS generation, as noted in a previous report (*1*). Therefore, the inhibitors had bell-shape (inhibited and increased) ROS generation. The H_2O_2, O_2^-, and •OH ratios may depend on the H_2O_2-decomposing capacity of catalase. Another possibility is unknown ROS generated in a milieu of 3-AT or sodium azide. •OH scavengers L-mannitol and dimethylthiourea (DMTU) showed neither inhibitory nor stimulatory effects on catalase's ROS generation (Table 2). In addition, the inhibition of ROS generation by Edaravone, noted to be a •OH scavenger (*24*), was not very potent especially in the lower concentration range. These results suggest that •OH might not be a major

ROS which is induced by catalase under UVB light. Determining any of the ROS from water induced by catalase and UVB as the main species might be difficult. On the other hand, Indigo Carmine, known to be a O_3 quencher (*6*), potently inhibited ROS generation but in a biphasic manner, suggesting that O_3 is one of the reactive species generated by catalase. The natural and intrinsic antioxidants ascorbic acid and α-tocopherol, which are reported to inhibit UV-induced human skin inflammation (*25*), effectively inhibited ROS generation in a dose-dependent manner (Table 2 and Figure 6). Melanin, a polymer of tyrosine that is produced in the skin by sunlight, was also found to be one of the most effective inhibitors among the drugs tested. Melanin may protect the skin against damage by UV light at least partly through its inhibitory effect on catalase-induced ROS generation, possibly in combination with antioxidative vitamins. Diphenylisobenzofuran and β-carotene are quenchers rather specific to $^1O_2$ and inhibited catalase-generated ROS (Figure 6d); though was less sensitive to DCFH•DA. Sodium azide is also known to be an effective scavenger of $^1O_2$ as well as a catalase inhibitor. $^1O_2$ should be considered a major ROS produced by catalase under UVB light.

The current authors previously reported (*7*) that IgG generated ROS under UV (280 nm) light irradiation for one hour. Interferon-γ and tumor necrotizing factor α, but not Cu, Zn-SOD, BSA, and histone, also increased absorption at 340 nm due to NADH oxidation as a result of UV irradiation, indicating ROS generation. ROS generation mediated by IgG was inhibited by dexamethasone, piroxicam, and dichlofenac but not by indomethacin (*7*). In this work, the NSAIDs tested, including piroxicam and dicrofenac, were found to be effective in the inhibition of catalase-induced ROS generation with UVB (310 nm) irradiation although their potencies differed. Indomethacin showed the strongest inhibitory effect and, in contrast, the steroidal dexamethasone had no effect (Table 2). Taken together, both catalase and IgG can generate ROS under UV light but probably *via* different mechanisms. The dihydropyridine Ca-entry blocker nifedipine, an anti-inflammatory, was a comparatively strong inhibitor of ROS generation (Figure 6f), while a non-dihydropyridine Ca-blocker, verapamil, showed no effect (Table 2). It appears that NSAIDs may generally inhibit ROS generation by catalase. NSAIDs are known to lower $^1O_2$ and H_2O_2 *via* the inhibition of NAD(P)H oxidase by macrophages (*8*) and leukocytes (*9*). The inhibitory effects of NSAIDs on catalase-induced ROS might need to be taken into account when considering their anti-inflammatory effects *in vivo*. The current results for antioxidants and anti-inflammatory drugs appear to be supported by several reports. Sulindac protected UVB-induced phototoxicity in the skin of SKH-1 hairless mice (*26*). Para-aminobenzoic acid scavenged ROS and protected DNA against UV and free radical damage *in vitro* (*18*). Salicylic acid protected catalase inactivation by damaging or substituting catalase-bound NADPH (*27*). Thus, investigating the relationship between catalase's ability to degrade H_2O_2 and generate ROS with other drugs in the future may prove interesting; this is especially true since the two contradictory actions might be influenced by factors such as the concentration of H_2O_2, the pH, and the lipophilicity of drugs. The site of initial ROS generation, which was reported to lie at the IGKD site for IgG (*4*), is likely to be important. IgG-UV-generated ROS are reported to be bactericidal without binding to antigens. The bactericidal effect of leucocytes may also be due to O_3 generated by antibodies (*28*). The current data is not sufficient grounds for speculation that catalase plays an important role in bactericidal or tumoricidal functions in skin or other organs; however, catalase's efficiency at generating ROS (five times that of IgG, Table 1) cannot be ignored. Catalase is, like IgG, also considered an evolutionarily important non-specific host defense tool.

In conclusion, catalase was found to be a unique protein that not only can decompose ROS (H_2O_2) but also efficiently generate ROS when specific energy such as UVB irradiation is supplied, although the major reactive species it generated have yet to be determined. ROS generation can be inhibited by numerous anti-inflammatory and antioxidative drugs. Natural antioxidants such as ascorbic acid, α-tocopherol, and melanin might play an important role in preventing damage due to possible catalase-induced ROS generation *in vivo*, and especially in the skin.

References

1. Heck DE, Vetrano AM, Mariano TM, Laskin JD. UVB light stimulates production of reactive oxygen species: Unexpected role for catalase. J Biol Chem 2003; 278:22432-22436.
2. Wentworth AD, Jones LH, Wentworth P Jr, Janda KD, Lerner RA. Antibodies have the intrinsic capacity to destroy antigens. Proc Natl Acad Sci USA 2000; 97:10930-10935.
3. Valkonen M, Kuusi T. Spectrophotometric assay for total peroxyl radical-trapping antioxidant potential in human serum. J Lipid Res 1997; 38:823-882.
4. Datta D, Vaidehi N, Xu X, Goddard WA 3rd. Mechanism for antibody catalysis of the oxidation of water by singlet dioxygen. Proc Natl Acad Sci USA 2002; 99:2636-2641.
5. Khan AD, Kovacis D, Kolbanovsky A, Desoi A, Frenkel K, Geacintov NE. The decomposition of peroxinitrite to nitroxyl anion (NO^-) and singlet oxygen in aqueous solution. Proc Natl Acad Sci USA 2000; 97:2984-2989.
6. Wentworth P, MacDann P Jr, Wentworth AD, Takeuchi C, Nieva J, Jones T, Bautista C, Ruedi JM, Gutierrez A, Janda KD, Babior BM, Eschenmoser A, Lerner RA. Evidence for antibody-catalyzed ozone formation and inflammation. Science 2002; 298:2195-2199.
7. Oyanagui Y, Taniguchi M, Iwata M, Murakami M. Inhibition of immunoglobulin G-catalyzed hydrogen

peroxide generation by dexamethasone and piroxicam. Life Sci 2003; 73:1333-1346.

8. Oyanagui Y. Inhibition of superoxide anion production in macrophages by anti-inflammatory drugs. Biochem Pharmaco 1976; 25:1473-1480.
9. Oyanagui Y. Inhibition of superoxide anion production in non-stimulated guinea pig peritoneal exudate cells by anti-inflammatory drugs. Biochem Pharmacol 1978; 27:777-782.
10. Morgan PE, Dean RT, Davies MJ. Protective mechanisms against peptide and protein peroxides generated by singlet oxygen. Free Radic Biol Med 2004; 36:484-496.
11. McCormick JP, Thomason T. Near-ultraviolet photooxidation of tryptophan. Proof of formation of superoxide ion. J Am Chem Soc 1978; 100:312-313.
12. Srivastava SK, Modak MJ. Rose bengal mediated inhibition of DNA polymerases: Mechanism of inhibition of avian myeloblastosis virus reverse transcriptase under photooxidative conditions. Biochemistry 1983; 22:2283-2288.
13. Brüne B, Schmidt KU, Ullrich V. Activation of soluble guanylate cyclase by carbon monoxide and inhibition by superoxide anion. Eur J Biochem 1990; 192:683-688.
14. Bus JS, Aust SD, Gibson JE. Superoxide- and singlet oxygen-catalyzed lipid peroxidation as a possible mechanism for paraquat (methyl viologen) toxicity. Biochem Biophys Res Commun 1974; 58:749-755
15. Chance B, Maehly AC. Assay of catalases and peroxidases, Methods Enzymol, Academic Press, New York, 1955; 136:764-775.
16. Aronoff S. Catalase: kinetics of photooxidation. Science 1965; 150:72-73.
17. Masaki H, Okano Y, Sakurai H. Differential role of catalase and glutathione peroxidase in cultured human fibroblasts under exposure of H_2O_2 or ultraviolet B light. Arch Dermatol Res 1998; 290:113-118.
18. Hu ML, Chen YK, Chen LC, Sano M. Para-aminobenzoic acid scavenges reactive oxygen species and protects DNA against UV and free radical damage. J Nutr Biochem 1995; 6:504-508.
19. Lledías F, Rangel P, Hansberg W. Oxidation of catalase by singlet oxygen. J Biol Chem 1998; 273:10630-10637.
20. Szatrowski TP, Nathan CF. Production of large amounts of hydrogen peroxide by human tumor cells. Cancer Res 1991; 51:794-798.
21. Halliwell B, Whiteman M. Measuring reactive species and oxidative damage *in vivo* and in cell culture: how should you do it and what do the results mean? Br J Pharmacol 2004; 142:231-255.
22. Bilski P, Belanger AG, Chignell CF. Photosensitized oxidation of 2',7'-dichlorofluorescin: singlet oxygen does not contribute to the formation of fluorescent oxidation product 2',7'-dichlorofluorescein. Free Radic Biol Med 2002; 33:938-946.
23. Sato K, Akaike T, Kohno M, Ando M, Maeda H. Hydroxyl radical production by H_2O_2 plus Cu, Zn-superoxide dismutase reflects the activity of free copper released from the oxidatively damaged enzyme. J Biol Chem 1992; 267:25371-25377.
24. Sueishi K, Mishima K, Makino K, Itoh Y, Tsuruya K, Hirakata H, Oishi R. Protection by a radical scavenger edaravone against cisplatin-induced nephrotoxicity in rats. Eur J Pharmacol 2002; 451:203-208.
25. Fuchs J, Kern H. Modulation of UV-light-induced skin inflammation by D-alpha-tocopherol and L-ascorbic acid: a clinical study using solar simulated radiation. Free Radic Biol Med 1998; 25:1006-1012.
26. Athar M, An KP, Tang X, Morel KD, Kim AL, Kopelovich L, Bickers DR. Photoprotective effects of sulindac against ultraviolet B-induced phototoxicity in the skin of SKH-1 hairless mice. Toxicol Appl Pharmacol 2004; 195:370-378.
27. Durner J, Klessig DF. Salicylic acid is a modulator of tobacco and mammalian catalases. J Biol Chem 1996; 271:28492-28501.
28. Babior BM, Takeuchi C, Ruedi J, Gutierrez A, Wentworth P Jr. Investigating antibody-catalyzed ozone generation by human neutrophils. Proc Natl Acad Sci USA 2003; 100:3031-3034.

(*Received December 6, 2007; Revised February 19, 2008; Accepted February 25, 2008*)

Drug Discov Ther 2008; 2(2):94-107.

Original Article

Formulation and hypoglycemic activity of pioglitazone-cyclodextrin inclusion complexes

Ahmed Abd Elbary[1], Mahfouz A. Kassem[2], Mona M. Abou Samra[2], Rawia M. Khalil[2,]*

[1] *Faculty of Pharmacy, Cairo University, Cairo, Egypt;*
[2] *Department of Pharmaceutical Technology, National Research Centre, Dokki, Cairo, Egypt.*

ABSTRACT: Pioglitazone is a thiazolidinedione derivative used for the treatment of type 2 diabetes. The drug's poor aqueous solubility and slow dissolution rate are the main causes of its limited therapeutic action in some cases. The aim of the present study is to formulate a more soluble product of pioglitazone at physiological pH. The potential interaction of pioglitazone with cyclodextrins and water-soluble polymers was investigated to enhance the drug's bioavailability and improve its efficacy. The interaction of pioglitazone with β-cyclodextrin, HP-β-cyclodextrin, and dimethyl-β-cyclodextrin was evaluated by spectrophotometric and solubility methods. Both methods revealed the formation of 1:1 inclusion complexes. The phase solubility diagram of pioglitazone-cyclodextrin systems with or without water-soluble polymers was classified as the AL type. The solubilization strength of cyclodextrins and the apparent stability constant of systems increased upon addition of water-soluble polymers. Inclusion complexes of pioglitazone in cyclodextrins with or without water-soluble polymers were prepared by the kneading method. Binary systems were characterized and confirmed by IR spectroscopy, X-ray diffractometry, and thermogravimetric analysis. The dissolution rates of pioglitazone, pioglitazone-cyclodextrin physical mixtures, pioglitazone-cyclodextrin complexes, and ternary systems containing water-soluble polymers were determined using a USP dissolution tester; results revealed enhanced dissolution properties of cyclodextrin complexes compared to drug and physical mixtures, and all of the ternary systems displayed higher dissolution efficiency than corresponding binary systems. The permeation of pioglitazone and pioglitazone-cyclodextrin complexes through a cellulose membrane with and without water-soluble polymers (PVP and HPMC) present increased and the release pattern follows the kinetics of a Higuchi equation. Assessment of the hypoglycemic effect of the free drug and its cyclodextrin complexes in normal rats *via* measurement of blood glucose levels (BGL) after administration of a single oral dose revealed that the hypoglycemic effect of pioglitazone-cyclodextrin complexes was greater than that of the free drug and that a pioglitazone-DM β-cyclodextrin complex had the greatest effect. In conclusion, the physicochemical and biological properties of pioglitazone improved as a result of complexation with cyclodextrins, and the improvement of physicochemical properties was more prominent after water-soluble polymers were associated with pioglitazone-cyclodextrin systems.

Keywords: Cyclodextrins, Water-soluble polymers, Dissolution rate, Complexation, Solubility

1. Introduction

Type 2 diabetes is the most prevalent form of diabetes mellitus. Approximately 90% of diabetic cases are the non-insulin-dependent phenotype (*1*). Impaired insulin secretion and resistance to the action of insulin, rather than an absolute insulin deficiency, characterize patients with type 2 diabetes.

Thiazolidinediones (TZDs) are a new class of oral antidiabetic agents that act to improve insulin sensitivity and decrease the insulin resistance of peripheral tissues (*2*). Newer TZDs such as pioglitazone are now available and have been approved by health authorities worldwide for use in patients with inadequate glycemic control (*3*). Pioglitazone decreases insulin resistance in the periphery and in the liver, resulting in increased insulin-dependent glucose disposal and decreased hepatic glucose output. Pioglitazone is a potent and highly selective agonist for peroxisome proliferator-activated receptor gamma (PPARγ). PPAR receptors are found in tissues critical to insulin action such as adipose tissue, skeletal muscle, and the liver. Activation of PPARγ nuclear receptors modulates the transcription

---

**Correspondence to:* Dr. Rawia M. Khalil, National Research Centre, Department of Pharmaceutical Technology, Cairo, Egypt;
e-mail: rawia_khalil@yahoo.com

of a number of insulin-responsive genes involved in the control of glucose and lipid metabolism (*4,5*).

Pioglitazone is a drug that is essentially water-insoluble. The poor aqueous solubility and slow dissolution rate of the drug may have a negative impact on its bioavailability and subtherapeutic plasma drug levels and may lead to therapeutic failure in some cases.

Drug-cyclodextrin complexation is an important approach for development of oral drug delivery systems. The addition of cyclodextrins increases the water solubility of several poorly water-soluble substances; in most cases this results in improving a drug's bioavailability and increasing its pharmacological effect, allowing a reduction in the dose of the drug administered and decrease in side effects (*6*). Cyclodextrins have been used to optimize the bioavailability of many oral anti-diabetic drugs (*7,8*).

Moreover, the complexation efficiency and solubilizing effect of cyclodextrins in aqueous solutions have been increased by adding water-soluble polymers (*9*). This strategy is a useful way to decrease the amount of cyclodextrin needed in oral dosage form and decrease cost and toxicity, thus increasing the pharmaceutical usefulness of cyclodextrins.

The main goal of this study was to improve the biological performance of pioglitazone by inclusion complexation of the drug in cyclodextrins.

2. Materials and Methods

2.1. *Materials*

Pioglitazone, Hera, Hyderabad, India was kindly donated by Medical Union Pharmaceutical, Abu-Sultan, Ismailia, Egypt. β-cyclodextrin (β-CD), Heptakis (2,6-Di-*O*-methyl)-β-cyclodextrin (DM-β-CD, MW 1331.4), hydroxypropyl-β-cyclodextrin (HP-β-CD, MW 1380), and hydroxypropyl methylcellulose were purchased from Sigma-Aldrich, St. Louis, USA. Polyvinylpyrrolidone (K-30) was purchased from Sisco Research Laboratories (Bombay, India). Methanol, sodium dihydrogen phosphate, citric acid, and hydrochloric acid were all analytical grade.

2.2. *Elucidation of the stoichiometric ratio of Pioglitazone cyclodextrin complexes*

Using spectrophotometric measurements, the stoichiometric ratio of pioglitazone-cyclodextrin complexes was determined using the continuous variation method (*10*).

2.3. *Effect of cyclodextrins on the solubility of pioglitazone with and without water-soluble polymers*

Phase solubility studies for both binary and ternary systems were carried out according to the method of Higuchi and Connors (*11*). An excess amount of pioglitazone was added to different concentrations of cyclodextrins in distilled water with or without a fixed PVP concentration of 0.25% (w/v) or fixed HPMC concentration of 0.1% (w/v). All glass containers were sealed; for ternary systems, containers were heated in an autoclave at 120ºC for 20 min. All suspensions obtained were shaken at 25 ± 0.5°C until reaching equilibrium (about 72 h). Filtration of all suspensions was carried out through Millipore filters (0.45 µm), and filtrates were spectrophotometrically analyzed for drug content at 266 nm.

2.4. *Preparation of pioglitazone-cyclodextrin physical mixtures*

In accordance with the stoichiometric ratio of the complexes (1:1), a homogenous blend of pioglitazone and cyclodextrin derivative was prepared by mixing using a porcelain mortar. The mixture was then sieved through a 250-µm sieve.

2.5. *Preparation of pioglitazone-cyclodextrin complexes*

Using the kneading method (*12*), complexes of pioglitazone in cyclodextrins were prepared; pioglitazone was added to cyclodextrin in a molar ratio equivalent to its corresponding stoichiometric ratio in the complex (1:1) and then kneaded thoroughly with a minimal amount of water to obtain a paste. The paste was then dried under vacuum at room temperature in the presence of phosphorus pentoxide as a drying agent. The dried mass was pulverized and sieved through a 250-µm sieve.

2.6. *Preparation of pioglitazone-cyclodextrin-polymer complexes*

Ternary systems consisting of pioglitazone, cyclodextrin, and a water-soluble polymer were prepared by the kneading method. Two water soluble polymers were used, namely PVP and HPMC in respective concentrations of 0.25% and 0.1% (w/v). Pioglitazone and cyclodextrins were used in a molar ratio of 1:1. The three components were kneaded thoroughly with a minimal amount of water. The paste formed was then dried under vacuum at room temperature in the presence of phosphorus pentoxide as a drying agent. The dried mass was pulverized and sieved through a 250-µm sieve.

2.7. *Characterization of pioglitazone-cyclodextrin complexes*

2.7.1. *X-ray diffractometry*

The x-ray diffractometer patterns of pioglitazone, physical mixtures, and complexes were obtained using a Diano X-ray diffractometer equipped with CoK α. The tube operated at 45 kV, 9 mA.

2.7.2. *Infrared spectroscopy*

Infrared spectra of pioglitazone, cyclodextrin derivatives, physical mixtures, and complexes were determined as KBr discs using a Shimadzu 435 U-04 IR spectrophotometer.

2.7.3. *Thermal measurement*

Using a thermogravimetric technique (TGA), the stability and thermal behavior of pioglitazone, physical mixtures, and complexes were determined. A TGA scan was carried out using a computerized Perkin Elmer TGA series under a dynamic N2 purging gas atmosphere at a constant rate of 50 mL/min and a heating rate of 5°C/min.

2.8. *In vitro dissolution studies*

Using the USP Dissolution Tester Apparatus 1 (rotating basket), the dissolution of pioglitazone was assessed; dissolution media were 900 mL of 0.1 N HCl (pH 1.2 simulating gastric pH), citrate, or phosphate buffers (pH 4.6 and 6.8 simulating duodenal and intestinal pH values) at a rotation rate of 50 rpm. Powder samples containing 30 mg of pioglitazone or an equivalent amount of complex or physical mixtures with cyclodextrins in were prepared using transparent hard gelatin capsules (number 0). Aliquots of 5 mL each were withdrawn from the dissolution medium at intervals of 15, 30, 60, 90, and 120 min and replaced by an equal volume of fresh dissolution medium. The samples were filtered through Millipore filters (0.45 µm) and analyzed for pioglitazone content by measuring its absorbance at 266 nm using fresh dissolution medium as a blank. Experiments for each dissolution study were carried out in triplicate.

2.9. *Effect of cyclodextrins on the permeation of pioglitazone through a cellulose membrane with and without water-soluble polymers present*

The permeation of pioglitazone and its cyclodextrin complexes with or without water-soluble polymers through a semipermeable cellulose membrane (dialysis tubing, high retention seamless cellulose tubing, 12,000 daltons) was investigated. The cellulose membrane was placed in Franz-type diffusion cells; the surface area of membrane in the diffusion cells was 5 cm^2. The receptor phase consisted of 60 mL phosphate buffer solution (PBS) (pH 7.4) containing cyclodextrin (0.5%, w/v) as a solubilizing agent for permeated pioglitazone. The receptor phase was sonicated under vacuum prior to usage to remove dissolved air. The membrane of diffusion cells was stirred with a magnetic bar and kept at 37ºC by circulating water through an external jacket. The donor phase consisted of a 10 mL aqueous suspension or solution of 30 mg pioglitazone or its equivalent amount of pioglitazone-cyclodextrin complexes with or without water-soluble polymers. The aqueous solutions contained pioglitazone-cyclodextrin complexes and 0.25% (w/v) PVP or 0.1% (w/v) HPMC. Water-soluble polymers were heated in an autoclave (120ºC for 20 min) before use. Samples of receptor fluid (2 mL) were withdrawn at various intervals up to 4 h and replaced with fresh buffer solution. The samples were analyzed spectrophotometrically at 266 nm.

2.10. *Effect of complexation with cyclodextrins on the hypoglycemic efficacy of pioglitazone in normal rats*

2.10.1. *Animals*

Male Albino rats (150-250 g) purchased from the animal house of the National Research Center were used in the experiment. They were kept for one week in the laboratory before the experiment for acclimatization to laboratory conditions and were given a standard diet and water. Prior to experimental treatments, animals fasted overnight but were allowed free access to water. Ten animals were used for each study group.

2.10.2. *Determination of the blood glucose levels*

Blood glucose concentrations (mg/100 mL) were determined using a glucometer (Dr-gluco) with electrochemical biosensors. Blood samples were collected from the orbital sinus of the animal.

2.10.3. *Protocol*

The fasting blood glucose level of each animal was determined at the beginning of the experiment, *i.e.* after overnight fasting with free access to water. Animals in the control group received 0.5% carboxy-methyl cellulose (CMC) only. The test groups of animals were treated with the test samples suspended in the same vehicle in a parallel group design. Intragastric tubing was used to administer a single dose of 10 mg/kg of the free drug or the equivalent amount of complexes. Blood samples were collected at 2, 4, 6, 8, 10, 24 h after the oral administration of test samples.

Hypoglycemic response was evaluated as a percentage decrease in blood glucose levels (BGL) calculated as follows:

$$\textbf{\% decrease in BGL} = \frac{[\textbf{BGL at } t = 0] - [\textbf{BGL at } t]}{[\textbf{BGL at } t = 0]} \times 100$$

The pharmacodynamic parameters taken into consideration were the maximum percentage decrease in BGL, time of maximum percentage decrease in BGL(t_{max}), and area under the percentage decrease in BGL versus time curve ($AUC_{0\text{-}24\ h}$), which was calculated using the trapezoidal rule (*13*). Other parameters were also considered when assessing the duration of drug action such as mean residence time

(MRT) and time of half-peak percentage decrease in BGL ($t_{½p}$).

Statistical analysis of the results was performed using one-way analysis of variance (ANOVA), followed by a least-significance test (LSD). This statistical analysis was computed with SPSS software.

3. Results and Discussion

3.1. *Elucidation of the stoichiometric ratio of pioglitazone-cyclodextrin complexes*

The absorbance values of solutions with a fixed total concentration (0.048 mM) and containing different mole fractions of pioglitazone and β-CD, HP-β-CD, and DM-β-CD were measured at 266 nm. Results revealed that the absorbance values of these solutions were not equivalent to the sum of the corresponding values of their components. This serves as evidence of complex formation between pioglitazone and these cyclodextrins. The calculated absorbance differences were plotted against mole fractions (Figure 1). For constant total concentration of the two species of complex, the complex is in its greatest concentration at the point where the two species are combined at the ratio in which they occur in the complex. Figure 1 shows that maximum extent of sharp changes in absorbance occurs at a mole fraction of 0.5, indicating the formation of an equimolecular complex (1:1) between pioglitazone and β-CD, HP-β-CD, and DM-β-CD.

3.2. *Effect of cyclodextrins on the solubility of pioglitazone with and without water-soluble polymers present*

The effect of cyclodextrins, namely, β-CD, HP-β-CD, and DM-β-CD, on the solubility of pioglitazone in distilled water at 25ºC was investigated. Figures 2 and 3 reveal that the aqueous solubility of pioglitazone increased linearly as a function of increasing cyclodextrin concentration. The phase-solubility diagram was classified as an AL type, which indicates the formation of 1:1 pioglitazone-cyclodextrin complexes over the investigated range of cyclodextrin concentration. The slope values in all diagrams were less than one, suggesting the formation of 1:1 complexes in solution and allowing the calculation of apparent stability constants of the drug complexes. The apparent stability constants (K_C) of these complexes were calculated from the slopes and intercept of the straight lines of the phase-solubility diagram according to the following equation (*11*):

$$K_C = \frac{\textbf{slope}}{\textbf{S}_0\textbf{(1-slope)}}$$

where S_0 is the solubility of pioglitazone in water at 25°C (2 M × 10^{-4}) with no cyclodextrins present. The stability constant values for the investigated cyclodextrin complexes were computed and found to be 464.92 M^{-1}, 381.44 M^{-1}, and 567.00 M^{-1} for β-CD, HP-β-CD, and DM-β-CD, respectively. Equimolecular complexes with DM-β-CD were found to be the most stable, followed by β-CD and HP-β-CD. The lower value for the complex stability constant observed for HP-β-CD than for β-CD suggested that the presence of a hydroxypropyl substituent could interfere with the inclusion of the drug into the cyclodextrin cavity

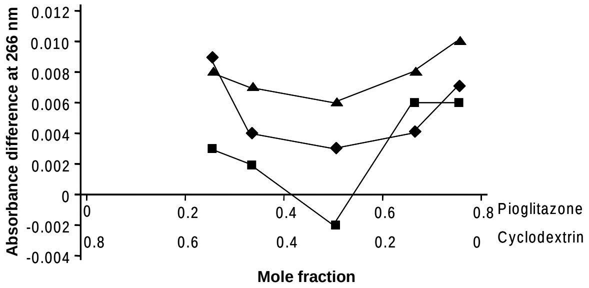

Figure 1. Elucidation of the stoichiometric ratio of pioglitazone-cyclodextrin complexes spectrophotometrically: Pioglitazone-β-CD complex (♦); Pioglitazone-HP-β-CD complex (■); Pioglitazone-DM-β-CD complex (▲).

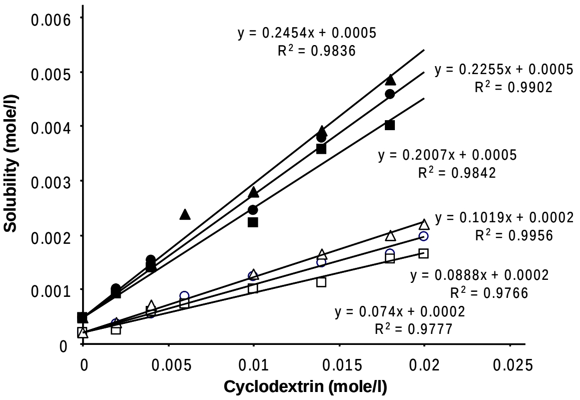

Figure 2. Effect of cyclodextrins on the solubility of pioglitazone in absence or presence of (HPMC): Pioglitazone-β-CD system (○); Pioglitazone-HP-β-CD system (□); Pioglitazone-DM-β-CD system (Δ); pioglitazone-β-CD-HPMC system (●); Pioglitazone-HP-β-CD-HPMC system (■); Pioglitazone-DM-β-CD-HPMC system (▲).

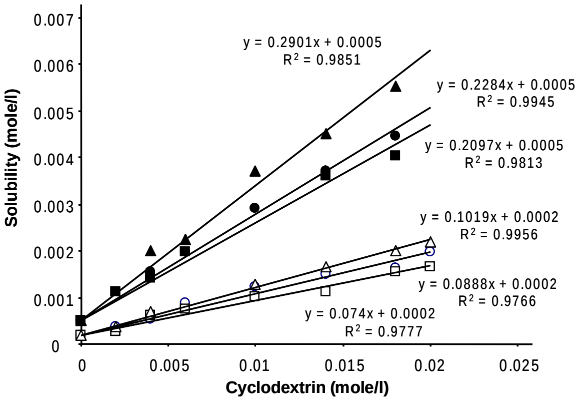

Figure 3. Effect of cyclodextrins on the solubility of pioglitazone in absence or presence of (PVP): pioglitazone-β-CD system (○); Pioglitazone-HP-β-CD system (□); Pioglitazone-DM-β-CD system (Δ); pioglitazone-β-CD-PVP system (●); Pioglitazone-HP-β-CD-PVP system (■); Pioglitazone-DM-β-CD-PVP system (▲).

because of the partial obstruction of its opening (*14*). An analogous phenomenon was previously observed for other drugs such as ibuprofen (*15*), ibuproxam (*16*), nicardipine hydrochloride (*17*) and glyburide (*18*). The increment of pioglitazone solubility seems to be related to the inclusion ability of the cyclodextrin molecules in water. The solubilization strength of the investigated cyclodextrins with respect to the drug, calculated as moles pioglitazone solubilized per mole of cyclodextrin, reveals that the solubilization strength of cyclodextrins decreases in the following order: DM-β-CD > β-CD > HP-β-CD.

Figures 2 and 3 reveal that the addition of water-soluble polymers to the cyclodextrin solution did not change the type of phase solubility diagram (AL type) obtained for binary systems. *K*c values in the presence of water-soluble polymers were found to be 592.01, 530.68, and 819.49 M^{-1} for pioglitazone-β-CD, pioglitazone-HP-β-CD, and pioglitazone-DM-β-CD, respectively, in the presence of PVP; these values were 594.19, 512.44, and 663.68 M^{-1} for pioglitazone-β-CD, pioglitazone-HP-β-CD, and pioglitazone-DM-β-CD, respectively, in the presence of HPMC. These results are in agreement with the previous finding obtained by other authors (*19-21*) who demonstrated that the addition of small amounts of water-soluble polymers has improved the complexing and solubilizing efficiency of cyclodextrins. The observed enhancement of K_C upon the addition of polymers shows that they are able to interact in a different way with drug-cyclodextrin binary complexes depending on their structures; this is because the polymers can interact differently with cyclodextrin and drug molecules such as hydrophobic bonds, Van der Waals dispersion forces, or hydrogen bonds (*22*).

3.3. *Characterization of pioglitazone-cyclodextrin complexes*

3.3.1. *X-ray diffractometry (XRD)*

Figure 4 shows the powder x-ray diffraction patterns of pioglitazone and its cyclodextrin complexes. The x-ray pattern of free pioglitazone revealed a drug fingerprint with intense and sharp peaks, indicating its crystalline nature.

The diffraction pattern for the complex differs significantly from that of each constituent and constitutes a new solid phase. Some peaks disappeared,

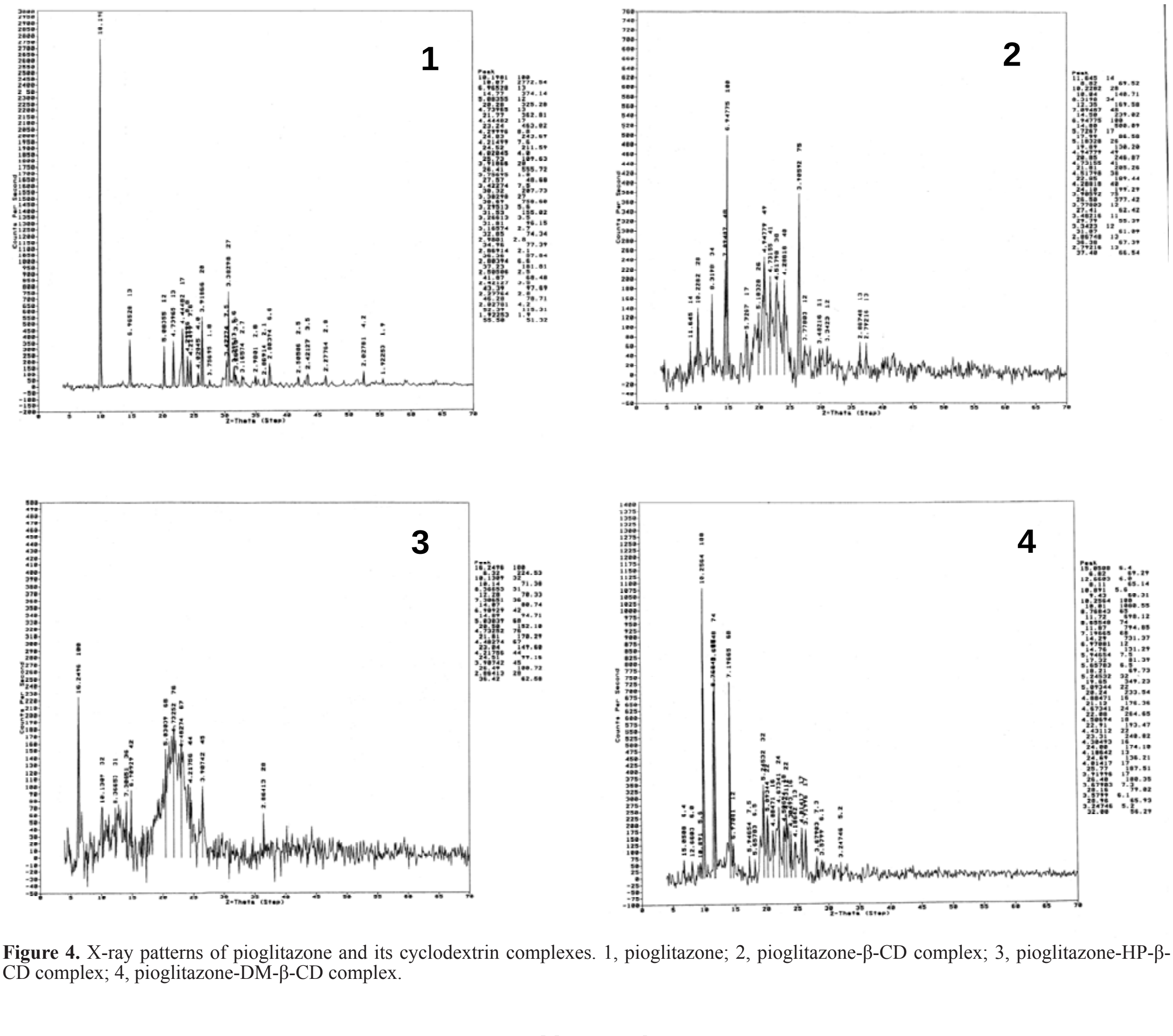

Figure 4. X-ray patterns of pioglitazone and its cyclodextrin complexes. 1, pioglitazone; 2, pioglitazone-β-CD complex; 3, pioglitazone-HP-β-CD complex; 4, pioglitazone-DM-β-CD complex.

some new peaks appeared, and the height of some peaks decreased. A reduction in crystallinity was observed in complexes with all investigated cyclodextrins. Crystallinity was determined by comparing the heights of several representative peaks in the diffraction patterns of the binary systems with those of a reference. The relationship used for calculation of crystallinity was the relative degree of crystallinity (RDC), as indicated by:

$$RDC = Is/Ir$$

where Is is the peak height of the sample under investigation and Ir is the peak height at the same angle for the reference with the highest intensity (*23*). Free drug peaks at 10.07, 24, and 26.4 (2θ) were used as a reference to calculate the RDC of kneaded and physical mixture binary systems (Table 1). A reduction in crystallinity was observed in the complexes; all investigated cyclodextrins had reduced diffraction peaks attributable to a new solid phase with low crystallinity, thus indicating inclusion complex formation with these cyclodextrins (more water-soluble) (*24*). The reduction in RDC values for pioglitazone-cyclodextrin complexes in comparison to the corresponding physical mixtures could be explained by the presence of reciprocal interaction in the solid state between host and guest, namely the formation of mixed particles during the drying process (*25*).

3.3.2. *Infrared spectroscopy*

The IR spectrum of pioglitazone (Figures 5-7) reveals the presence of a peak at 3083 cm^{-1} due to N-H stretching while peaks at 2928 and 2741 cm^{-1} corresponded to CH stretching. Strong absorption peaks observed at 1742 and 1685 cm^{-1} were assigned to drug carbonyl stretching vibration (C=O). A peak at 1608 cm^{-1} indicates the aromatic ring and a peak at 1242 cm^{-1} is due to C-O-Ar group. The rest of the fingerprint absorption bands appear at 1176.21, 1148.12, 1038.21, 930.61, 872.6, 850.03, 790.23, 711.8, 738.56, 659.21, 584.91, 602.22, and 519.59 cm^{-1}.

The IR spectrum of the investigated cyclodextrins is characterized by intense bands at 3300-3500 cm^{-1} due to OH stretching vibrations. The vibration at CH and CH_2 groups appears in the 2800-3000 cm^{-1} region. As can be seen in the spectral pattern of the physical mixture, it corresponds simply to superposition of the IR spectra of the two components.

The IR spectra of pioglitazone-cyclodextrins complexes have considerable differences in comparison to those of their corresponding constituents. A decrease in frequency of a specific peak is generally seen on complexation, indicating an ordering of the molecule (*26,27*). In IR spectrum of pioglitazone-cyclodextrin complexes, the amide-NH stretching vibration at 3,083 cm^{-1} was not detected; a broad band that might be due to co-occurrence of the N-H band of the drug did

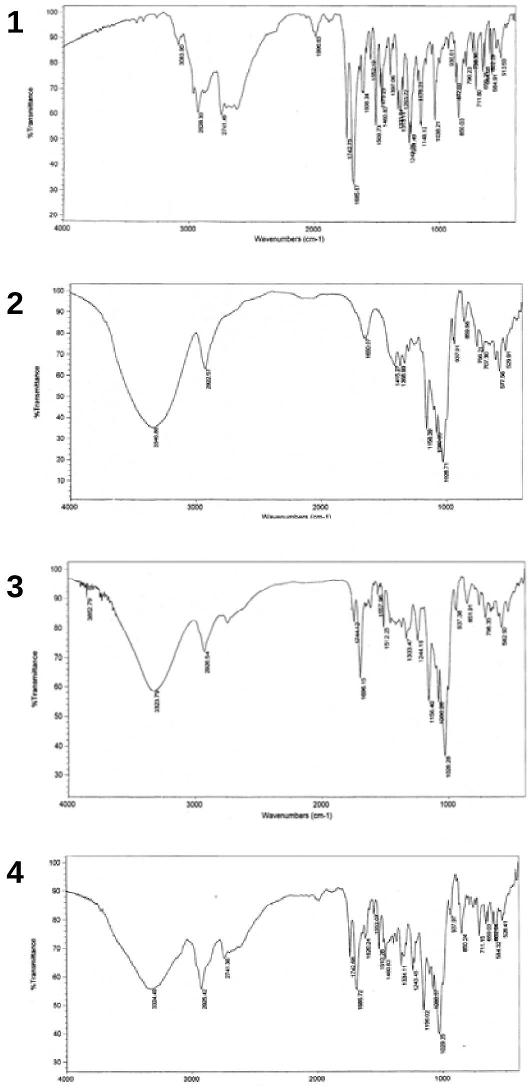

Figure 5. IR spectra of pioglitazone and pioglitazone-β-CD systems. 1, pioglitazone; 2, β-CD; 3, pioglitazone-β-CD complex; 4, pioglitazone-β-CD physical mixture.

Table 1. Relative degree of crystallinity (RDC) of pioglitazone-cyclodextrin complexes and pioglitazone-cyclodextrin physical mixtures

Pioglitazone-cyclodextrin systems	RDC at (2θ)		
	10.07°	24°	26.4°
Piog-β-CD complex	0.05075	0.818	0.679
Piog-HP-β-CD complex	0.0257	0.407	0.181
Piog-DM-β-CD complex	0.3897	0.714	0.325
Piog-β-CD physical mixture	0.3548	1.310	1.507
Piog-HP-β-CD physical mixture	0.19279	0.607	0.424
Piog-DM-β-CD physical mixture	0.4614	0.805	0.973

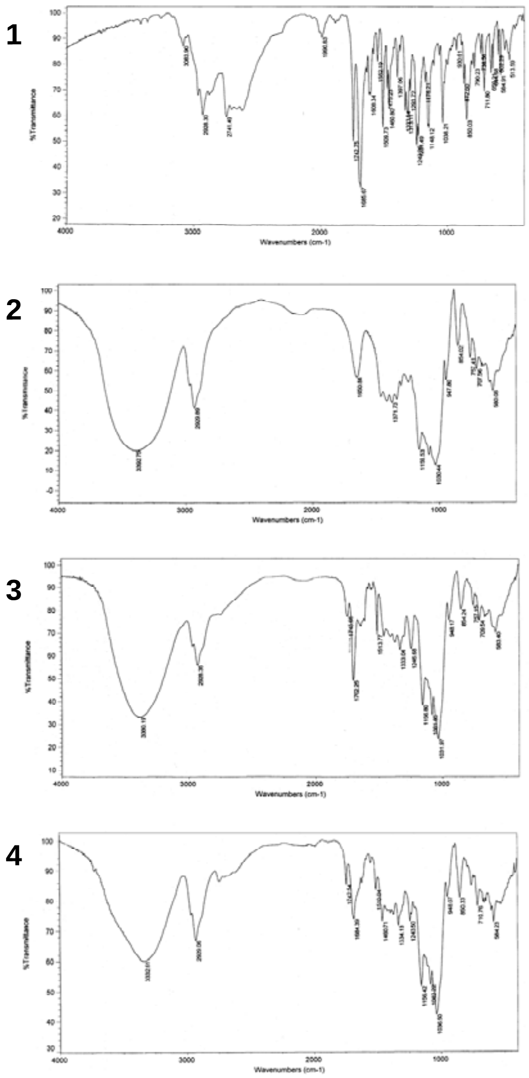

Figure 6. IR spectra of pioglitazone and pioglitazone-HP-β-CD systems. 1, pioglitazone; 2, HP-β-CD; 3, pioglitazone-HP-β-CD complex; 4, pioglitazone-HP-β-CD physical mixture.

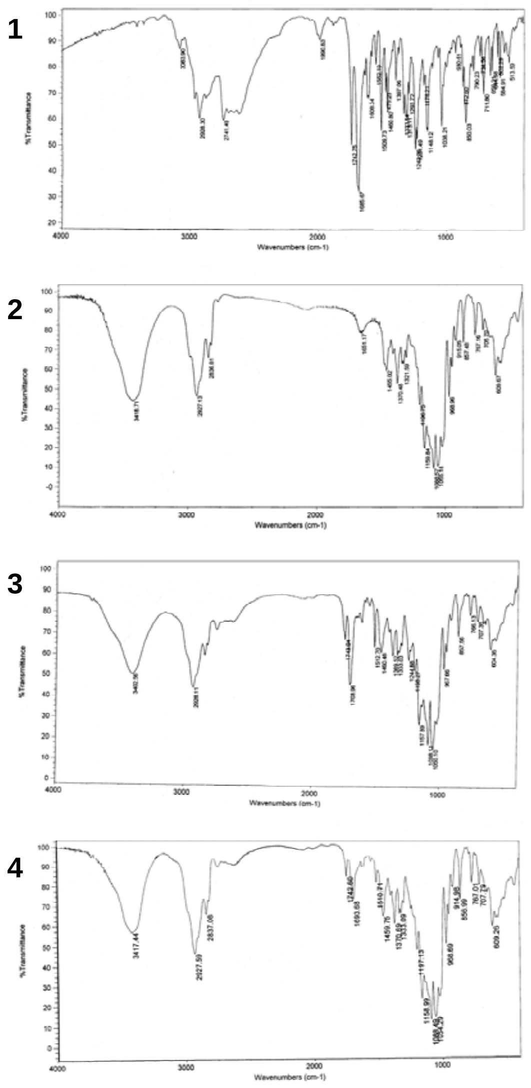

Figure 7. IR spectra of pioglitazone and pioglitazone-DM-β-CD systems. 1, pioglitazone; 2, DM-β-CD; 3, pioglitazone-DM-β-CD complex; 4, pioglitazone-DM-β-CD physical mixture.

appear with the OH intensified band of cyclodextrins at 3327-3425 cm^{-1}. This indicates a strong interaction and complex formation of pioglitazone with cyclodextrins. The absorption band that appears at 1685.07 cm^{-1} due to carbonyl groups of pioglitazone broadened and shifted to a higher wave number for pioglitazone-CD complexes as follows: 1696.15 cm^{-1} for pioglitazone-β-CD, 1702.25 cm^{-1} for pioglitazone-HP-β-CD, and 1703.96 cm^{-1} for pioglitazone-DM-β-CD. The intensities of the bands appearing at 1724.75, 1608.34, 1509.73, 1460.80, and 1242 cm^{-1} were also affected by such an interaction.

All these modifications clearly indicate the presence of host-guest interaction and the formation of stable hydrogen bonds between pioglitazone and cyclodextrins; this is because spectral changes always involve the C-OH, CH_2, and CH groups of the cyclodextrins (*28,29*).

3.3.3. *Thermo gravimetric analysis (TGA)*

Thermo-gravimetric analysis (TGA) was carried out to investigate the thermal stability of pioglitazone-cyclodextrin complexes (Figures 8-10). As is clear from TGA thermo-grams of the cyclodextrins investigated, the weight change due to water loss was 13.294% for β-CD, 4.56% for HP-β-CD, and 0.503% for DM-β-CD and occurred up to a temperature of 130°C. This water content within the cavity of the cyclodextrins molecules stabilizes their ring structure (*30*).

Figures 8-10 show the TGA curves of free pioglitazone; in these curves a maximum rate of weight loss was observed at 308.96°C; this indicated a thermal event due to melting and was associated with a 67.49% loss in weight. A second thermal event was observed at 504°C. For pioglitazone-cyclodextrins complexes, weight change due to water loss from the cyclodextrins cavities occurs up to 130°C. The complexation of pioglitazone with cyclodextrins was accompanied by weight loss, and the temperature of the maximum weight loss differed from that of the drug.

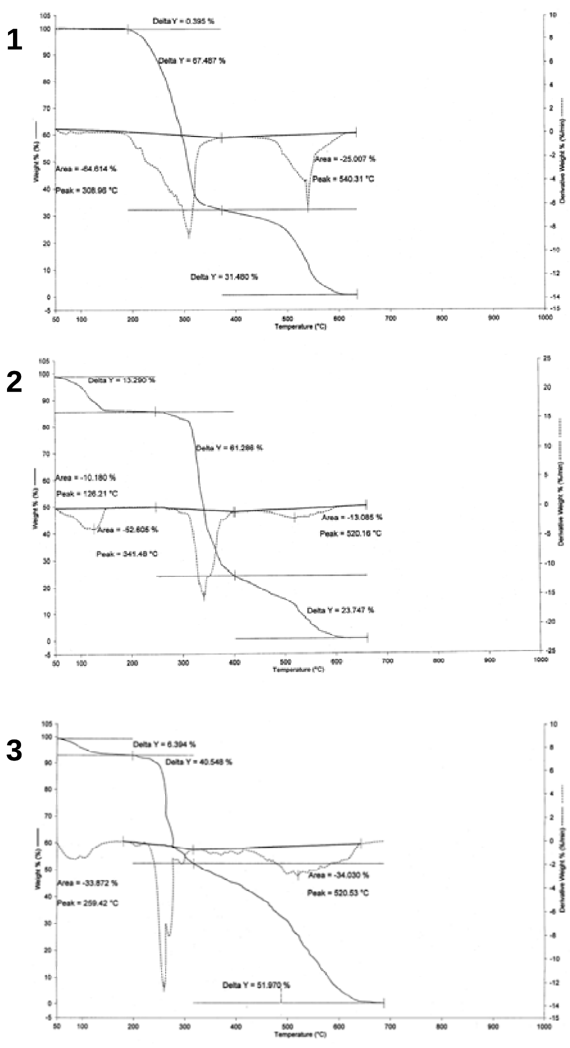

Figure 8. TGA thermograms of pioglitazone and pioglitazone-β-CD systems. 1, pioglitazone; 2, β-CD; 3, pioglitazone-β-CD complex.

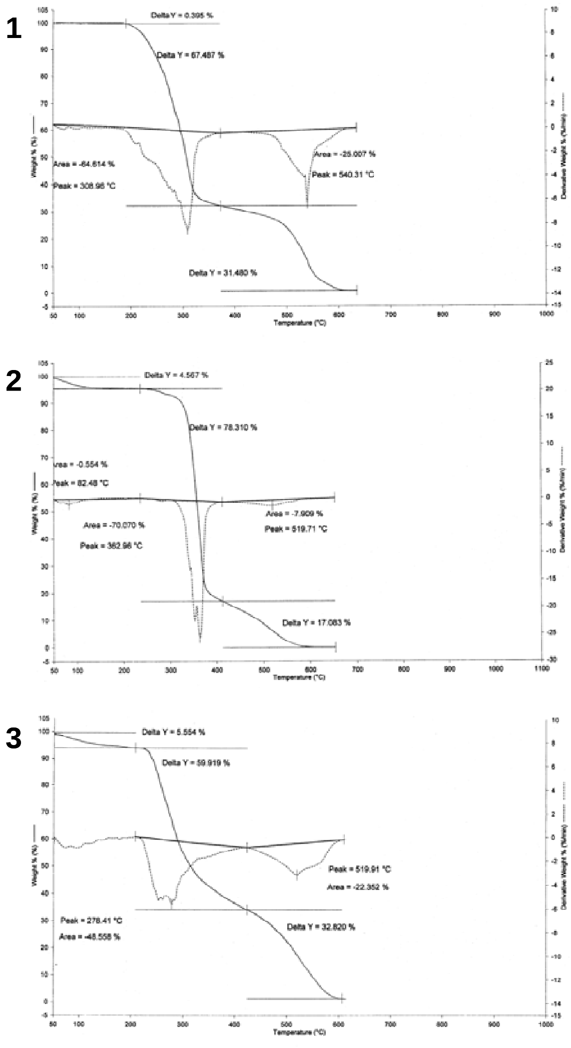

Figure 9. TGA thermograms of pioglitazone and pioglitazone-HP-β-CD systems. 1, pioglitazone; 2, HP-β-CD; 3, pioglitazone-HP-β-CD complex.

For a pioglitazone-β-CD complex, a maximum rate of weight loss occurred at 259.4°C (40.53% weight loss). Additional thermal events are observed within the temperature range of 278°C up to 300°C. For pioglitazone-HP-β-CD, a maximum rate of weight loss appeared at 278.41°C (weight loss: about 59.911%). For DM-β-CD, a maximum rate of weight loss appeared at 401.44°C (79.35% weight loss). This indicates that complexation induced changes in the thermal behavior of the drug.

Based on this information, pioglitazone decomposed at 308.96°C before it was included in DM-β-CD but an inclusion complex in DM-β-CD decomposed at 401.44°C. These findings show that the thermal stability of pioglitazone improved when it was included in DM-β-CD. The complexation of pioglitazone with cyclodextrins was accompanied by a change in the rate of decomposition of the drug, which clearly indicates the existence of new compounds in the solid state and points to inclusion of the drug in cyclodextrins.

3.4. *Effect of cyclodextrins on the dissolution rate of pioglitazone with and without water-soluble polymers present*

Figure 11 shows that the dissolution of pioglitazone in acidic medium (0.1 N HCl, pH 1.2) was incomplete even after 120 min. All the binary systems with cyclodextrins displayed better dissolution properties than pioglitazone alone, being immediately dispersed and completely dissolved within 15 min. As expected, Figures 12 and 13 demonstrate that all preparations had a lower percentage of drug dissolved at duodenal and intestinal pH values (citrate buffer, pH 4.6, and phosphate buffer, pH 6.8) in comparison to gastric fluid 0.1 N HCl (pH 1.2). The dissolution rate decreased with the increasing pH (4.6 to 6.8) of the dissolution medium. Evident from Figures 12 and 13 is the fact that the dissolution rate of the drug is enhanced in presence of cyclodextrins and that the dissolution rate of the prepared complexes is higher than that of the corresponding physical mixtures. In all cases, DM-β-CD had a greater effect on enhancing the dissolution rate of the drug. The inclusion complexation of pioglitazone in cyclodextrins increased the dissolution rate of the drug in the following order: DM-β-CD > HP-β-CD > β-CD. This result coincides with the water solubility of these cyclodextrins (*31*).

The heightened effectiveness of DM-β-CD can be explained on the basis of its greater water solubility and greater ability to amorphize, wet, solubilize, and complex pioglitazone in a solid state. The increase in drug dissolution rate observed for physical mixtures may be mainly attributed to the hydrophilic effect of the carriers, which can reduce the interfacial tension between the poorly soluble drug and the dissolution medium, thus leading to a higher dissolution rate (*32*). As is well known, the mere presence of a hydrophilic carrier cannot improve the dissolution properties of the drug, also requiring the participation of several factors such as increase in particle surface, formation of a soluble complex, changes in crystallinity or amorphization, and a significant dispersion degree in a hydrophilic carrier.

Thus, negligible improvement was registered for the physical mixtures, whereas the kneading method

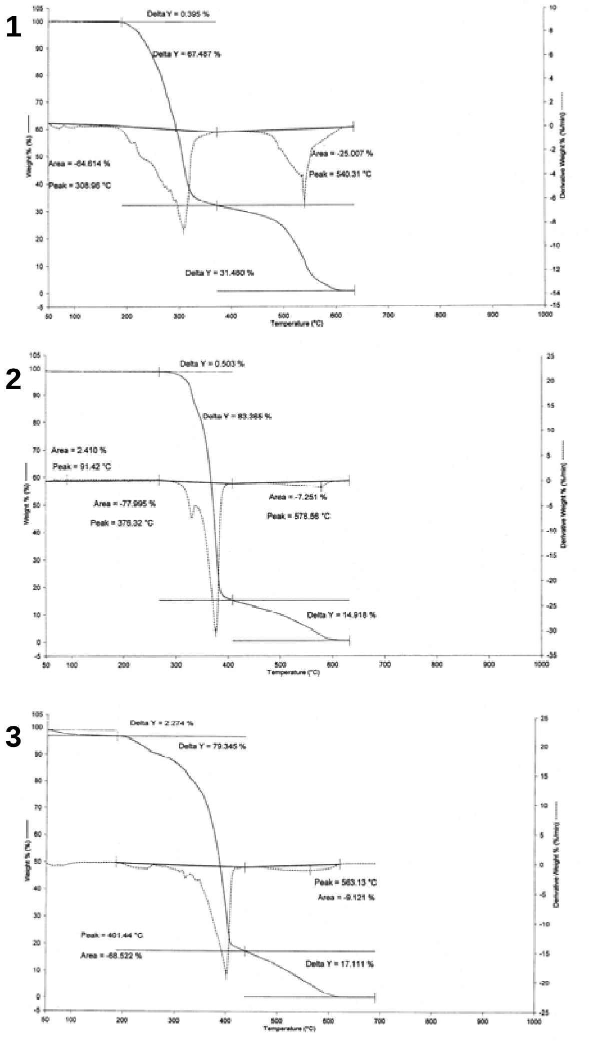

Figure 10. TGA thermograms of pioglitazone and pioglitazone-DM-β-CD systems. 1, pioglitazone; 2, DM-β-CD; 3, pioglitazone-DM-β-CD complex.

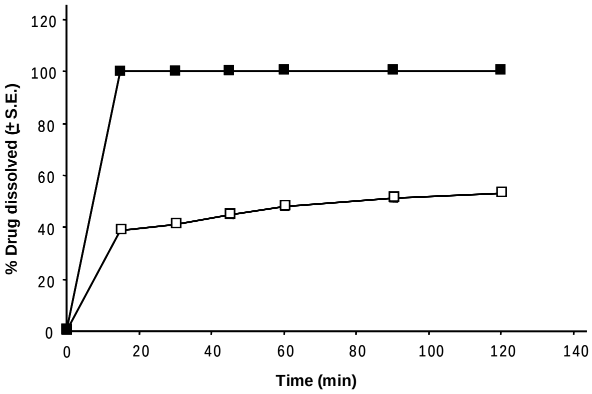

Figure 11. Effect of cyclodextrins on the dissolution rate of pioglitazone in pH 1.2: Free pioglitazone (□); Piog-β-CD complex (■); Piog-β-CD physical mixture (■); Piog-HP-β-CD complex (■); Piog-HP-β-CD physical mixture (■); Piog-DM-β-CD complex (■); Piog-DM-β-CD physical mixture (■).

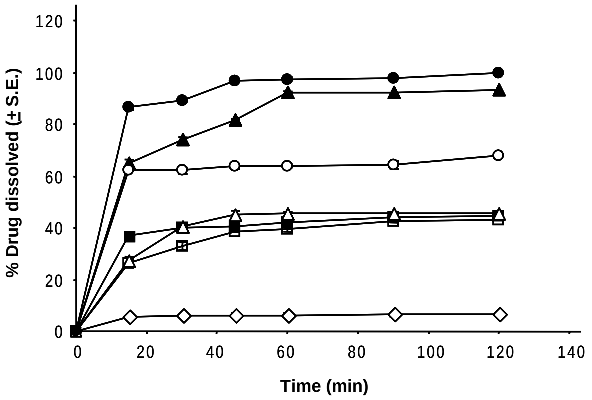

Figure 12. Effect of cyclodextrins on the dissolution rate of pioglitazone in pH 4.6: Free pioglitazone (◊); Piog-β-CD complex (■); Piog-β-CD physical mixture (□); Piog-HP-β-CD complex (▲); Piog-HP-β-CD physical mixture (Δ); Piog-DM-β-CD complex (●); Piog-DM-β-CD physical mixture (○).

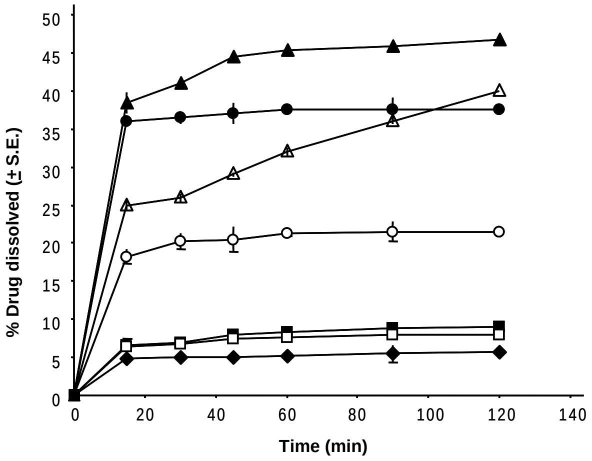

Figure 13. Effect of cyclodextrins on the dissolution rate of pioglitazone in pH 6.8: Free pioglitazone (♦); Piog-β-CD complex (■); Piog-β-CD physical mixture (□); Piog-HP-β-CD complex (●); Piog-HP-β-CD physical mixture (○); Piog-DM-β-CD complex (▲); Piog-DM-β-CD physical mixture (Δ).

enhanced the dissolution rate of the drug somewhat.

The dissolution profiles of pioglitazone and pioglitazone-cyclodextrin ternary systems containing water-soluble polymers, namely (0.25% PVP or 0.1% HPMC) at simulated intestinal pH (4.6 and 6.8), are shown in Figures 14-17. As is evident from the figures, the addition of hydrophilic polymers markedly enhanced the dissolution rate of pioglitazone compared to the binary system in all cases. DM-β-CD ternary systems had the greatest effect on enhancing the dissolution rate of the drug, followed by HP-β-CD ternary systems. The dissolution rate of the pioglitazone decreases with the increase in pH of the dissolution medium from 4.6 to 6.8. The order of hydrophilic polymers in terms of enhancing the dissolution rate of pioglitazone-cyclodextrin complexes was: PVP > HPMC. Thus, inclusion of hydrophilic polymers in the cyclodextrin complexes yielded rates of dissolution higher than those for pioglitazone or its complexes with cyclodextrins. This result is in agreement with the previous investigation performed by Chowdary and Srinivas (*20*), which demonstrated that inclusion of a hydrophilic polymer in a celecoxib-HP-β-CD complex yielded a higher dissolution rate than that of celecoxib and its complexes with HP-β-CD. The increase in the dissolution rate of the drug in presence of these water-soluble polymers could be interpreted to mean that in ternary preparations the molecules of pioglitazone-cyclodextrin complex are supposed to be present in a more or less intimate dispersed state within the polymer matrix through interaction between the exterior of the complex and the polymer (*19*).

In the current study, the presence of hydrophilic polymers increased the dissolution efficiency of pioglitazone-cyclodextrin complexes. The differences in the dissolution efficiencies of ternary systems might be due to different complexation efficiency of the cyclodextrins in presence of these polymers. This may be due to different types of linkages established with the polymers and the drug (*21*).

3.5. *In vitro permeation studies*

3.5.1. *Effect of cyclodextrins on the permeation of*

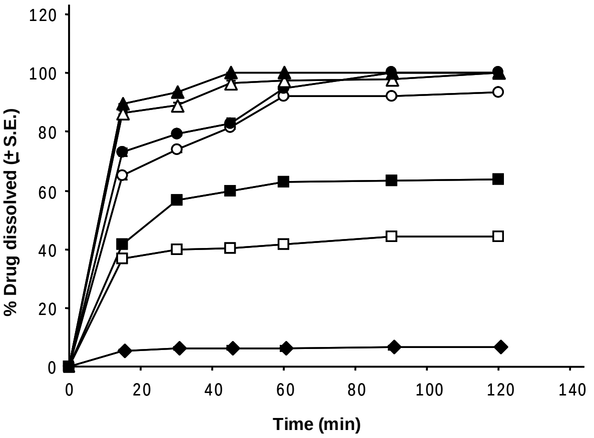

Figure 14. Effect of PVP on the dissolution rate of pioglitazone-cyclodextrin complexes in pH 4.6: Free pioglitazone (♦); Piog-β-CD PVP complex (■); Piog-β-CD complex (□); Piog-HP-β-CD PVP complex (●); Piog-HP-β-CD complex (○); Piog-DM-β-CD PVP complex (▲); Piog-DM-β-CD complex (Δ).

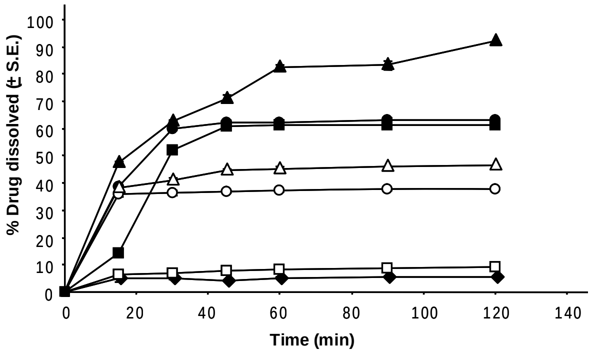

Figure 15. Effect of PVP on the dissolution rate of pioglitazone-cyclodextrin complexes in pH 6.8: Free pioglitazone (♦); Piog-β-CD PVP complex (■); Piog-β-CD complex (□); Piog-HP-β-CD PVP complex (●); Piog-HP-β-CD complex (○); Piog-DM-β-CD PVP complex (▲); Piog-DM-β-CD complex (Δ).

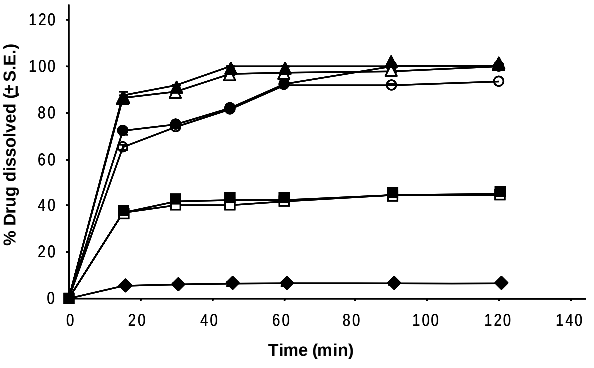

Figure 16. Effect of HPMC on the dissolution rate of pioglitazone-cyclodextrin complexes in pH 4.6: Free pioglitazone (♦); Piog-β-CD HPMC complex (■); Piog-β-CD complex (□); Piog-HP-β-CD HPMC complex (●); Piog-HP-β-CD complex (○); Piog-DM-β-CD HPMC complex (▲); Piog-DM-β-CD complex (Δ).

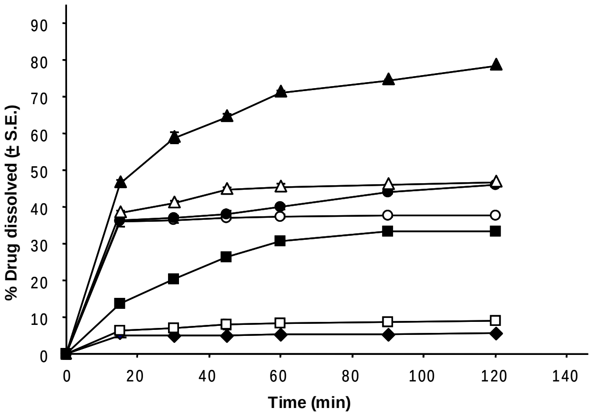

Figure 17. Effect of HPMC on the dissolution rate of pioglitazone-cyclodextrin complexes in pH 6.8: Free pioglitazone (♦); Piog-β-CD HPMC complex (■); Piog-β-CD complex (□); Piog-HP-β-CD HPMC complex (●); Piog-HP-β-CD complex (○); Piog-DM-β-CD HPMC complex (▲); Piog-DM-β-CD complex (Δ).

pioglitazone through a cellulose membrane with and without water-soluble polymers present

To evaluate the effect of complexation on the oral bioavailability of the included pioglitazone, an *in vitro* study was performed to measure the permeation through a cellulose membrane as a barrier model. In this study, permeation were performed using pioglitazone-β-CD, pioglitazone-HP-β-CD, and pioglitazone-DM-β-CD complexes in 1:1 molar ratios in comparison to uncomplexed pioglitazone. Table 2 shows that there was a significant increase in total pioglitazone that permeated through the membrane when the drug was complexed with cyclodextrins. This trend may due to rapid dissolution of the complex in comparison to pioglitazone alone, thus enhancing the availability of the drug in solution at the absorption site. The extent of enhancement of drug permeation was found to be dependent on the type of cyclodextrin; DM-β-CD had the highest rate of drug permeation. The enhancement of drug permeation was in the order of DM-β-CD > β-CD > HP-β-CD. This ranking was the same as that found for the effect of cyclodextrins on the solubility of pioglitazone. The data presented in Table 2 were mathematically processed using a Higuchi equation (*33*) and zero-order and first-order kinetics. Results indicated that the permeation pattern follows the kinetics of the Higuchi equation (*33*):

$$Q = RT_{1/2}$$

where Q is the amount of drug that permeated per unit area at time T and R is the rate of drug permeation; this is indicated by the very high correlation coefficient for most formulations. General opinion is that cyclodextrin molecules do not penetrate biological membranes but act as a carrier by keeping the hydrophobic drug in solution, delivering it to the surface of the biological membranes where it is inserted into the barrier (*34,35*). Cyclodextrins act as penetration enhancers by assuring constant high concentration of dissolved drug at the membrane surface (*36*).

The current results parallel those of Uekama *et al.* (*37*) which proved that the permeation of oral benzodiazepine through a cellulose membrane was significantly increased by complexation with γ-cyclodextrin.

Table 2 also shows that the presence of water-soluble polymers increased the amount of pioglitazone transferred across the cellulose membrane. The release pattern was found to follows the kinetics of a Higuchi equation (*33*). The permeation as measured by the flux improved significantly when pioglitazone was complexed with cyclodextrins, and this improvement was more prominent in the presence of water-soluble polymers. There appear to be few interpretations of this result other than that the free pioglitazone concentration in these systems was greater than that for pioglitazone solubility in a phosphate buffer solution at 37ºC. In addition, preheating pioglitazone suspensions at 120ºC should easily result in a higher free pioglitazone concentration as the aqueous solubility of organic compounds is generally temperature-dependent. As the temperature is allowed to drop back to 37ºC, PVP, a well-known nucleation and crystal growth inhibitor, can sustain the supersaturated state for long periods of time. The current results are in agreement with the previous investigation performed by Shaker *et al.* (*38*) which demonstrated that the addition of PVP increased the flux of corticosterone from suspensions in the presence of HP-β-CD after autoclaving at 120ºC. That work suggested that the increased flux is related to an increased corticosterone-CD complexation binding constant.

3.6. *Effect of complexation with cyclodextrins on the hypoglycemic efficacy of pioglitazone for normal rats.*

Figure 18 represents the mean % decrease in BGL after administration of free pioglitazone and pioglitazone-cyclodextrin complexes as a function of time. As is evident from the figure, there was a marked difference between the mean % decrease in BGL over time for

Table 2. *In vitro* permeation characteristics of pioglitazone and its cyclodextrin complexes in presence or absence of water soluble polymers through cellulose membrane (values ± S.E.)

Time (min)	Percentage drug permeated from:									
	Free Piog.	Pioglitazone			PVP			HPMC		
		β-CD	HP-β-CD	DM-β-CD	Piog.β-CD	Piog.HP-β-CD	Piog.DM-β-CD	Piog-β-CD	Piog-HP-β-CD	Piog.DM-β-CD
15	2.23±0.63	9.35±0.13	9.80±1.17	9.20±1.54	11.11±1.46	9.30±0.69	9.20±0.93	11.00±0.79	10.61±0.73	8.56±0.33
30	2.53±0.50	11.40±0.25	10.53±0.87	10.45±1.25	11.78±1.56	10.00±0.70	10.45±0.61	11.83±1.07	10.76±0.72	9.72±0.12
60	3.30±0.75	12.51±0.22	11.00±0.83	11.50±1.31	12.79±2.07	10.50±0.46	12.96±1.66	13.32±1.82	12.06±1.10	12.16±0.79
90	3.57±0.37	13.48±0.25	11.64±1.09	12.65±0.55	13.95±2.22	12.00±1.57	13.98±2.03	13.47±1.20	13.16±1.06	14.64±1.18
120	3.66±0.14	13.85±0.29	12.00±0.98	13.43±0.02	14.22±1.82	13.00±0.4	14.81±2.38	14.90±1.60	13.36±0.82	14.27±0.84
150	3.90±0.54	14.48±0.43	12.80±1.04	14.50±0.72	15.70±1.86	13.70±1.34	15.31±1.94	15.99±1.50	14.00±1.14	15.10±0.28
180	4.10±0.94	14.74±0.49	13.00±1.11	15.44±1.08	16.70±1.13	14.20±1.72	17.01±1.66	16.08±1.40	15.00±2.03	16.50±0.36
210	4.50±0.64	15.60±0.09	13.66±1.33	16.50±0.57	16.99±1.06	14.30±2.08	18.69±1.34	16.70±1.48	15.16±1.54	17.06±0.59
240	4.90±0.54	16.05±0.21	14.02±1.14	17.46±0.66	17.01±0.42	14.70±1.57	19.18±1.42	16.82±0.52	15.66±0.54	17.48±0.78
R*	0.012	0.030	0.021	0.041	0.033	0.029	0.050	0.031	0.027	0.047

R*(mg•cm^2•min$^{1/2}$) = rate of drug released pioglitazone and pioglitazone-cyclodextrin complexes as well as for the control. The maximum decrease in BGL for all the investigated systems appears to occur 6 h post-dosing. The effect on BGL fades in about 24 h, while the effect was maintained to different degrees at this time point for the complexes. Figure 18 shows that pioglitazone-cyclodextrin complexes have a greater effect on decreasing BGL in comparison to uncomplexed pioglitazone. The greatest peak increase occurs after administration of a pioglitazone-DM-β-CD complex.

Table 3 shows the effect of pioglitazone-cyclodextrin complexes on the maximum percentage decrease in BGL compared to the control and free pioglitazone. The maximum % decrease in BGL is the least for the control, followed by the free drug. The pioglitazone-cyclodextrin complexes behave differently, not only from the control but also from the free drug. Pioglitazone-DM-β-CD complex displayed the highest maximum decrease in BGL. The difference in the maximum percentage decrease in BGL between the pioglitazone-DM-β-CD complex and all investigated systems is very highly statistically significant ($p < 0.001$). These results point to a statistically significant increase in the intensity of action of pioglitazone when present in the form of a pioglitazone-DM-β-CD complex.

Table 3 shows that t_{max} is reached for the free drug earlier than for the pioglitazone-cyclodextrin complexes. Pioglitazone-DM-β-CD complex had the greatest delay in maximum response.

Statistical analysis of the data on the time of maximum percentage decrease in BGL indicated that the differences in t_{max} for most of the investigated systems are insignificant ($p > 0.05$). The difference between the free drug and pioglitazone-DM-β-CD is statistically significant ($p < 0.05$). This indicates that the time of the maximum effect of drug action is delayed for a pioglitazone-DM-β-CD complex.

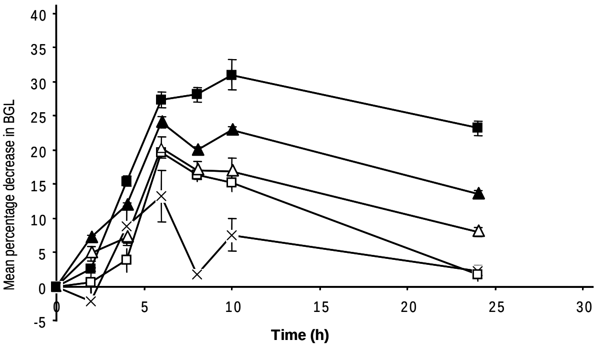

Figure 18. Mean percentage decrease in blood glucose levels of normal rats after administration of free pioglitazone and its complexes: Control (×); Free pioglitazone (□); Piog-HP-β-CD complex (Δ); Piog-β-CD complex (▲); Piog-DM-β-CD complex (■).

The $AUC_{0\text{-}24\,h}$ values for all the investigated systems are higher than for the control and the free drug and are highest for a pioglitazone-DM-β-CD complex. The differences in $AUC_{0\text{-}24\,h}$ values between the different test groups are in most cases very highly significant ($p < 0.001$). This indicates a pronounced and statistically significant augmentation of the bioavailability of pioglitazone when prepared in the form of pioglitazone-cyclodextrin complexes and especially when prepared as a pioglitazone-DM-β-CD complex.

The relative bioavailability was calculated according to the following equation:

$$\textbf{Relative bioavailability} = \frac{\textbf{Mean AUC}_{\textbf{0-24 h}}\textbf{ (Complex)}}{\textbf{Mean AUC}_{\textbf{0-24 h}}\textbf{ (Drug)}} \times \textbf{100}$$

The values indicate an increase in relative bioavailability of the drug *via* complexation. The increased relative bioavailability was more prominent for pioglitazone-DM-β-CD complex, with the mean value reaching 261% in comparison to 190% and 135% for pioglitazone-β-CD complex and pioglitazone-HP-β-CD complex, respectively. These results indicated that pioglitazone was not bioequivalent to any of its complexes according to FDA standards and that a dose correction was required for the complexes.

Table 3 shows the values of $t_{1/2p}$ for the prepared pioglitazone-cyclodextrin complexes was higher than those for the free drug and the control. Pioglitazone-DM-β-CD complex had the highest $t_{1/2p}$ value. Statistical analysis of the data on $t_{1/2p}$ showed that the difference between the free drug and pioglitazone-HP-β-CD is not significant ($p > 0.05$). At the same time, the differences between the free pioglitazone and pioglitazone-β-CD and pioglitazone-DM-β-CD are very highly significant ($p < 0.001$). These results point to the longer duration of drug action when formulated as pioglitazone-β-CD or pioglitazone-DM-β-CD complexes.

Quotient R was calculated for the investigated groups according to the following equation:

$$\textbf{R}\Delta\ (39) = \frac{\textbf{Mean } t_{1/2p}\textbf{ (complex)}}{\textbf{Mean } t_{1/2p}\textbf{ (drug)}}$$

The values indicated an increase in the duration of the drug action *via* complexation as revealed by the values of RΔ being higher than unity. The increase in duration of drug action is more prominent for pioglitazone-DM-

Table 3. Pharmacodynamic parameters for free pioglitazone and pioglitazone-cyclodextrin complexes (value ± S.E.)

Formulations	Max % decrease in BGL	$T_{max\,(h)}$	$AUC_{0\text{-}24\,h}$	$t_{1/2\,h}$	MRT (h)
Control	17.716±2.52	6.333±0.62	145.983±29.90	7.133±1.18	8.602±0.73
Free pioglitazone	19.788±0.71	6.800±0.44	213.119±12.14	9.040±0.75	8.587±0.38
Pioglitazone-β-CD complex	24.607±0.56	8.000±0.66	404.781±5.43	20.640±1.37	9.567±0.04
Pioglitazone-HP-β-CD complex	23.391±1.25	7.200±0.53	289.242±18.72	10.640±1.37	9.186±0.26
Pioglitazone-DM-β-CD complex	33.099±1.84	8.600±0.60	558.021±24.73	29.600±1.80	10.127±0.11

β-CD complex where the mean value is equal to 3.27 in comparison to 2.28 for pioglitazone-β-CD complex and 1.17 for pioglitazone-HP-β-CD complex.

Table 3 shows that the greatest augmentation in MRT was observed for pioglitazone-cyclodextrin complexes, and pioglitazone-DM-β-CD displayed the highest MRT value, followed by pioglitazone-β-CD complex. Statistical analysis of the data showed that the difference between the free drug and pioglitazone-DM-β-CD is highly significant ($p < 0.01$) while other differences are insignificant ($p > 0.05$). These results point to the augmentation of the duration of drug action for a pioglitazone-DM-β-CD complex.

In conclusion, the bioavailability, intensity, and duration of drug action increased when pioglitazone was prepared in the form of pioglitazone-cyclodextrin complexes, and the greatest increase took place with a pioglitazone-DM-β-CD complex.

References

1. LaMonte MJ, Blair SN, Church TS. Physical activity and diabetes prevention. J Appl Physiol 2005; 99:1205-1213.
2. Miyazaki Y, Mahankali A, Matsuda M, Glass L, Mahankali S, Ferrannini E, Cusi K, Mandarino LJ, DeFronzo RA. Improved glycemic control and enhanced insulin sensitivity in type 2 diabetic subjects treated with pioglitazone. Diabetes Care 2001; 24:710-719.
3. O'Moore-Sullivan TM, Prins JB. Thiazolidinediones and type 2 diabetes: new drugs for an old disease. Med J Aust 2002; 176:381-384.
4. Olefsky JM. Treatment of insulin resistance with peroxisome proliferator activated receptor γ-agonists. J Clin Invest 2000; 106:467-470.
5. Belcher G, Lambert C, Edwards G, Urquhart R. Safety and tolerability of pioglitazone, metformin, and gliclazide in the treatment of type 2 diabetes. Diabetes Res Clin Pract 2005; 70:53-62.
6. Martin del Valle M. Cyclodextrins and their uses: a review. Process Biochemistry 2004; 39:1033-1046.
7. Moyano JR, Arias-Blanco MJ, Gines JM, Giordano F. Solid state characterization and dissolution characteristics of gliclazide-β-cyclodextrin inclusion complexes. Int J Pharm 1997; 148:211-217.
8. Ammar HO, Salama HA, Ghorab M, Mahmoud AA. Formulation and biological evaluation of glimepiride-cyclodextrin-polymer systems. Int J Pharm 2006; 309:129-138.
9. Ammar HO, Salama HA, Ghorab M, Mahmoud AA. Implication of inclusion complexation of glimipiride in cyclodextrin-polymer systems on its dissolution, stability and therapeutic efficacy. Int J Pharm 2006; 320:53-57.
10. Martin A, Bustamante P, Chun AHC. Physical pharmacy: Physical chemical principles in pharmaceutical sciences, 4th ed., Lippincott William and Wilkins, Philadelphia, PA , USA, 1993; pp. 260-261.
11. Higuchi T, Connors KA. Advances in analytical chemistry and instrumentation. Interscience Publishers, New York, 1965.
12. Uekema K, Horiuchi Y, Kikuchi M, Hirayama F, Ijitsu T, Ueno M. Enhanced dissolution and oral bioavailability of R-tocopheryl esters by dimethyl-β-cyclodextrin complexation. J Incl Phenom 1988; 6:167-174.
13. Wagner SG. Fundamentals of clinical pharmacokinetics,1st ed., Drug Intelligence Publications Inc., Hamilton, IL, USA, 1975.
14. Prankerd R, Stone H, Sloan K, Perrin J. Degradation of aspartame in acidic aqueous media and its stabilization by complexation with cyclodextrins or modified cyclodextrins. Int J Pharm 1992; 88:189-199.
15. Mura P, Bettinetti GP, Manderioli A, Faucci MT, Bramanti GB, Sorrenti M. Interactions of ketoprofen and ibuprofen with β-cyclodextrin in solution and in the solid state. Int J Pharm 1998; 166:189-203.
16. Mura P, Zerrouk N, Faucci MT, Maestrelli F, Chemtob C. Comparative study of ibuproxam complexation with amorphous β-cyclodextrin derivatives in solution and in the solid state. Eur J Pharm Biopharm 2002; 54:181-191.
17. Zerrouk N, Corti G, Anallotti S, Maestrelli F, Cirri M, Mura P. Influence of cyclodextrins and chitosan separately or in combination, on glyburide solubility and permeability. Eur J Pharmac Biopharm 2006; 62:241-246.
18. Fernandes CM, Teresa Vieira M, Veiga FJB. Physicochemical characterization and *in vitro* dissolution behavior of nicardypine-cyclodextrins inclusion compounds. Eur J Sci 2002; 15:79-88.
19. Mura P, Faucci MT, Bettinetti GP. The influence of polyvinylpyrolidone on naproxen complexation with hydroxyl propyl-β cyclodextrin. J Pharm Sci 2001; 13:187-194.
20. Chowdary KPR, Srinivas SV. Influence of hydrophilic polymers on celecoxib complexation with hydroxypropyl-β cyclodextrin. AAPS PharmSciTech 2006; 7:79.
21. Ribeiro L SS, Ferreira DC, Veiga FJP. Physicochemical investigation of the effect of water soluble polymers on vinpocetine complexation with β cyclodextrin and its sulfobutyl ether derivative in solution and solid state. Eur J Pharm Sci 2003; 20:253-266.
22. Faucci MT, Mura P. Effect of water-soluble polymers on naproxen complexation with natural and chemically modified β-cyclodextrins. Drug Dev Ind Pharm 2001; 27:909-917.
23. Ryan JA, Compressed pellet X-ray diffraction monitoring for optimization of crystallinity in lyophilized solids: imipenem; cilastin sodium case. J Pharm Sci 1986; 75:805-807.
24. Calabro ML, Tommasini S, Donato P, Raneri D, Stancanelli R, Ficarra P, Ficarra R, Costa C, Catania S, Rustichelli C, Gamberini G. Effect of α- and β-cyclodextrin complexation on the physicochemical properties and antioxidant activity of some 3-hydroxyflavones. J Pharm Biomed Anal 2004; 35:365-377.
25. Veiga MD, Diaz PJ, Ahsan F. Interaction of griseofulvin with cyclodextrins in solid binary systems. J Pharm Sci 1998; 81:891-900.
26. Kurazumi M, Nambu N, Nagai T. Inclusion compounds of non steroidal anti-inflammatory and other slightly water soluble drugs with alpha and beta-cyclodextrins in powdered form. Chem Pharm Bull 1975; 23:3062-3068.
27. Winters CS, York P, Timmins P. Solid state examination of a gliclazide:beta-cyclodextrin complex. Eur J Pharm Sci 1997; 5:209-214.
28. Jug M, Becirevic-Lacan M. Influence of hydroxypropyl-β-cyclodextrin complexation on piroxicam release

from buccoadhesive tablets. Eur J Pharm Sci 2004; 21:251-260.

29. Fernandes CM, Vieira MT, Veigaa F. Physicochemical characterization and *in vitro* dissolution behavior of nicardipine-cyclodextrins inclusion compounds. Eur J Pharm Sci 2004; 15:79-88.
30. Furo I, Pocsik I, Tompa K, Teeaar R, Lippmaa E. C.P.-D. D.-M.A.S. ^{13}C-N.M.R investigations of anhydrous and hydrated cyclomalto-oligosaccharides: the role of water of hydration. Carbohydr Res 1987; 66:27-33.
31. Wade A., Weller PJ (eds.). Handbook of pharmaceutical excipients, 2nd ed., American Pharmaceutical Association, Washington, USA, 1994.
32. Mura P, Faucci MT, Maestrelli F, Furlanetto S, Pinzauti S. Characterization of physicochemical properties of naproxen systems with amorphous β-cyclodextrin-epichlorhydrin polymers. J Pharm Biomed Anal 2002; 29:1015-1024.
33. Higuchi T. Rate of release of medicaments from ointment bases containing drugs in suspension. J Pharm Sci 1961; 50:874-875.
34. Loftsson T, Frioriksdottir H, Ingvasdottir G, Jonsdottir B, Siguroardottir AM. The influence of 2-hydroxypropyl-β-cyclodextrin on diffusion rates and transdermal delivery of hydrocortisone. Drug Dev Ind Pharm 1994; 20:1699-1708.
35. Loftsson T, Olafsdottir Bj, Bodor N. The effects of cyclodextrin on transdermal delivery of drugs. Eur J Pharmacol Biopharmacol 1991; 37:30-33.
36. Loftsson T, Stefansson E. Effect of cyclodextrin on the topical delivery of drugs to the eye. Drug Dev Ind Pharm 1997; 23:473-476.
37. Uekama K, Narisawa S, Hirayama F, Otagiri M. Improvement of dissolution and absorption characteristics of benzodiazepines by cyclodextrin complexation. Int J Pharm 1983; 16:327-338.
38. Shaker DS, Ghanem A-H, Li SK, Warner KS, Hashem FM, Higuchi WI. Mechanistic studies of the effect of hydroxyl propyl-β-cyclodextrin on *in vitro* transdermal permeation of corticosterone through hairless mouse skin. Int J Pharm 2003; 253:1-11.
39. Meier J, Noesch E, Shmidt R. Pharmacokinetic criteria for the evaluation of retard formulations. Eur J Clin Pharmacol 1974; 7:429-432.

(*Received March 8, 2008; Revised March 24, 2008; Accepted April 6, 2008*)

Original Article

Reconstituted powder for suspension of antitubercular drugs formulated as microspheres for pediatric use

Abdus Samad[1], Yasmin Sultana[1,*], Roop K. Khar[1], Mohd Aqil[1], Krishna Chuttani[2], Anil K. Mishra[2]

[1] *Department of Pharmaceutics, Faculty of Pharmacy, Jamia Hamdard, New Delhi, India;*
[2] *Department of Radiopharmaceuticals, Institute of Nuclear Medicine and Allied Sciences (INMAS), Delhi, India.*

ABSTRACT: The aim of the present investigation was to develop a novel dosage form of rifampicin and isoniazid to minimize degradation of rifampicin in acidic medium, to modulate the release of rifampicin in the stomach and isoniazid in the intestine, and to provide pediatric compliance. Rifampicin slowly diffuses out through this hydrogel matrix, thereby sustaining its release (50.08%). The release of isoniazid was thus very low in an acidic environment, *i.e.* simulated gastric fluid (SGF) pH 1.2 (18.98%), while in simulated intestinal fluid (SIF) pH 7.4 the release was sustained and prolonged (76.98%). Good results were obtained for a period of 36 h in SIF pH 7.4 with isoniazid-alginate microspheres. The drug content was calculated on the basis of the drug entrapment efficiency of the individual microsphere formulation (gelatin, 82.32% and sodium alginate blends, 89.31%). Results revealed that an optimized formulation had a sedimentation volume of 0.4. This optimized formulation was found to be stable. Degradation of isoniazid was faster than that of rifampicin. The degradation rate constant at 25°C was found to be 1.9286×10^{-4} (day^{-1}), so the formulation was predicted to have a shelf life of 1.518 years.

Keywords: Reconstituted powder, Suspension, Antitubercular drugs, Degradation, Pediatric use

Introduction

Tuberculosis is a major cause of childhood morbidity and mortality. Estimates indicate that about 6-8%, *i.e.* 1.3 million, of all new Tuberculosis (TB) cases and 4.5 lac deaths are in the pediatric age group (*1*). Although children can present with TB at any stage, the majority of the cases is seen at ages 1-4 due to children's low resistance to progression of disease infection. Despite this, a surprising fact is that, globally, national TB control programs have continued to accord a low priority to childhood TB (*2*).

Sodium alginate is a purified carbohydrate product extracted from brown seaweed by the use of dilute alkali. It consists chiefly of the sodium salt of alginic acid; a polyuronic acid composed of β-(1→4)-D-mannosyluronic acid and α-(1→4)-L-gulosyluronic acid residues linked so that the carboxyl group of each unit is free while the aldehyde group is shielded by a glycosidic linkage (*3,4*).

Chitin, the polysaccharide polymer from which chitosan is derived, is a cellulose-like polymer consisting mainly of unbranched chains of *N*-acetyl-D-glucosamine. Deacetylated chitin, or chitosan, is comprised of chains of D-glucosamine. When ingested, chitosan can be considered a dietary fiber (*5,6*).

Gelatin contains a large number of glycine (almost 1 in 3 residues, arranged every third residue), proline and 4-hydroxyproline residues. A typical structure is [Ala-Gly-Pro-Arg-Gly-Glu-4Hyp-Gly-Pro] (*7*).

Isoniazid (INH) is an antimycobacterial agent widely used in first-line therapy for tuberculosis. The drug is characterized by a short half-life ranging from 1-4 h, depending on the rate of metabolism. INH has a pronounced absorption from all the three sections of the small intestine (*8*) and from intramuscular (IM) injection sites. INH is inactivated in the liver, mainly by acetylation and dehydrazination; the rate of acetylation is genetically determined and subject to individual variation. Long-term continuous therapy with INH leads to hepatotoxicity and peripheral neuritis. Thus, a drug formulation must have controlled release of INH, especially in the small intestine. Rifampicin was selected as a model drug for this research. Rifampicin with a naphthaquinone group is an antitubercular drug used for the treatment of tuberculosis. Rifampicin is

---

**Correspondence to:* Dr. Yasmin Sultana, Department of Pharmaceutics, Faculty of Pharmacy, Jamia Hamdard, New Delhi 110062, India;
e-mail: yasmin013@yahoo.com

completely eliminated from the gut after oral intake. On account of the high dose, attempts were made to develop a controlled-release formulation of rifampicin for sustained action (*9*).

Studies are being carried out in the authors' laboratory to determine the reason for the drop in bioavailability of rifampicin from certain fixed-dose combination (FDC) antituberculosis products. Data were provided earlier to show that rapid decomposition of rifampicin in the presence of isoniazid in FDC antituberculosis products in an acidic stomach environment was the likely reason behind the appearance of the problem (*10-13*). In one recent investigation, the focus was primarily on understanding why the bioavailability problem of rifampicin in FDC products appeared more prominent when bioequivalence studies were done on multiple marketed formulations (*14,15*) than when studies involved single test formulations (*16,17*).

Thus aim of this work is to improve the oral bioavailability of isoniazid in the presence of rifampicin by minimizing the chemical interaction between the metabolites of rifampicin with isoniazid under acidic conditions. Isoniazid and rifampicin are both first-line antitubercular drugs with a half-life ranging from 3-4 h and are available on the market in solid dosage form, leading to low compliance in pediatrics. Hence, formulation of a reconstituted powder for suspension using micro-particulate technology can resolve this problem.

Materials and Methods

Isoniazid was generously donated by Lupin Research Park (Pune, India), sodium alginate was purchased from Central Drug House (CDH, India), and all other materials and solvents were from Sigma (St. Louis, MO, USA). Rifampicin was generously donated by Lupin Research Park (Pune, India). Gelatin type B (250 blooms, pH of 1% aqueous solution of 4-5) was purchased from Sigma. Sucrose was purchased from CDH (India) and all other materials and solvents were from Sigma.

Preparation of microspheres

Sodium alginate solutions (3-5%) were prepared by dissolving sodium alginate in 10 mL of warm water. To this solution was added 1% of chitosan dissolved in acetic acid. The whole solution was stirred for 2 h at a temperature of 40ºC and then 0.8 mL of plasticizer, dibutyl phthalate, and isoniazid (5%) were added. The resulting polymer solution was emulsified in light liquid paraffin containing 2% Span 80. The emulsion was stirred for 1 h to ensure complete emulsification. To this was added calcium chloride solution, and the dispersion was stirred for another 10 min. Microspheres were collected by filtration, washed with isopropanol three times, and finally dried at room temperature.

To the 15% gelatin solution were added 3-5% of sucrose and 2% rifampicin. The resulting solution was warmed to 40°C and the warm solution was mixed with 40 mL of liquid paraffin which was kept at 40°C. The mixture was stirred for 5 min with a three-blade paddle (diameter: 35 mm) at 2,000 rpm to form a water-in-oil emulsion. Next, the emulsion was rapidly cooled to 15°C and then 150 mL of acetone were added in order to dehydrate and flocculate the coacervated droplets. The residual solvent was removed with *n*-hexane. After preparation, the microspheres were maintained at room temperature in a desiccator until use.

Preparation of reconstituted powder for suspension

The oral drug delivery system was prepared by using an equivalent amount of isoniazid-alginate blends and rifampicin-gelatin microspheres as in marketed FDC products. Sugar and vanilla were added to the equivalent amount of microspheres as a sweetening agent and flavoring agent, respectively, to increase the palatability of the formulation. Xanthum gum and sodium benzoate were added to the formulation as a viscosity enhancer and preservative, respectively.

Evaluation of the reconstituted powder for suspension

Sedimentation volume determination

Sedimentation volume (F) was determined by measuring the ultimate volume of sediment with respect to the total volume of suspension. The optimized formulation of powder was dissolved in 10 mL of distilled water. The suspension was kept undisturbed for 10 min in a 10-mL measuring cylinder. The volume of sediment was measured after 10 min.

In vitro dissolution studies

In vitro dissolution studies of the formulation were carried out in simulated gastric fluid (SGF) pH 1.2 and simulated intestinal fluid (SIF) pH 7.4 to study drug interaction and to assess the efficacy of the combination product. Samples were taken at regular intervals and replaced with fresh dissolution medium. The absorbance was measured and the concentration was determined by the UV method at 262 nm and 473 nm for isoniazid and rifampicin, respectively.

In vivo study

Gamma scintigraphy studies were carried out to determine the location and distribution of microspheres upon oral administration and the extent of transit through the gastro-intestinal tract (GIT). For this study, the microspheres were labeled with ^{99m}Tc-pertechnetate, eluted from a ^{99}Mo-^{99m}Tc generator supplied by Amersham Biosciences (USA), and the experimental animals were New Zealand white rabbits (3-3.5 kg) and Adult Wistar rats of either sex (300-350 g, 15-20 weeks old).

^{99m}Tc-pertechnetate-isoniazid-alginate blend microspheres were prepared by dissolving 3.5 mg of microspheres in 1 mL of distilled water in a sterile glass vial followed by different concentrations of stannous chloride dehydrates (25-200 µg); pH varied from 5-7.5. The contents were filtered through a 0.22-mm membrane filter into a sterile vial. Approximately 18.5 MBq ^{99m}Tc-pertechnetate were added to this, and the result was mixed and incubated for 5-10 min. Then, the complex was subjected to quality control.

Radiolabelling efficiency was evaluated with Instant Thin Layer Chromatography-Silica gel (ITLC-SG) strips as the stationary phase and acetone 100% as the mobile phase.

$$\textbf{\% Radiolabelling} = \frac{\textbf{Radioactivity (counts) retained in the lower half of the strip}}{\textbf{Initial radioactivity associated (total count present) with the strip}} \times 100$$

Radiochemical impurity that is likely to exist in the form of unconjugated technetium was determined by ascending ITLC-SG.

$$\textbf{\% R/H technetium} = \frac{\textbf{Counts present in the lower part of strip}}{\textbf{Total count present in the strip}} \times 100$$

For whole-body imaging, 37 MBq of activity in 1 mL of preparation was administered orally to four rabbits weighing between 3-3.5 kg. The microspheres were administered by gavage in a dose of 2 mg/mL after overnight fasting for 8-10 h. Animals were given free access to water, but food was restored 1-2 h after dosing. The animals were anaesthetized with diazepam and serial scintigraphic examination was done at 4 and 24 h to assess the mobilization of the microspheres in the GIT using a large field view gamma camera (Siemens) equipped with a high-resolution, parallel-hole collimator and linked to a dedicated computer. Images were recorded for a preset time of 5 min/view with a 15% window centered to include the 140 KeV photo peak of ^{99m}Tc.

Stability study of the formulation

A stability study of optimized formulation was carried out as per WHO Guidelines. For the estimation of drug content in the microspheres, the stability-indicating HPTLC method was used. Microspheres were packed in laminated aluminium foil and kept ina stability chamber maintained at temperatures of 40 ± 0.5°C, 50 ± 0.5°C, and 60 ± 0.5°C for 90 days. Samples were taken at intervals of 0, 30, 60, and 90 days. The samples were analyzed for their drug content by HPTLC analysis using a standard curve (For isoniazid, AUC = 1.7426 × concentration; for rifampicin, AUC = 4.4781 × concentration).

The slope of each line was obtained and degradation rate constant (K) was calculated by the formula

$$\text{Slope} = -K/2.303$$

where K is the degradation rate constant. The value of K at 25°C (K_{25}) was obtained by extrapolation of the plot and shelf life was then calculated by substituting K_{25} in the following equation

$$T_{0.9} = 0.1054/K_{25}$$

where $T_{0.9}$ is the time required for 10% drug degradation and is referred to as shelf life.

Result and Discussion

Sugar was added as a sweetening agent and vanilla was used as a flavoring agent in an equivalent amount of microspheres, increasing the palatability of the formulation. Xanthum gum and sodium benzoate were added to the formulation as a viscosity enhancer and preservative, respectively (Table 1).

The present study was an attempt to develop a suitable oral drug delivery system for isoniazid and rifampicin in order to prevent their interaction in gastric medium. Microparticulate technology has been substantially explored for the targeted delivery of drugs by the parenteral route. It has also been utilized for oral delivery of drugs and bioactives primarily to bypass first-pass hepatic metabolism and sustain drug levels. An extensive survey of the literature survey indicated the potential for such a delivery system to achieve the desired purpose.

Reported data on drug permeability studies suggested that rifampicin was absorbed well from the stomach and isoniazid from the intestine (*18*). A wide range of both enteric as well as non-enteric biodegradable polymers was thus screened for the study. Sodium alginate and gelatin were selected due to the ease of preparation of microspheres from these polymers.

Chemically, sodium alginate is a carbohydrate and is

Table 1. Formula of optimized formulation of the reconstituted powder for suspension

Ingredients	Formulae
Microspheres	266.20 mg
Sugar	133.10 mg
Xanthum Gum	3%
Vanilla flavor	1%
Sodium benzoate	0.5%

made up of homopolymeric blocks of mannuronic and guluronic acids. Calcium ions bind to the polyuronic acid groups present in the polymer chains to form a 3D-network, which swells when water is consumed. In situ drug loading was done by dissolving or dispersing a known quantity of each drug in an aqueous polymer solution before emulsification in the oil phase. Water-soluble drugs are present in the internal phase of the w/o emulsion and thus are efficiently entrapped in the hydrogel matrix.

Chemically, gelatin is a protein and is made up of large numbers of glycin, proline, and 4-hydroxyproline amino acids. Sugar binds to the free amino groups present in the polymer chains to form a 3D-network, which swells when water is consumed. In situ drug loading was done by dissolving or dispersing a known quantity of each drug in an aqueous polymer solution before emulsification in the oil phase.

Gelatin swells in an acidic environment (SGF pH 1.2), forming minute hydrogel microparticles. Rifampicin slowly diffuses out through this hydrogel matrix, thereby sustaining its release (50.08%). However, burst release was observed in SIF pH 7.4 due to erosion of the matrix. Sodium alginate-blend microspheres also release the drug by diffusion in SGF pH 1.2 while in SIF pH 7.4 the drug release mechanism involves both diffusion of the drug through the capillaries formed as well as slow erosion of the matrix. The release of isoniazid was thus very low in an acidic environment (18.98%), while in SIF pH 7.4 the release was sustained and prolonged (76.98%). Good results were obtained for a period of 36 h in SIF pH 7.4 with isoniazid-alginate microspheres.

A reconstituted powder for suspension was formulated to consist of an accurately weighed amount of drug-loaded microspheres, sweetening agent, viscosity enhancer, and flavoring agent for greater compliance in pediatrics. The drug content was calculated on the basis of the drug entrapment efficiency of the individual microsphere formulation (gelatin, 82.32% and sodium alginate blends, 89.31%) and drug-loaded microspheres containing an amount of drug (182.22 mg of rifampicin-gelatin microspheres and 83.98 mg of isoniazid-alginate blends microspheres) equivalent to that of the standard FDC product approved by the WHO (150 mg rifampicin + 75 mg isoniazid) were used.

The sedimentation volume normally ranges from less than one to one and it may exceed one. The sedimentation volume decreases with an increase in xanthum gum, *i.e.* from 0.1% to 0.9%. The optimized formulation was concluded to have a sedimentation volume of 0.4.

In vitro dissolution studies of marketed formulations consisting of single drugs and a combination of isoniazid and rifampicin suggested the existence of an interaction between the two drugs in SGF pH 1.2 (Figure 1). Only minor differences were seen in the extent of drug release of both drugs in SIF pH 7.4 (Figure 2).

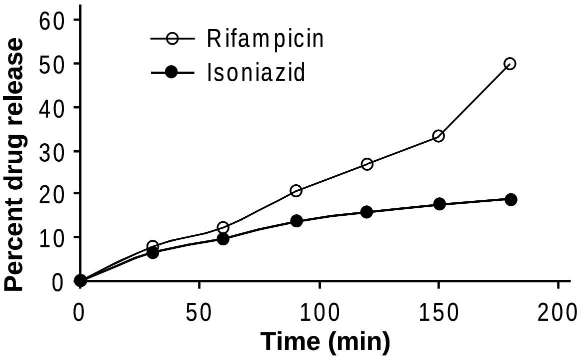

Figue 1. Dissolution profile of oral formulation of isoniazid and rifampicin (combination) in SGF pH 1.2.

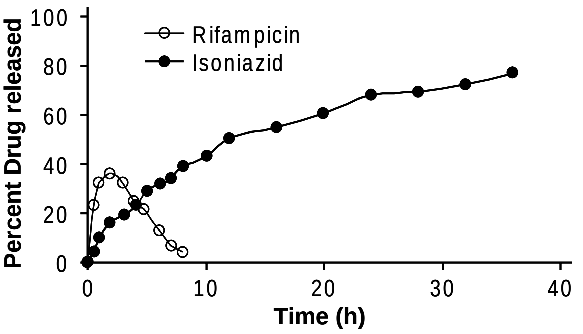

Figue 2. Dissolution profile of oral formulation of isoniazid and rifampicin (combination) in SIF pH 7.4.

However, this drug delivery system was largely successful in preventing the drug interaction due to reduced release of isoniazid from alginate microspheres into the gastric medium. The maximum extent of rifampicin was released into the gastric medium while gelatin microspheres had a burst release in SIF.

In gamma scintigraphy analysis, the section of GIT was analyzed in detail, revealing substantial differentiation. The presence of microspheres was marked in the intestinal lumen after 4 h (Figure 3). Microspheres were also be detected in different organs like the kidney, liver, lungs and lower part of the intestine after 24 h (Figure 4). Such prolonged retention of the formulation could be due to the small particle size of the formulation and the bio-adhesive nature of the preparation.

HPTLC analysis of the drug combination was based on the reported method (*19*). The following are the instrument specifications and chromatographic conditions: Solvent system: *n*-hexane/2-propanolol/acetone/ammonia/formic acid (3:3.8:2.8:0.3:0.1, v/v); wavelength at 254 nm (Figure 5).

Results of observations are shown in Tables 2 and 3. The log % of the remaining drug was plotted against time (Figures 6 and 7). The effect of temperature on the degradation was studied by plotting Log K versus $1/T$

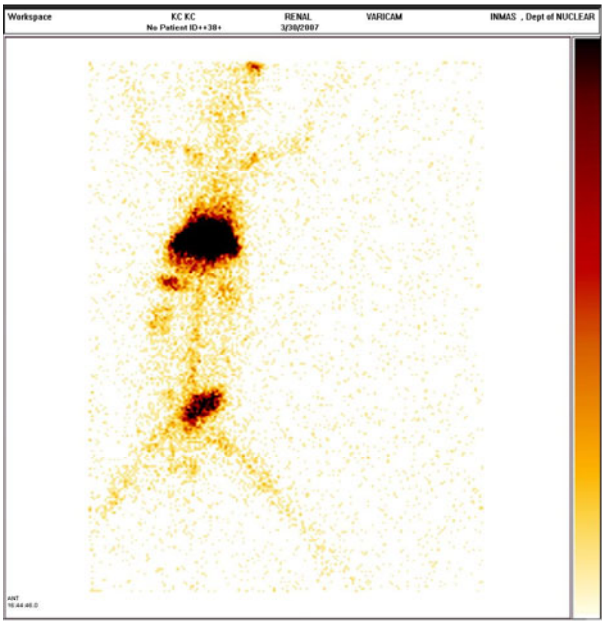

Figue 3. Whole body γ-scintigraphy of rabbit after 4 h of oral administration of ^{99m}Tc-pertechnetate-reconstited powder of microspheres.

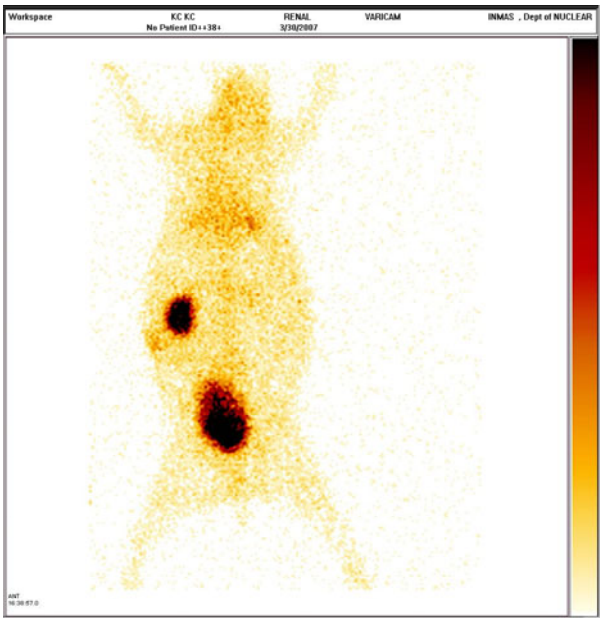

Figue 4. Whole body γ-scintigraphy of rabbit after 24 h of oral administration of ^{99m}Tc-pertechnetate-reconstited powder of microspheres.

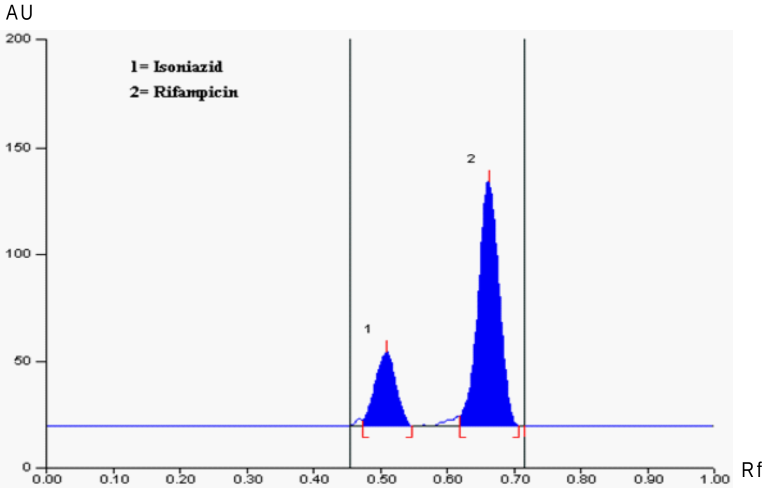

Figue 5. HPTLC graph of isoniazid and rifampicin by the reported method.

(Figures 8 and 9).

The optimized formulation was found to be stable. Degradation of isoniazid was faster than that of rifampicin. Thus, the shelf life can be predicted using the isoniazid shelf life. Higher temperatures ($K = 2.303 \times 10^{-4}$ day^{-1} at 60°C) led to more than 2% degradation of isoniazid at the end of 90 days. The degradation rate constant at 25°C was found to be 1.9286×10^{-4} (day^{-1}), so the formulation was predicted to have a shelf life of 1.518 years.

Conclusions

The present work was an attempt to develop a reconstituted powder for suspension of antitubercular drug microspheres for pediatric use in order to reduce the interaction between two drugs. The following conclusions were drawn from the results obtained:

(i) *In vitro* drug release was obtained for 36 h for isoniazid-alginate microspheres and for 4 h for rifampicin-gelatin microspheres.

(ii) The developed formulation provided more prolonged release of the drug than did the marketed preparation.

(iii) Gamma-scintigraphic analysis revealed the presence of alginate microspheres in the intestine for a period of more than 24 h.

(iv) Stability studies indicated that the developed formulation was stable for three months.

(v) The formulation, a reconstituted powder for

Table 2. Degradation of isoniazid in the optimized formulation according to WHO guidelines

Temp (°C)	Time (Days)	Mean area (±SD)	Conc. (ng/µL)	Contents (mg)	% Remained	% Log remained
40 ± 0.5	0	1306.95	750.0	75.00	100.00	2.000
	30	1298.93	745.4	74.54	99.39	1.997
	60	1286.74	738.4	73.84	98.45	1.993
	90	1282.38	735.9	73.59	98.12	1.991
50 ± 0.5	0	1306.95	750.0	75.00	100.00	2.000
	30	1297.01	744.3	74.43	99.24	1.996
	60	1285.69	737.9	73.78	98.37	1.992
	90	1280.46	734.8	73.48	97.97	1.991
60 ± 0.5	0	1306.95	750.0	75.00	100.00	2.000
	30	1296.49	744.0	74.00	98.67	1.994
	60	1282.72	736.1	73.61	98.15	1.992
	90	1279.59	734.3	73.43	97.91	1.990

Table 3. Degradation of rifampicin in the optimized formulation according to WHO guidelines

Temp (°C)	Time (Days)	Mean area (±SD)	Conc. (ng/µL)	Contents (mg)	% Remained	% Log remained
40 ± 0.5	0	6717.25	1500.0	150.00	100.00	2.000
	30	6674.16	1490.4	149.04	99.36	1.997
	60	6671.47	1489.8	148.98	99.32	1.997
	90	6656.25	1486.4	148.64	99.09	1.996
50 ± 0.5	0	6717.25	1500.0	150.00	100.00	2.000
	30	6668.34	1489.1	148.91	99.27	1.996
	60	6659.83	1487.2	148.72	99.15	1.996
	90	6651.77	1485.4	148.54	99.03	1.995
60 ± 0.5	0	6717.25	1500.0	150.00	100.00	2.000
	30	6663.41	1488.0	148.80	99.20	1.996
	60	6655.35	1486.2	148.62	99.08	1.995
	90	6649.53	1484.9	148.49	98.99	1.995

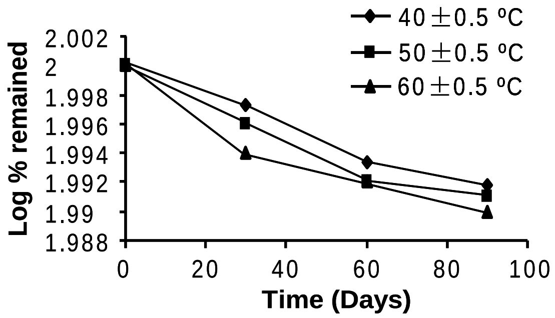

Figue 6. Degradation kinetics of isoniazid in optimized formulation according to WHO guidelines.

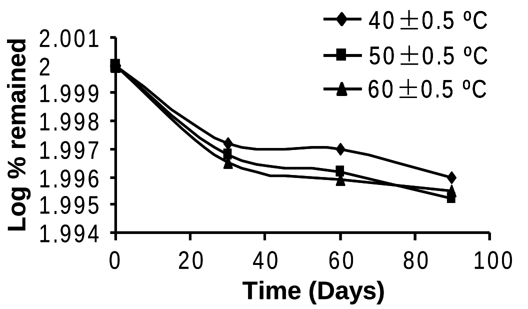

Figue 7. Degradation kinetics of rifampicin in optimized formulation according to WHO guidelines.

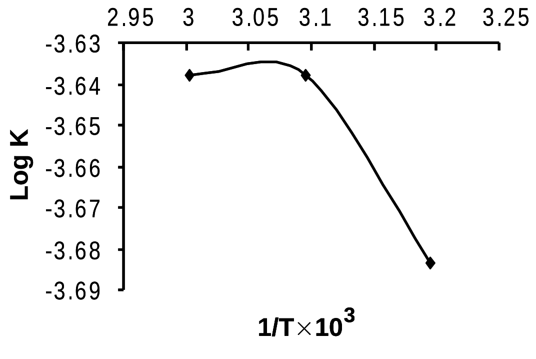

Figue 8. Graph for calculation of shelf life of isoniazid (Log degradation rate constant, K versus $1/T \times 10^3$).

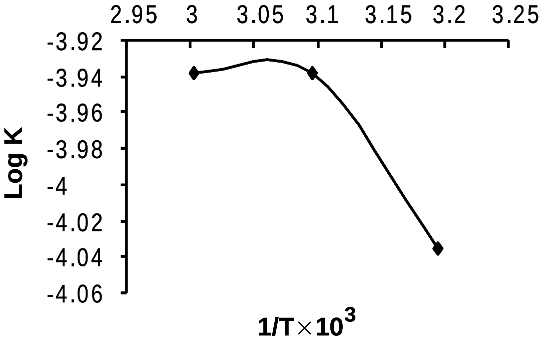

Figue 9. Graph for calculation of shelf life of rifampicin (Log degradation rate constant, K versus $1/T \times 10^3$).

suspension, thus has potential clinical usefulness and may contribute to patient compliance through better delivery of two first-line antitubercular agents.

Extensive chemotherapeutic studies are however, required to adjust the dosage regimen for this formulation.

References

1. Mitchison DA. Basic mechanism of chemotherapy. Chest 1979; 76:771-781.
2. Mitchinson DA. The action of anti tuberculosis drugs in short course chemotherapy. Tubercle 1985; 66:219-225.
3. Rastogi R, Sultana Y, Aqil M, Ali A, Kumar S, Chuttani K, Mishra AK. Alginate microspheres of isoniazid for oral sustained drug delivery. Int J Pharm 2007; 334:71-77.
4. Smidsrod O, Skjak-Braek G. Alginate as an immobilization matrix for cells. Trends Biotechnol 1990; 8:71-78.
5. Thanoo BC, Sunny MC, Jayakrishnan A. Cross-linked chitosan microspheres: preparation and evaluation as a matrix for the controlled release of pharmaceuticals. J Pharm Pharmacol 1992; 44:283-286.
6. Ko JA, Park HJ, Hwang SJ, Park JB, Lee JS. Preparation and characterization of chitosan microparticles intended for controlled drug delivery. Int J Pharm 2002; 249:165-174.
7. Lou Y, Olson WP, Tian XX, Klegerman ME, Groves MJ. Interaction between fibronectin-bearing surfaces and Bacillus Calmette-Guerin (BCG) or gelatin microparticles. J Pharm Pharmacol 1995; 47:177-181.
8. Nolan CM, Goldberg SV. Treatment of isoniazid-resistant tuberculosis with isoniazid, rifampin, ethambutol, and pyrazinamide for 6 months. Int J Tuberc Lung Dis 2002; 6:952-958.
9. Centers for Disease Control and Prevention. Targeted tuberculin testing and treatment of latent tuberculosis infection. Morb Mortal Wkly Rep 2000; 49:1-51.
10. Singh S, Mariappan TT, Sharda N, Kumar S, Chakraborti AK. The reason for an increase in decomposition of rifampicin in the presence of isoniazid under acid conditions. Pharm Pharmacol Commun 2000; 6:405-410.
11. Singh S, Mariappan TT, Sharda N, Singh B. Degradation of rifampicin, isoniazid and pyrazinamide from prepared mixtures and marketed single and combination products under acid conditions. Pharm Pharmacol Commun 2000; 6:491-494.
12. Singh S, Mariappan TT, Shankar R, Sharda N, Singh B. A critical review of the probable reasons for the variable bioavailability of rifampicin from anti-tuberculosis fixed-dose combination (FDC) products, and the likely solutions to the problem. Int J Pharm 2001; 228:5-17.
13. Singh S. Efforts of the WHO/IUATLD to solve the problem of poor bioavailability of rifampicin from FDC anti-tuberculosis products: is a change required in the direction of the approach in the view of recent findings? Int J Tuberc Lung Dis 2001; 5:880-882.
14. Acocella G. Human bioavailability studies. Bull Int Union Tuberc Lung Dis 1989; 64:38-40.
15. Pillai G, Fourie PB, Padayatchi N, Onyebujoh PC, McIlleron H, Smith PJ, Gabriels G. Recent bioequivalence studies on fixed dose combination anti tuberculosis drug formulations available on the global market. Int J Tuberc Lung Dis 1999; 3:S309-S316.
16. Panchagnula R, Singh I, Kaur KJ, Kaul CL. Bioequivalence study of rifampicin in fixed dose combination of rifampicin and isoniazid *vs*. separate formulations. Exp Clin Pharmacol 1999; 21:625-628.
17. Panchagnula R, Kaur KJ, Singh I, Kaul CL. The WHO simplified study protocol in practice: investigation of combined formulations supplied by the WHO. Int J Tuberc Lung Dis 1999; 3:S336-S342.
18. Sankar R, Sharda N, Singh S. Behaviour of decomposition of rifampicin in the presence of isoniazid in the pH range 1-3. Drug Dev Ind Pharm 2003; 29:733-738.
19. Małgorzata T, Jolanta F, Halina S. Simultaneous densitometric determination of rifampicinand isoniazid by high-performance thin-layer chromatography. Journal of Planar Chromatography 2005; 18:207-211.

(*Received February 19, 2008; Revised March 4, 2008; Accepted March 5, 2008*)

Original Article

Synthesis and biological evaluation of substituted phenylpyrazole[4,5-*b*]oleanane derivatives as inhibitors of glycogen phosphorylase

Jun Chen[1], Yanchun Gong[1], Jun Liu[2], Luyong Zhang[2], Weiyi Hua[1], Hongbin Sun[1,*]

[1] *Center for Drug Discovery, School of Pharmacy, China Pharmaceutical University, Nanjing, China;*
[2] *Jiangsu Center for Drug Screening, China Pharmaceutical University, Nanjing, China.*

ABSTRACT: A series of substituted phenylpyrazole[4,5-*b*]oleanane derivatives have been synthesized and biologically evaluated as inhibitors of glycogen phosphorylase (GP). The structure of phenylpyrazole moiety in compound 17 was determined by ROESY. All of the synthesized oleanane derivatives were biologically evaluated against rabbit muscle GPa. Within this series of compounds, pyrazole triterpene 7 (IC_{50} = 10.8 μM) exhibited slightly more potent activity than its parent compound 1. Preliminary SAR analysis of the pyrazoleoleanane derivatives as GP inhibitors is discussed.

Keywords: Phenylpyrazole[4,5-*b*]oleanane derivatives, Glycogen phosphorylase, Inhibitors, Synthesis, Diabetes

1. Introduction

Pentacyclic triterpenoids are very common constituents in the plant kingdom. A variety of biological properties have been ascribed to this class of compounds including anti-inflammation (*1*), anti-HIV (*2,3*), suppression of tumor promotion (*4,5*), and protection of the liver against toxic injury (*6-8*). The most well-known member of this family of compounds is probably oleanolic acid (OA, **1**) (Figure 1) which has been clinically used as a liver protective drug for more than 20 years in China. Previously, the current authors first reported that **1** and related pentacyclic triterpenes (*e.g.* maslinic acid and corosolic acid; Figure 1) represented a new class of inhibitors of glycogen phosphorylase (GP) (*9-12*). GP inhibitors have been regarded as a promising therapeutic approach to treatment of type 2 diabetes, and several GP inhibitors have shown efficacy in lowering blood glucose in clinical trials (*13*).

Given the significant biological importance and potential clinical utility of OA as a promising modulator of glycogen metabolism, synthesis and biological evaluation of new OA derivatives should prove helpful in finding more potent therapeutic agents with better pharmacokinetic properties. Recently, the current authors reported the synthesis and biological evaluation of several pyrazole[4,3-*b*]oleanane derivatives as GP inhibitors (*9*). This paper describes the synthesis, GP inhibitory activity, and structure–activity relationships of fifteen novel substituted phenylpyrazole [4,5-*b*]oleanane derivatives. To the extent known, all of the OA derivatives in this study have not yet to be reported.

2. Materials and Methods

2.1 *Chemistry*

2.1.1 *General methods*

The reagents (chemicals): Shanghai Chemical Reagent Company. Column chromatography (CC): silica gel 60 (200-300 mesh). TLC: silica gel 60 F254 plates (250 μm, Qindao Ocean Chemical Company, China). Melting points (M.p.): capillary tube; uncorrected. Infrared (IR) spectra: Shimadzu FTIR-8400S spectrometer; in cm^{-1}. ^1H- and ^{13}C-NMR spectra: ACF* 300Q Bruker, $CDCl_3$ unless otherwise indicated; δ in ppm, *J* in Hz. LR-MS: Hewlett-Packard 1100 LC/MSD spectrometer.

2.1.2 *Synthesis*

Benzyl 2-Hydroxymethylene-3-oxooleana-12-en-28-oate (**4**)

A mixture of **3** (*10*) (1 g, 1.84 mmol), NaOMe (1 g, 18.52 mmol), and HCO_2Et (1.5 mL, 18.58 mmol) in CH_2Cl_2 (20 mL) was stirred at r.t. for 10 h, and then the reaction mixture was evaporated *in vacuo*. Brine was added to the residue, and the mixture was extracted with AcOEt. The organic layer was washed with H_2O, dried (Na_2SO_4), and concentrated under reduced pressure. The crude product was purified by flash CC

**Correspondence to:* Dr. Hongbin Sun, Center for Drug Discovery, School of Pharmacy, China Pharmaceutical University, 24 Tongjia Xiang, Nanjing 210009, China;
e-mail: hbsun2000@yahoo.com

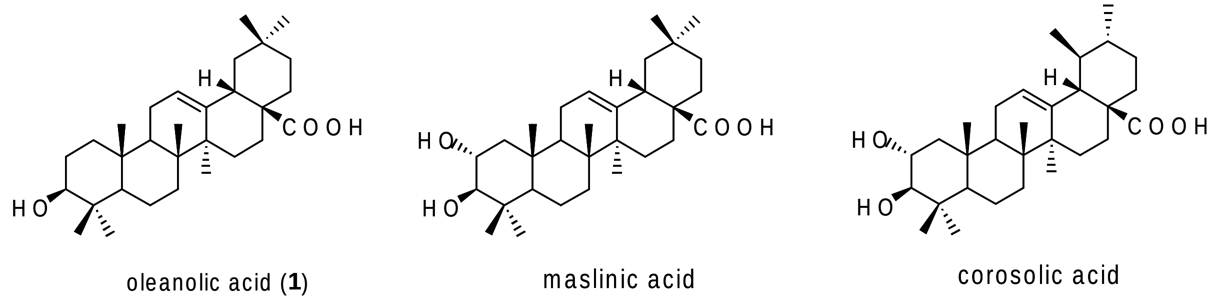

Figure 1. Several natural pentacyclic triterpenes as GP inihibitors.

(silica gel; heptane/AcOEt 50:1) to afford 0.84 g (80%) of **4** as a white solid. M.p. 143-145°C. IR (KBr): 3431, 2943, 1726, 1166. ^{1}H-NMR (300 MHz): 0.66 (3H, *s*); 0.88 (3H, *s*); 0.90 (3H, *s*); 0.93 (3H, *s*); 1.11 (3H, *s*); 1.14 (3H, *s*); 1.18 (3H, *s*); 2.26 (1H, *d*, J = 14.4 Hz); 2.93 (1H, *dd*, J = 4.0, 13.8 Hz); 5.05 (1H, *d*, J = 12.5 Hz); 5.10 (1H, *d*, J = 12.5 Hz); 5.33 (1H, *t*, J = 3.5 Hz); 7.29~7.35 (5H, *m*); 8.56 (1H, *s*). ESI-MS: 595 ([M+Na]$^+$).

Benzyl 1'-phenylpyrazole[4,5-b]olean-12-en-28-oate (**5**)

A mixture of **4** (0.5 g, 0.87 mmol) and phenylhydrazine hydrochloride (0.13 g, 0.92 mmol) in EtOH (20 mL) was heated under reflux for 20 h. Brine was added to the residue, and the mixture was extracted with AcOEt. The organic layer was washed with H_2O, dried (Na_2SO_4), and concentrated under reduced pressure. The crude product was purified by flash CC (SiO_2; heptane/AcOEt 50:1) to afford 0.41 g (72%) of **5** as a white solid. M.p. 118-120°C. IR (KBr): 3454, 2947, 1726, 1627, 1384. ^{1}H-NMR (300MHz): 0.68 (3H, *s*); 0.91 (6H, *s*); 0.94 (3H, *s*); 1.01 (3H, *s*); 1.05 (3H, *s*); 1.15 (3H, *s*); 2.11 (1H, *d*, J = 14.9 Hz); 2.62 (1H, *d*, J = 14.9 Hz); 2.92~2.97 (1H, *m*); 5.05 (1H, *d*, J = 12.5 Hz); 5.11 (1H, *d*, J = 12.5 Hz); 5.37 (1H, br *s*); 7.32~7.46 (11H, *m*). ESI-MS: 645 ([M+H]$^+$). Anal. calc. for $C_{44}H_{56}N_2O_2$: C 81.94, H 8.75, N 4.34; Found: C 81.80, H 8.89, N 4.11.

Benzyl 1'-(p-tolyl)pyrazole[4,5-b]olean-12-en-28-oate (**6**)

Following the procedure for the preparation of **5**, treatment of **4** (0.5 g, 0.87 mmol) with *p*-tolylhydrazine hydrochloride (0.15 g, 0.92 mmol) afforded 0.49 g (85%) of **6**. M.p. 113-115°C. IR (KBr): 3429, 2925, 1724, 1384. ^{1}H-NMR (300 MHz, DMSO-d_6): 0.60 (3H, *s*); 0.84 (3H, *s*); 0.89 (9H, *s*); 0.93 (3H, *s*); 0.98 (3H, *s*); 1.12 (3H, *s*); 2.05 (1H, *d*, J = 15.2 Hz); 2.38 (3H, *s*); 2.83~2.88 (1H, *m*); 5.04 (2H, *m*); 5.27 (1H, br *s*); 7.20~7.40 (10H, *m*). ^{13}C-NMR (75 MHz): 176.3; 145.2; 143.0; 139.6; 138.4; 137.4; 136.3; 128.8; 128.7; 128.3; 127.8; 127.6; 122.6; 122.0; 113.1; 65.2; 54.0; 46.1; 45.6; 45.3; 41.3; 41.1; 38.5; 38.1; 37.5; 36.4; 34.1; 33.1; 32.6; 31.9; 31.7; 30.3; 29.1; 27.1; 25.2; 23.2; 22.7; 22.6; 22.0; 20.6; 18.6; 16.2; 14.9. ESI-MS: 659 ([M+H]$^+$). Anal. calc. for $C_{45}H_{58}N_2O_2$: C 82.02, H 8.87, N 4.25; Found: C 81.73, H 8.92, N 3.78.

Benzyl 1'-(4"-chlorophenyl)pyrazole[4,5-b]olean-12-en-28-oate (**7**)

Following the procedure for the preparation of **5**, treatment of **4** (0.5 g, 0.87 mmol) with (4-chlorophenyl) hydrazine hydrochloride (0.16 g, 0.92 mmol) afforded 0.49 g (83%) of **7**. M.p. 125-127°C. IR (KBr): 3440, 2947, 1724, 1159. ^{1}H-NMR (300 MHz, DMSO-d_6): 0.60 (3H, *s*); 0.84 (3H, *s*); 0.89 (6H, *s*); 0.93 (3H, *s*); 0.98 (3H, *s*); 1.12 (3H, *s*); 2.05 (1H, *d*, J = 15.1 Hz); 2.83~2.89 (1H, *m*); 5.04 (2H, *m*); 5.27 (1H, br *s*); 7.30~7.43 (8H, *m*); 7.53~7.58 (2H, *m*). ^{13}C-NMR (75 MHz): 176.3. 145.6; 143.1; 141.0; 138.0; 136.3; 133.5; 130.8; 128.6; 128.3; 127.8; 127.6; 122.0; 113.6; 75.3; 53.9; 46.1; 45.6; 41.4; 41.1; 40.4; 37.5; 35.3; 34.1; 33.2; 32.6; 31.9; 31.7; 30.3; 29.2; 27.2; 25.3; 23.2; 22.8; 22.6; 22.2; 18.6; 16.3; 14.9. ESI-MS: 679 ([M+H]$^+$). Anal. calc. for $C_{44}H_{55}ClN_2O_2$: C 77.79, H 8.16, N 4.12; Found: C 77.74, H 8.32, N 3.84.

Benzyl 1'-(4"-isopropylphenyl)pyrazole[4,5-b]olean-12-en-28-oate (**8**)

Following the procedure for the preparation of **5**, treatment of **4** (0.5 g, 0.87 mmol) with (4-isopropylphenyl)hydrazine hydrochloride (0.17 g, 0.92 mmol) afforded 0.49 g (81%) of **8**. M.p. 95-97°C. IR (KBr): 3431, 2952, 1726, 1460, 1384, 1159. ^{1}H-NMR (300 MHz): 0.68 (3H, *s*); 0.91 (6H, *s*); 0.94 (3H, *s*); 1.01 (3H, *s*); 1.05 (3H, *s*); 1.15 (3H, *s*); 2.10 (1H, *d*, J = 15.1 Hz); 2.60 (1H, *d*, J = 14.9 Hz); 2.92~3.01 (2H, *m*); 5.05 (1H, *d*, J = 12.5 Hz); 5.09 (1H, *d*, J = 12.5 Hz); 5.37 (1H, br *s*); 7.27~7.36 (10H, *m*). ESI-MS: 687 ([M+H]$^+$). Anal. calc. for $C_{47}H_{62}N_2O_2$: C 82.17, H 9.10, N 4.08; Found: C 81.98, H 9.10, N 3.88.

Benzyl 1'-(3",5"-difluorophenyl)pyrazole[4,5-b]olean-12-en-28-oate (**9**)

Following the procedure for the preparation of **5**, treatment of **4** (0.5 g, 0.87 mmol) with (3,5-difluorophenyl)hydrazine hydrochloride (0.17 g, 0.92 mmol) afforded 0.49 g (83%) of **9**. M.p. 95-96°C. IR (KBr): 3425, 2949, 1726, 1616, 1458, 1122. ^{1}H-NMR (300 MHz, DMSO-d_6): 0.61 (3H, *s*); 0.85 (3H, *s*); 0.89 (6H, *s*); 0.98 (3H, *s*); 1.02 (3H, *s*); 1.12 (3H, *s*); 2.07 (1H, *d*, *J* = 15.1 Hz); 2.83~2.89 (1H, *m*); 5.04 (2H, *m*); 5.27 (1H, br *s*); 7.22~7.39 (8H, *m*); 7.43~7.52 (1H, *m*). ^{13}C-NMR (75 MHz): 176.2; 163.2; 163.1; 159.8; 145.7; 144.5; 144.3; 144.1; 143.0; 138.4; 136.2; 128.2; 127.7; 127.6; 122.0; 113.8; 113.3; 113.2; 113.0; 112.9; 105.2; 104.9; 104.6; 65.2; 54.0; 46.1; 45.6; 45.3; 41.3; 41.1; 37.5; 36.3;34.0; 33.1; 32.6; 31.9; 31.7; 30.2; 29.1; 27.1; 25.2; 23.2; 22.7; 22.6; 22.4; 22.2; 18.6; 16.2. ESI-MS: 681 ($[M+H]^+$). Anal. calc. for $C_{44}H_{54}F_2N_2O_2$: C 77.61, H 7.99, N 4.11; Found: C 77.60, H 8.25, N 3.68.

Benzyl 1'-(4"-cyanophenyl)pyrazole[4,5-b]olean-12-en-28-oate (**10**)

Following the procedures for the preparation of **5**, treatment of **4** (0.5 g, 0.87 mmol) with 4-hydrazinylbenzonitrile hydrochloride (0.16 g, 0.92 mmol) afforded 0.47 g (80%) of **10**. M.p. 135-137°C. IR (KBr): 3442, 2947, 1724, 1382, 1159. ^{1}H-NMR (300 MHz, DMSO-d_6): 0.60 (3H, *s*); 0.85 (3H, *s*); 0.89 (6H, *s*); 0.94 (3H, *s*); 0.97 (3H, *s*); 1.12 (3H, *s*); 2.07 (1H, *d*, *J* = 15.3 Hz); 2.55 (1H, *d*, *J* = 15.1 Hz); 2.83~2.89 (1H, *m*); 5.04 (2H, *m*); 5.27 (1H, br *s*); 7.28~7.40 (6H, *m*); 7.58~7.62 (2H, *m*); 7.97~8.02 (2H, *m*). ^{13}C-NMR (75 MHz): 176.8; 146.6; 146.4; 143.6; 139.2; 136.8; 133.4; 130.5; 128.8; 128.3; 128.2; 122.6; 118.6; 114.6; 65.8; 54.5; 46.7; 46.2; 45.9; 41.9; 41.7; 39.1; 38.0; 36.8; 34.6; 33.7; 33.2; 32.5; 32.2; 30.8; 29.8; 27.6; 25.8; 23.8; 23.3; 23.2; 22.9; 19.2; 16.8; 15.5. ESI-MS: 670 ($[M+H]^+$). Anal. calc. for $C_{45}H_{55}N_3O_2$: C 80.68, H 8.27, N 6.27; Found: C 80.55, H 8.46, N 5.99.

Benzyl 1'-(4"-carboxyphenyl)pyrazole[4,5-b]olean-12-en-28-oate (**11**)

Following the procedures for the preparation of **5**, treatment of **4** (0.5 g, 0.87 mmol) with 4-hydrazinylbenzoic acid hydrochloride (0.17 g, 0.92 mmol) afforded 0.28 g (47%) of **11**. M.p. 165-167°C. IR (KBr): 3425, 2945, 1726, 1379, 1163. ^{1}H-NMR (300 MHz, DMSO-d_6): 0.60 (3H, *s*); 0.85 (3H, *s*); 0.89 (6H, *s*); 0.93 (3H, *s*); 0.97 (3H, *s*); 1.12 (3H, *s*); 2.06 (1H, *d*, *J* = 15.0 Hz); 2.54 (1H, *d*, *J* = 15.0 Hz); 2.84~2.88 (1H, *m*); 5.03 (1H, *d*, *J* = 13.0 Hz); 5.06 (1H, *d*, *J* = 13.0 Hz); 5.27 (1H, *t*, *J* = 3.2 Hz); 7.30~7.37 (6H, *m*); 7.60~7.62 (2H, *m*); 7.98~8.00 (2H, *m*). ^{13}C-NMR (75 MHz): 176.3; 146.1; 145.9; 143.1; 138.7; 136.3; 132.9; 130.0; 128.3; 127.8; 127.7; 122.1; 118.1; 114.1; 111.8; 65.3; 53.9; 46.1; 45.6; 45.3; 41.4; 41.1; 39.0; 38.7; 37.5; 36.3; 34.1; 33.1; 32.6; 31.9; 31.7; 30.3; 29.3; 27.1; 25.2; 23.2; 22.8; 22.6; 22.3; 18.6; 16.2; 14.9. ESI-MS: 689 ($[M+H]^+$). Anal. calc. for $C_{45}H_{56}N_2O_4$: C 78.45, H 8.19, N 4.07; Found: C 78.26, H 8.50, N 3.91.

Benzyl 1'-(4"-methoxyphenyl)pyrazole[4,5-b]olean-12-en-28-oate (**12**)

Following the procedures for the preparation of **5**, treatment of **4** (0.5 g, 0.87 mmol) with (4-methoxyphenyl)hydrazine hydrochloride (0.16 g, 0.92 mmol) afforded 0.37 g (62%) of **12**. M.p. 171-173°C. IR (KBr): 3423, 2945, 1726, 1516, 1250. ^{1}H-NMR (300 MHz): 0.67 (3H, *s*); 0.89 (3H, *s*); 0.91 (3H, *s*); 0.94 (3H, *s*); 1.03 (3H, *s*); 1.08 (3H, *s*); 1.15 (3H, *s*); 2.64 (1H, *d*, *J* = 14.9 Hz); 2.92~2.98 (1H, *m*); 3.86 (3H, *s*); 5.05 (1H, *d*, *J* = 12.5 Hz); 5.10 (1H, *d*, *J* = 12.5 Hz); 5.36 (1H, *t*, *J* = 3.6 Hz); 6.90~6.98 (2H, *m*); 7.29~7.36 (7H, *m*); 7.49 (1H, *s*). ESI-MS: 675 ($[M+H]^+$). Anal. calc. for $C_{45}H_{58}N_2O_3$: C 80.08, H 8.66, N 4.15; Found: C 79.85, H 8.72, N 3.93.

Benzyl 1'-(2"-ethylphenyl)pyrazole[4,5-b]olean-12-en-28-oate (**13**)

Following the procedures for the preparation of **5**, treatment of **4** (0.5 g, 0.87 mmol) with (2-ethylphenyl) hydrazine hydrochloride (0.16 g, 0.92 mmol) afforded 0.51 g (87%) of **13**. M.p. 108-110°C. IR (KBr): 3440, 2947, 1726, 1456, 1382. ^{1}H-NMR (300 MHz, DMSO-d_6): 0.59 (3H, *s*); 0.70 (3H, *s*); 0.81 (3H, *s*); 0.83 (3H, *s*); 0.89 (6H, *s*); 1.02 (3H, *s*); 2.83~2.89 (1H, *m*); 5.02~5.06 (2H, *m*); 5.27 (1H, br *s*); 7.29~7.47 (10H, *m*). ^{13}C-NMR (75 MHz): 176.2; 145.0; 144.9; 143.0; 142.7; 142.6; 140.4; 140.3; 137.6; 137.5; 136.2; 129.4; 129.3; 129.2; 129.1; 128.4; 128.3; 127.8; 127.6; 125.5; 122.0; 113.3; 113.1; 65.2; 53.9; 46.1; 45.7; 45.5; 45.3; 45.3; 41.4; 41.1; 38.4; 38.3; 38.2; 37.6; 37.5; 36.3; 34.1; 34.0; 33.1; 32.6; 31.9; 31.7; 30.3; 29.7. 27.3; 27.1; 25.2; 25.2; 23.2; 23.0; 23.0; 22.8; 22.6; 22.4; 20.2; 18.6; 16.3; 16.2; 15.1; 14.6; 14.4; 14.3. ESI-MS: 673 ($[M+ H]^+$).

Benzyl 1'-(3"-chloro-4"-methylphenyl)pyrazole[4,5-b]olean-12-en-28-oate (**14**)

Following the procedures for the preparation of **5**, treatment of **4** (0.5 g, 0.87 mmol) with (3-chloro-4-methylphenyl)hydrazine hydrochloride (0.18 g, 0.92 mmol) afforded 0.51 g (85%) of **14**. M.p. 92-93°C. IR (KBr): 3452, 2947, 1726, 1159. ^{1}H-NMR (300 MHz): 0.68 (3H, *s*); 0.90 (3H, *s*); 0.91 (3H, *s*); 0.94 (3H, *s*); 1.02 (3H, *s*); 1.06 (3H, *s*); 1.16 (3H, *s*); 2.09 (1H, *d*, *J* = 15.0 Hz); 2.44 (3H, *s*); 2.59 (1H, *d*, *J* = 14.9 Hz); 2.93~2.97 (1H, *m*); 5.05 (1H, *d*, *J* = 12.5 Hz); 5.10 (1H, *d*, *J* = 12.5 Hz); 5.37 (1H, br *s*); 7.17~7.20 (1H, *m*); 7.27~7.40 (8H, *m*). ^{13}C-NMR (75 MHz): 177.5; 146.3; 143.6; 141.2; 138.7; 137.1; 136.5; 133.9; 130.5; 129.7; 128.5; 128.0; 127.9; 127.3; 122.6; 114.3; 66.0; 54.7; 46.4; 45.9; 45.9; 41.9; 41.6; 39.3; 38.07; 36.9; 34.7; 33.9; 33.1; 32.4; 32.3; 30.7; 29.5; 27.7; 25.6; 23.6; 23.3; 23.1; 22.4; 19.8; 19.2; 16.6; 15.2. ESI-MS: 693 ($[M+H]^+$).

3-Oxoleana-12-en-28-oic acid (**15**)

To a solution of **1** (OA) (2 g, 4.3 mmol) in acetone (100 mL) was added Jones reagent (8 mL) at 0°C. The resulting mixture was stirred for 30 min. Then the reaction mixture was quenched by EtOH. After removing most solvents by evaporation under reduced pressure, to the residue was added EtOAc (50 mL) and THF (10 mL). The organic layer was washed with brine, dried (Na_2SO_4) and concentrated under reduced pressure. The crude product was purified by flash CC (SiO_2; heptane/AcOEt 15:1) to afford 1.6 g (80%) of **15**. M.p. 199-201°C. IR (KBr): 3448, 2945, 1701, 1460, 1384. ^{1}H-NMR (300 MHz): 0.81 (3H, *s*); 0.91 (3H, *s*); 0.93 (3H, *s*); 1.03 (3H, *s*); 1.05 (3H, *s*); 1.09 (3H, *s*); 1.15 (3H, *s*); 2.30~2.48 (1H, *m*); 2.49~2.65 (1H, *m*); 2.84 (1H, *dd*, *J* = 4.0, 13.7 Hz); 5.30 (1H, br *s*). ESI-MS: 453 ($[M-H]^-$).

2-Hydroxymethylene-3-oxooleana-12-en-28-oic acid (**16**)

A mixture of **15** (0.84 g, 1.85 mmol), NaOMe (1 g, 18.52 mmol) and HCO_2Et (1.5 mL, 18.58 mmol) in CH_2Cl_2 (20 mL) was stirred at r.t. for 10 h, and then the reaction mixture was evaporated *in vacuo*. Brine was added to the residue, and the mixture was extracted with AcOEt. The organic layer was washed with H_2O, dried (Na_2SO_4) and concentrated under reduced pressure. The crude product was purified by flash CC (silica gel; heptane/AcOEt 10:1) to afford 0.7 g (78%) of **16**. White solid. M.p. 212-214°C. IR (KBr): 2945, 1691, 1581. ^{1}H-NMR (300 MHz, DMSO-d_6): 0.76 (6H, *s*); 0.86 (6H, *s*); 1.10 (9H, *s*); 2.29 (1H, *d*, *J* = 14.5 Hz); 2.75 (1H, *dd*, *J* = 3.7, 13.9 Hz); 5.20 (1H, *s*); 8.73 (1H, *s*); 11.98 (1H, *s*); 14.28 (1H, br *s*). ESI-MS: 481 ($[M-H]^-$).

1'-Phenylpyrazole[4,5-b]olean-12-en-28-oisc acid (**17**)

A mixture of **16** (0.5 g, 1.04 mmol) and phenylhydrazine hydrochloride (0.16 g, 1.09 mmol) in EtOH (20 mL) was heated under reflux for 20 h. Brine was added to the residue, and the mixture was extracted with AcOEt. The organic layer was washed with H_2O, dried (Na_2SO_4) and concentrated under reduced pressure. The crude product was purified by flash CC (SiO_2; CH_2Cl_2/MeOH 100:1) and then recrystallization from AcOEt to afford 0.42g (73%) of **17**. White solid. M.p. > 300°C. IR (KBr): 2904, 1722, 1458, 1382. ^{1}H-NMR (300 MHz, DMSO-d_6): 0.80 (3H, *s*); 0.89 (9H, *s*); 0.94 (3H, *s*); 0.98 (3H, *s*); 1.13 (3H, *s*); 2.07 (1H, *d*, *J* = 14.9 Hz); 2.55 (1H, *d*, *J* = 14.9 Hz); 2.76~2.83 (1H, *m*); 5.25 (1H, br *s*); 7.29 (1H, *s*); 7.33~7.38 (2H, *m*); 7.45~7.52 (3H, *m*); 12.01 (1H, *s*). ^{13}C-NMR (75 MHz): 178.7; 145.5; 143.7; 142.3; 137.8; 129.2; 129.1; 128.6; 121.7; 113.5; 54.2; 45.9; 45.8; 45.7; 41.6; 41.1; 37.8; 36.6; 34.3; 33.5; 33.0; 32.2; 32.0; 30.5; 29.3; 27.4; 25.5; 23.5; 23.0; 22.8; 22.3; 18.9; 16.7; 15.2. HRMS: Calcd for $C_{37}H_{49}N_2O_2$: 553.3794 ($[M-H]^-$), Found 553.3795 ($[M-H]^-$). Anal. calc. for $C_{37}H_{50}N_2O_2$: C 80.10, H 9.08, N 5.05; Found: C 79.77, H 8.85, N 4.98.

1'-(p-Tolyl)pyrazole[4,5-b]olean-12-en-28-oic acid (**18**)

Following the procedures for the preparation of **17**, treatment of **16** (0.5 g, 1.04 mmol) with *p*-tolylhydrazine hydrochloride (0.17 g, 1.09 mmol) afforded 0.38 g (65%) of **18**. M.p. > 300°C. IR (KBr): 2950, 1718, 1515, 1384. ^{1}H-NMR (300 MHz, DMSO-d_6): 0.79 (3H, *s*); 0.89 (9H, *s*); 0.94 (3H, *s*); 0.99 (3H, *s*); 1.13 (3H, *s*); 2.05 (1H, *d*, *J* = 14.9 Hz); 2.39 (3H, *s*); 2.76~2.81 (1H, *m*); 5.25 (1H, br *s*); 7.20~7.30 (5H, *m*); 12.01 (1H, br *s*). ^{13}C-NMR (75 MHz): 178.7; 145.5; 143.8; 139.8; 138.6; 137.7; 129.0; 128.9; 121.7; 113.3; 54.3; 45.9; 45.8; 45.7; 41.6; 41.1; 37.8; 34.3; 33.5; 32.9; 32.2; 32.0; 30.5; 29.3; 25.5; 23.5; 23.0; 22.8; 22.3; 22.3; 20.9; 18.9; 16.7; 15.2. HRMS: Calcd for $C_{38}H_{51}N_2O_2$: 567.3951 ($[M-H]^-$), Found 567.4000 ($[M-H]^-$). Anal. calc. for $C_{38}H_{52}N_2O_2$: C 80.24, H 9.21, N 4.92; Found: C 80.06, H 9.11, N 4.82.

1'-(4''-Chlorophenyl)pyrazole[4,5-b]olean-12-en-28-oic acid (**19**)

Following the procedures for the preparation of **17**, treatment of **16** (0.5 g, 1.04 mmol) with (4-chlorophenyl) hydrazine hydrochloride (0.19 g, 1.09 mmol) afforded 0.38 g (62%) of **19**. M.p. 260-262°C. IR (KBr): 3443, 2945, 1700, 1613. ^{1}H-NMR (300 MHz): 0.88 (3H, *s*); 0.97 (6H, *s*); 1.00 (3H, *s*); 1.06 (3H, *s*); 1.13 (3H, *s*); 1.22 (3H, *s*); 2.69 (1H, *d*, *J* = 14.9 Hz); 2.89~2.96 (1H, *m*); 5.42 (1H, br *s*); 7.38~7.55 (5H, *m*). ESI-MS: 587 ($[M-H]^-$).

1'-(4''-Isopropylphenyl)pyrazole[4,5-b]olean-12-en-28-oic acid (**20**)

Following the procedures for the preparation of **17**, treatment of **16** (0.5 g, 1.04 mmol) with (4-isopropylphenyl)hydrazine hydrochloride (0.2 g, 1.09 mmol) afforded 0.45 g (73%) of **20**. M.p. 243-245°C. IR (KBr): 3440, 2943, 1693, 1610. ^{1}H-NMR (300 MHz, DMSO-d_6): 0.76 (3H, *s*); 0.86 (9H, *s*); 0.92 (3H, *s*); 0.96 (3H, *s*); 1.10 (3H, *s*); 2.03 (1H, *d*, *J* = 14.9 Hz); 2.74~2.78 (1H, *m*); 2.91~3.00 (1H, *m*); 5.22 (1H, br *s*); 7.21~7.33 (5H, *m*); 11.97 (1H, br *s*). ESI-MS: 595 ($[M-H]^-$).

1'-(3'',5''-Difluorophenyl)pyrazole[4,5-b]olean-12-en-28-oic acid (**21**)

Following the procedures for the preparation of **17**, treatment of **16** (0.5 g, 1.04 mmol) with (3,5-difluorophenyl)hydrazine hydrochloride (0.2 g, 1.09 mmol) afforded 0.43 g (78%) of **21**. M.p. 208-210°C. IR (KBr): 3448, 2947, 1703, 1616, 1122. ^{1}H-NMR (300 MHz,

DMSO-d_6): 0.80 (3H, *s*); 0.89 (9H, *s*); 0.99 (3H, *s*); 1.03 (3H, *s*); 1.13 (3H, *s*); 2.05 (1H, *d*, J = 15.1 Hz); 2.79 (1H, *dd*, J = 3.5, 13.4 Hz); 5.25 (1H, br *s*); 7.23~7.27 (2H, *m*); 7.35 (1H, *s*); 7.44~7.51 (1H, *m*); 12.02 (1H, br *s*). ^{13}C-NMR (75 MHz): 178.5; 163.3; 163.1; 160.0; 159.8; 145.7; 144.3; 144.1; 143.6; 138.5; 121.5; 113.9; 113.4; 113.2; 113.0; 105.3; 105.0; 104.6; 54.0; 45.7; 45.5; 41.4; 40.9; 40.3; 37.5; 36.3; 34.1; 33.3; 32.7; 32.0; 31.7; 30.3; 29.2; 27.2; 25.3; 23.3; 22.8; 22.6; 22.2; 18.7; 16.5; 14.9. ESI-MS: 589 ([M-H]$^-$).

2.2 *Enzymatic activity assays*

The inhibitory activity of the test compounds against rabbit muscle GPa was monitored using a microplate reader (BIO-RAD) based on the published method (*14*). In brief, GPa activity was measured in the direction of glycogen synthesis by the release of phosphate from glucose-1-phosphate. Each test compound was dissolved in DMSO and diluted at different concentrations for IC_{50} determination. The enzyme (GPa) was added to 100 µL of buffer containing 50 mM Hepes (pH 7.2), 100 mM KCl, 2.5 mM $MgCl_2$, 0.5 mM glucose-1-phosphate, 1 mg/mL glycogen, and the test compound in 96-well microplates (Costar). After the addition of 150 µL of 1 M HCl containing 10 mg/mL ammonium molybdate and 0.38 mg/mL malachite green, reactions were run at 22°C for 25 min. And then the phosphate absorbance was measured at 655 nm. The IC_{50} values were estimated by fitting the inhibition data to a dose-dependent curve using a logistic derivative equation.

3. Results and Discussion

3.1 *Chemistry*

The synthesis of substituted phenylpyrazole [4,5-*b*]oleanane derivatives is illustrated in Schemes 1-3. Following the procedures reported previously (*9-11*), esterification of **1** (OA) with benzyl chloride afforded benzyl ester **2**. Treatment **2** with PCC afforded ketone **3**. Formylation of **3** with ethyl formate in the presence of NaOMe in CH_2Cl_2 gave compound **4**. Treatment of **4** with substituted phenylhydrazine hydrochloride in EtOH at reflux temperature afforded pyrazole triterpene **5~14** (47~87%).

As shown in Scheme 2, the attempted hydrogenolysis of **5** in order to obtain the corresponding phenylpyrazole triterpene acid was unsuccessful, resulting in a complex mixture. Thus, a new approach for synthesis of phenylpyrazole triterpene acid was designed (*Scheme 3*).

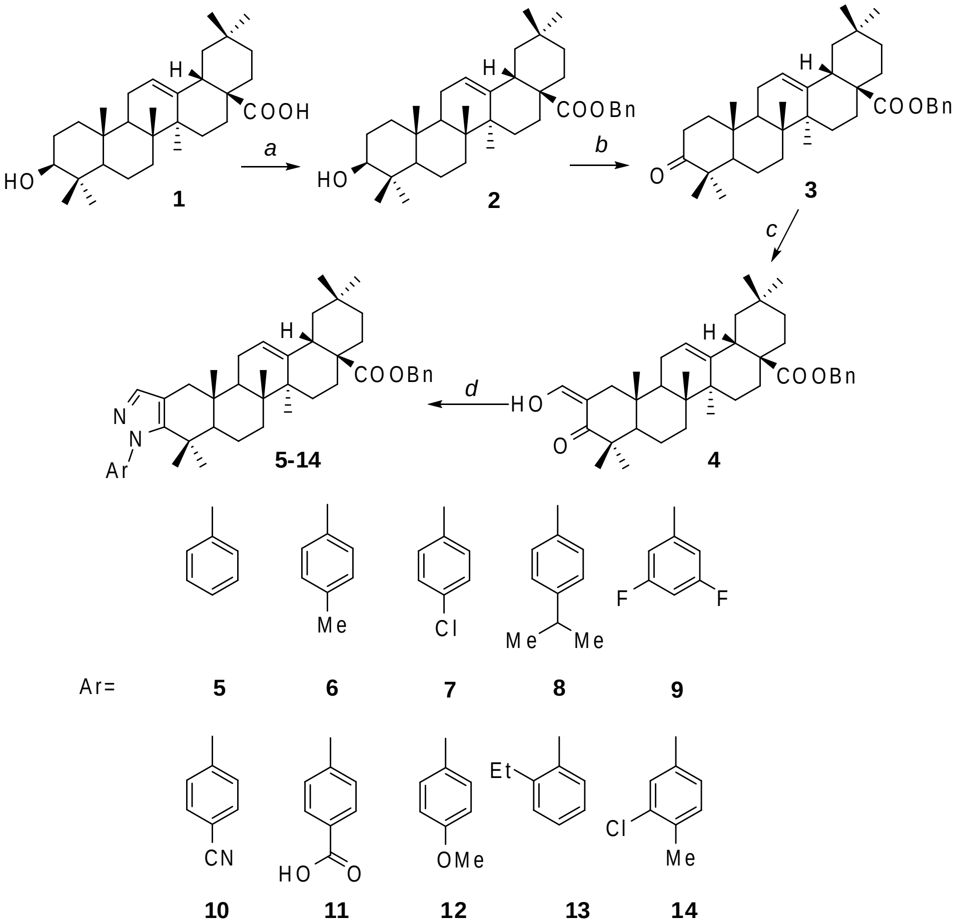

Scheme 1. Reagents and conditions: *a)* BnCl, K_2CO_3, DMF, 50°C; *b)* PCC, CH_2Cl_2, r.t; *c)* HCO_2Et, NaOMe, CH_2Cl_2, r.t, 80%; *d)* for **5-14**: $ArNH_2NH_2$•HCl, EtOH, reflux, 47-87%.

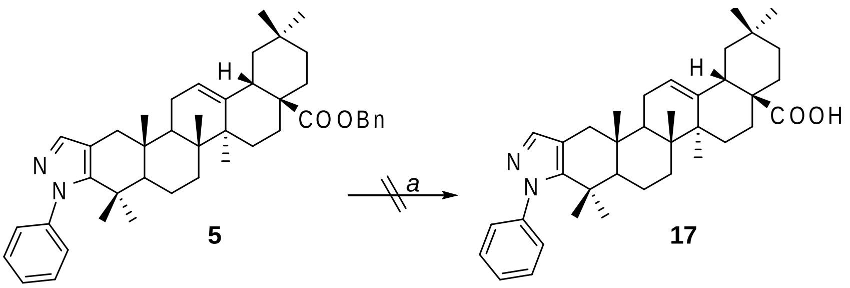

Scheme 2. Reagents and conditions: *a)* H_2, 10% Pd-C, AcOH/1M HCl, r.t.

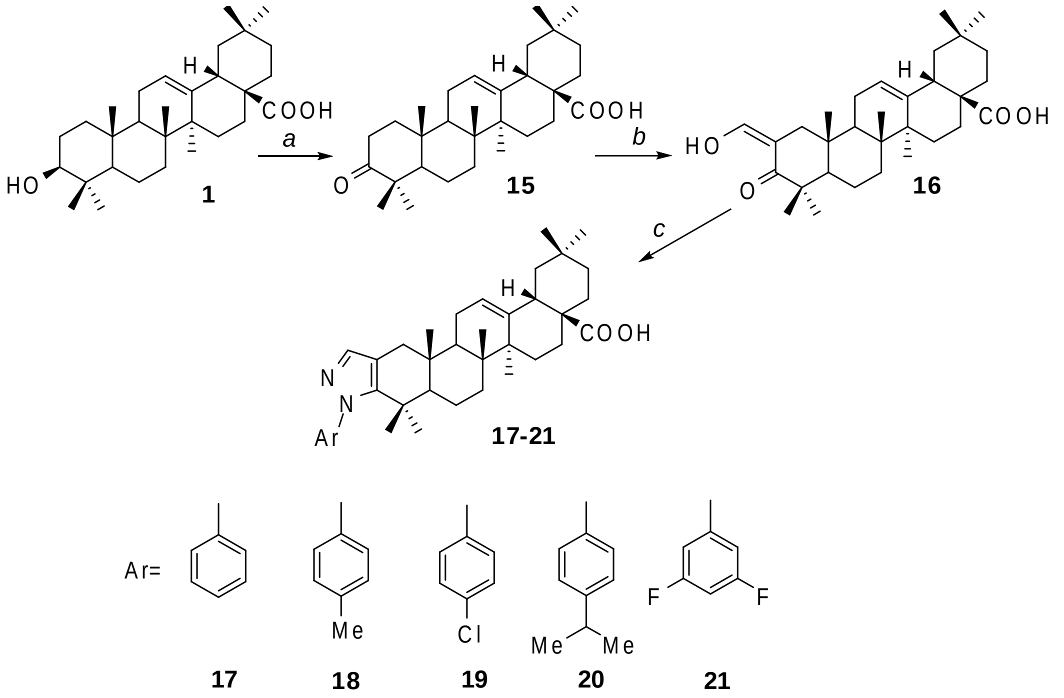

Scheme 3. Reagents and conditions: *a)* Jones regent, acetone, 0°C to r.t, 80%; *b)* HCO_2Et, NaOMe, CH_2Cl_2, r.t, 78%; *c)* for **17**-**21**: $ArNH_2NH_2$• HCl, EtOH, reflux, 62-73%.

Oxidation of **1** (OA) with Jones reagent in acetone gave keto-acid **15**. Formylation of **15** with ethyl formate in the presence of NaOMe in CH_2Cl_2 gave compound **16**. Treatment of **16** with substituted phenylhydrazine hydrochloride in EtOH at reflux temperature afforded substituted phenylpyrazole triterpene acid **17**~**21** (62~73%).

The structure of **17** was unambiguously determined by NMR and HRMS data (*see 2.1.2 Synthesis*), including ROESY analysis.

3.2 *Biological evaluation*

The synthesized phenylpyrazole[4,5-*b*]oleanane derivatives were biologically evaluated for their inhibitory activity against rabbit muscle GPa. The activity of rabbit muscle GPa was measured by detecting the release of phosphate from glucose -1-phosphate in the direction of glycogen synthesis (*14*). The assay results showed that most of the newly synthesized pyrazole triterpenes exhibited inhibitory activity against rabbit muscle GPa with IC_{50} values in the range of 10.8–535 μM (Table 1).

Table 1. Inhibition of rabbit muscle GPa by compounds **1**, **5**-**21**

Compounds	RMGPa IC_{50}[a] (μM)
1(OA)	14
5	NI[b]
6	57
7	10.8
8	NI
9	NI
10	257.2
11	NI
12	13.4
13	NI
14	535
17	35.1
18	18.3
19	241.7
20	69.6
21	46.9
caffeine[c]	114

[a] Values are means of three experiments; [b] NI means no inhibition; [c] Caffeine was used as a positive control.

3.3 *SAR analysis*

Preliminary structure-activity relationship (SAR) analysis showed that incorporation of a phenylpyrazole structural unit in the A-ring of oleanolic acid resulted in a slight increase in GPa inhibitory potency in some cases (*e.g.* **7** and **12**). C(28) Triterpene acids were more potent than the corresponding C(28) benzyl esters (*e.g.* **5** *vs.* **17**; **6** *vs.* **18**; **8** *vs.* **20**; **9** *vs.* **21**), indicating a preference for hydrophilic groups over hydrophobic groups at the C(28) position, agreeing with the authors' previous studies (*9,10*).

4. Conclusion

Fifteen new phenylpyrazole[4,5-*b*]oleanane derivatives have been synthesized and biologically evaluated for their inhibitory activity against rabbit muscle GPa. Within this series of compounds, **7** (IC_{50} = 10.8 μM) exhibited slightly more potent activity than its parent compound, **1** (OA). Preliminary SAR analysis showed a clear preference for hydrophilicity over hydrophobicity at both the C(28) and pyrazole unit in terms of GPa inhibition. Further biological evaluation of these phenylpyrazole triterpenes is ongoing and these results will be reported in due course.

Acknowledgements

This program was financially supported by the National Natural Science Foundation of China (grants 30672523 and 90713037), research grants from Chinese Ministry of Education (grants 706030 and 20050316008), the program for New Century Excellent Talents in University (NCET-05-0495).

References

1 Singh GB, Singh S, Bani S, Gupta BD, Banerjee SK. Anti-inflammatory activity of oleanolic acid in rats and mice. J Pharm Pharmacol 1992; 44:456-458.

2 Mengoni F, Lichtner M, Battinelli L, Marzi M, Mastroianni CM, Vullo V, Mazzanti G. *In vitro* anti-HIV activity of oleanolic acid on infected human mononuclear cells. Planta Med 2002; 68:111-114.

3 Zhu YM, Shen JK, Wang HK, Cosentino LM, Lee KH. Synthesis and anti-HIV activity of oleanolic acid derivatives. Bioorg Med Chem Lett 2001; 11:3115-3118.

4 Hsu HY, Yang JJ, Lin CC. Effects of oleanolic acid and ursolic acid on inhibiting tumor growth and enhancing the recovery of hematopoietic system postirradiation in mice. Cancer Lett 1997; 111:7-13.

5 Tan GT, Lee S, Lee IS, Chen J, Leitner P, Besterman JM, Kinghorn AD, Pezzuto JM. Natural-product inhibitors of human DNA ligase I. Biochem J 1996; 314:993-1000.

6 Liu Y, Hartley DP, Liu J. Protection against carbon tetrachloride hepatotoxicity by oleanolic acid is not mediated through metallothionein. Toxicol Lett 1998; 95:77-85.

7 Jeong HG. Inhibition of cytochrome P450 2E1 expression by oleanolic acid: hepatoprotective effects against carbon tetrachloride-induced hepatic injury. Toxicol Lett 1999; 105:215-222.

8 Liu J, Liu Y, Parkinson A, Klaassen CD. Effect of oleanolic acid on hepatic toxicant-activating and detoxifying systems in mice. Exp Ther 1995; 275:768-774.

9 Chen J, Gong YC, Liu J, Hua WY, Zhang LY, Sun HB. Synthesis and biological evaluation of novel pyrazole[4,3-*b*]oleanane derivatives as inhibitors of glycogen phosphorylase. Chem Biodiv 2008; in press.

10 Chen J, Liu J, Zhang LY, Wu GZ, Hua WY, Wu XM, Sun HB. Pentacyclic Triterpenes. Part 3: Synthesis and biological evaluation of oleanolic acid derivatives as novel inhibitors of glycogen phosphorylase, Bioorg Med Chem Lett 2006; 16:2915-2919.

11 Wen XA, Sun HB, Liu J, Wu GZ, Zhang LY, Wu XM, Ni ZP. Pentacyclic Triterpenes. Part 1: The first examples of naturally occurring pentacyclic triterpenes as a new class of inhibitors of glycogen phosphorylases. Bioorg Med Chem Lett 2005; 15:4944-4948.

12 Wen XA, Zhang P, Liu J, Zhang LY, Wu XM, Ni PZ, Sun HB. Pentacyclic Triterpenes. Part 2: Synthesis and biological activity of maslinic acid derivatives as inhibitors of glycogen phosphorylase. Bioorg Med Chem Lett 2006; 16:722-726.

13 Kurukulasuriya R, Link JT, Madar DJ, Pei Z, Rohde JJ, Richards SJ, Souers AJ, Szczepankiewicz BG. Prospects for pharmacologic inhibition of hepatic glucose production. Curr Med Chem 2003; 10:99-121.

14 Martin WH, Hoover DJ, Armento SJ, Stock IA, McPherson RK, Danley DE, Stevenson RW, Barrett EJ, Treadway JL. Discovery of a human glycogen phosphorylase inhibitor that lowers blood glucose *in vivo*. Proc Natl Acad Sci USA 1998; 95:1776-1781.

(*Received February 15, 2008; Accepted February 27, 2008*)

Original Article

Using factorial design to improve the solubility and *in-vitro* dissolution of nimesulide hydrophilic polymer binary systems

Ibrahim S. Khattab*, **Saleh M. Al-Saidan, Aly H. Nada, Abdel-Azim A. Zaghloul**

Department of Pharmaceutics, Faculty of Pharmacy, Kuwait University, Kuwait.

ABSTRACT: The aim of the present study was to use factorial design to enhance the dissolution rate of nimesulide using solid binary systems with the hydrophilic carriers D-mannitol and polyethylene glycol (PEG 4000). Two-factor full factorial design was employed to investigate the effects of the drug/carrier ratio (X_1, 10 and 20%) and the method of preparation (X_2, physical or co-melted mixture) on the percent drug release after 60 min (Y_1). Drug-carrier co-melted mixtures were prepared by melting the carriers D-mannitol or PEG with the drug. For physical mixtures, the drug and carrier were mixed thoroughly in a mortar until a homogeneous mixture was obtained. Drug-carrier interactions were investigated by differential scanning calorimetry (DSC). All prepared mixtures were filled in hard gelatin capsules, size 0, and then their dissolution rate was tested. The results showed an increase in the solubility of the drug with increasing polymer concentrations. Thermal analysis revealed no notable differences regarding thermal events of nimesulide, D-mannitol, PEG 4000, and their physical or co-melted mixtures. The percent drug released after 60 min was 29.5% for nimesulide alone, 37.14 and 32.0% for a PEG/Physical mixture with a 10 or 20% drug/polymer ratio, and 69.7 and 53.1% for a PEG/Co-melted mixture with the same ratios. For nimesulide/D-mannitol, this percent drug released was 33.57 and 29.6% for a physical mixture and 63.13 and 48.04% for a co-melted mixture. Formulations with PEG showed an increase in solubility as well as dissolution in comparison to those prepared with D-mannitol. Factorial design was successfully used to optimize the dissolution rate of nimesulide. The chosen polymers caused a notable increase in drug solubility and co-melted formulations generally showed a higher dissolution than those prepared with physical mixtures.

Keywords: Nimesulide, Binary systems, Factorial design

1. Introduction

Nimesulide is a non-steroidal anti-inflammatory agent that differs from many similar compounds in that it is acidic by virtue of a sulfonanilide rather than a carboxyl group. It is an inhibitor of cyclo-oxygenase 2, hence it inhibits the synthesis of destructive prostaglandins and spares cytoprotective prostaglandins. Nimesulide is practically insoluble in water (0.01 mg/mL). The poor aqueous solubility and wettability of the drug give rise to difficulties in the pharmaceutical formulation of oral preparations or solutions and may lead to its varying bioavailability. Increasing the aqueous solubility of nimesulide is an important way to overcome these drawbacks (*1*).

The improvement of both solubility and dissolution rate by inserting a drug into a solid dispersion has been widely discussed and reported in a number of articles (*2-6*).

The selection of the carrier has ultimate influence on dissolution characteristics. Research has shown that water soluble carriers result in a fast release of the drug from the matrix. Poorly soluble carriers, however, lead to slow release of the drug from the matrix (*7*). To date, several methods have been used to increase the water solubility of poorly soluble drugs such as physical modification of the drug and use of co-solvents, nanoparticles, a film coating, a complexation approach, and solid dispersion technology (*8-13*). Polyethylene glycols have been used extensively as water-soluble carriers and stabilizers for pharmaceutical dosage forms because of their favorable solution properties and low toxicity and cost (*14-16*). D-Mannitol is primarily used in pharmaceutical preparations as a diluent. It has been also used to improve the dissolution and bioavailability of thiazolidinedione and triamterene (*17-19*).

The purpose of the present study was to employ an experimental design to develop an optimization strategy to increase the water dissolution of nimesulide by using carriers such as D-mannitol and polyethylene glycol at various drug/polymer concentrations. A two-factor, two-level factorial experimental design was employed to determine whether a particular treatment or combination of treatments was satisfactorily significant

---

**Correspondence to:* Dr. Ibrahim S. Khattab, Pharmaceutics Faculty of Pharmacy, Kuwait University, Kuwait;
e-mail: Khattab@hsc.edu.kw

in influencing system response. Mathematical elaboration of experimental data was carried out by the computer program Design Expert®.

2. Materials and Methods

2.1. *Materials*

Nimesulide (NS) was from Sigma (Italy), and Polyethylene Glycol 4000 (PEG 4000) and D-mannitol (DM) were from Fluka (Germany). Empty capsules were generously supplied by KSPICO (Kuwait). All other materials and solvents were of analytical grade and used as received.

2.2. *Preparation of physical mixtures and binary systems*

2.2.1. *Preparation of physical mixtures*

Physical mixtures were prepared according to the design; NS content was at a concentration of 10 and 20% (w/w) with a carrier of DM or PEG 4000. The drug and carrier were accurately weighed, pulverized, and then mixed thoroughly by titration in a glass mortar until a homogeneous mixture was obtained. The systems were designated NS/DM10, NS/DM20, NS/PEG10, and NS/PEG20 for the drug D-mannitol and the drug PEG, respectively.

2.2.2. *Melting carrier method*

Solid dispersions of NS with carriers were prepared by the melting method at ratios of 1:9 and 2:8 (NS: PEG or DM). The required amount of each carrier was melted over a thermostatically controlled magnetic stirrer at its respective melting point, *i.e.* 50-60°C for PEG and 165°C for DM. When the carrier appeared to have completely melted, the required amount of NS was incorporated into the molten carrier mass. The blend was heated at the corresponding temperature for 5 min with constant mixing. The resultant melted mixture was transferred to a glass mortar and mixed thoroughly for another 5 min and then left to cool at room temperature. After solidification, the solid obtained was ground and passed through a no. 60 sieve, and the fraction between 50-200 µm fractions was selected. All prepared solid dispersions or physical mixtures were filled into hard gelatine capsules (size 0) such that each capsule contained 10 or 20% drug in different carriers.

2.3. *Phase solubility studies*

The apparent solubility of NS pure drug and binary mixtures in water was obtained at 37°C. Various quantities (1, 2, 3, 10 and 20%, w/v) of aqueous solutions of PEG and DM were prepared, and 50 mL of these solutions were placed in conical flasks with screw caps. An excess amount of NS was added to the flasks. The flasks containing NS-mixtures were shaken mechanically for 12 h at 37 ± 2°C in a mechanical shaker, rpm 175 (Elico Pvt. Ltd, Mumbai, India). These solutions were allowed to equilibrate for the next 24 h and then centrifuged for 5 min at 2,000 rpm. The supernatant of each flask was filtered through Whatman filter paper no. 1; the filtrate was diluted and analyzed spectrophotometrically at 393 nm. Solubility studies were performed in triplicate ($n = 3$).

2.4. *Differential scanning calorimetry*

Thermal analysis was carried out by a Setaram instrument (model 41 L, Caluire, France WB/M00) under a dry nitrogen purging gas flux. Thermoregulation of the instrument head was guaranteed by connection to a cooling system. About 5 mg of samples were weighed in a standard open aluminum pan. An empty pan of the same type was utilized as a reference. Heating and cooling rates of 5°C/min in the temperature range of 25-360°C were used. Calibration of temperature and heat flow was performed with indium.

2.5. *In vitro dissolution test*

A paddle dissolution apparatus, USP23/NF (model DT80, Erweka, Germany), was used. Dissolution fluid was 900 mL of a pH 7.4 phosphate buffer. Temperature was thermostated at 37 ± 0.5°C and the buffer was stirred at 50 rpm. Sample solution (2.5 mL) was withdrawn at predetermined time intervals, and the fluid was filtered (0.45 nm membrane) prior to entering the working cell and analyzed spectrophotometrically at 393 nm; each test was performed in triplicate ($n = 3$). An equal amount of fresh dissolution medium was replaced after withdrawal of the test sample. The considered parameters were: the initial dissolution rate and the percent NS released after 1 h of dissolution.

2.6. *Experimental design*

To optimize the *in-vitro* dissolution of NS from different carriers, a two-factor full factorial design was employed to investigate the effects of the drug/carrier ratio (X_1, 10-20%), represented by –1 and +1 and analogous to the respective low and high values, and the method of preparation (X_2, physical or co-melted mixture) on the percent drug release after 1 h (Y), with X_1 and X_2 serving as independent variables. The polynomial equations that completely describe the system were also calculated. The general expression for these equations is as follows:

$$Y = b_0 + b_1X_1 + b_2X_2$$

Mathematical elaboration of experimental data was carried out by the computer program DESIGN EXPERT®. Analysis of variance (ANOVA) was also performed on the resulting data.

3. Results

3.1. *Phase solubility studies*

The solubility of NS increased as the PEG concentration increased, while with DM a slight change occurred in comparison to solubility with pure NS, as indicated by the solubility data given in Table 1 and shown in Figure 1. The enhancement of solubility with PEG as directly relates to the increase in the polymer content may be attributed to the hydrophilic nature of the carrier.

3.2. *DSC studies*

Differential scanning calorimetry (DSC) analysis is widely used to investigate the structure of solid dispersions and to demonstrate possible drug/matrix interactions through the shape of the peaks, the melting temperatures, and the specific melting heats offered by the thermograms.

The thermograms were carried out separately with the drug and excipient. NS shows quite a narrow melting peak and a melting point at 146°C. The melting point for PEG is at 58°C, with a wide and asymmetric peak due to its chemical composition, which is a mixture of macromolecules with a molecular mass around 4,000. The thermograms of DM gave rise to two sharp melting endotherms at 170.15°C and 345.17°C (Figure 2).

Thermal analysis revealed no notable differences regarding thermal events of NS, PEG, DM, and their physical or co-melted mixtures, even though some NS influence on thermal crystallization of PEG can be appreciated. The main reason for this is that the situation inside the system is altered as far as scanning proceeds.

Table 1. Summary of NS/polymer solubility studies

Polymer conc (%)	NS/PEG (x 10^{-5} M)	St/So*	NS/DM (x 10^{-5} M)	St/So*
1	2.36	1.00	2.00	0.85
2	2.40	1.17	2.20	0.93
5	3.24	1.37	2.46	1.04
10	4.45	1.89	2.87	1.22
20	7.37	3.12	1.78	0.75

* St/So, solubility change; So, solubility of nimesulide in water (2.36 x 10^{-5} M).

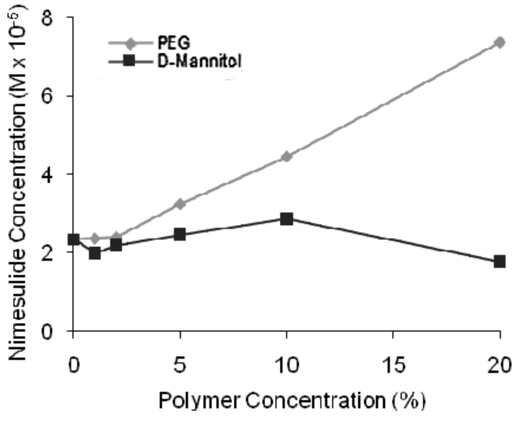

Figure 1. Phase solubility diagram of NS with (PEG/ Mannitol) solutions.

3.3. *Experimental design*

A full factorial experimental design was adopted to investigate the effect of the drug/carrier ratio (X_1) and method of preparation (X_2) on the percent drug release (Y) as illustrated in Table 2. In a full factorial design, the two variables polymer ratio and method of preparation at two levels are represented by –1 and +1, analogous to low and high values. Response surface methodology was used to generate contour plots to visually illustrate the impact of the tested variables on dissolution. Response surfaces were generated by employing one of the following mathematical equations.

Linear model: $Y = b_0 + b_1X_1 + b_2X_2$
Interaction model: $Y = b_0 + b_1X_1 + b_2X_2 + b_3X_1X_2$
Quadratic model: $Y = b_0 + b_1X_1 + b_2X_2 + b_3X_1X_2 + X_1^2 + X_2^2$

where Y represents the dependent variables, X_1 and X_2 are the independent variables (X_1 represents the polymer ratio and X_2 is the method of preparation),

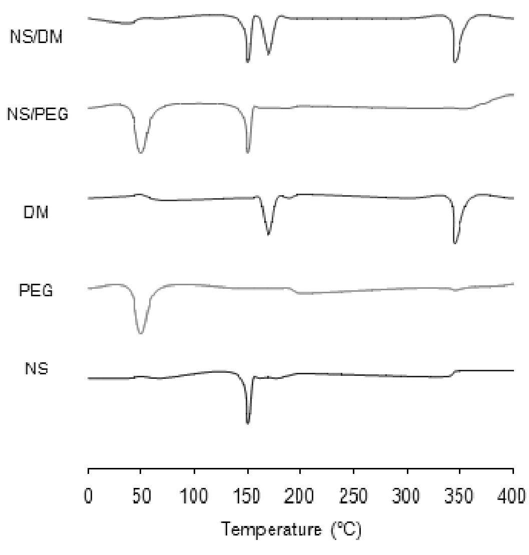

Figure 2. DSC thermogram of nimesulide, PEG 4000, and D-mannitol and NS/PEG and NS/DM (2:8) binary systems.

Table 2. Two-factor, two-level full factorial design

Run No.	Controlled factor	
	X_1	X_2
1	–1	–1
2	1	–1
3	–1	1
4	1	1
5	–1	–1
6	1	–1
7	–1	1
8	1	1

and the coefficients b_0, b_1, b_2 and b_3 are the least square regression coefficients.

The results indicate an increase in the solubility of the drug with increasing polymer concentrations. Dissolution of NS from its physical mixtures was slightly higher than that for the pure drug, but maximum improvement in the dissolution rate was observed with co-melted mixtures. The percent drug released after 60 min (R_{60}) was 29.5% for NS alone, 37.14 and 32.06% for PEG/PM with a 10 or 20% drug/polymer ratio, and 69.7 and 53.1% for PEG/CM with the same ratios. For NS/DM, this percent drug released was 33.57 and 29.5% for PM and 63.13 and 48.04% for CM. Formulations with PEG showed a notable increase in solubility as well as dissolution in comparison to those prepared with D-mannitol (Figures 3 and 4).

To optimize the percent NS release, mathematical relationships were generated between the dependent and independent variables; the resulting polynomial equations for dissolution after 60 min in terms of coded factors are as follows:

$$R_{60}\ (\text{NS/DM}) = 43.64 - 4.96X_1 + 11.87X_2 - 2.7X_1X_2$$
$$R_{60}\ (\text{NS/PEG}) = 47.88 - 5.32X_1 + 13.05X_2 - 3.02X_1X_2$$

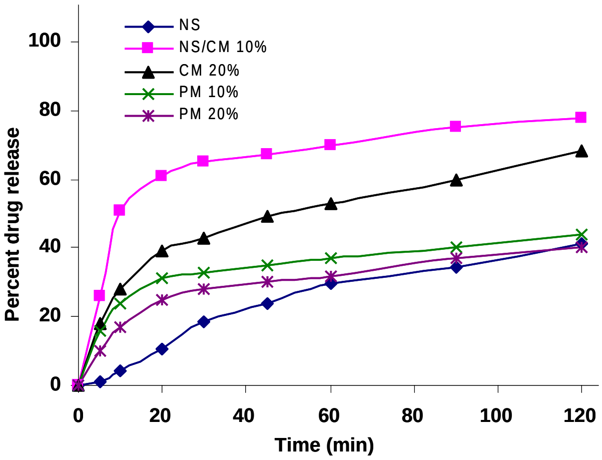

Figure 3. Dissolution profiles of NS alone and with PEG 4000 from different mixtures ratios (10% or 20%) prepared by different methods (PM, Physical mixture; CM, Co-melted mixture).

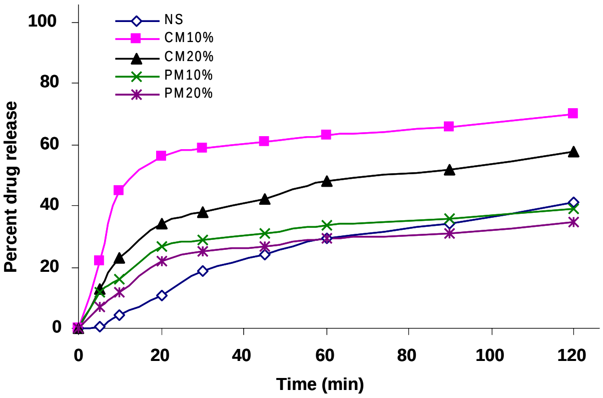

Figure 4. Dissolution profiles of NS alone and with D-mannitol from different mixtures ratios (10% or 20%) prepared by different methods (PM, Physical mixture; CM, Co-melted).

Generating the respective model equations allows selection not only of the best formulation experimentally prepared but also of the best formulation within the experimental range.

The observed, predicted, and residual values are shown in Tables 3 and 4. The "Predicted R-Squared" of 0.9965 is in reasonable agreement with the "Adjusted R-Squared" of 0.9985 for NS/PEG after time of 60 min. The same finding applied to NS/DM, which had a "Predicted R-Squared" of 0.9996 and "Adjusted R-Squared" of 0.9993. As the "Adequate Precision" measures the signal-to-noise ratio, a ratio greater than 4 is desirable; the resulting ratios of 86.68 for NS/PEG and 131.388 for NS/DM indicate an adequate signal.

Figures 5 and 6 represent response surface plots showing the influence of the percent NS released from capsules containing D-mannitol or PEG 4000, which explains the relationships between the dependent and independent variables. The figures show the effect of drug concentration and method of preparation on the response in terms of percent NS release. The results indicate that the effect of the increase in polymer concentration was more significant with co-melted mixtures than with physical ones.

Using the least square regression coefficients b_0, b_1, b_2 and b_3 in the model, one can find which X(s) produces the maximum drug release value (optimization). An experiment was performed under optimal conditions corresponding to 10% PEG 4000 using the co-melted method; the results conformed to the predicted values, indicating that the response surface

Table 3. Actual, predicted, and residual values for percent of nimesulide released after 60 min from capsules containing a NS/DM (X_1: 10 and 20%) physical mixture or co-melted mixture (X_2)

Standard order	X_1	X_2	Actual value	Predicted value	Residual value
1	–1	–1	33.57	33.49	0.08
2	1	–1	29.50	30.12	–0.62
3	–1	1	63.13	63.42	–0.29
4	1	1	48.04	48.19	–0.15
5	–1	–1	33.02	32.88	0.14
6	1	–1	30.51	30.80	0.29
7	–1	1	64.42	63.80	0.62
8	1	1	47.87	47.95	–0.08

Table 4. Actual, predicted, and residual values for percent of nimesulide released after 60 min from capsules containing a NS/PEG (X_1: 10 and 20%) physical mixture or co-melted mixture (X_2)

Standard order	X_1	X_2	Actual value	Predicted value	Residual value
1	–1	–1	37.14	36.84	0.30
2	1	–1	32.00	32.15	–0.09
3	–1	1	69.72	70.03	–0.31
4	1	1	53.08	53.17	0.09
5	–1	–1	40.27	40.10	0.17
6	1	–1	32.47	32.65	0.18
7	–1	1	71.75	71.93	–0.18
8	1	1	52.11	52.27	–0.16

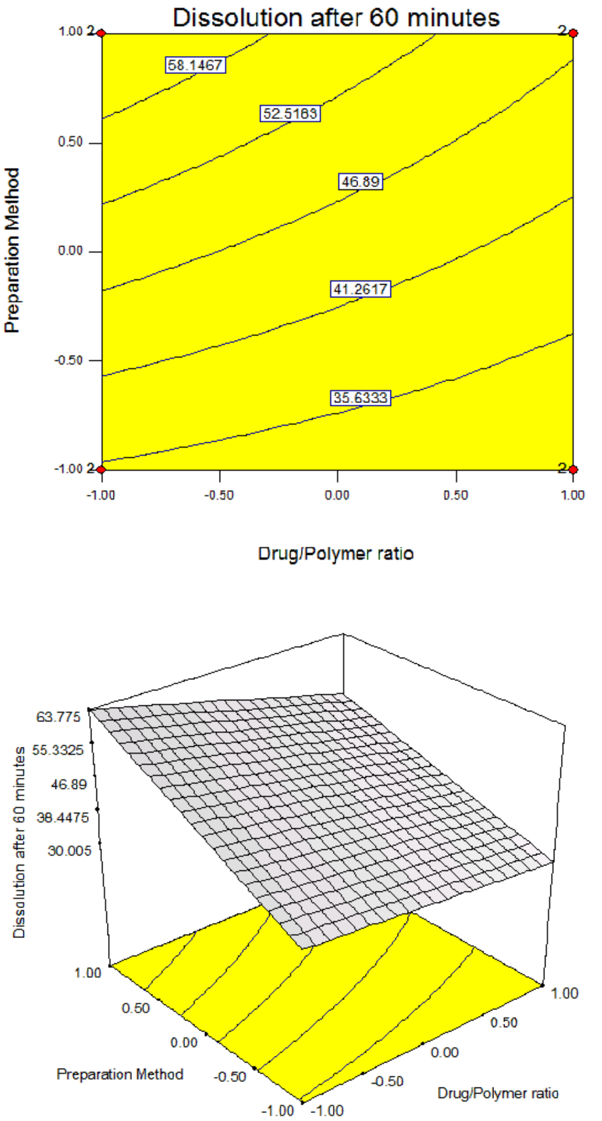

Figure 5. Response surface plot showing the influence of the NS/DM ratio (X_1) and method of preparation (X_2, Physical mixture or Co-melted mixture) on the nimesulide dissolution rate after 60 min.

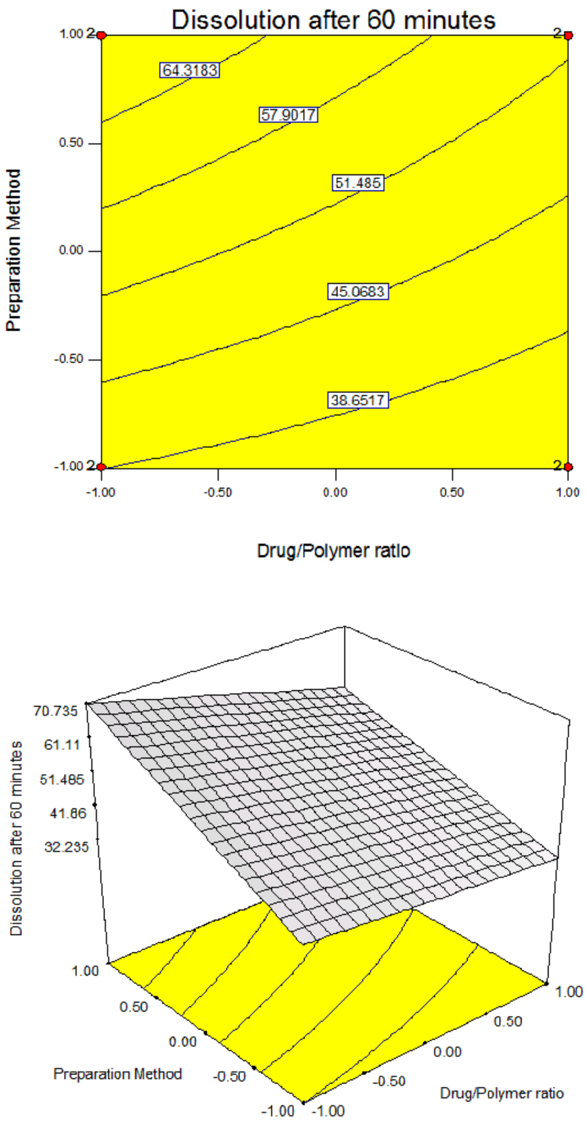

Figure 6. Response surface plot showing the influence of the NS/PEG ratio (X_1) and method of preparation (X_2, Physical mixture or Co-melted mixture) on the nimesulide dissolution rate after 60 min.

methodology optimization technique was quite useful in optimizing *in-vitro* dissolution of nimesulide.

4. Conclusions

Thermal analysis revealed no notable differences regarding thermal events of NS, PEG, DM, and their physical or co-melted mixtures. A co-melted binary system showed higher solubility as well as dissolution in comparison to NS alone or a physical mixture. Capsules containing PEG show a higher dissolution compared to those containing DM. Binary systems of NS/PEG 4000, formulated as solid dispersions, produce satisfactory drug release from capsules after 1 h. A factorial experimental design is an excellent way to optimize both formulation and process factors as well as to save time by reducing number of runs.

Acknowledgment

This work was supported by a Kuwait University Research Grant [No. PP02/04].

References

1. Cyclolab Ltd. New nimesulide salt cyclodextrin inclusion complexes PCT /HU94/00014 WO 94/28031, 1994.
2. Serajuddin ATM. Solid dispersion of poorly water-soluble drugs: Early promises, subsequent problems, and recent breakthroughs. J Pharm Sci 1999; 88:1058-1065.
3. Craig DQM. The mechanisms of drug release from solid dispersions in water-soluble polymers. Int J Pharm 2002; 231:131-144.
4. Khan N, Craig DQM. The influence of drug incorporation on the structure and release properties of solid dispersions in lipid matrices. J Control Release

2003; 3:355-368.

5. Shah JC, Chen JR, Chow D. Preformulation study of etoposide: Increased solubility and dissolution rate by solid-solid dispersions. Int J Pharm 1995; 113:103-111.
6. Damian F, Blaton N, Naesens L, Balzarini J, Kinget R, Augustijns P, Van den Mooter G. Physicochemical characterization of solid dispersions of the antiviral agent UC-781 with polyethylene glycol 6000 and Gelucire 44/14. Eur J Pharm Sci 2000; 10:311-322.
7. Barker SA. Matrix solid-phase dispersion J Chromatogr A 2000; 885:115-127.
8. Darwish I, El-Kamel A. Dissolution enhancement of glibenclamide using liquisolid tablet technology. Acta Pharm 2001; 51:173-181.
9. Hu J, Johnston KP, Williams RO 3rd. Nanoparticle engineering processes for enhancing the dissolution rates of poorly water soluble drugs. Drug Dev Ind Pharm 2004; 30:233-245.
10. Kaukonen AM, Boyd BJ, Charman WN, Porter CJ. Drug solubilisation behaviour during *in vitro* digestion of suspension formulations of poorly water-soluble drugs in triglycerides lipids. Pharm Res 2004; 21:254-260.
11. Munday DL. Film coated pellets containing verapamil hydrochloride: enhanced dissolution into neutral medium. Drug Dev Ind Pharm 2003; 29:575-583.
12. Pan RN, Chen JH, Chen RR. Enhancement of dissolution and bioavailability of piroxicam in solid dispersion. Drug Dev Ind Pharm 2000; 26:989-994.
13. Shawn AM, Thomas DR, Tina PD. A compaction process to enhance dissolution of poorly soluble drugs using hydroxypropyl methylcellulose. Int J Pharm 2003; 250:3-11.
14. Worthing H. Propylene Glycol. In: Handbook of Pharmaceutical Excipients (Wade A, Weller PJ, eds), American Pharmaceutical Association/The Pharmaceutical Press, Washington, DC/London, 1994; pp. 241-242.
15. Spiegel AJ, Noseworthy, MM. Use of non-aqueous solvents in parenteral products. J Pharm Sci 1963; 52:917-927.
16. Mura P, Manderioli A, Bramanti G, Ceccarelli L. Properties of solid dispersions of naproxen in various polyethylene glycols. Drug Dev Ind Pharm 1996; 22:909-916.
17. Kubo H, Mizobe M. Improvement of dissolution rate and oral bioavailability of a sparingly water-soluble drug, (+/-)-5-[[2-(2-naphthalenylmethyl)-5-benzoxazolyl]-methyl]-2,4-thiazolidinedione, in co-ground mixture with D-mannitol. Biol Pharm Bull 1997; 20:460-463.
18. Arias MJ, Gines JM, Moyano JR, Rabasco AM. The application of solid dispersion technique with D-mannitol to the improvement in oral absorption of triamterene. J Drug Target 1994; 2:45-51.
19. Arias MJ, Ginés JM, Moyano JR, Pérez-Martínez JI, Rabasco AM. Influence of preparation method of solid dispersions on dissolution rate: study of triammterene-D-mannitol system. Int J Pharm 1995; 123:25-31.

(*Received March 11, 2008; Revised March 27, 2008; Accepted April 25, 2008*)

Original Article

Iontophoretic delivery of 5-fluorouracil through excised human stratum corneum

Brahma N. Singh, Shyam B. Jayaswal

Department of Pharmaceutics, Institute of Technology, Banaras Hindu University, Varanasi - 221 005 (Uttar Pradesh), India.

ABSTRACT: The objective of this study was to determine the effects of ionization, current density and penetration enhancers on the iontophoretic delivery of 5-fluorouracil (5-FU) through excised human stratum corneum (HSC). The iontophoretic (cathodal) transport of 5-FU was assessed *in vitro* at three physiologically relevant pH values of 5.0, 7.4 and 8.0, at various levels of current density ranging between 0.15 to 0.98 mA/cm^2, and in the presence of suitable penetration enhancers, namely Azone® (AZ), lauryl alcohol (LA), and isopropyl myristate (IPM). The steady-state flux at constant current density (0.47 mA/cm^2) was increased by approximately 19, 10 and 27 fold at pH 5, 7.4 and 8.0, respectively. The effect of current density at pH 7.4 exhibited a linear correlation between current density and steady-state flux ($r = 0.98$, $p = 0.002$), which indicates the potential of iontophoresis for controlled transdermal delivery of 5-FU. The combination of cathodal iontophoresis with IPM produced an additive enhancement which may be attributed to aggravated skin perturbation effect and increased skin conductivity. Other enhancers such as AZ and LA produced negative or no further enhancement respectively, when used in conjunction with cathodal iontophoresis. It may be therefore concluded that pH and current density play critical role during iontophoretic delivery of 5-FU, and combination of a chemical penetration enhancer and iontophoresis can not be always viewed as a synergistic strategy which should be evaluated on a case-by-case basis for each drug candidate/enhancer combination.

Keywords: 5-FU, Cathodal iontophoresis, Penetration enhancers, Transdermal, Current density

**Correspondence to:* Dr. Brahma N. Singh, Department of Formulation, Pharmaceutical Research & Development, Forest Laboratories, Inc., 49 Mall Drive, Commack, New York 11725, USA;
e-mail: brahmasingh@hotmail.com

1. Introduction

5-fluorouracil (5-FU) is an antineoplastic antimetabolite, which is commercially available as topical solution and cream (Effudex®; Valeant Pharmaceuticals, CA, USA). Another topical cream formulation is marketed as Fluoroplex® by Allergan, Inc. (CA, USA). These formulations are recommended for the topical treatment of multiple actinic (solar) keratoses, and have also been recently approved by the US FDA for the treatment of superficial basal cell carcinomas when conventional (*i.e.*, surgical) methods are not feasible. Topical 5-FU has also been considered as an effective treatment for psoriasis and Bowen's disease. Although conventional topical formulations of 5-FU are effective, their efficacy may be limited because of inadequate penetration through the stratum corneum, leading to suboptimal concentrations of 5-FU into the target tissue. Other disadvantages may include poor patient compliance because of prolonged treatment period required (*1*), frequent remission (*2*), and unacceptable irritation (*3*). Consequently, there remains need for a convenient, safe and efficacious method of 5-FU delivery for treatment of skin disorders, particularly basal cell carcinomas and psoriasis.

The inadequate penetration of 5-FU through the stratum corneum is mainly attributed to poor transcellular transport due to its hydrophilic nature (*4*), and restricted pore transport due to permselective properties of the skin. The isoelectric point (pI) of the human stratum corneum (HSC) is 3.7 (*5*), which implies that membrane is essentially neutral at pH ≈ 4. The pores are positively charged at pH below 4 and above 4 they bear a negative charge. Consequently, under normal physiological conditions (pH 7.4), the transport of 5-FU, an anionic drug (pK_a = 8.0), through charged pores is less likely to be favored owing to electrostatic repulsion across the negatively charged skin membrane. Therefore, to maximize the delivery of 5-FU, the formulation pH should be acidic (pH ≤ 5) which can affect drug solubility and skin irritation. One potential approach to overcome these limitations is iontophoresis, which utilizes an additional driving force, namely an electrical potential gradient across the skin and takes advantage of the fact that like charges repel (*6*).

The clinical benefit of iontophoresis has been well documented for the treatment of psoriasis, Bowen's disease and various types of skin cancer (*1,7-9*). More recently, it has been utilized for delivery of acyclovir for the treatment of cold sores (*10*). An alternate approach to effectively deliver anticancer drugs across skin is electroporation (*11*).

The key advantage of iontophoretic delivery is that flux of a therapeutic drug can be controlled externally (by adjusting the applied current), thus tailored to the specific needs of the patient. In addition, a drug can be delivered in a pulsatile manner, which is advantageous for effective topical therapy of psoriasis (*2*). Yet, another important benefit of iontophoresis, which is clinically relevant for the treatment of Bowen's disease and other localized malignancies of the skin is that high concentrations of ionized drugs can be efficiently introduced in a relatively limited area with minimal exposure to normal surrounding tissues (*12*). This localized delivery, besides reducing the toxic effects, also has potential to avoid the necessity of a surgical treatment which is most common for Bowen's disease (*1*). These potential advantages of iontophoresis and the limited efficacy of conventional approaches make 5-FU an ideal candidate for iontophoretic delivery. Since 5-FU exists in anionic forms in solution (at pH > 5), a cathodal iontophoresis was used in the present investigation.

The specific objectives of this study were to (a) determine the degree to which the transdermal flux of 5-FU can be enhanced by constant current iontophoresis; (b) examine the role of pH; (c) study the effects of current density; and (d) to explore whether iontophoresis of the drug in the presence of chemical penetration enhancers further potentiates percutaneous transport. To the best of our knowledge, this is first reported investigation on the *in-vitro* iontophoretic delivery of 5-FU through human skin, both alone as well as in combination with penetration enhancers.

2. Materials and Methods

2.1. *Materials*

5-FU and Azone® (1-dodecylazacycloheptan-2-one) were gifts from Biochem Pharmaceutical Industries Ltd. (Mumbai, India) and Nelson Research and Development Co. (Irvine, CA, USA), respectively. Lauryl alcohol (1-dodecanol) and isopropyl myristate were purchased from Sisco Research Laboratories Pvt. Ltd. (Mumbai, India). All other chemicals were of analytical grade and used without any further purification.

2.2. *Fabrication of iontophoretic delivery device*

A constant current power source was designed and fabricated at the University Science and Instrumentation Center of Banaras Hindu University. The unit could supply a direct current (DC) ranging between 50 µA to 25 mA. Platinum wires (99.9% purity, 0.5 mm dia; Jai Scientific Corporation, Varanasi, India) were used as electrodes, which had an effective working length of 10 mm.

2.3. *Iontophoretic transport studies*

The experimental methods for preparation of HSC and *in-vitro* transport studies have been described previously (*4*). Briefly, the HSC was rehydrated in water for 1 h and subsequently mounted in side-by-side permeation chambers with the support of a wire mesh. The dermal side of HSC faced the receiver chamber filled with phosphate buffer pH 7.4, while the donor chamber contained 4 mL of solution formulations of 5-FU (1 mg/mL). Samples of receiver solution (0.5 mL) were taken at regular intervals, and were replenished with same volume of fresh receiver solution. To perform cathodal iontophoresis, a pair of platinum electrodes was immersed in the solutions with the cathode in the donor chamber and anode in the receiver chamber. These electrodes were connected to an adjustable constant current source with simple DC features as described in section 2.2. The electric current was applied continuously, without interruption (except during sampling the current was turned ‘off) for 6 h. The effective surface area of HSC available for drug permeation was 2.54 cm^2. All experiments were performed in triplicates at 37 ± 0.5°C.

2.4. *Effect of ionization*

The effect of ionization was determined at three physiologically relevant pH (donor solution) values of 5.0, 7.4 and 8.0 at a constant current density of 0.47 mA/cm^2 while maintaining the pH of receiver solution at 7.4. The buffer solutions were composed of equal proportions (30 mM) each of trisodium citrate, sodium dihydrogen orthophosphate and glycine. Minor changes in pH during iontophoresis were monitored and corrected for by the addition of micoliter amounts of 1 M HCl or 1 M NaOH solutions. By this method, the pH was kept within ± 0.2 units of the desired pH as determined at the end of the experiment.

2.5. *Effect of current density*

The influence of current density was investigated at the experimental conditions as described in section 2.3. The current density was varied between 0.15 to 0.98

mA/cm^2. The pH of both donor and receiver solutions was maintained at 7.4.

2.6. *Effect of iontophoresis in combination with penetration enhancers*

Three penetration enhancers, namely Azone®, lauryl alcohol and isopropyl myristate were studied. The concentrations of these enhancers in the respective donor solutions were 3% (w/v), 5% (w/v), and 5% (w/w), respectively. The preparation of donor solution with Azone® prompted an emulsification with 0.11% (w/v) of polysorbate 20, as suggested previously (*13*). All of these studies were performed at the physiological pH (that is, the pH of the donor and receiver solutions were 7.4) and at a constant current density of 0.47 mA/cm^2.

2.7. *Analytical method and data analysis*

The steady-state flux (*J*ss) and enhancement factor were determined using equations as described in previous publication (*4*). The fraction change in steady-state flux was determined using the following equation (*14*):

$$\text{Fraction change in the flux} = \frac{(\text{Iontophoretic flux} - \text{Passive flux})}{\text{Iontophoretic flux}}$$

Other formulae used in data analysis are given in Tables 1-3. The method for drug analysis was same as described previously (*4*).

2.8. *Statistical analyses*

Statistical comparisons were made using Student's paired *t*-test, with a two-tailed distribution. For the evaluation of any correlation, Pearson's correlation test was performed, and the correlation coefficients and associated probability values (two-tailed) were calculated using a statistical software (Graph PAD Instat®, CA, USA). The level of significance was considered at $p < 0.05$.

3. Results and Discussion

3.1. *Effect of ionization*

Formulation pH is a critical variable in iontophoresis because it affects drug ionization, net charge on the skin and electroosmotic flow (*15*). Accordingly, in the present study, three pH values higher than pI of the HSC were selected to determine the potential of iontophoresis at various ionization levels while simultaneously taking the advantage of the permselective property of the skin. In addition, minor drifts in pH that occurred during iontophoresis were monitored and adjusted when the difference between observed and original values were higher than ± 0.2 units. Such shifts in pH are often associated with use of platinum electrodes due to hydrolysis of water, which generates hydrogen ions. This in turn can affect the ionization state of the drug molecules and hence rate of iontophoretic transport (*16*).

The cumulative amount of 5-FU permeated at various pH is shown in Figure 1. The calculated values of fraction change in the steady-state flux and enhancement factor for iontophoretic transport of 5-FU are shown in Table 1. The data clearly show that at pH 5, 7.4 and 8.0, the flux is increased during iontophoresis by approximately 19, 10 and 27 fold, respectively. Apparently, the values of fraction change in the steady-state flux for 5-FU during iontophoresis are not solely related to their corresponding degrees of ionization.

It is clear from Table 1 that as the pH is increased from 7.4 to 8.0, the iontophoretic flux increased

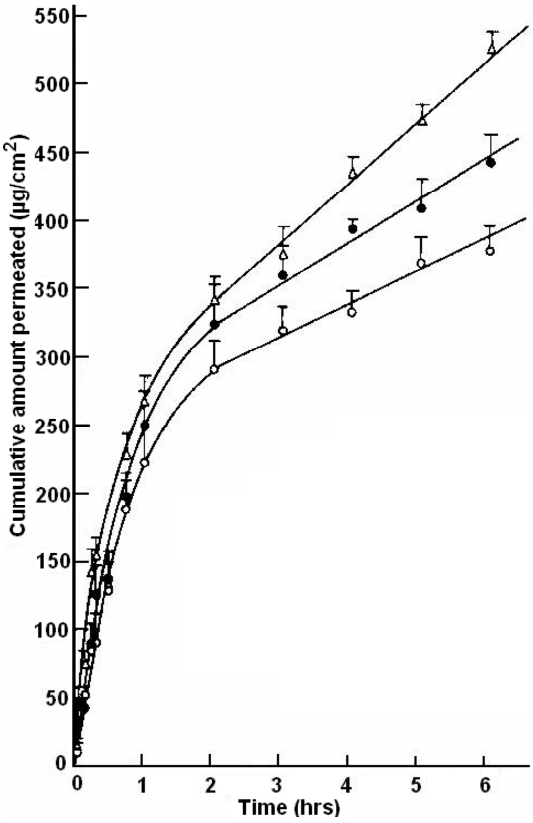

Figure 1. *In-vitro* permeation profiles of 5-FU through human stratum corneum at different pH values during cathodal iontophoresis (△, pH 7.4; ●, pH 8; ○, pH 5) (Mean ± SD of three determinations; Only half bars have been shown for clarity).

Table 1. Effect of pH on the steady-state flux, fraction change in the flux and enhancement factor (Mean ± S.D. of three determinations) for iontophoretic transport of 5-FU through excised HSC at 0.47 mA/cm^2

pH	Fraction ionized[a]	Steady-state flux (μg/cm^2/h)	Fraction change in the flux[b]	Enhancement factor[c]
5.0	0.001	201.57 ± 8.81	0.948 ± 0.002	19.11 ± 0.78
7.4	0.201	170.06 ± 3.40	0.904 ± 0.006	10.40 ± 0.60
8.0	0.500	242.40 ± 6.58	0.962 ± 0.005	26.84 ± 3.50

[a] Calculated by considering its pK$_{a1}$ value of 8.0

[b] Calculated using passive flux values from Singh *et al.* (*4*)

[c] $\text{Enhancement factor} = \frac{\text{Iontophoretic flux}}{\text{Passive flux}}$

which may be attributed to increase in the extent of ionization. However, the flux decreased unexpectedly when pH was increased from 5.0 to 7.4. Theoretically, a lower iontophoretic (cathodal) flux is expected at pH 5.0 compared to 7.4. The higher flux at pH 5 may be explained as follows.

At a pH of 5.0, the skin bears a net negative charge and only a small fraction of 5-FU (0.1%) is ionized in the donor solution. Under these conditions, the total flux of 5-FU during cathodal iontophoresis (J_t) may be represented by following equation which is modified from Merino *et al.* (*17*):

$$J_t = J_p + J_{er} - J_{eo} \qquad (1)$$

where J_p is the passive flux, J_{er} represents flux due to electrorepulsive migration (*i.e.*, anions repelled into the skin from the cathode), and J_{eo} is electroosmotic flux which represents net transport of uncharged molecules of 5-FU due to electroosmosis. This transport occurs due to electrically induced convective solvent flow that carries uncharged molecules in the direction of positive ions flow *i.e.*, anode-to-cathode direction (*18*). The negative sign signifies the fact that J_{eo} has a negative contribution to the total flux of 5-FU because it occurs in the direction opposite to electrorepulsive delivery (cathode-to-anode direction) (*17*).

Despite the fact that J_p at pH 7.4 (16.4 ± 1.28 μg/cm^2/h) was higher than at pH 5.0 (10.54 ± 0.04 μg/cm^2/h) (*4*), and that a higher electrorepulsive contribution is expected at pH 7.4, the total flux at pH 5 is higher than at pH 7.4. This clearly suggests that negative contribution of electroosmotic flow was relatively smaller (or negligible) at pH 5.0 than at pH 7.4.

Theoretical aspects of our interpretation may be further corroborated by acknowledging an apparent relationship between pH, electroosmotic flow and permselective properties of the skin. When the skin bears a net negative charge (at pH > pI), it preferentially allows the passage of counterions (*i.e.*, cations). This cation permselectivity of the skin is an inherent property and is unlikely to be abolished due to imposition of an asymmetric pH gradient across the skin (in our study, 5.0 in cathode chamber, 7.4 in the anode chamber) (*19*). However, at lower donor pH of 5.0 it is possible that net negative charge at the skin surface may be decreased due to partial neutralization by hydronium ions. In fact, an excess concentration of hydronium ions at a very acidic donor pH (~3) has been observed to reverse the net charge of skin and therefore the direction of electroosmotic flow to cathode-to-anode direction (*17*). Based on this mechanism, the degree of preferential cation passage would be abated at pH 5.0. Accordingly, the magnitude of J_{eo} will be lower, and hence J_t will be higher at pH 5.0 compared to pH 7.4.

Finally, at pH 8.0, 5-FU is 50% ionized and the flux is 1.43 times higher than pH 7.4. This indicates that contribution of electrorepulsive migration is significant, which overwhelms the negative effect of electroosmosis (*6*). Collectively, these findings suggest that the relative contribution of electrorepulsive migration, electroosmotic flow and passive transport to total flux of 5-FU may be different than theoretically expected depending on the pH.

3.2. *Effect of current density*

In the absence of an electric current, 5-FU permeates through the skin at a low rate (J_{ss} = 16.4 ± 1.28 μg/cm^2/h). This permeation rate was significantly enhanced by cathodal iontophoresis at all current density values ($p <$ 0.05). The corresponding values of enhancement factor are shown in Table 2. As predicted theoretically, the cumulative permeation of 5-FU was observed to increase with increasing applied current density (Figure 2).

The application of smaller iontophoretic current (0.16 and 0.31 mA/cm^2) produced a linear increase in the cumulative drug transport up to 6 h. Interestingly, doubling the current density from 0.16 to 0.31 mA/cm^2 increased the steady-state flux by almost two-fold. Further increases in current density also caused enhancement in the flux but did not commensurate in the same proportion. Overall, a positive linear relationship between current density and steady-state flux was observed (Figure 3), which was significant (r = 0.98, p = 0.002).

The linear dependence of the 5-FU flux on the applied current density may be described by Faraday's law which is represented by following equation (*20*):

$$J_i = \frac{t_i I}{F Z_i} \qquad (2)$$

where J_i, Z_i are the flux and charge (valency) of 5-FU anion, I is the applied current density and F is the Faraday's constant. In Eq (2), t_i is a proportionality constant which denotes the transport number of 5-FU anion. Remarkably, a linear relationship between 5-FU transport and current strength has also been demonstrated for *in-vivo* iontophoresis to rabbit eyes. In

Table 2. Effect of current density on the steady-state flux and enhancement factor (Mean ± S.D. of three determinations) for iontophoretic transport of 5-FU through excised HSC at pH 7.4

Current intensity (mA)	Current density (mA/cm^2)	Steady-state flux (μg/cm^2/h)	Enhancement factor[b]
0.0 (Passive)	-	16.40 ± 1.28[a]	1.0
0.4	0.16	26.53 ± 0.99[*]	1.62 ± 0.08
0.8	0.31	48.67 ± 0.73[*]	2.98 ± 0.19
1.2	0.47	63.37 ± 2.44[*]	3.87 ± 0.20
2.5	0.98	92.69 ± 2.34[*]	5.67 ± 0.41

[*] Significantly different from passive flux (p < 0.05)
[a] From Singh *et al.* (*4*)
[b] Enhancement factor = $\frac{\text{Iontophoretic flux}}{\text{Passive flux}}$

this particular study, the mean 5-FU concentration in the cornea increased linearly ($R^2 = 0.97$) when the current was increased from 0 - 0.75 mA (*12*).

In the present study, the ionic strength and pH of donor solution (*i.e.*, the % ionized fraction) was kept constant for all current density levels tested. It therefore follows that linear increase in flux occurred primarily due to proportional decreases in electrical resistance of the HSC, which is supported by previous findings (*21*). Further, studies have also shown that changes in electrical properties of the skin are associated with proportional microscopic changes in the structure of stratum corneum. Craane-van Hinsberg *et al.* (*22*) studied the ultrastructure of the HSC after iontophoresis using current density in the range of 0.013 - 13 mA/cm^2. Their findings demonstrated that application of iontophoretic current causes disordering of the intercellular lipids of HSC and these perturbations are more pronounced with increasing current density. They attributed the lipid disordering effect to the polarization of the lipid head groups induced by the electric field, followed by mutual repulsion. These changes are microscopically noticed as loosening of epidermal cells and distention in intercellular space that commensurate with increasing current density (*23*).

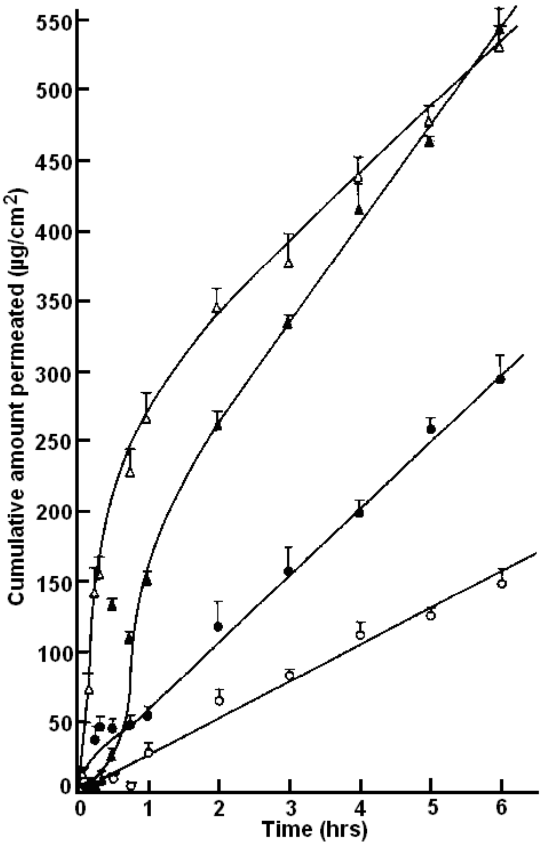

Figure 2. *In-vitro* permeation profiles of 5-FU through human stratum corneum at different current densities (▲, 0.98 mA/cm^2; △, 0.47 mA/cm^2; ●, 0.31 mA/cm^2; ○, 0.16 mA/cm^2) (Mean ± S.D. of three determinations; Only half bars have been shown for clarity).

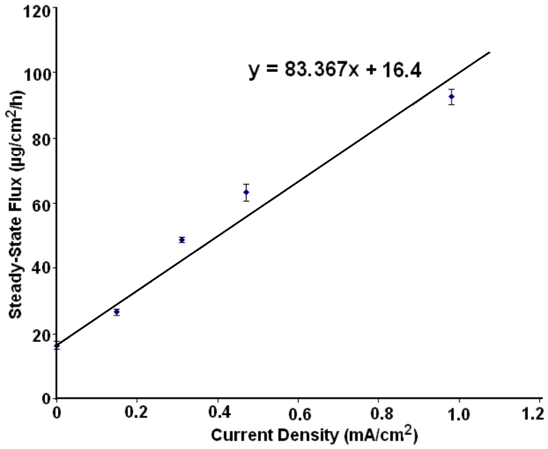

Figure 3. Relationship between steady-state flux of 5-FU and applied current density (Mean ± S.D. of three determinations).

The existence of a linear relationship between current density and flux has a considerable therapeutic relevance because it indicates the potential of 5-FU iontophoresis for controlled and individualized dose administration in patients.

3.3. *Effect of iontophoresis in combination with penetration enhancers*

The effect of various penetration enhancers on the iontophoretic transport of 5-FU across excised HSC is shown in Figure 4. All these experiments were performed

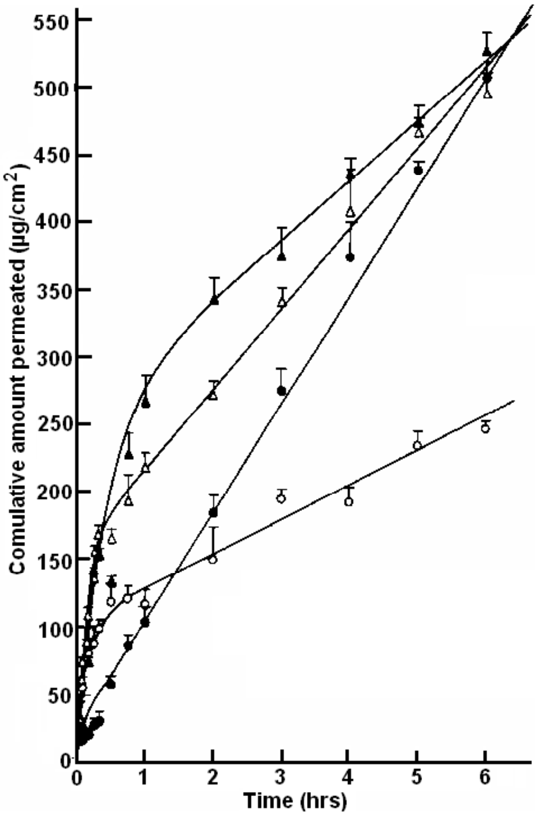

Figure 4. Effect of various penetration enhancers on the iontophoretic permeation of 5-FU through human stratum corneum (○, AZ; ●, IPM; △, LA; ▲, Control) (Mean ± S.D. of three determinations; Only half bars have been shown for clarity).

Table 3. Effect of penetration enhancers on the steady-state flux, enhancement factor, and synergy factor (Mean ± S.D. of three determinations) for iontophoretic transport of 5-FU through excised HSC at pH 7.4 and current density of 0.47 mA/cm^2

Penetration enhancers (PE)	Conc.	Steady-state flux (µg/cm^2/h)	K_p (cm/h × 10^4)	Enhancement factor[a]	Synergy factor[b]
None (Control)	N/A	63.37 ± 2.44	3.17 ± 0.12	1.0	-
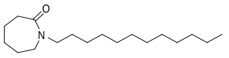 Azone (Mol. Wt = 281.49)	3% w/v	28.79 ± 3.17	1.44 ± 0.16*	0.45 ± 0.05	0.06 ± 0.01
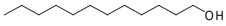 Lauryl alcohol (Mol. Wt. = 186.34)	5% w/v	63.74 ± 2.44	3.19 ± 0.12	1.01 ± 0.08	0.52 ± 0.07
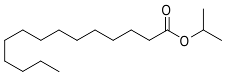 Isopropyl myristate (Mol. Wt. = 270.46)	5% w/w	85.36 ± 1.14	4.27 ± 0.06*	1.35 ± 0.04	0.79 ± 0.03

* Significantly different from control ($p < 0.05$)

[a] $$\text{Enhancement factor} = \frac{\text{Iontophoretic } K_p \text{ with PE}}{\text{Iontophoretic } K_p \text{ w/o PE}}$$

[b] $$\text{Synergy factor} = \frac{\text{Iontophoretic } K_p \text{ with PE}}{\text{Iontophoretic } K_p \text{ w/o PE} + {}^{c}\text{Passive } K_p \text{ with PE}}$$

c = Passive K_p from Singh *et al.* (*4*)

at constant current density of 0.47 mA/cm^2, which is close to the acceptable limit of current for tolerable iontophoretic delivery (0.5 mA/cm^2, Ref. *24*). The values of steady-state flux for iontophoretic and passive delivery in presence of various enhancers are compared in Figure 5. The corresponding data along with calculated values of permeability coefficient (K_p), enhancement and synergy factors are summarized in Table 3.

The permeability coefficient of 5-FU was significantly increased ($p < 0.05$) in the presence of IPM when compared to the control. However, the permeability coefficient remained unaltered ($p > 0.05$) or significantly decreased ($p < 0.05$) in presence of LA and AZ, respectively. In the presence of IPM, the cumulative drug transport increased linearly (Figure 4), and the enhancement in K_p of 5-FU was 1.35 times greater compared to control (Table 3). Furthermore, the combination of IPM and iontophoresis produced greater enhancement (5.2-fold) than iontophoresis alone (3.9-fold) and passive transport in presence of IPM (2.7-fold, Ref. *4*). Apparently, this was an additive effect, which is also evident by a lower than unity value of synergy factor (Table 3).

The additive enhancement may be attributed to direct and indirect effects of IPM. The direct effect of IPM involves interaction with the skin resulting in the perturbation of the lipid bilayers of the stratum corneum (*4*). The indirect effect has been attributed to ability of IPM to retard the rate of water loss from the skin, which results in an increase of skin conductivity and iontophoretic flux of the drug (*25*). Nevertheless, this finding is relevant because IPM is included in one of commercially available cream formulations of 5-FU (Fluoroplex®).

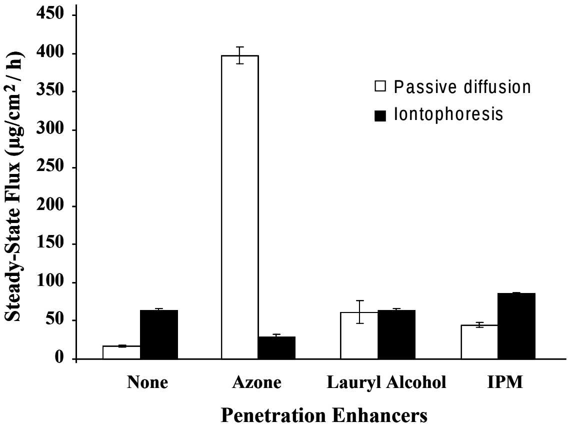

Figure 5. Comparison of steady-state flux during passive diffusion and iontophoresis of 5-FU in the presence of penetration enhancers (Mean ± S.D. of three determinations). Passive diffusion data replotted from Singh et al. (*4*).

As shown in Figure 5, the steady-state flux for combination (AZ + iontophoresis) is significantly lower compared to control (iontophoresis w/o AZ) as well as passive transport in presence of AZ. This further implies that combination of AZ and iontophoresis inhibits transport of 5-FU through both transcellular as well as hydrophilic (pores) pathways. The chemical structure of AZ is similar to that of a surfactant comprising of a polar head (lactam ring) and a lipophilic (dodecyl) side chain (Table 3). From mechanistic point of view, this structure provides an active configuration ("spoon-shaped form") in which polar head group is at an angle relative to the alkyl chain (*26*). Accordingly, it is possible that inhibitory effect of AZ in the present study might be related to the effect of electric current on the charge distribution of the polar region of AZ molecules which in turn might affect their ability to interact with the components of the stratum corneum. Another possible reason might be due to an interaction between 5-FU and AZ which has been implicated for reduced enhancing efficiency (*27*). However, the role of skin-current interactions leading to development of a skin polarization potential can not be completed ignored. The latter has been known to reduce the efficiency of iontophoresis (*28*). Other investigators have also observed negative effect of AZ on the iontophoretic transport (*25,29*), but in other cases a synergistic enhancement has been reported (*28,30-31*). The lack of a synergistic effect of IPM and an effect of LA in the present study indicates that concentrations of these enhancers and current density level were probably not optimal which should be further explored both *in-vitro* as well as *in-vivo*.

It is obvious that three selected enhancers in this study produced distinctly different results when combined with iontophoresis. Some of the observed differences between findings of our study and other studies could be explained based on differences in the experimental protocol. For instance, in our study, the enhancers were added together with the drug. This is in sharp contrast to most of the reported studies in which skin specimens are pretreated with enhancers prior to iontophoretic transport studies, and other cosolvents like propylene glycol and ethanol are often used in combination with penetration enhancers. Skin pretreatment with a penetration enhancer has been reported to produce greater enhancement than the coapplication of the drug and an enhancer in the vehicle (*27*). Other variables that might explain differences are physicochemical properties of the drug (pK_a, solubility), formulation composition (pH, drug and enhancer concentrations, ionic strength), current density level, and differences in skin types. Consequently, the combination of iontophoresis with chemical enhancers can not be always viewed as a 'magic strategy' and should be evaluated on a case-by-case basis for each drug/enhancer combination.

4. Conclusions

The results generated in this series of investigation have demonstrated that, with the application of cathodal iontophoresis, the transdermal delivery of 5-FU could be substantially enhanced compared to passive diffusion. Moreover, this work explores the feasibility of a combination strategy involving a chemical penetration enhancer and iontophoresis as a technique for controlled transdermal delivery of 5-FU. Other enhancer systems more suited for practical applications need to be investigated. A successful combination of iontophoresis and a well-tolerated permeation enhancer such as IPM appears promising for controlled transdermal delivery of 5-FU. Thus by proper optimization of the electrical and physico-chemical factors, 5-FU can be delivered through the intact skin at a controlled rate and with a desirable dosing pattern. Eventually, such controlled delivery systems can offer convenience of outpatient therapy and assuage patients plagued by the side effects of chemotherapy with 5-FU.

Acknowledgements

This research was supported by the University Grants Commission (UGC), Government of India in the form of Junior Research Fellowship to Brahma Singh. Authors would also like to thank Dr. Sanjay Singh for his technical assistance, Dr. C. B. Tripathi (Head, Department of Forensic Medicine, Institute of Medical Sciences, BHU, Varanasi) for providing cadaver skin specimens, and University Science and Instrumentation center of BHU for fabrication of the constant current source. Authors gratefully acknowledge Prof. Ajay K. Banga (Mercer University) for critically reviewing the manuscript.

References

1. Welch ML, Grabski WJ, McCollough ML, Skelton HG, Smith KJ, Menon PA, Anderson LL. 5-fluorouracil iontophoretic therapy for Bowen's disease. J Am Acad Dermatol 1997; 36:956-958.
2. Pearlman DL. Method for treating psoriasis with cytotoxic agents. U.S. Patent 4853388, August 1, 1989.
3. Goette DK. Topical chemotherapy with 5-fluorouracil. A review. J Am Acad Dermatol 1981; 4:633-649.
4. Singh BN, Singh RB, Singh J. Effects of ionization and penetration enhancers on the transdermal delivery of 5-fluorouracil through excised human stratum corneum. Int J Pharm 2005; 298:98-107.
5. Wilkerson VA. The chemistry of human epidermis. II. The isoelectric points of the stratum corneum, hair, and nails as determined by electrophoresis. J Biol Chem 1935; 112:329-335.
6. Kalia YN, Naik A, Garrison J, Guy RH. Iontophoretic drug delivery. Adv Drug Del Rev 2004; 56:619-658.
7. Bacro TR, Holladay EB, Stith MJ, Maize JC, Smith CM. Iontophoresis treatment of basal cell carcinoma with cisplatin: a case report. Cancer Detect Prev 2000; 24:610-619.
8. Tiwari SB, Ravikumar BC, Udupa N, Balachandran C. Topical methotrexate delivered by iontophoresis in the treatment of recalcitrant psoriasis – a case report. Int J Dermatol 2003; 42:157-159.
9. Smith KJ, Konzelman JL, Lombardo FA, Skelton HG 3rd, Holland TT, Yeager J, Wagner KF, Oster CN, Chung R. Iontophoresis of vinblastine into normal skin and for treatment of Kaposi's sarcoma in human immunodeficiency virus-positive patients. The military medical consortium for applied retroviral research. Arch Dermatol 1992; 128:1365-1370.
10. Morrel EM, Spruance SL, Goldberg DI. Iontophoretic acyclovir cold sore study group. Topical iontophoretic administration of acyclovir for the episodic treatment of herpes labialis: a randomized, double-blind, placebo-

controlled, clinic-initiated trial. Clin Infect Dis 2006; 15:460-467.

11. Singh BN, Dwivedi C. Antitumor drug delivery by tissue electroporation. Anti-Cancer Drugs 1999; 10:139-146.
12. Kondo M, Araie M. Iontophoresis of 5-fluorouracil into conjunctiva and sclera. Invest Ophthalmol Vis Sci 1989; 30:583-585.
13. Morimoto Y, Sugibayashi K, Hosoya K, Higuchi WI. Penetration enhancing effect of Azone on the transport of 5-fluorouracil across the hairless rat skin. Int J Pharm 1986; 32:31-38.
14. Siddiqui O, Roberts MS, Polack AE. Iontophoretic transport of weak electrolytes through the excised human stratum corneum. J Pharm Pharmacol 1989; 41:430-432.
15. Costello CT, Jeske AH. Iontophoresis: applications in transdermal medication delivery. Phys Ther 1995; 75:554-563.
16. Hale RL, Lu A, Solas D, Selick HE, Oldenburg KR, Zaffaroni AC. Compositions and methods for enhanced drug delivery. U.S. Patent 5607691, March 4, 1997.
17. Merino V, López A, Kalia YN, Guy RH. Electrorepulsion versus electroosmosis: effect of pH on the iontophoretic flux of 5-fluorouracil. Pharm Res 1999; 16:758-761.
18. Pikal MJ. The role of electroosmotic flow in transdermal iontophoresis. Adv Drug Del Rev 2001; 46:281-305.
19. Kim A, Green PG, Rao G, Guy RH. Convective solvent flow across the skin during iontophoresis. Pharm Res 1993; 10:1315-1320.
20. Phipps JB, Gyory JR. Transdermal ion migration. Adv Drug Del Rev 1992; 9:137-176.
21. Inada H, Ghanem AH, Higuchi WI. Studies on the effects of applied voltage and duration on human epidermal membrane alteration/recovery and the resultant effects upon iontophoresis. Pharm Res 1994; 11:687-697.
22. Craane-van Hinsberg IW, Verhoef JC, Spies F, Bouwstra JA, Gooris GS, Junginger HE, Boddé HE. Electroperturbation of the human skin barrier *in vitro*: II. Effects on stratum corneum lipid ordering and ultrastructure. Microsc Res Tech 1997; 37:200-213.
23. Singh S, Bi M, Jayaswal SB, Singh J. Effect of current density on the iontophoretic permeability of benzyl alcohol and surface characteristics of human epidermis. Int J Pharm 1998; 166:157-166.
24. Prausnitz MR. The effects of electric current applied to skin: a review for transdermal drug delivery. Adv Drug Del Rev 1996; 18:395-425.
25. Fang JY, Huang YB, Lin HH, Tsai YH. Transdermal iontophoresis of sodium nonivamide acetate. IV. Effect of polymer formulations. Int J Pharm 1998; 173:127-140.
26. Kim N, El-Kattan AF, Asbill CS, Kennette RJ, Sowell JW Sr, Latour R, Michniak BB. Evaluation of derivatives of 3-(2-oxo-1-pyrrolidine) hexahydro-1H-azepine-2-one as dermal penetration enhancers: side chain length variation and molecular modeling. J Controlled Rel 2001; 73:183-196.
27. Chow DS, Kaka I, Wang TI. Concentration-dependent enhancement of 1-dodecylazacyclohetan-2-one on the percutaneous penetration kinetics of triamcinolone acetonide. J Pharm Sci 1984; 73:1794-1799.
28. Meidan VM, Al-Khalili M, Michniak BB. Enhanced iontophoretic delivery of buspirone hydrochloride across human skin using chemical enhancers. Int J Pharm 2003; 264:73-83.
29. Hirvonen J, Kontturi K, Murtomäki L, Paronen P, Urtti A. Transdermal iontophoresis of sotalol and salicylate; the effect of skin charge and penetration enhancers. J Controlled Rel 1993; 26:109-117.
30. Ganga S, Ramarao P, Singh J. Effect of Azone on the iontophoretic transdermal delivery of metoprolol tartrate through human epidermis *in vitro*. J Controlled Rel 1996; 42:57-64.
31. Femenía-Font A, Balaguer-Fernández C, Merino V, López-Castellano A. Combination strategies for enhancing transdermal absorption of sumatriptan through skin. Int J Pharm 2006; 323:125-130.

(*Received April 25, 2008; Accepted April 29,2008*)

Drug Discoveries & Therapeutics

Guide for Authors

1. Scope of Articles

Drug Discoveries & Therapeutics mainly publishes articles related to basic and clinical pharmaceutical research such as pharmaceutical and therapeutical chemistry, pharmacology, pharmacy, pharmacokinetics, industrial pharmacy, pharmaceutical manufacturing, pharmaceutical technology, drug delivery, toxicology, and traditional herb medicine. Studies on drug-related fields such as biology, biochemistry, physiology, microbiology, and immunology are also within the scope of this journal.

2. Submission Types

Original Articles should be reports new, significant, innovative, and original findings. An Article should contain the following sections: Title page, Abstract, Introduction, Materials and Methods, Results, Discussion, Acknowledgments, References, Figure legends, and Tables. There are no specific length restrictions for the overall manuscript or individual sections. However, we expect authors to present and discuss their findings concisely.

Brief Reports should be short and clear reports on new original findings and not exceed 4000 words with no more than two display items. *Drug Discoveries & Therapeutics* encourages younger researchers and doctors to report their research findings. Case reports are included in this category. A Brief Report contains the same sections as an Original Article, but Results and Discussion sections must be combined.

Reviews should include educational overviews for general researchers and doctors, and review articles for more specialized readers.

Policy Forum presents issues in science policy, including public health, the medical care system, and social science. Policy Forum essays should not exceed 2,000 words.

News articles should not exceed 500 words including one display item. These articles should function as an international news source with regard to topics in the life and social sciences and medicine. Submissions are not restricted to journal staff - anyone can submit news articles on subjects that would be of interest to Drug Discoveries & Therapeutics' readers.

Letters discuss material published in *Drug Discoveries & Therapeutics* in the last 6 months or issues of general interest. Letters should not exceed 800 words and 6 references.

3. Manuscript Preparation

Preparation of text. Manuscripts should be written in correct American English and submitted as a Microsoft Word (.doc) file in a single-column format. Manuscripts must be paginated and double-spaced throughout. Use Symbol font for all Greek characters. Do not import the figures into the text file but indicate their approximate locations directly on the manuscript. The manuscript file should be smaller than 5 MB in size.

Title page. The title page must include 1) the title of the paper, 2) name(s) and affiliation(s) of the author(s), 3) a statement indicating to whom correspondence and proofs should be sent along with a complete mailing address, telephone/fax numbers, and e-mail address, and 4) up to five key words or phrases.

Abstract. A one-paragraph abstract consisting of no more than 250 words must be included. It should state the purpose of the study, basic procedures used, main findings, and conclusions.

Abbreviations. All nonstandard abbreviations must be listed in alphabetical order, giving each abbreviation followed by its spelled-out version. Spell out the term upon first mention and follow it with the abbreviated form in parentheses. Thereafter, use the abbreviated form.

Introduction. The introduction should be a concise statement of the basis for the study and its scientific context.

Materials and Methods. Subsections under this heading should include sufficient instruction to replicate experiments, but well-established protocols may be simply referenced. *Drug Discoveries & Therapeutics* endorses the principles of the Declaration of Helsinki and expects that all research involving humans will have been conducted in accordance with these principles. All laboratory animal studies must be approved by the authors' Institutional Review Board(s).

Results. The results section should provide details of all of the experiments that are required to support the conclusions of the paper. If necessary, subheadings may be used for an orderly presentation. All figures, tables, and photographs must be referred in the text.

Discussion. The discussion should include conclusions derived from the study and supported by the data. Consideration should be given to the impact that these conclusions have on the body of knowledge in which context the experiments were conducted. In Brief Reports, Results and Discussion sections must be combined.

Acknowledgments. All funding sources should be credited in the Acknowledgments section. In addition, people who contributed to the work but who do not fit the criteria for authors should be listed along with their contributions.

References. References should be numbered in the order in which they appear in the text. Cite references in text using a number in parentheses. Citing of unpublished results and personal communications in the reference list is not recommended but these sources may be mentioned in the text. For all references, list all authors, but if there are more than fifteen authors, list the first three authors and add "*et al.*" Abbreviate journal names as they appear in PubMed. Web references can be included in the reference list.

Example 1:
Hamamoto H, Kamura K, Razanajatovo IM, Murakami K, Santa T, Sekimizu K. Effects of molecular mass and hydrophobicity on transport rates through non-specific pathways of the silkworm

larva midgut. Int J Antimicrob Agents 2005; 26:38-42.

Example 2:
Mizuochi T. Microscale sequencing of *N*-linked oligosacchaides of glycoproteins using hydrazinolysis, Bio-Gel P-4, and sequential exoglycosidase digestion. In: Methods in Molecular Biology: Vol. 14 Glycoprotein analysis in biomedicine (Hounsell T, ed.). Humana Press, Totowa, NJ, USA, 1993; pp. 55-68.

Example 3:
Drug Discoveries & Therapeutics. Hot topics & news: China-Japan Medical Workshop on Drug Discoveries and Therapeutics 2007. http://www.ddtjournal.com/hotnews.php (accessed July 1, 2007).

Figure legends. Include a short title and a short explanation. Methods described in detail in the Materials and methods section should not be repeated in the legend. Symbols used in the figure must be explained. The number of data points represented in a graph must be indicated.

Tables. All tables should have a concise title and be typed double-spaced on pages separate from the text. Do not use vertical rules. Tables should be numbered with Roman numerals consecutively in accordance with their appearance in the text. Place footnotes to tables below the table body and indicate them with lowercase superscript letters.

Language editing. Manuscripts submitted by authors whose primary language is not English should have their work proofread by a native English speaker before submission. The Editing Support Organization can provide English proofreading, Japanese-English translation, and Chinese-English translation services to authors who want to publish in *Drug Discoveries & Therapeutics* and need assistance before submitting an article. Authors can contact this organization directly at http://www.iacmhr.com/iac-eso .

IAC-ESO was established in order to facilitate manuscript preparation by researchers whose native language is not English and to help edit work intended for international academic journals. Quality revision, translation, and editing services are offered by our staff, who are native speakers of particular languages and who are familiar with academic writing and journal editing in English.

4. Figure Preparation

All figures should be clear and cited in numerical order in the text. Figures must fit a one- or two-column format on the journal page: 8.3 cm (3.3 in.) wide for a single column; 17.3 cm (6.8 in.) wide for a double column; maximum height: 24.0 cm (9.5 in.). Only use the following fonts in the figure: Arial and Helvetica. Provide all figures as separate files. Acceptable file formats are JPEG and TIFF. Please note that files saved in JPEG or TIFF format in PowerPoint lack sufficient resolution for publication. Each Figure file should be smaller than 10 MB in size. Do not compress files. A fee is charged for a color illustration or photograph.

5. Online Submission

Manuscripts should be submitted to *Drug Discoveries & Therapeutics* online at http://www.ddtjournal.com. The manuscript file should be smaller than 10 MB in size. If for any reason you are unable to submit a file online, please contact the Editorial Office by e-mail: office@ddtjournal.com .

Editorial and Head Office
Wei TANG, MD PhD
Secretary-in-General
TSUIN-IKIZAKA 410
2-17-5 Hongo, Bunkyo-ku
Tokyo 113-0033
Japan
Tel: 03-5840-9697
Fax: 03-5840-9698
E-mail: office@ddtjournal.com

Cover letter. A cover letter from the corresponding author including the following information must accompany the submission: name, address, phone and fax numbers, and e-mail address of the corresponding author. This should include a statement affirming that all authors concur with the submission and that the material submitted for publication has not been previously published and is not under consideration for publication elsewhere and a statement regarding conflicting financial interests.

Authors may recommend up to three qualified reviewers other than members of Editorial board. Authors may also request that certain (but not more than three) reviewers not be chosen.

The cover letter should be submitted as a Microsoft Word (.doc) file (smaller than 1 MB) at the same time the work is submitted online.

6. Accepted Manuscripts

Proofs. Rough galley proofs in PDF format are supplied to the corresponding author via e-mail. Corrections must be returned within 4 working days of receipt of the proofs. Subsequent corrections will not be possible, so please ensure all desired corrections are indicated. Note that we may proceed with publication of the article if no response is received.

Transfer of copyrights. Upon acceptance of an article, authors will be asked to agree to a transfer of copyright. This transfer will ensure the widest possible dissemination of information. A letter will be sent to the corresponding author confirming receipt of the manuscript. A form facilitating transfer of copyright will be provided. If excerpts from other copyrighted works are included, the author(s) must obtain written permission from the copyright owners and credit the source(s) in the article.

Cover submissions. Authors whose manuscripts are accepted for publication in *Drug Discoveries & Therapeutics* may submit cover images. Color submission is welcome. A brief cover legend should be submitted with the image.

Revised February 2008

IACMHR CO., LTD.

Drug Discoveries & Therapeutics

IACMHR CO., LTD.

Editorial Office

TSUIN-IKIZAKA 410
2-17-5 Hongo, Bunkyo-ku
Tokyo 113-0033, Japan

Tel: 03-5840-9697
Fax: 03-5840-9698
E-mail: office@ddtjournal.com
URL: www.ddtjournal.com

JOURNAL PUBLISHING AGREEMENT

Ms No:

Article entitled:

Corresponding author:

To be published in Drug Discoveries & Therapeutics

Assignment of publishing rights:

I hereby assign to International Advancement Center for Medicine & Health Research Co., Ltd. (IACMHR Co., Ltd.) publishing Drug Discoveries & Therapeutics the copyright in the manuscript identified above and any supplemental tables and illustrations (the articles) in all forms and media, throughout the world, in all languages, for the full term of copyright, effective when and if the article is accepted for publication. This transfer includes the rights to provide the article in electronic and online forms and systems.

I understand that I retain or am hereby granted (without the need to obtain further permission) rights to use certain versions of the article for certain scholarly purpose and that no rights in patent, trademarks or other intellectual property rights are transferred to the journal. Rights to use the articles for personal use, internal institutional use and scholarly posting are retained.

Author warranties:

I affirm the author warranties noted below.
1) The article I have submitted to the journal is original and has not been published elsewhere.
2) The article is not currently being considered for publication by any other journal. If accepted, it will not be submitted elsewhere.
3) The article contains no libelous or other unlawful statements and does not contain any materials that invade individual privacy or proprietary rights or any statutory copyright.
4) I have obtained written permission from copyright owners for any excerpts from copyrighted works that are included and have credited the sources in my article.
5) I confirm that all commercial affiliations, stock or equity interests, or patent-licensing arrangements that could be considered to pose a financial conflict of interest regarding the article have been disclosed.
6) If the article was prepared jointly with other authors, I have informed the co-authors(s) of the terms of this publishing agreement and that I am signing on their behalf as their agents.

Your Status:

☐ I am the sole author of the manuscript.

☐ I am one author signing on behalf of all co-authors of the manuscript.

Please tick one of the above boxes (as appropriate) and then sign and date the document in black ink.

Signature: **Date:**

Name printed:

Please return the completed and signed original of this form by express mail or fax, or by e-mailing a scanned copy of the signed original to:

Drug Discoveries & Therapeutics office
TSUIN-IKIZAKA 410, 2-17-5 Hongo,
Bunkyo-ku, Tokyo 113-0033, Japan
E-mail: proof-editing@ddtjournal.com
Fax: +81-3-5840-9698